OSAKA UNIVERSITY
GRADUATE SCHOOL OF SCIENCE

T H E S I S

for

Doctor of Science

Three-Body Dynamics Induced by Loosely Bound Nuclei

Tokuro FUKUI

Research Center for Nuclear Physics (RCNP), Osaka University,
Ibaraki, Osaka 567-0047, Japan

Defended on February 4, 2014

Juries:

Adviser:	Kazuyuki OGATA	-	RCNP
Chief Examiner:	Atsushi HOSAKA	-	RCNP
Examiners:	Nori AOI	-	RCNP
	Tadashi SHIMODA	-	Department of Physics
	Atsushi TAMII	-	RCNP

For my parents

"The things I once imagined would be my greatest achievements were only the first steps toward a future I can only begin to fathom."

—Jace Beleren

Three-Body Dynamics Induced by Loosely Bound Nuclei

Abstract: The main object of this thesis is to correctly understand nuclear dynamics when the system consists of a three-body system including loosely bound nuclei. If a projectile is bound loosely, it can break up into its continuum state in the intermediate state of scattering process. Thus the channel couplings among bound and continuum states of the projectile is expected to be important to precisely describe the dynamics. By explicitly taking into account the channel couplings with the method of the continuum-discretized coupled-channels (CDCC), we clarify how the continuum channels of loosely bound nuclei are significant.

First, we focus on transfer reactions. We construct a precise reaction model based on the coupled-channel Born approximation (CCBA), which explicitly treats the channel couplings among bound and continuum states of both a projectile and a residual nucleus in the initial and final channels, respectively, by means of the CDCC method. From the CCBA analysis of transfer reactions, it has been found that the interference between the elastic transfer (ET) and the breakup transfer (BT) can be important. The former is the transfer process from an ground state to an ground state in each channel, whereas the latter is the transfer process from or into continuum states in the initial or final channels, respectively. Furthermore, it has also pointed out that transferred angular momenta can vary due to the channel couplings.

Second, we concentrate on breakup reactions with a low incident energy, in particular when a target nucleus is heavy and thus there is a strong Coulomb field. In such a case, it was reported that the eikonal approximation, which can efficiently treat breakup reactions by assuming that a distorted wave between a projectile and target does not deviate from a plane wave, does not work. To solve this difficulty, we propose an efficient way to extend the eikonal model to low energy reactions. As a result we found that the Coulomb correction based on the distance of closest approach in Rutherford scattering works well. It suggests that a concept of a "trajectory" is held and thus a simple picture for dynamics remains in complicated reaction process.

Third, the α-clustering phenomena, which is the localization of α-particles at surface region of nuclei, has been investigated through α-transfer reactions. Wave functions in a structure part of nuclei are calculated by means of a microscopic cluster model. By comparing calculated transfer cross sections with experimental data, we can extract an "α-cluster probability" at surface region of nuclei. The probability is different from neither a spectroscopic factor, which have been regarded as an indicator of the clustering, or an asymptotic normalization coefficient (ANC).

Keywords: Nuclear reaction, continuum state, coupled-channels method, transfer reaction, breakup reaction

Acknowledgments

I would like to acknowledge the guidance of Prof. Kazuyuki Ogata with his wise insight for research and earnest effort for education. It would have been impossible to complete this thesis if there were no support of him. I am very grateful to Prof. Masanobu Yahiro for giving unerring suggestion for research. I would also greatly appreciate Prof. Pierre Capel for fruitful discussions and his wonderful hospitality for my visit to Brussels. A very nice collaboration with Prof. Yoshiko Kanada-En'yo, Dr. Yasutaka Taniguchi, and Dr. Tadahiro Suhara encourages my passion for physics. I express my gratitude to them.

I really respect Prof. Atsushi Hosaka. His broad interest and intuitive interpretation on physics broaden my vision for study. I thank Prof. Takayuki Myo, Dr. Kazuhito Mizuyama, Dr. Yuma Kikuchi, Dr. Kosho Minomo, and Kazuki Yoshida for fruitful discussions and giving helpful comments. I also wish to thank Prof. Yasunori Iseri for valuable discussions. His computer code RANA serves as a useful reference to construct my computer code for transfer reactions.

I appreciate staffs of theory group at Research Center for Nuclear Physics (RCNP), Prof. Noriyoshi Ishii, Prof. Hiroyuki Kamano, Dr. Takayasu Sekihara, and Dr. Junko Yamagata-Sekihara for their supports. I express my great thanks to our secretary Ms. Mika Tambara for her tenderness and smile. I was very happy to share a valuable moment and discuss physics with former RCNP students, Dr. Kaori Horii, Dr. Shunsuke Ohkoda, and Dr. Yasuhiro Yamaguchi, and present students, Takuya Shibata, Sangho Kim, Takashi Ezoe, and Takuya Sugiura.

I thank all of members of RCNP who provide us suitable environment for research. This research was supported in part by Grant-in-Aid of the Japan Society for the Promotion of Science (JSPS) for JSPS Fellows (Grant No. 24-2396).

Finally, I would express special thanks to my family, in particular, my parents. Your love and wisdom always give me a supportive push forward.

Tokuro Fukui

Contents

CHAPTER 1

Introduction

Contents

1.1 Three-body dynamics

In nuclear physics, nucleon-nucleon, nucleon-nucleus, and nucleus-nucleus scattering have been studied to reveal the nuclear interaction and nuclear structures. The correct interpretation of the mechanism for these nuclear reactions is also an important subject of physics. It is, however, not easy to understand correctly the reaction mechanism when system can be regarded as the three-body system. If two particles are bound loosely and form a projectile, the system including a target nucleus should be treated as the three-body system. For example, let us consider the scattering of deuteron and a target nucleus A. In a naive picture, it can be understood as scattering of d by the nuclear and Coulomb field produced by A. However, in this picture the degree of freedom of nucleons, which is the fact that d consists of proton and neutron, is ignored. The dynamics that proceeds by the interactions between the nucleons in d and A is desired to be considered when one nucleus is loosely bound. We would like to discuss how the picture of nuclear reactions changes when we consider this kind of the three-body dynamics. In this thesis, we focus on the effect due to breakup of a nucleus in the intermediate state of the scattering.

In the direct nuclear reaction picture [1,2], nuclear reactions can be categorized as elastic scattering, inelastic scattering, which includes breakup reactions, and transfer reactions. Below we discuss important features of these reactions which are characterized by loosely bound nuclei.

1.1.1 Elastic scattering

Among nuclear reactions, elastic scattering is the simplest reaction, in which a projectile is ejected with having the same energy as in the initial state. However, it does not necessarily mean that an incident nucleus is inert throughout the scattering process. For example,

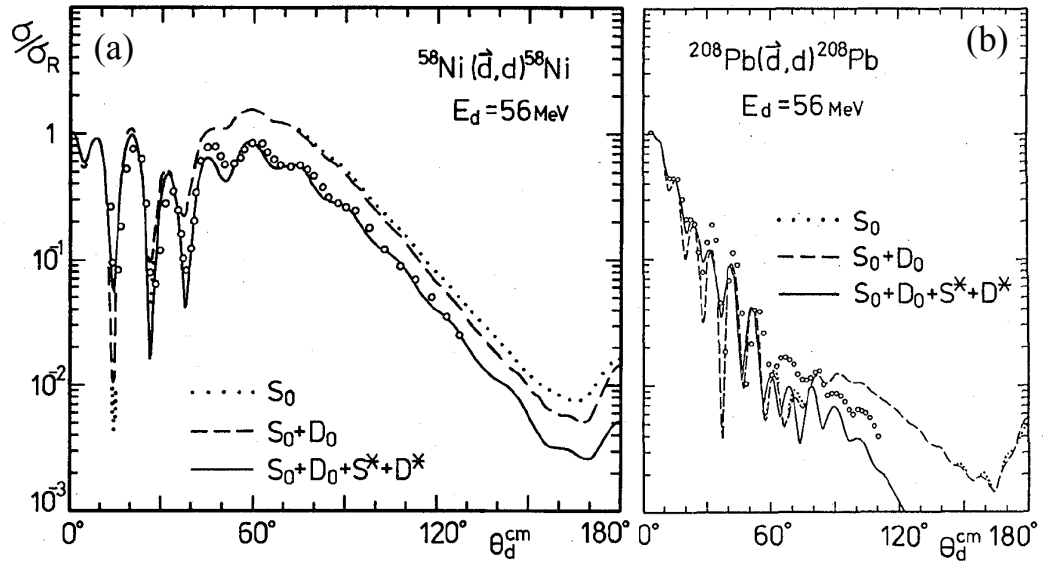

Figure 1.1: (a) Rutherford ratio of the elastic cross section as a function of the scattering angle of d for the d+^{58}Ni at 56 MeV. (b) Same as in panel (a) but for the d+^{208}Pb system. In each panel the solid line stands for the result of the CDCC calculation, which explicitly takes into account the virtual breakup process of d with its s- and d-wave states. The dashed (dotted) line stands for the result which dose not include the breakup states of d with (without) the d-wave component in the ground state of d. This figure is taken from Ref. [3]. In each panel, circles are the experimental data taken from Ref. [4].

in Fig. 1.1 we show the Rutherford ratio of the elastic cross section as a function of the scattering angle of d for (a) the d+^{58}Ni at 56 MeV and (b) d+^{208}Pb at 56 MeV [3]. In each case, if one neglects any effects of the breakup states of d, the dashed and dotted lines are obtained. Note that the former (latter) includes (does not include) the d-wave component in the s-wave ground state of d. They cannot well reproduce the experimental data (circles) [4]. The solid line is for the result calculated with the method of the continuum-discretized coupled-channels (CDCC) [3, 5, 6], which explicitly takes into account the channel-couplings of the breakup channels. In Chap. 2 we mention CDCC in detail. It reproduces well the experimental data even at backward angles. This fact indicates the importance of treating the virtual breakup process of d. Note that it is called the virtual breakup that a projectile breaks up in intermediate states of elastic scattering.

To understand the virtual breakup, we show the behavior of the dynamical polarization potential (DPP) of unstable nuclei reported in Ref. [7]. The optical potential $U_{\rm opt}$, which describes the elastic scattering, and the DPP are defined by

$$U_{\rm opt} = PVP + U_{\rm DPP}, \tag{1.1}$$

$$U_{\rm DPP} = PVQ \lim_{\varepsilon\to 0} \frac{1}{E + i\varepsilon - QHQ} QVP, \tag{1.2}$$

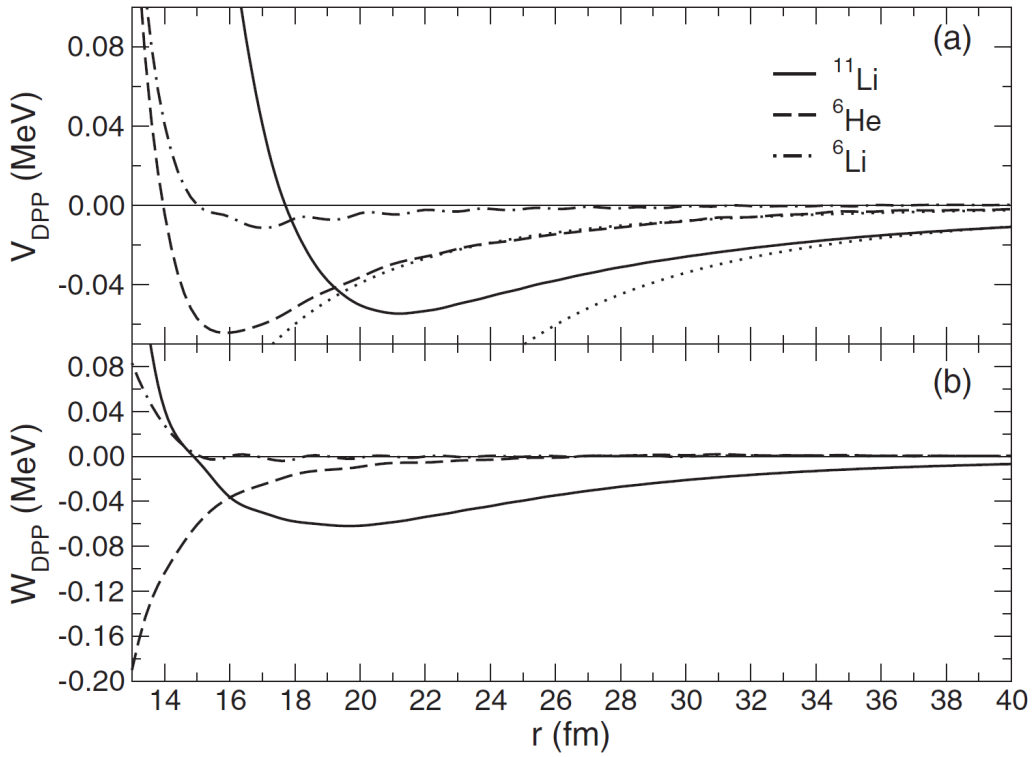

Figure 1.2: Trivially equivalent local form the DPPs of ^{11}Li (solid line), ^{6}He (dashed line), and ^{6}Li (dash-dotted line) on the target nucleus ^{208}Pb. The panel (a) and (b) respectively correspond to the real and imaginary parts of the DPP. The dotted lines denote the Coulomb polarization potentials for ^{11}Li and ^{6}He. The detail of the calculation is given in Ref. [7].

where H (V) is the many-body Hamiltonian (interaction) of the projectile-target system. E and ε are the total energy and the infinitesimal value, which ensures an outgoing boundary condition, respectively. The operator P projects onto the elastic channel (P space) and $Q = 1 - P$ is the projection operator onto the non elastic channels (Q space). The first term of Eq. (1.1) is the folding potential describing the interaction that does not go through the Q space. The folding potential is real, local, and energy independent. The second term $U_{\rm DPP}$, which is complex, non-local, and energy dependent function, describes the channel couplings between the P and Q spaces. Thus, by seeing the behavior of $U_{\rm DPP}$, we can estimate the contribution of the coupling with the Q space. In Fig. 1.2, DPPs in the so called trivially equivalent local potential [8] of the projectiles, ^{11}Li (solid line), ^{6}He (dashed line), and ^{6}Li (dash-dotted line), for the scattering on the ^{208}Pb target nucleus at 29.8 MeV, 18 MeV, and 29 MeV, respectively, are shown as a function of the relative distance of each projectile and the target. In panels (a) and (b) their real and imaginary parts are respectively plotted. These calculations were performed with CDCC in Ref. [7]. The DPPs of the unstable nuclei, ^{11}Li and ^{6}He, have a quite long tail compared to that of the DPP for the

stable ^{6}Li nucleus. In Ref. [7] it was reported that the calculated cross sections with CDCC including breakup channels of each projectile well reproduce experimental data [9–11] of the elastic cross section for each system, whereas CDCC without their breakup channels does not. Therefore, this unusual feature of the DPP for the unstable nuclei suggests that a strong coupling with the Q space, the breakup states of unstable nuclei in particular, is necessarily taken into account to correctly describe the elastic scattering.

Thus, in elastic scattering the importance of the three-body dynamics, the breakup effects of loosely bound nuclei in particular, is well known, and their dynamics can be well described through the analysis by means of CDCC. We should clarify how the three-body dynamics of loosely bound nuclei is important in other reactions. CDCC can provide us with clear interpretation of reaction mechanisms. The formulation of CDCC is given in Chap. 2.

1.1.2 Inelastic scattering

In this thesis we do not discuss usual inelastic reactions, which proceed with an excitation of a target nucleus. We focus on breakup reactions that can be regarded as inelastic scattering in a broad sense. In breakup reactions, a projectile breaks up into its fragments, and hence their description trivially requires the channel couplings of elastic and breakup channels. If we consider a breakup reaction on a heavy ion target, not only nuclear interaction but also Coulomb interaction play an important role. In such a case, sometimes the following assumption is adopted. The reaction is dominated by the Coulomb interaction between the projectile and the target, and proceeds with the one-step process, in which the transition from a bound state to a continuum state is described by the Born approximation. The virtual photon theory (VPT) [12], which is one of such naive models, is often used for analyses of Coulomb-dominant breakup reactions, because it is difficult to explicitly treat the long-ranged Coulomb interaction in coupled-channels (CC) calculations. If one aims to explicitly treat the Coulomb breakup with full quantum mechanics, sometimes the scattering wave function needs to calculate up to more than 1000 fm with the number of partial waves of more than 10000 $\hbar$. Thus, VPT simplifies the Coulomb breakup reaction by regarding the reaction as the dissociation of a projectile by the Coulomb dipole (E1) photon absorption. However, it is not trivial that the picture by VPT is correct. The role of the quadrupole (E2) component, nuclear interaction, and the multistep process, which are not taken into account in VPT, should be investigated. Note that Eλ is the electric multipole moment when one expands the Coulomb interaction by means of the Legendre polynomial P_λ with its multipolarity λ. The multipole expansion of the Coulomb interaction is written in Appx. B.

For example, we discuss the importance of these effects in the ^{208}Pb(^{8}B,p^7Be) breakup reaction reported in Ref. [13]. In Fig. 1.3 the breakup cross section of the ^{208}Pb(^{8}B,p^7Be) is plotted as a function of the scattering angle θ_8 of the center of mass (c.m) of the p-^{7}Be system. The cross section corresponds to the breakup energy ε_{17} of the p-^{7}Be system ranging from 500 keV to 750 keV. The solid line stands for the calculated cross section with CDCC, which includes all orders of the nuclear and Coulomb breakups as well as all the multipolarities of the Coulomb interaction. When the nuclear breakup is ignored, one

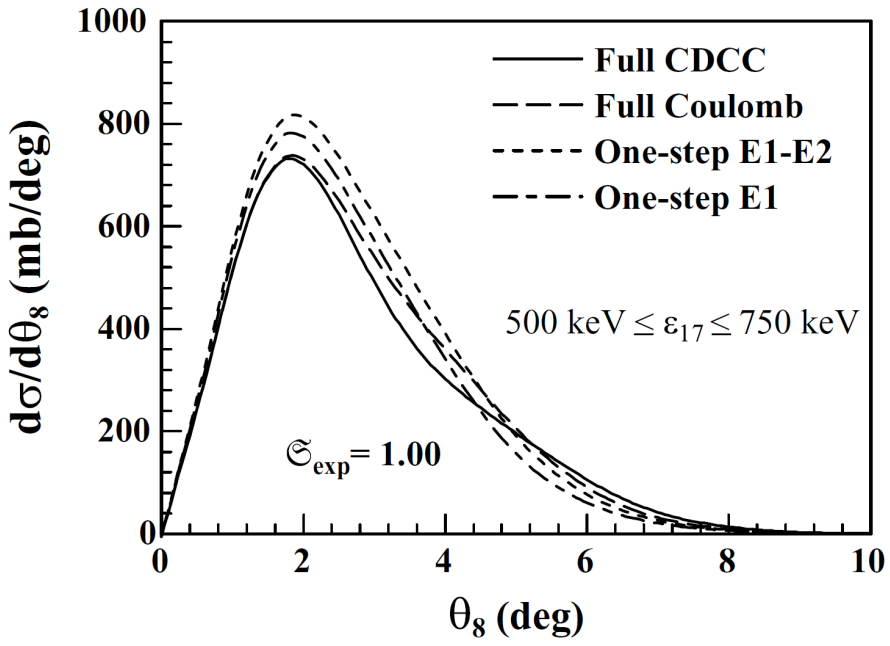

Figure 1.3: The breakup cross section calculated with CDCC of ^{8}B on ^{208}Pb at 52 MeV/nucleon as a function of the scattering angle θ_8 in the center of mass (c.m.) of the p-^{7}Be system. The cross section corresponds to the breakup energy ε_{17} of the p-^{7}Be system ranging from 500 keV to 750 keV. The solid line is obtained by CDCC with all orders of the nuclear and Coulomb breakups. The cross section for only the Coulomb breakups with all orders of the multipolarity of the Coulomb interaction is shown by the dashed line. When multistep processes and the higher multipolarity than E2 (E1) are neglected, the dotted (dash-dotted) line is obtained. See Ref. [13] for more detail.

obtains the dashed line. Furthermore, if one assumes a one-step transition process with only the E1 and E2 (E1) of the multipolarities, the dotted (dash-dotted) line is obtained. The E1 one-step calculation, which essentially corresponds to VPT, is often adopted. These results indicate that the higher multipolarity and multistep transition exist non-negligibly even for heavy ion targets.

In Refs. [13, 14] the reaction model based on CDCC, which can treat the Coulomb breakup precisely and conveniently by adopting the eikonal approximation, is developed, that is, the eikonal-CDCC (E-CDCC). The eikonal approximation is based on the concept that, for high energy reactions, variation of the projectile-target distorted wave from a plane wave is expected to be small. E-CDCC has an advantage that it has high accuracy with less computational cost than full quantum calculation. The details of E-CDCC is given in Chap. 2.

In the same period as E-CDCC had been established, another reaction model based on the eikonal approximation that is, the model with the dynamical eikonal approximation (DEA), was proposed [15, 16]. For low energy reactions, the eikonal approximation is

expected to be not applicable, and recently it is found that DEA is difficult to reproduce a full quantum calculation at low incident energies, say 20 MeV/nucleon [17].

Therefore it is demanded to build up a reliable and economical reaction model, which can be applied to low energy reactions. In this thesis the construction of such a reaction model is done by adopting a simple correction for the Coulomb trajectory. E-CDCC and DEA have same philosophy to efficiently treat the Coulomb breakups, based on the eikonal approximation, except how to calculate the projectile's wave function in each model. The former uses a partial wave expansion, and the latter calculates the wave function with three-dimensional points. Thus, comparison of E-CDCC and DEA given in Chap. 4 is important to describe the Coulomb breakups efficiently.

1.1.3 Transfer reaction

Transfer reactions have been widely used to investigate a single-particle structure of nuclei. As an example let us consider the transfer reaction $A(a,b)B$. When one aims to seek a single-particle structure of the residual nucleus B in its ground state, an low incident energy is usually adopted to make the momentum matching better. Here the momentum matching means how small the energy difference between an incident energy and a single-particle energy is. If the energy difference is small, the matching is good. For naive understanding, sometimes it is used the metaphorical expression that *one jumps from a running train into another running train*. It is not easy to jump if each velocity of the two trains differs from each other. Since a single-particle energy of B is merely from several MeV to several tens MeV, an incident energy also should be taken as in similar order.

In conventional description of the transfer reaction, the breakup states of a and B are neglected by using the distorted-wave Born approximation (DWBA). Because it is difficult and it requires a large computational cost to perform CC calculation for breakup states in transfer reactions. Thus, in DWBA, the transfer process is described by a one-step transition between the ground states in the initial and final channels. At energies typically adopted for transfer reactions, there is enough "time" for particles to interact each other, and couplings to several complicated channels such as breakup or rearrangement channels may be important. In transfer reaction, since deuteron, which is a loosely bound nucleus, is often used as the projectile a to reproduce a single-particle state of B, the breakup channels of d, in particular, are expected to play a significant role. Furthermore, if B is a loosely bound nucleus, its breakup channels should also be taken into account.

To explicitly take into account these breakup effects, in the mid-1960s, the coupled-channels Born approximation (CCBA) was proposed by Penny and Satchler [18] and Iano and Austern [19]. From the end of 1960s to the 1970s, a large number of the CCBA calculations were performed [20–96] by using some computational codes for the CCBA calculation, for example CHUCK [97], SATURN-MARS [98, 99], and OUKID [100]. Note that, at that time, the channel-couplings with only a few bound excited states of the projectile a and/or the residual nucleus B in the region of stable nuclei were taken into account in these codes. For example, in Ref. [101], the authors clarified the importance of the channel-couplings with some resonance states of the target nucleus in order to resolve a failure of DWBA on the heavy-ion induced transfer reaction ^{40}Ca(^{13}C,^{14}N)^{39}K [102]. In Fig. 1.4(a),

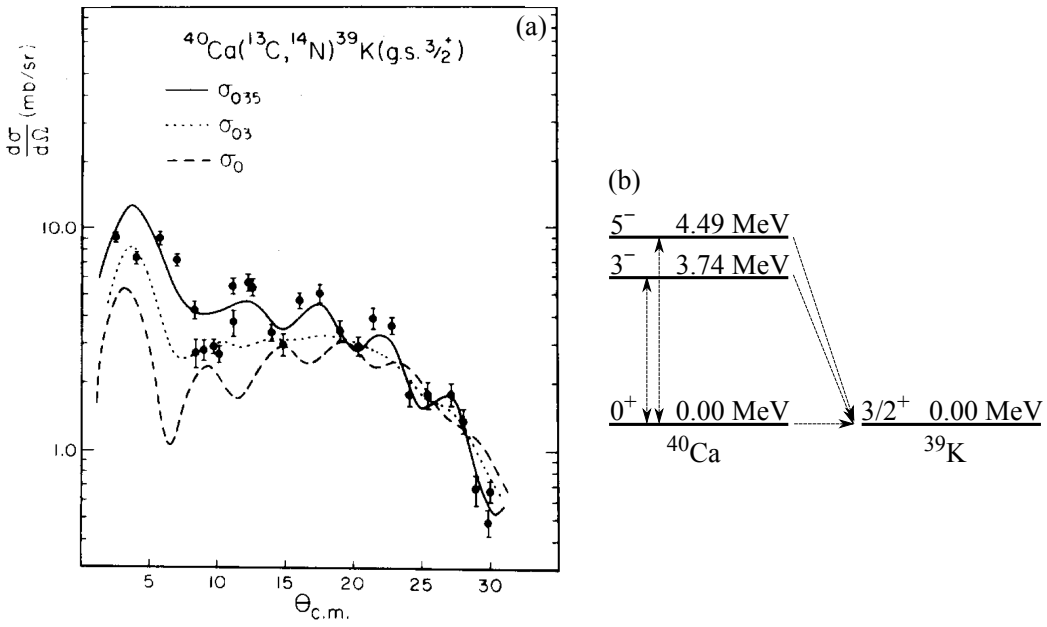

Figure 1.4: (a) The cross section of the ^{40}Ca(^{13}C,^{14}N)^{39}K reaction at 68 MeV. Horizontal axis is the emitting angle of ^{14}N in the c.m. frame. The solid (dashed) line is the CCBA result including the channel-couplings among 0^+, 3^-, and 5^- (between 0^+ and 3^-) states of ^{40}Ca. Experimental data are taken from Ref. [102]. (b) A schematic picture of the path of the transfer process with the CC effects. See Ref. [101] for more detail.

we show the cross section of the ^{40}Ca(^{13}C,^{14}N)^{39}K reaction at 68 MeV as a function of the ^{14}N emitting angle. If one neglects all channel-couplings regarding the excited states of ^{40}Ca, the dashed line, which corresponds to the DWBA result, is obtained. It is not able to reproduce the oscillation pattern of the experimental data [102]. The dotted line is the result for the CCBA calculation, which takes into account the channel-couplings between 0^+ and 3^- states of ^{40}Ca. When the couplings to the 5^- state of ^{40}Ca is also added, the solid line is obtained. Note that these excites states are bound states since the proton separation energy of ^{40}Ca is 8.33 MeV. They agree with the experimental data even at forward angles, where the DWBA calculation fails to reproduce the data. Thus CCBA has been achieved success. Though the importance of the CC effects was argued by these works, the continuum states of a and/or B were not taken into account owing to a limitation of the computational power at that time.

After establishment of CDCC in the end of 1980s, several CCBA calculations with CDCC were performed to treat breakup states involving both resonant and non resonant states of loosely bound nuclei by using computer codes FRESCO [103, 104], RANA [105], and so on. Note that, in CDCC, infinite number of states, not only resonance states but also non resonant continuum states, of the projectile a and/or the residual nucleus B are in principle considered. For instance, in Ref. [106], the effects of the ^{6}Li breakup into α and

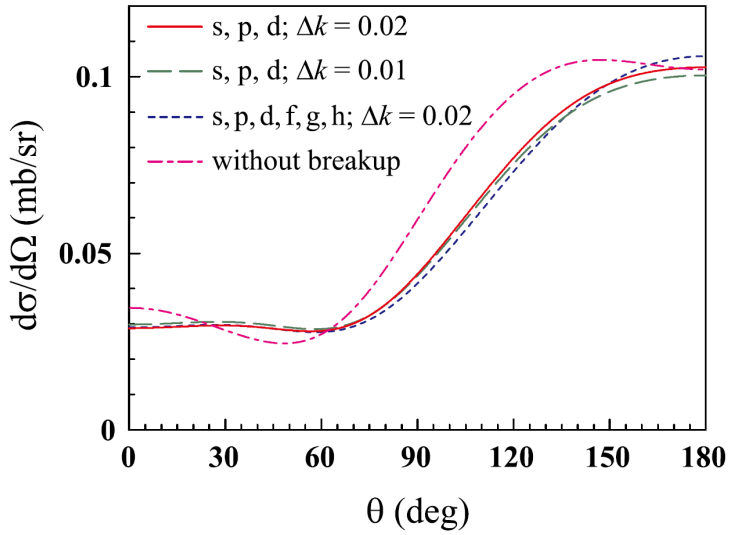

Figure 1.5: The cross sections calculated with the ZR-CCBA of the ^{13}C(^{6}Li,d)^{17}O reaction at 3.6 MeV are plotted as a function of the deuteron emitting angle. In the calculation the breakup effects of ^{6}Li was taken into account. The figure indicates that the breakup channels of ^{6}Li are important, and a treatment of them requires a huge model space. See Ref. [106] for more detail.

d on the transfer reaction ^{13}C(^{6}Li,d)^{17}O was investigated within the CDCC framework. In Fig. 1.5, the calculated cross sections of the ^{13}C(^{6}Li,d)^{17}O reaction at 3.6 MeV are plotted as a function of the deuteron emitting angle. The dash-dotted line and the others respectively correspond to the results including and not including the breakup channels of ^{6}Li. The differences among the solid, dashed, and dotted lines are due to the model space dependence of the calculation. These results indicate that the breakup channels of ^{6}Li play an important role and a huge model space is needed for the calculation. In Ref. [106], although the breakup effects of ^{6}Li is explicitly taken into account, those of ^{17}O are not. Moreover, the zero-range (ZR) approximation, in which the product of the α-d interaction and its wave function is assumed to be represented by a δ-function, was adopted to save the computational task. At this moment, there is only one CCBA work [107], in which the breakup states of both a projectile and a residual nucleus were considered, simultaneously. However the detail of the breakup mechanism of a projectile and a residual nucleus has not been discussed yet.

From these points of view, we need a more precise CCBA model, which explicitly takes into account the breakup channels of both a and B in order to investigate the breakup effects of a and B. Thus, in Chap. 3, we construct such a CCBA model, in which the exact finite-range (FR) integration instead of the ZR approximation is adopted. This CCBA model enables us to describe transfer reactions in detail and correctly.

1.2 Construction of thesis

This thesis is constructed as follows. In Chap. 2 the formulation of CDCC is given. E-CDCC is also formulated there. As mentioned above, the three-body dynamics, breakup effects of nuclei in particular, is expected to be important for loosely bound system. CDCC explicitly treats CC of the breakup channels of nuclei, and enables us to correctly interpret the picture of dynamics. First, the three-body dynamics on transfer reactions is discussed in Chap. 3. The CCBA framework, which can perform the CC calculation regarding the breakup channels both in the initial and final channels, are proposed. As an application, the ^{8}B(d,n)^{9}C reaction, which is paid attention with an astrophysical interest [108], is analyzed with the CCBA model and the breakup effects of d and ^{9}C are investigated. As for breakup reactions, in Chap. 4, we propose a method for treating Coulomb breakup reactions with efficient and precise models. As a specific reaction, the breakup reaction ^{208}Pb(^{15}C,n^{14}C) is described with two reaction models, E-CDCC and DEA, which are based on the eikonal approximation. In Chap. 5, α-clustering phenomena, which is the localization of α particles at surface region of nuclei, are investigated through α-transfer reactions by using a microscopic wave function for the structure part. We summarize this thesis in Chap. 6.

Main purpose of this thesis is to correctly understand the three-body dynamics induced by loosely bound nuclei by means of precise and efficient reaction models.

CHAPTER 2

Formulation

Contents

The method of the continuum-discretized coupled-channels (CDCC), which explicitly takes into account the channel-couplings between elastic-breakup and breakup-breakup channels, is described in this Chapter. CDCC has been successful in describing various reactions. In Ref. [109], it is confirmed that CDCC wave function for the three-body system explicitly corresponds to the 0th-order term of the distorted-wave Faddeev wave function [110] which is the exact solution of three-body scattering. Moreover, the first-order term of the Faddeev component is expected to be small. Therefore the reliability of the wave function described by CDCC is well established. These facts are summarized in Appx. A. Details of the formulation and the development of CDCC are given in Ref. [3, 5, 6].

2.1 Continuum-discretized coupled-channels (CDCC) formalism

2.1.1 Truncation and discretization of three-body wave function

We consider the scattering of the projectile a and the target nucleus A. To take into account explicitly the breakup effects of a, we regard a as a two-body system consisting of x and y.

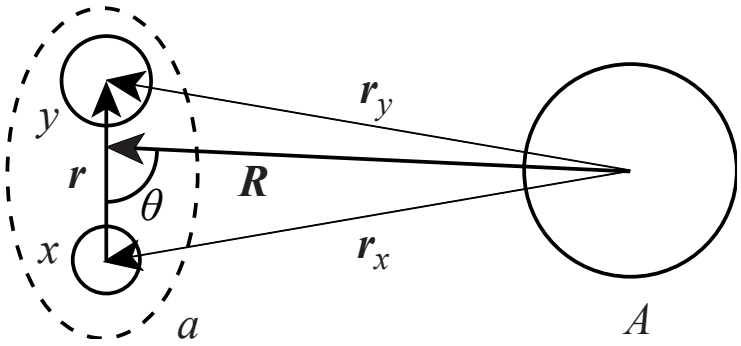

Figure 2.1: Coordinates of the three-body system ($x + y + A$).

Thus we work with the three-body model ($x + y + A$) shown in Fig. 2.1. The Hamiltonian of the three-body system is given by

$$H = T_R + V_x^{(\mathrm{N})}(\boldsymbol{r}_x) + V_x^{(\mathrm{C})}(\boldsymbol{r}_x) + V_y^{(\mathrm{N})}(\boldsymbol{r}_y) + V_y^{(\mathrm{C})}(\boldsymbol{r}_y) + h, \tag{2.1}$$

$$h = T_r + V_x^{(\mathrm{N})}(\boldsymbol{r}) + V_x^{(\mathrm{C})}(\boldsymbol{r}), \tag{2.2}$$

where $\boldsymbol{r}$ ($\boldsymbol{R}$) is the relative coordinate between x (the center of mass of the x-y system) and y (A), and T_R is the kinetic energy operator for the coordinate $\boldsymbol{R}$. $V_x^{(\mathrm{N})}$ ($V_y^{(\mathrm{N})}$) and $V_x^{(\mathrm{C})}$ ($V_y^{(\mathrm{C})}$) respectively represent the nuclear and Coulomb interactions between x (y) and A. The internal Hamiltonian for the x-y system is expressed by h.

The orbital angular momenta $\boldsymbol{L}$ and $\boldsymbol{\ell}$, which respectively correspond to the coordinates $\boldsymbol{R}$ and $\boldsymbol{r}$, satisfy

$$\boldsymbol{J} = \boldsymbol{L} + \boldsymbol{\ell}, \tag{2.3}$$

where $\boldsymbol{J}$ is the total angular momentum. The three-body wave function Ψ satisfies the Schödinger equation

$$(H - E)\Psi(\boldsymbol{r}, \boldsymbol{R}) = 0, \tag{2.4}$$

where E is the total energy of the system and M is the z-component of $\boldsymbol{J}$. In CDCC we expand Ψ with the internal wave function $\psi_{\ell m}$ of a, which approximately forms the complete set as follows:

$$\begin{aligned}\Psi(\boldsymbol{r}, \boldsymbol{R}) = &\sum_{|J-\ell|<L<|J+\ell|} \left[\psi_\ell(k_0, \boldsymbol{r}) \otimes \chi^J_{\ell L M_L}(K_0, \boldsymbol{R})\right]_{JM} \\ &+ \sum_{\ell=0}^{\infty} \sum_{|J-\ell|<L<|J+\ell|} \int_0^\infty dk \left[\psi_\ell(k, \boldsymbol{r}) \otimes \chi^J_{\ell L M_L}(K, \boldsymbol{R})\right]_{JM}, \end{aligned} \tag{2.5}$$

$$\left[\psi_\ell \otimes \chi^J_{\ell L M_L}\right]_{JM} \equiv \sum_{m, M_L} (\ell m L M_L | J M)\, \psi_{\ell m} \chi^J_{\ell L M_L}, \tag{2.6}$$

where $\chi^J_{\ell L M_L}$ represents the distorted wave of the a-A system. m (M_L) is the z-component of $\boldsymbol{\ell}$ ($\boldsymbol{L}$), and the relative momentum for the x-y (a-A) system is denoted by $\hbar k$ ($\hbar K$). From the energy conservation, the total energy E satisfies

$$E = \frac{\hbar^2 k^2}{2\mu_r} + \frac{\hbar^2 K^2}{2\mu_R}. \tag{2.7}$$

Here μ_r (μ_R) is the reduces mass of the x-y (a-A) system. The first term of Eq. (2.5) stands for the elastic component in which x and y are bound and form the ground state of a, while the second term corresponds to the breakup component in which the x-y system is in continuum states. $\psi_{\ell m}$ satisfies

$$(h - \varepsilon)\psi_{\ell m}(k, \boldsymbol{r}) = 0, \tag{2.8}$$

with the eigenenergy ε of the x-y system defined by

$$\varepsilon = \frac{\hbar^2 k^2}{2\mu_r}. \tag{2.9}$$

It is difficult to handle the second term of Eq. (2.5), since it has infinite number of "channels". Therefore, in CDCC, the breakup component $\Psi_{\rm bu}$, that is the second term of Eq. (2.5) is approximated as

$$\begin{aligned}
\Psi_{\rm bu} &\equiv \sum_{\ell=0}^{\infty} \sum_{|J-\ell|<L<|J+\ell|} \int_0^{\infty} dk \left[\psi_\ell(k, \boldsymbol{r}) \otimes \chi^J_{\ell L}(K, \boldsymbol{R})\right]_{JM} \\
&\approx \sum_{\ell=0}^{\ell_{\rm max}} \sum_{|J-\ell|<L<|J+\ell|} \int_0^{k_{\rm max}} dk \left[\psi_\ell(k, \boldsymbol{r}) \otimes \chi^J_{\ell L}(K, \boldsymbol{R})\right]_{JM} \\
&= \sum_{\ell=0}^{\ell_{\rm max}} \sum_{|J-\ell|<L<|J+\ell|} \sum_{n}^{n_{\rm max}} \int_{k_{n-1}}^{k_n} dk \left[\psi_\ell(k, \boldsymbol{r}) \otimes \chi^J_{\ell L}(K, \boldsymbol{R})\right]_{JM} \\
&\approx \sum_{\ell=0}^{\ell_{\rm max}} \sum_{|J-\ell|<L<|J+\ell|} \sum_{n}^{n_{\rm max}} \left[\hat{\psi}_{n\ell}(\boldsymbol{r}) \otimes \hat{\chi}^J_{n\ell L}(\boldsymbol{R})\right]_{JM}.
\end{aligned} \tag{2.10}$$

Equation (2.10) means that CDCC first truncates the model space at $\ell_{\rm max}$ and $k_{\rm max}$. Next we divide the momentum space $[0, k_{\rm max}]$ and then discretize it by a specific procedure. This concept is shown as a schematic picture in Fig. 2.2. For the procedure we have tow methods, one is the average method and the other is the pseudostate method. Below the detail of the two procedures of the discretization is given.

2.1.2 Average method

In this method the momentum space $[0, k_{\rm max}]$ is divided into several ranges called "bin" states specified by the momentum width $\Delta k_n = k_n - k_{n-1}$. Then $\psi_{\ell m}$ in each bin is taken as an average;

$$\hat{\psi}_{n\ell m}(\boldsymbol{r}) = \frac{1}{\sqrt{\Delta k_n}} \int_{k_{n-1}}^{k_n} \psi_{\ell m}(k, \boldsymbol{r}) dk, \tag{2.11}$$

$$\hat{\chi}^J_{n\ell L M_L}(\boldsymbol{R}) = \sqrt{\Delta k_n}\, \chi^J_{\ell L M_L}(K, \boldsymbol{R}). \tag{2.12}$$

This prescription is called the average method for discretization. $\hat{\psi}_{n\ell m}$ has an orthonormality:

$$\left\langle \hat{\psi}_{n\ell m}(\boldsymbol{r}) | \hat{\psi}_{n'\ell' m'}(\boldsymbol{r}) \right\rangle = \delta_{nn'}\delta_{\ell\ell'}\delta_{mm'}.. \tag{2.13}$$

The diagonalization of h results in

$$\left\langle \hat{\psi}_{n\ell m}(\boldsymbol{r}) \left| h \right| \hat{\psi}_{n'\ell' m'}(\boldsymbol{r}) \right\rangle = \hat{\varepsilon}_n \delta_{nn'}\delta_{\ell\ell'}\delta_{mm'}, \tag{2.14}$$

where the discretized eigenenergy $\hat{\varepsilon}_n$ is calculated as

$$\begin{aligned} \hat{\varepsilon}_n &= \frac{1}{\Delta k_n}\int_{k_{n-1}}^{k_n} \frac{\hbar^2 k^2}{2\mu_r} dk \\ &= \frac{\hbar^2}{2\mu_r}\frac{1}{3}(k_n^2 + k_{n-1}^2 + k_n k_{n-1}) \\ &= \frac{\hbar^2 \hat{k}_n^2}{2\mu_r}, \end{aligned} \tag{2.15}$$

$$\hat{k}_n \equiv \frac{(k_n + k_{n-1})^2}{4} + \frac{(\Delta k_n)^2}{12}. \tag{2.16}$$

Thus, from the total energy conservation, we have

$$E = \hat{\varepsilon}_0 + \frac{\hbar^2 K_0^2}{2\mu_R} = \hat{\varepsilon}_n + \frac{\hbar^2 K_n^2}{2\mu_R}, \tag{2.17}$$

where $\hat{\varepsilon}_0 = \varepsilon_0$ is the ground stated energy of the projectile a and K_n, which is the discretized form of K, is defined by Eq. (2.17). The average method is adopted in the calculation for breakup reactions discussed in Chap. 4.

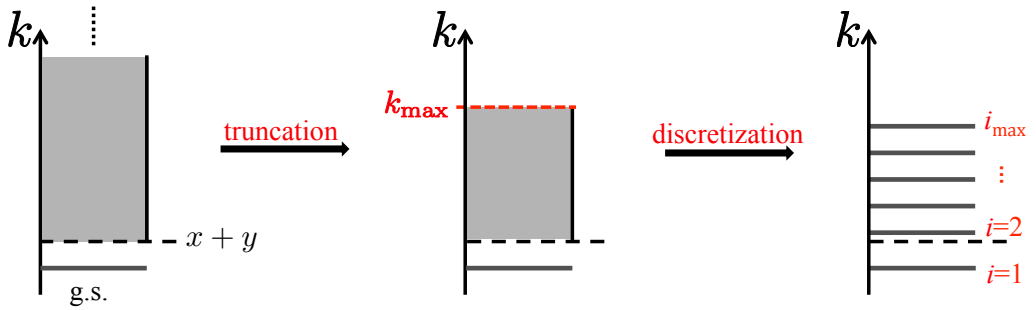

Figure 2.2: Schematic picture of the truncation and discretization in CDCC.

2.1.3 Pseudostate method

In this method $\psi_{\ell m}$ is expanded with some basis functions. We adopt the Gaussian basis in this thesis,

$$\psi_{\ell m}(\boldsymbol{r}) = \phi_\ell(r) i^\ell Y_{\ell m}(\hat{\boldsymbol{r}}), \tag{2.18}$$

$$\phi_\ell(r) = \sum_i^{i_{\max}} c_i \varphi_{\ell i}(r), \tag{2.19}$$

$$\varphi_{\ell i}(r) = N_i r^\ell \exp\left[-\left(\frac{r}{\rho_i}\right)^2\right], \tag{2.20}$$

where the range parameter ρ_i is determined by using the relation of the geometric series,

$$\rho_i = \rho_{\min} a^{i-1}, \tag{2.21}$$

$$a = \left(\frac{\rho_{\max}}{\rho_{\min}}\right)^{1/((i_{\max})-1)}. \tag{2.22}$$

Here $\rho_{\min}$ ($\rho_{\max}$) stands for the first (final) term of the series. The normalization factor N_i is determined from the condition,

$$\langle \varphi_{\ell i} \,|\, \varphi_{\ell i} \rangle = 1. \tag{2.23}$$

The expansion coefficient c_i is evaluated from the variation principle in which we minimize the expectation value of the energy $\langle \varepsilon \rangle$ as

$$\langle \varepsilon \rangle = \frac{\langle \phi_\ell \,|\, h \,|\, \phi_\ell \rangle}{\langle \phi_\ell \,|\, \phi_\ell \rangle} = \frac{\sum_{ij} c_i^* c_j \langle \varphi_{\ell i} \,|\, h \,|\, \varphi_{\ell j} \rangle}{\sum_{ij} c_i^* c_j \langle \varphi_{\ell i} \,|\, \varphi_{\ell j} \rangle}, \tag{2.24}$$

$$\frac{\partial \langle \varepsilon \rangle}{\partial c_i^*} = \frac{\left\langle \varphi_{\ell i} \middle| h \middle| \sum_j c_j \varphi_{\ell j} \right\rangle}{\sum_{ij} c_i^* c_j \langle \varphi_{\ell i} \,|\, \varphi_{\ell j} \rangle} - \frac{\sum_{ij} c_i^* c_j \langle \varphi_{\ell i} \,|\, h \,|\, \varphi_{\ell j} \rangle}{\sum_{ij} c_i^* c_j \langle \varphi_{\ell i} \,|\, \varphi_{\ell j} \rangle} \frac{\left\langle \varphi_{\ell i} \middle| \sum_j c_j \varphi_{\ell j} \right\rangle}{\sum_{ij} c_i^* c_j \langle \varphi_{\ell i} \,|\, \varphi_{\ell j} \rangle} = 0. \tag{2.25}$$

Then we obtain

$$\left\langle \varphi_{\ell i} \middle| h \middle| \sum_j c_j \varphi_{\ell j} \right\rangle = \varepsilon \left\langle \varphi_{\ell i} \middle| \sum_j c_j \varphi_{\ell j} \right\rangle. \tag{2.26}$$

This can be rewritten with the matrix expression;

$$\left[\left(\mathcal{H}_{ij} \right) - \varepsilon \left(\mathcal{N}_{ij} \right) \right] \left(c_j \right) = 0, \tag{2.27}$$

where

$$\mathcal{H}_{ij} = \langle \varphi_{\ell i} \,|\, h \,|\, \varphi_{\ell j} \rangle = \int_0^\infty \varphi_{\ell i}^*(r) h \varphi_{\ell j}(r), \tag{2.28}$$

$$\mathcal{N}_{ij} = \langle \varphi_{\ell i} \,|\, \varphi_{\ell j} \rangle = \int_0^\infty \varphi_{\ell i}^*(r) \varphi_{\ell j}(r). \tag{2.29}$$

By diagonalizing the generalized eigen-equation Eq. (J.8), we obtain the eigenenergy ε, which is discrete. We regard the pseudostate energy ε, which depends on the basis parameters, for example, the number of the bases $i_{\max}$ and the range parameter ρ_i, as the energy $\hat{\varepsilon}_n$ of the nth channel. We adopt the pseudostate method in the calculation for transfer reactions in Chap. 3.

2.1.4 Comparison of two procedures of discretization

Here we compare the average and pseudostate methods. To take an overlap of the true scattering wave function ψ_{lm} and the discretized-continuum wave function $\hat{\psi}_{nlm}$ is useful to understand what the discretized-continuum states stand for. For the average method, it can be calculated analytically;

$$\begin{aligned}
\left\langle \psi_{lm}(k,\boldsymbol{r}) \,\middle|\, \hat{\psi}_{nlm}(\boldsymbol{r}) \right\rangle_{\boldsymbol{r}} &= \int \psi_{lm}(k,\boldsymbol{r}) \left(\frac{1}{\sqrt{\Delta k_n}} \int_{k_{n-1}}^{k_n} \psi_{\ell m}(k',\boldsymbol{r}) dk' \right) d\boldsymbol{r} \\
&= \frac{1}{\sqrt{\Delta k_n}} \int_{k_{n-1}}^{k_n} \delta(k-k') dk' \\
&= \begin{cases} 1/\sqrt{\Delta k_n} & (k_{n-1} \le k \le k_n), \\ 0 & (k < k_{n-1},\ k > k_n). \end{cases}
\end{aligned} \tag{2.30}$$

As shown in Fig. 2.3(a), this stands for that we sum up the continuum states ψ_{lm} from k_{n-1} to k_n with the constant weight $1/\sqrt{\Delta k_n}$. For the pseudostate method, it can be calculated numerically. As a result shown in Fig. 2.3(b), it has the peak at $k = \hat{k}_n$. It corresponds to the summation up ψ_{lm} with a certain weight.

Furthermore, the good agreement of observables calculated with two procedures was reported [111]. Thus the discretized-continuum states obtained from each procedure are expected to be equivalent to each other if we adopt a proper model space.

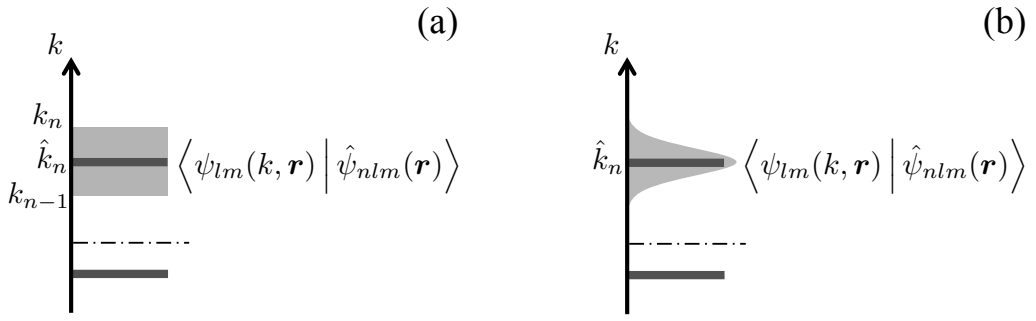

Figure 2.3: Schematic picture of the value of overlap $\left\langle \psi_{lm}(k,\boldsymbol{r}) \,\middle|\, \hat{\psi}_{nlm}(\boldsymbol{r}) \right\rangle_{\boldsymbol{r}}$ within (a) the average method and (b) the pseudostate method. Horizontal axis is the value of the overlap.

2.1.5 CDCC equation

To obtain the distorted wave $\hat{\chi}^J_{c'}$ and then calculate observables from the scattering matrix $\hat{S}^J_{cc_0}$, we derive the following CDCC equation by inserting Eqs. (2.5) and (2.10) into Eq. (2.4), and multiplied by $\left[\hat{\psi}_{n\ell}(\boldsymbol{r}) \otimes i^L Y_L(\hat{\boldsymbol{R}})\right]_{JM}$ from the left;

$$\left\langle \left[\hat{\psi}_{n\ell}(\boldsymbol{r}) \otimes i^L Y_L(\hat{\boldsymbol{R}})\right]_{JM} |H - E|\, \Psi_{JM}(\boldsymbol{r}, \boldsymbol{R}) \right\rangle_{\boldsymbol{r},\hat{\boldsymbol{R}}} = 0, \tag{2.31}$$

$$\left[-\frac{\hbar^2}{2\mu_R}\frac{d^2}{dR^2} + \frac{\hbar^2}{2\mu_R}\frac{L'(L'+1)}{R^2} - E_n\right] \hat{\chi}^J_c(R) = -\sum_{cc'} F_{cc'}(R)\hat{\chi}^J_{c'}(R), \tag{2.32}$$

where

$$E_n \equiv \frac{\hbar^2 K_n^2}{2\mu_R} = E - \hat{\varepsilon}_n, \tag{2.33}$$

and for simplicity the quantum numbers $\{n, \ell, L\}$ are expressed as c. The coupling potential $F_{cc'}$ is defined by

$$F_{cc'}(R) = F^{(\mathrm{N})}_{cc'}(R) + F^{(\mathrm{C})}_{cc'}(R), \tag{2.34}$$

$$F^{(\mathrm{N})}_{cc'}(R) = \left\langle \left[\hat{\psi}_{n\ell}(\boldsymbol{r}) \otimes i^L Y_L(\hat{\boldsymbol{R}})\right]_{JM} \left| V^{(\mathrm{N})}_x + V^{(\mathrm{N})}_y \right| \left[\hat{\psi}_{n'\ell'}(\boldsymbol{r}) \otimes i^{L'} Y_{L'}(\hat{\boldsymbol{R}})\right]_{JM} \right\rangle_{\boldsymbol{r},\hat{\boldsymbol{R}}}, \tag{2.35}$$

$$F^{(\mathrm{C})}_{cc'}(R) = \left\langle \left[\hat{\psi}_{n\ell}(\boldsymbol{r}) \otimes i^L Y_L(\hat{\boldsymbol{R}})\right]_{JM} \left| V^{(\mathrm{C})}_x + V^{(\mathrm{C})}_y \right| \left[\hat{\psi}_{n'\ell'}(\boldsymbol{r}) \otimes i^{L'} Y_{L'}(\hat{\boldsymbol{R}})\right]_{JM} \right\rangle_{\boldsymbol{r},\hat{\boldsymbol{R}}}. \tag{2.36}$$

$F^{(\mathrm{N})}_{cc'}$ and $F^{(\mathrm{C})}_{cc'}$ are the nuclear and Coulomb coupling potentials, respectively. One obtains the distorted wave $\hat{\chi}^J_{c'}$ and the scattering matrix (S matrix) $\hat{S}^J_{cc'}$ by solving Eq. (2.32) up to $R = R_{\max}$ and then at $R_{\max}$ connecting $\hat{\chi}^J_{c'}$ with the boundary condition

$$\hat{\chi}^J_{c'}(R) \to \begin{cases} H^{(-)}_{L,\eta_n}(K_n R)\delta_{cc'} - \sqrt{K_0/K_n}\hat{S}^J_{cc'} H^{(+)}_{L,\eta_n}(K_n R) & \text{for } E_n \geq 0, \quad (2.37) \\ -\hat{S}^J_{cc'} W_{-\eta_n, L+1/2}(-2iK_n R) & \text{for } E_n < 0. \quad (2.38) \end{cases}$$

When the channels are open ($E_n \geq 0$), the boundary condition is expressed by Eq. (2.37). Here $H^{(-)}_{L,\eta}$ ($H^{(+)}_{L,\eta}$) is the Coulomb function having the incoming (outgoing) asymptotic form. The Sommerfeld parameter η_n is defined by

$$\eta_n \equiv \frac{\mu_R Z_a Z_A e^2}{\hbar^2 K_n}, \tag{2.39}$$

where Z_a and Z_A are the atomic numbers of a and A, respectively. On the other hand, when the channel is closed ($E_n < 0$), $\hat{\chi}^J_c$ is connected with the Wittaler function $W_{-\eta_n, L+1/2}$ as shown in Eq. (2.38).

2.1.6 Cross section

If we neglect the Coulomb interaction between the projectile a and the target nucleus A, the asymptotic form of the Ψ can be written as

$$\Psi_\alpha(\boldsymbol{r}_\alpha, \boldsymbol{R}_\alpha) \sim e^{i\boldsymbol{K}_\alpha\cdot\boldsymbol{R}_\alpha}\psi_\alpha + \frac{1}{(2\pi)^{3/2}}\sum_\beta \frac{e^{iK_\beta R_\beta}}{R_\beta} f_{\beta\alpha}(\Omega_\beta)\psi_\beta + \phi_{\rm sc}, \tag{2.40}$$

where we put the subscript α and β to explicitly represent the transition from an α channel to a β channel. ψ_γ is the projectile's wave function in the γ channel and $\phi_{\rm sc}$ is the wave function when the system is in a three-body or more many-body configuration. The relative wave number $\boldsymbol{K}_\gamma$ corresponds to $\boldsymbol{K}$. Using the S matrix in Eq. (2.37), the scattering amplitude $f_{\beta\alpha}$ regarding the angle $\Omega_\beta = (\theta, \phi)$ is given by

$$\begin{aligned} f_{\beta\alpha}(\Omega_\beta) &= \delta_{\alpha\beta} f_\alpha^{\rm Coul}(\Omega_\beta) \\ &\quad + \frac{2\pi}{K_\alpha}\sqrt{\frac{v_\beta}{v_\alpha}} \sum_{JLL'} e^{i(\sigma_L^\alpha + \sigma_{L'}^\beta)} \left(\delta_{\alpha\beta}\delta_{LL'} - S_{cc'}\right) \\ &\quad \times \sum_{MM_LM'_L} (\ell m L M_L | JM) \left(\ell' m' L' M'_L | JM\right) Y^*_{LM_L}(\hat{\boldsymbol{K}}_\alpha) Y_{L'M'_L}(\Omega_\beta), \end{aligned} \tag{2.41}$$

where the Coulomb scattering amplitude $f_\alpha^{\rm Coul}$ is explicitly written as

$$f_\alpha^{\rm Coul}(\Omega_\beta) = -\frac{\eta_n}{2K_\alpha}{\rm cosec}^2\left(\frac{\theta}{2}\right)\exp\left[-i\eta_n \ln\left(\sin^2\frac{\theta}{2}\right) + 2i\sigma_0^\alpha\right]. \tag{2.42}$$

The factor σ_L^γ is the Coulomb phase shift in the γ channel and that with $L = 0$ is given by

$$\begin{aligned} \sigma_0^\gamma &= \frac{1}{2i}\ln\frac{\Gamma(1+i\eta_n)}{\Gamma(1-i\eta_n)} \\ &= \arg\Gamma(1+i\eta_n). \end{aligned} \tag{2.43}$$

The velocity v_γ is defined by

$$v_\gamma = \frac{\hbar K_\gamma}{\mu_R}. \tag{2.44}$$

If we take the z axis to the direction of $\boldsymbol{K}_\alpha$, we obtain the scattering amplitude for the scattering angle θ;

$$\begin{aligned} f_{\beta\alpha}(\theta) &= \delta_{\alpha\beta} f_\alpha^{\rm Coul}(\theta) \\ &\quad + \frac{i}{2K_\alpha}\sqrt{\frac{v_\beta}{v_\alpha}} \sum_{JLL'} e^{i(\sigma_L^\alpha + \sigma_{L'}^\beta)} \hat{L}\hat{L'} \left(\delta_{\alpha\beta}\delta_{LL'} - S_{cc'}\right) \\ &\quad \times \sum_{M'_L} (-)^{(M'_L - |M'_L|)/2} \sqrt{\frac{(L' - |M'_L|)!}{(L' - M'_L)!}} \\ &\quad \times (\ell m L 0 | Jm) \left(\ell' m' L' M'_L | JM\right) P_{L'|M'_L|}(\cos\theta), \end{aligned} \tag{2.45}$$

where $P_{L'|M'_L|}$ is the Legendre function.

The "discretized" differential cross section is defined by

$$\frac{d\sigma_{c'}}{d\Omega} = \sigma_{c'}(\theta) = \frac{1}{2\ell+1}\sum_{mm'}|f_{\beta\alpha}(\theta)|^2. \tag{2.46}$$

For the elastic scattering, $\alpha = \beta$ and $c' = c$, it is often used the Rutherford ratio $\sigma_c(\theta)/\sigma_{\rm Rut}(\theta)$ with the Rutherford cross section

$$\sigma_{\rm Rut}(\theta) = |f_\alpha^{\rm Coul}(\theta)|^2. \tag{2.47}$$

For the breakup reaction, the cross section is calculated from Eq. (2.46) with $\alpha \neq \beta$ and $c' \neq c$. In particular, we use the double differential cross section $d^2\sigma/d\Omega d\varepsilon$ defined by

$$\frac{d^2\sigma}{d\Omega d\varepsilon} = \mathcal{G}(\varepsilon)\sum_{\ell'\neq\ell}\frac{d\sigma_{c'}}{d\Omega}. \tag{2.48}$$

Here we introduce the smoothing function $\mathcal{G}$ in order to obtain the continuous function regarding ε by interpolating the differential cross section Eq. (2.46) for the energy index n'. For the interpolation in our numerical code, we adopt the Lagrange's polynomial method [112] with before and after 3 points. The angular distribution $d\sigma_{\rm bu}/d\Omega$ of the breakup cross section is given by

$$\frac{d\sigma_{\rm bu}}{d\Omega} = \int d\varepsilon \frac{d^2\sigma}{d\Omega d\varepsilon}. \tag{2.49}$$

Similarly, by integrating over the scattering angle of the c.m. of system, we obtain the energy distribution or energy spectrum $d\sigma_{\rm bu}/d\varepsilon$ of the breakup cross section as

$$\frac{d\sigma_{\rm bu}}{d\varepsilon} = \int d\Omega \frac{d^2\sigma}{d\Omega d\varepsilon}. \tag{2.50}$$

The partial cross section is defined by

$$\sigma_{\beta\alpha}(L) = \frac{1}{2\ell+1}\frac{\pi}{K_0^2}\sum_{J,L'}(2J+1)\left|\delta_{\alpha\beta}\delta_{LL'} - S^J_{cc'}\right|^2. \tag{2.51}$$

In particular the partial breakup cross section $\sigma_{\rm bu}^{n_0 l}$ is given by

$$\sigma_{\rm bu}^{n_0\ell}(L) = \sum_{n,\ell'}\tilde{\sigma}_{\rm bu}^{n_0\ell;n\ell'}(L), \tag{2.52}$$

$$\tilde{\sigma}_{\rm bu}^{n_0\ell;n\ell'}(L) = \frac{1}{2\ell+1}\frac{\pi}{K_0^2}\sum_{J,L'}(2J+1)\left|S^J_{cc'}\right|^2. \tag{2.53}$$

2.2 Coupling potential

In this section the formulation of the coupling potential $F_{cc'}$ defined by Eq. (2.34) is given. Note that in this work we include only the central part of the nuclear potentials $V_x^{(\mathrm{N})}$ and $V_y^{(\mathrm{N})}$. To calculate the integral in Eq. (2.35), we expand $V_x^{(\mathrm{N})}$ with the multipole λ of the Legendre polynomial $P_\lambda(\cos\theta)$,

$$\begin{aligned} V_x^{(\mathrm{N})}(\boldsymbol{r}_x) &= \sum_\lambda V_x^{\lambda(\mathrm{N})}(\alpha r, R) P_\lambda(w) \\ &= \sum_\lambda V_x^{\lambda(\mathrm{N})}(\alpha r, R) \frac{4\pi}{\hat{\lambda}^2} \sum_\mu Y_{\lambda\mu}(\hat{\boldsymbol{R}}) Y^*_{\lambda\mu}(\hat{\boldsymbol{r}}) \\ &= 4\pi \sum_\lambda \frac{(-)^\lambda}{\hat{\lambda}} V_x^{\lambda(\mathrm{N})}(\alpha r, R) \sum_\mu (\lambda\mu\lambda - \mu|00)\, Y_{\lambda\mu}(\hat{\boldsymbol{R}}) Y^*_{\lambda,-\mu}(\hat{\boldsymbol{r}}) \\ &= 4\pi \sum_\lambda \frac{(-)^\lambda}{\hat{\lambda}} V_x^{\lambda(\mathrm{N})}(\alpha r, R) \left[Y_\lambda(\hat{\boldsymbol{R}}) \otimes Y_\lambda(\hat{\boldsymbol{r}}) \right]_{00}, \end{aligned} \tag{2.54}$$

$$V_x^{\lambda(\mathrm{N})}(\alpha r, R) = \frac{\hat{\lambda}^2}{2} \int_{-1}^{1} V_x^{(\mathrm{N})}(r_x) P_\lambda(w) dw, \tag{2.55}$$

where μ is the z-component of λ and we have used

$$\boldsymbol{r}_x = \boldsymbol{R} - \frac{m_y}{m_x + m_y}\boldsymbol{r} \equiv \boldsymbol{R} - \alpha\boldsymbol{r}, \tag{2.56}$$

$$r_x = \sqrt{R^2 + \alpha^2 r^2 + 2\alpha R r w}, \tag{2.57}$$

$$\boldsymbol{r}_y = \boldsymbol{R} + \frac{m_x}{m_x + m_y}\boldsymbol{r} \equiv \boldsymbol{R} + \beta\boldsymbol{r}, \tag{2.58}$$

$$r_y = \sqrt{R^2 + \alpha^2 r^2 - 2\alpha R r w}. \tag{2.59}$$

Here m_x (m_y) stands for the mass of x (y), and we use $\hat{\lambda} = \sqrt{2\lambda+1}$ and $w = \cos\theta$, where θ is the angle between $\boldsymbol{r}$ and $\boldsymbol{R}$ shown in Fig. 2.1. Equation (2.55) is obtained by integrating $V_x^{(\mathrm{N})}(\boldsymbol{r}_x) P_\lambda(w)$ over w for $-1 \le w \le 1$.In the integration the orthogonal condition of the Legendre polynomial is used;

$$\int_{-1}^{1} dw P_\lambda(w) P_{\lambda'}(w) = \frac{2}{\hat{\lambda}^2}\delta_{\lambda'\lambda}. \tag{2.60}$$

Other interactions, $V_y^{\lambda(\mathrm{N})}$, $V_x^{\lambda(\mathrm{C})}$, and $V_y^{\lambda(\mathrm{C})}$ can be similarly expanded as

$$V_y^{\lambda(\mathrm{N})}(\beta r, R) = \frac{\hat{\lambda}^2}{2} \int_{-1}^{1} V_y^{(\mathrm{N})}(r_y) P_\lambda(w) dw, \tag{2.61}$$

$$V_x^{\lambda(\mathrm{C})}(\alpha r, R) = \frac{\hat{\lambda}^2}{2} \int_{-1}^{1} V_x^{(\mathrm{C})}(r_x) P_\lambda(w) dw, \tag{2.62}$$

$$V_y^{\lambda(\mathrm{C})}(\beta r, R) = \frac{\hat{\lambda}^2}{2} \int_{-1}^{1} V_y^{(\mathrm{C})}(r_y) P_\lambda(w) dw. \tag{2.63}$$

Bellow we give the specific forms of the nuclear and Coulomb coupling potentials.

2.2.1 Nuclear coupling potential

If we write $\hat{\psi}_{n\ell m}$ as

$$\hat{\psi}_{n\ell m}(\boldsymbol{r}) = \frac{\hat{\phi}_{n\ell}(r)}{r} i^{\ell} Y_{\ell m}(\hat{\boldsymbol{r}}), \tag{2.64}$$

we can factorize Eq. (2.35) into the radial and angular parts;

$$F^{(\mathrm{N})}_{n'\ell'L',n\ell L}(R) = \sum_{\lambda} f^{(\mathrm{N})}_{n'\ell' n\ell\lambda}(R) Z(\ell' L' \ell L; \lambda J), \tag{2.65}$$

where

$$f^{(\mathrm{N})}_{n'\ell' n\ell\lambda}(R) = \int_0^\infty \hat{\phi}^*_{n'\ell'}(r) \left(V_x^{\lambda(\mathrm{N})}(\alpha r, R) + V_y^{\lambda(\mathrm{N})}(\beta r, R) \right) \hat{\phi}_{n\ell}(r) dr, \tag{2.66}$$

$$\begin{aligned} &Z(\ell' L' \ell L; \lambda J) \\ &\quad = 4\pi \frac{(-)^{\lambda}}{\hat{\lambda}} \\ &\quad \times \left\langle \left[i^{\ell'} Y_{\ell'}(\hat{\boldsymbol{r}}) \otimes i^{L'} Y_{L'}(\hat{\boldsymbol{R}}) \right]_{JM} \middle| \left[Y_{\lambda}(\hat{\boldsymbol{r}}) \otimes Y_{\lambda}(\hat{\boldsymbol{R}}) \right]_{00} \middle| \left[i^{\ell} Y_{\ell}(\hat{\boldsymbol{r}}) \otimes i^{L} Y_{L}(\hat{\boldsymbol{R}}) \right]_{JM} \right\rangle_{\boldsymbol{r},\hat{\boldsymbol{R}}}. \end{aligned} \tag{2.67}$$

Here, by using the Wigner-Eckart theorem, $Z(\ell' L' \ell L; \lambda J)$ called Z factor is written as

$$\begin{aligned} Z(\ell' L' \ell L; \lambda J) = i^{\ell+\ell'+L+L'} (-)^{L+L'+J} \frac{\hat{\ell}\hat{\ell}'\hat{L}'\hat{L}'}{\hat{\lambda}^2} \\ \times \left(\ell' 0 \ell 0 | \lambda 0 \right) \left(L' 0 L 0 | \lambda 0 \right) W(\ell \ell' L L'; \lambda J). \end{aligned} \tag{2.68}$$

where $W(\ell\ell' LL'; \lambda J)$ is the Racah coefficient. $f^{(\mathrm{N})}$ vanishes at a finite value of R because of the short range property of the the nuclear potentials $V_x^{\lambda(\mathrm{N})}$ and $V_y^{\lambda(\mathrm{N})}$. The derivation of Eq. (2.68) is given in Appx. B.

2.2.2 Coulomb coupling potential

As for the Coulomb coupling potential, we can factorize Eq. (2.36) into

$$F^{(\mathrm{C})}_{n'\ell'L',n\ell L}(R) = \sum_{\lambda} f^{(\mathrm{C})}_{n'\ell' n\ell\lambda}(R) Z(\ell' L' \ell L; \lambda J) \tag{2.69}$$

with

$$f^{(\mathrm{C})}_{n'\ell' n\ell\lambda}(R) = \int_0^\infty \hat{\phi}^*_{n'\ell'}(r) \left(V_x^{\lambda(\mathrm{C})}(\alpha r, R) + V_y^{\lambda(\mathrm{C})}(\beta r, R) \right) \hat{\phi}_{n\ell}(r) dr \tag{2.70}$$

and the Z factor $Z(\ell' L' \ell L; \lambda J)$ given Eq. (2.67). After a few manipulations of Eq. (2.70) with the multipole expansion, we obtain

$$
\begin{aligned}
f^{(\mathrm{C})}_{x,n'\ell'n\ell\lambda}(R) = \frac{Z_x Z_y e^2}{R}\left[\delta_{n'n}\delta_{\ell'\ell} - \int_{\frac{R-R_\mathrm{C}}{\alpha}}^{r_\mathrm{max}} \hat{\phi}^*_{n'\ell'}(r)\hat{\phi}_{n\ell}(r)dr\theta\left(r_\mathrm{max} - \frac{R-R_\mathrm{C}}{\alpha}\right)\right] \\
+ \int_0^{\frac{R-R_\mathrm{C}}{\alpha}} \hat{\phi}^*_{n'\ell'}(r) + W^\lambda_{x,2}(r,R)\hat{\phi}_{n\ell}(r)dr \\
+ \int_{\frac{R-R_\mathrm{C}}{\alpha}}^{\frac{R+R_\mathrm{C}}{\alpha}} \hat{\phi}^*_{n'\ell'}(r)\left(X^\lambda_{x,3}(R) + W^\lambda_{x,3}(r,R)\right)\hat{\phi}_{n\ell}(r)dr\theta\left(r_\mathrm{max} - \frac{R-R_\mathrm{C}}{\alpha}\right) \\
+ \int_{\frac{R+R_\mathrm{C}}{\alpha}}^{r_\mathrm{max}} \hat{\phi}^*_{n'\ell'}(r)\left(X^\lambda_{x,1}(R) + W^\lambda_{x,1}(r,R)\right)\hat{\phi}_{n\ell}(r)dr\theta\left(r_\mathrm{max} - \frac{R-R_\mathrm{C}}{\alpha}\right),
\end{aligned}
\tag{2.71}
$$

where R_C is the Coulomb radius of the uniformly charged sphere. $\theta(r_1 - r_2)$ is the step function defined by

$$
\theta(r_1 - r_2) = \begin{cases} 0 & r_1 < r_2 \\ 1 & r_1 \geq r_2. \end{cases} \tag{2.72}
$$

The derivation of Eq. (2.71) and the specific forms of $X^\lambda_{x,i}$ and $W^\lambda_{x,i}$ are given in Appx. B. We have a similar form of the multipole decomposition of $V_y^{\lambda(\mathrm{C})}$.

2.3 CDCC with eikonal approximation

2.3.1 Eikonal-CDCC equation

In this section we formulate the model of CDCC with the eikonal approximation, called eikonal-CDCC (E-CDCC) [113, 114]. In E-CDCC the three-body wave function Ψ is expanded in terms of intrinsic states $\hat{\psi}_{n\ell m}$;

$$
\Psi(\boldsymbol{r}, \boldsymbol{R}) = \sum_{n\ell m} \hat{\psi}_{n\ell m}(\boldsymbol{r}) \sum_J e^{-i(m-m_0)\phi_R}\chi^J_{n\ell m}(R, \theta_R), \tag{2.73}
$$

where the coefficient $\sum_J e^{-i(m-m_0)\phi_R}\chi^J_{n\ell m}(R,\theta_R)$ represents the center of mass (c.m.) motion of a, and m_0 is the m in the initial state. Here we adopt the cylindrical coordinate as shown in fig. 2.4. ϕ_R is the azimuthal angle of $\boldsymbol{R}$. By inserting Eq. (2.73) into Eq. (2.4) with multiplied by $\hat{\psi}_{n\ell m}$ from the left and integrating over $\boldsymbol{r}$, one obtains CC equations for $\chi^J_{n\ell m}$;

$$
\begin{aligned}
&\sum_J e^{-i(m'-m_0)\phi_R}\left(T_{\boldsymbol{R}} + \hat{\varepsilon}_n - E\right)\chi^J_{n'\ell'm'}(R,\theta_R) \\
&\quad = -\sum_{n\ell m} F_{n'\ell'm';n\ell m}(\boldsymbol{R}) \sum_J e^{-i(m-m_0)\phi_R}\chi^J_{n\ell m}(R,\theta_R),
\end{aligned}
\tag{2.74}
$$

where $T_{\boldsymbol{R}}$ and the coupling potential $F_{n'\ell'm';n\ell m}$ are defined by

$$T_{\boldsymbol{R}} \equiv \frac{-\hbar^2}{2\mu_R}\nabla_{\boldsymbol{R}}, \tag{2.75}$$

$$\begin{aligned} F_{n'\ell'm';n\ell m}(\boldsymbol{R}) &\equiv \left\langle \hat{\psi}_{n'\ell'm'} \left| V_x^{(\mathrm{N})} + V_x^{(\mathrm{C})} + V_y^{(\mathrm{N})} + V_y^{(\mathrm{C})} - V_{\mathrm{C}} \right| \hat{\psi}_{n\ell m} \right\rangle \\ &\equiv \mathcal{F}_{c'c}(b,z) e^{-i(m'-m_0)\phi_R}, \end{aligned} \tag{2.76}$$

where we represent the set of the quantum numbers $\{n, \ell, m\}$ as c. The Coulomb interaction V_{C} between a and A is defined by

$$V_{\mathrm{C}}(R) = \frac{Z_a Z_A e^2}{R}. \tag{2.77}$$

We factorize $\chi^J_{n\ell m}$ with a plane wave as

$$\chi^J_{n\ell m}(R,\theta_R) \sim \xi_{cc_0}(b,z)\frac{1}{(2\pi)^{3/2}} e^{i\boldsymbol{K}_n\cdot\boldsymbol{R}}\phi_n^{(\mathrm{C})}(R) \tag{2.78}$$

with

$$K_n = \sqrt{\frac{2\mu_R\left(E-\hat{\varepsilon}_n\right)}{\hbar^2}}. \tag{2.79}$$

If there is interactions, the wave number K_n depends on b, and it can be written as

$$K_c(b) = \sqrt{\frac{2\mu_R\left(E-\hat{\varepsilon}_n\right)}{\hbar^2} - \frac{(m_0-m)^2}{b^2}}. \tag{2.80}$$

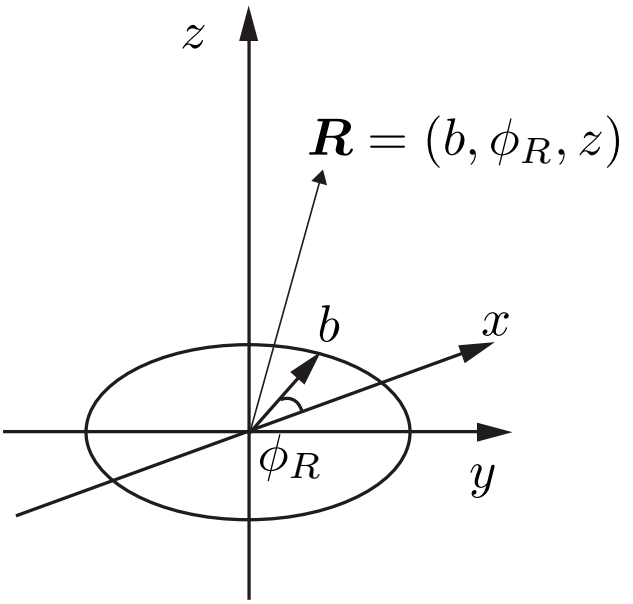

Figure 2.4: Cylindrical coordinates for E-CDCC.

In Eq. (2.78), the factor $\phi_n^{(\mathrm{C})}$, which is defined by

$$\phi_n^{(\mathrm{C})}(R) = e^{i\eta_n \ln[K_n R - K_n z]}, \tag{2.81}$$

represents deviation of the incident wave from corresponding plane wave due to the Coulomb interaction. Here η_n is the Sommerfeld parameter defined by Eq. (2.39).

When one inserts Eq. (2.78) into Eq. (2.74), the second-order derivative of ξ_{cc_0} can be neglected since it is expected to vary slowly compared with the plane wave $e^{i\boldsymbol{K}_N\cdot\boldsymbol{R}}$. This is the eikonal approximation. Then we obtain following CC equation called the E-CDCC equation for $\bar{\xi}_{cc_0} \equiv \sum_J \xi_{cc_0}$;

$$\frac{\partial}{\partial z}\bar{\xi}_{cc_0}(b,z) = \frac{1}{i\hbar v_n(R)} \sum_{c'} \mathcal{F}_{cc'}(b,z)\bar{\xi}_{cc_0}(b,z) e^{i(Kn'-K_n)z} \mathcal{R}_{nn'}(b,z), \tag{2.82}$$

where we commuted c and c'. Since Eq. (2.82) is the differential equation regarding z, the impact parameter b is no longer the dynamical variable. Thus Eq. (2.82) should be numerically solved in each b with the boundary condition

$$\lim_{z\to-\infty} \bar{\xi}_{cc_0}(b,z) = \delta_{cc_0}. \tag{2.83}$$

Here c_0 stands for c in the initial state. The velocity v_n for the a-A system is given by

$$v_n(R) = \frac{1}{\mu}\sqrt{\hbar^2 K_n^2 - 2\mu_R V_{\mathrm{C}}(R)}. \tag{2.84}$$

The factor $\mathcal{R}_{nn'}$ is defined by

$$\mathcal{R}_{nn'}(b,z) = \frac{(K_{n'}R - K_{n'}z)^{i\eta_{n'}}}{(K_n R - K_n z)^{i\eta_n}}. \tag{2.85}$$

The explicit form of $\mathcal{F}_{cc'}$ is given in Ref. [113, 114].

2.3.2 Scattering amplitude

The scattering amplitude f_{cc_0} for the transition to the channel specified by index c is given by

$$f_{cc_0} = -\frac{(2\pi)^2\mu_R}{\hbar^2}\left\langle \frac{\hat{\psi}_{c'}(r)}{r} i^\ell Y_{\ell' m'}(\hat{\boldsymbol{r}}) \frac{1}{(2\pi)^{3/2}} e^{i\boldsymbol{K}'_c(b)\cdot\boldsymbol{R}} \middle| \tilde{V} \middle| \Psi_{c_0,\boldsymbol{K}_n}(\boldsymbol{r},\boldsymbol{R}) \right\rangle, \tag{2.86}$$

where $\tilde{V} = V_x^{(\mathrm{N})} + V_x^{(\mathrm{C})} + V_y^{(\mathrm{N})} + V_y^{(\mathrm{C})} - V_{\mathrm{C}}$ and $\boldsymbol{K}'_c(b)$ is the relative wave number in the final channel. From Eqs. (2.73), (2.74), and (2.78), we obtain

$$f_{cc_0} = -\frac{\mu_R}{2\pi\hbar^2}\int d\boldsymbol{R} \sum_{c'} \mathcal{F}_{cc'}(b,z) e^{i(m_0-m)\phi_R} \bar{\xi}_{c'c'_0}(b,z) e^{i[\boldsymbol{K}_{c'}(b) - \boldsymbol{K}'_c(b)]\cdot\boldsymbol{R}}. \tag{2.87}$$

Here we evaluate the scalar product $[\boldsymbol{K}_{c'}(b) - \boldsymbol{K}'_c(b)] \cdot \boldsymbol{R}$. When we take the Madison convention and the scattering angle θ_f, the wave number vectors become

$$\boldsymbol{K}_{c'}(b) = (0, 0, K_{c'}(b)) \,, \tag{2.88}$$

$$\boldsymbol{K}_{c'}(b) = (K_c(b) \sin\theta_f, 0, K_c(b)\cos\theta_f) \,. \tag{2.89}$$

Since the coordinate $\boldsymbol{R}$ is $\boldsymbol{R} = (b\cos\phi_R, b\sin\phi_R, z)$, the scalar product is given by

$$\begin{aligned}\left[\boldsymbol{K}_{c'}(b) - \boldsymbol{K}'_c(b)\right] \cdot \boldsymbol{R} &= -K_c(b) b \sin\theta_f \cos\phi_R + \left[K_{c'}(b) - K_c(b)\cos\theta_f\right] z \\ &\sim -K_c(b) b\theta_f \cos\phi_R + \left[K_{c'}(b) - K_c(b)\right] z,\end{aligned} \tag{2.90}$$

where we assume the forward scattering and then we take the first order of θ_f in the trigonometric functions. Thus f_{cc_0} becomes

$$\begin{aligned}f_{cc_0} \sim -\frac{\mu_R}{2\pi\hbar^2} \int b db d\phi_R dz \sum_{c'} \mathcal{F}_{cc'}(b,z) e^{i(m_0-m)\phi_R} \bar{\xi}_{c'c'_0}(b,z) \\ \times e^{-iK_c(b)b\theta_f\cos\phi_R} e^{i[K_{c'}(b)-K_c(b)]z}.\end{aligned} \tag{2.91}$$

In Eq. (2.91), the z-integration can be done by using Eq. (2.82);

$$\begin{aligned}\int dz \sum_{c'} \mathcal{F}_{cc'}(b,z)\bar{\xi}_{c'c'_0}(b,z) e^{i[K_{c'}(b)-K_c(b)]z} &= \int_{-\infty}^{\infty} dz \frac{i\hbar^2}{\mu_R} K_c(b) \frac{\partial}{\partial z} \bar{\xi}_{cc_0}(b,z) \\ &= \frac{i\hbar^2}{\mu_R} K_c(b) \left[\bar{\xi}_{cc_0}(b,z)\right]_{-\infty}^{\infty}\end{aligned} \tag{2.92}$$

From Eqs. (2.83) and (2.92) we have

$$f_{cc_0} = \frac{1}{2\pi i} \int b db d\phi_R K_c(b) e^{i(m_0-m)\phi_R} e^{-iK_c(b)b\theta_f\cos\phi_R} \left(\mathcal{S}_{cc_0}(b) - \delta_{cc_0}\delta_{mm_0}\right), \tag{2.93}$$

where we define the eikonal S matrix $\mathcal{S}_{cc_0}$

$$\mathcal{S}_{cc_0}(b) \equiv \lim_{z\to\infty} \bar{\xi}_{cc_0}(b,z). \tag{2.94}$$

In E-CDCC, the b-integration in Eq. (2.93) is expressed by the following discretized summation;

$$\begin{aligned}f_{cc_0} \sim -\frac{1}{2\pi i} \sum_L \int_{b_L^{\min}}^{b_L^{\max}} b db \\ \times \int d\phi_R K_c(b) e^{i(m_0-m)\phi_R} e^{-iK_c(b)b\theta_f\cos\phi_R} \left(\mathcal{S}_{cc_0}(b) - \delta_{cc_0}\delta_{mm_0}\right),\end{aligned} \tag{2.95}$$

where the interval for the b-integration is determined from

$$K_c(b_L) b_L^{\min} \equiv L, \tag{2.96}$$

$$K_c(b_L) b_L^{\max} \equiv L+1. \tag{2.97}$$

If we assume each the b-dependence of $K_c(b)$, $e^{-iK_c(b)b\theta_f\cos\phi_R}$, and $\mathcal{S}_{cc_0}(b)$ is negligibly small, we obtain

$$f_{cc_0} \sim \frac{1}{2\pi i}\sum_L K_c(b_L)\left(\mathcal{S}_{cc_0}(b_L)-\delta_{cc_0}\delta_{mm_0}\right)\left\{\int_{b_L^{\min}}^{b_L^{\max}} bdb\right\} \times \int d\phi_R e^{i(m_0-m)\phi_R}e^{-iK_c(b)b\theta_f\cos\phi_R}, \tag{2.98}$$

where b_L is defined from

$$K_c(b_L)b_L \equiv L+\frac{1}{2}. \tag{2.99}$$

Thus the b-integration can be done;

$$\int_{b_L^{\min}}^{b_L^{\max}} bdb = \frac{1}{2(K_c(b))^2}\left[(L+1)^2-L^2\right] = \frac{2L+1}{2(K_c(b))^2}. \tag{2.100}$$

From the relation regarding the ϕ_R-integration,

$$\int d\phi_R e^{i(m_0-m)\phi_R}e^{-iK_c(b)b\theta_f\cos\phi_R} \sim 2\pi i^{(m_0-m)}\frac{\sqrt{4\pi}}{\hat{L}}Y_{L,m_0-m}(\theta_f,0), \tag{2.101}$$

the scattering amplitude f_{cc_0} becomes

$$\begin{aligned} f_{cc_0} &\sim \frac{1}{2\pi i}\sum_L K_c(b_L)\left(\mathcal{S}_{cc_0}(b_L)-\delta_{cc_0}\delta_{mm_0}\right)\frac{2L+1}{2(K_c(b))^2}2\pi i^{(m-m_0)}\frac{\sqrt{4\pi}}{\hat{L}}Y_{L,m_0-m}(\theta_f,0) \\ &= \frac{2\pi}{iK_n}\sum_L \frac{K_n}{K_c(b_L)}\frac{\hat{L}}{\sqrt{4\pi}}\left(\mathcal{S}_{cc_0}(b_L)-\delta_{cc_0}\delta_{mm_0}\right)i^{(m-m_0)}Y_{L,m-m_0}(\hat{\boldsymbol{K}}'_n) \\ &\equiv f^{\rm E}_{cc_0}. \end{aligned} \tag{2.102}$$

For the scattering amplitude $f^{\rm Q}_{cc_0}$ calculated by the quantum mechanics, we have Eq. (2.45). We rewrite it as

$$\begin{aligned} f^{\rm Q}_{cc_0} = \frac{2\pi}{iK_n}\sum_{JL_0L}\frac{\hat{L}_0}{\sqrt{4\pi}}\left(\ell_0 m_0 L_0 0|Jm_0\right)\left(\ell m L m_0-m|Jm_0\right) \\ \times\left(S^J_{cL,c_0L_0}-\delta_{cc_0}\delta_{LL_0}\right)i^{(m-m_0)}Y_{L,m-m_0}(\hat{\boldsymbol{K}}'_n). \end{aligned} \tag{2.103}$$

Here we neglect the Coulomb interaction for simplicity.

In the E-CDCC framework, by setting a critical value $L_{\rm C}$ at a proper point of L, the scattering amplitude described by the quantum mechanics and it by the eikonal approach can be connected, that is, we adopt Eq. (2.103) for $L \le L_{\rm C}$, and Eq. (2.102) for $L > L_{\rm C}$ as the "hybrid" scattering matrix $f^{\rm H}_{cc_0}$;

$$f^{\rm H}_{cc_0} = \frac{2\pi}{iK_n}\sum_{L\le L_{\rm C}} f^{\rm Q}_{L;cc_0}Y_{L,m-m_0}\left(\hat{\boldsymbol{K}}'\right) + \frac{2\pi}{iK_n}\sum_{L>L_{\rm C}} f^{\rm E}_{L;cc_0}Y_{L,m-m_0}\left(\hat{\boldsymbol{K}}'\right), \tag{2.104}$$

where the partial scattering amplitudes $f^{\rm Q}_{L;cc_0}$ and $f^{\rm E}_{L;cc_0}$ are respectively defined by

$$f^{\rm Q}_{L;cc_0} = \frac{2\pi}{iK_n} \sum_{J=|L-\ell|}^{L+\ell} \sum_{L_0=|J-\ell_0|}^{J+\ell_0} \frac{\hat{L}_0}{\sqrt{4\pi}} \left(\ell_0 m_0 L_0 0 | J m_0\right) \left(\ell m L_0 m_0 - m | J m_0\right) \times \left(S^J_{cL,c_0L_0} - \delta_{cc_0}\delta_{LL_0}\right) i^{(m-m_0)}, \tag{2.105}$$

$$f^{\rm E}_{L;cc_0} = \frac{K_n}{K_c(b_L)} \frac{\hat{L}}{\sqrt{4\pi}} \left(\mathcal{S}_{cc_0}(b_L) - \delta_{cc_0}\delta_{mm_0}\right) i^{(m-m_0)}. \tag{2.106}$$

The critical value $L_{\rm C}$ is determined so that the relation $f^{\rm Q}_{L;cc_0} = f^{\rm Q}_{L;cc_0}$ is satisfied. This hybrid procedure enables us to perform numerical calculation efficiently with high precision as well as that of the full quantum calculation [113, 114]. This can be regarded as the quantum mechanical correction.

CHAPTER 3

Transfer Reaction of Loosely Bound System

Contents

3.1 Introduction

Transfer reactions are useful to investigate a single-particle structure of nuclei because of its selectivity of kinetic and angular momenta, so called the momentum matching. For example by using the $A(d,p)B$ reaction, the single-particle structure of B with the n-A

configuration can be examined. In a conventional way, the (d,p) reaction is described with the distorted-wave Born approximation (DWBA), which assumes that n transfers to A through a one-step process. However, in particular, the breakup channels are expected to play an important role because the deuteron is bound with only 2.22 MeV. Furthermore, if the residual nucleus B is a loosely bound system such as unstable nuclei, its breakup channels also must be considered. In this chapter we discuss the role of the breakup channels of loosely bound nuclei in the transfer reaction.

3.2 Formal theory for transfer reaction

To include the breakup channels in the description of the transfer reaction, below the formulation of the coupled-channels Born approximation (CCBA), which explicitly takes into account the couplings of the breakup channels of both the projectile and the residual nucleus, is given. Below, we first show the formal theory of the scattering to introduce the transition matrix. Then, the CCBA formalism in terms of the method of the continuum-discretized coupled-channels (CDCC) is given.

3.2.1 Total wave function

We consider the transition of the state from the initial channel, the $a + A$ system, to the final channel, the $b+B$ system, as shown in Fig. 3.1. The former and latter are respectively represented by the indices α and β. The total wave function $\Psi_\alpha^{(+)}$ of the initial state can be expressed by

$$\Psi_\alpha^{(+)} = \sum_\alpha \psi_\alpha\left(\zeta_\alpha\right) \xi_\alpha^{(+)}(\boldsymbol{r}_\alpha), \tag{3.1}$$

which satisfies

$$\left[H - E\right] \Psi_\alpha^{(+)} = 0, \tag{3.2}$$

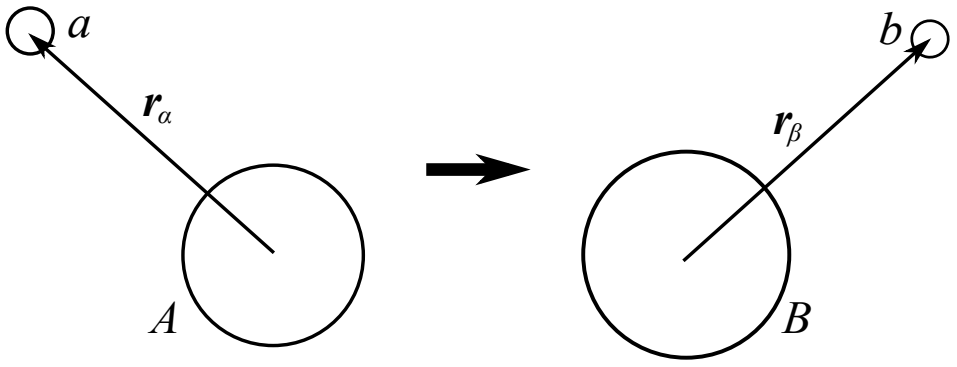

Figure 3.1: Illustration of the transfer reaction $a + A \to b + B$.

where E is the total energy of the system and the Hamiltonian H is defined by

$$\begin{aligned} H &= h_\alpha + K_\alpha + V_\alpha \\ &= h_\beta + K_\beta + V_\beta. \end{aligned} \tag{3.3}$$

Here V_α (K_α) is the interaction potential (kinetic operator) between a and A.

The explicit form of the internal Hamiltonian h_α is defined below. The wave function ψ_α is defined by

$$\psi_\alpha(\zeta_\alpha) \equiv \psi_a(\zeta_a)\,\psi_A(\zeta_A), \tag{3.4}$$

with the wave function ψ_X of the particle X ($X = a$ or A), which forms a complete set and the intrinsic variables are denoted by ζ. The expansion coefficient $\xi_\alpha^{(+)}$ describes the relative motion of the a-A system associated with its relative distance $\boldsymbol{r}_\alpha$. ψ_α and its components satisfy

$$[h_\alpha - \varepsilon_\alpha]\,\psi_\alpha = 0, \tag{3.5}$$
$$[h_a - \varepsilon_a]\,\psi_a = 0, \tag{3.6}$$
$$[h_A - \varepsilon_A]\,\psi_A = 0, \tag{3.7}$$

where internal Hamiltonian h_α is the sum of the Hamiltonian operators of each particle; $h_\alpha = h_a + h_A$. Thus, for the eigenenergy ε, we have the relation $\varepsilon_\alpha = \varepsilon_a + \varepsilon_A$. The sum, therefore, in Eq. (3.1) is taken over all intrinsic states of each particle. Using the orthonormality of ψ_α, $\xi_\alpha^{(+)}$ can be represented as

$$\begin{aligned} \xi_\alpha^{(+)}(\boldsymbol{r}_\alpha) &= \left\langle \psi_\alpha \,\middle|\, \Psi_\alpha^{(+)} \right\rangle \\ &= \int d\zeta_\alpha \psi_\alpha^*(\zeta_\alpha)\,\Psi_\alpha^{(+)}. \end{aligned} \tag{3.8}$$

The superscript $(+)$ and $(-)$, appears below, represent the outgoing and incoming boundary conditions for the scattering wave, respectively. For the final channel, we can similarly define the functions and variables.

3.2.2 Rearrangement component

In general, $\Psi_\alpha^{(+)}$ should contain the rearrangement component of other channels such as $\psi_\beta \xi_\beta^{(+)}$, i.e.,

$$\Psi_\alpha^{(+)} = \sum_\alpha \psi_\alpha(\zeta_\alpha)\,\xi_\alpha^{(+)}(\boldsymbol{r}_\alpha) + \sum_\beta \psi_\beta(\zeta_\beta)\,\xi_\beta^{(+)}(\boldsymbol{r}_\beta) + \cdots, \tag{3.9}$$

Note that the components $\psi_\alpha \xi_\alpha^{(+)}$ and $\psi_\beta \xi_\beta^{(+)}$ are not orthogonal. It means that the overlap of ψ_α and ψ_β is not zero;

$$O_{\alpha\beta} = \int d\zeta_\alpha \psi_\alpha^*(\zeta_\alpha)\,\psi_\beta(\zeta_\beta) \neq 0, \tag{3.10}$$

because ξ_β can be represented as a function of ζ_α and $\boldsymbol{r}_\alpha$. Explicit case is shown in Sec. 3.3.1. Moreover, we have the relation $O_{\alpha\beta} \neq O_{\beta\alpha}$.

Form Eq. (3.9) it is, in principle, possible to represent $\Psi_\alpha^{(+)}$ in terms of the β channel configuration;

$$\Psi_\alpha^{(+)} = \sum_\beta \psi_\beta\left(\zeta_\beta\right) \xi_\beta^{(+)}(\boldsymbol{r}_\beta). \tag{3.11}$$

The coefficient $\xi_\beta^{(+)}$ is defined from the analogy of Eq. (3.8) as

$$\begin{aligned} \xi_\beta^{(+)}\left(\boldsymbol{r}_\beta\right) &= \left\langle \psi_\beta \,\middle|\, \Psi_\alpha^{(+)} \right\rangle \\ &= \int d\zeta_\beta \psi_\beta^*\left(\zeta_\beta\right) \Psi_\alpha^{(+)}. \end{aligned} \tag{3.12}$$

3.2.3 Transition matrix

From Eq. (3.2) and (3.3), we obtain

$$\left[E - h_\beta - K_\beta\right] \Psi_\alpha^{(+)} = V_\beta \Psi_\alpha^{(+)}. \tag{3.13}$$

Then multiplying by ψ_β^* from the left and integrating over ζ_β lead

$$\left[E_\beta - K_\beta\right] \xi_\beta^{(+)}\left(\boldsymbol{r}_\beta\right) = \left\langle \psi_\beta \,\middle|\, V_\beta \,\middle|\, \Psi_\alpha^{(+)} \right\rangle, \tag{3.14}$$

where $E_\beta = E - \varepsilon_\beta$.

The formal solution of this equation can be obtained by following the standard Green's function procedure [2, 115, 116], that is,

$$\xi_\beta^{(+)}\left(\boldsymbol{r}_\beta\right) = e^{i\boldsymbol{k}_\alpha \cdot \boldsymbol{r}_\alpha} \delta_{\alpha\beta} - \frac{\mu_\beta}{2\pi\hbar^2} \int d\boldsymbol{r}'_\beta \frac{e^{ik_\beta \left|\boldsymbol{r}_\beta - \boldsymbol{r}'_\beta\right|}}{\left|\boldsymbol{r}_\beta - \boldsymbol{r}'_\beta\right|} \left\langle \psi_\beta \,\middle|\, V_\beta \,\middle|\, \Psi_\alpha^{(+)} \right\rangle, \tag{3.15}$$

with the boundary condition for the asymptotic form

$$\xi_\beta^{(+)}\left(\boldsymbol{r}_\beta\right) \sim e^{i\boldsymbol{k}_\alpha \cdot \boldsymbol{r}_\alpha} \delta_{\alpha\beta} + f_{\beta\alpha}(\hat{\boldsymbol{r}}_\beta, \boldsymbol{k}_\alpha) \frac{e^{ik_\beta \boldsymbol{r}_\beta}}{\boldsymbol{r}_\beta}. \tag{3.16}$$

Here the wave number k_γ is defined by $k_\gamma = \sqrt{2\mu_\gamma E_\gamma}/\hbar$ with the reduced mass μ_γ of the γ channel.

Now we may have

$$\left|\boldsymbol{r}_\beta - \boldsymbol{r}'_\beta\right| \approx r_\beta - \hat{\boldsymbol{r}}_\beta \cdot \boldsymbol{r}'_\beta = r_\beta - \hat{\boldsymbol{k}}_\beta \cdot \boldsymbol{r}'_\beta, \tag{3.17}$$

for the limit $r_\beta \gg r'_\beta$. Then we have the scattering amplitude $f_{\beta\alpha}$;

$$f_{\beta\alpha}(\boldsymbol{k}_\beta, \boldsymbol{k}_\alpha) = -\frac{2\pi\hbar^2}{\mu_\beta} T_{\beta\alpha}(\boldsymbol{k}_\beta, \boldsymbol{k}_\alpha), \tag{3.18}$$

with the transition matrix (T matrix) defined by

$$\begin{aligned} T_{\beta\alpha}(\boldsymbol{k}_\beta, \boldsymbol{k}_\alpha) &= \left\langle e^{i\boldsymbol{k}_\beta \cdot \boldsymbol{r}'_\beta} \psi_\beta \,\middle|\, V_\beta \,\middle|\, \Psi_\alpha^{(+)}\left(\boldsymbol{k}_\alpha\right) \right\rangle. \\ &= \int d\zeta_\beta d\boldsymbol{r}'_\beta e^{-i\boldsymbol{k}_\beta \cdot \boldsymbol{r}'_\beta} \psi_\beta^*\left(\zeta_\beta\right) V_\beta\left(\zeta_\beta, \boldsymbol{r}'_\beta\right) \Psi^{(+)}\left(\boldsymbol{k}_\alpha\right)_\alpha \end{aligned} \tag{3.19}$$

3.2.4 Gell-Mann, Goldberger transformation

Since Eq. (3.19) is not easy to calculate owing to the presence of the complicated interaction V_β, we introduce the auxiliary potential U_β. From Eq. (3.3), we have

$$\begin{aligned} H &= h_\beta + K_\beta + V_\beta \\ &= h_\beta + K_\beta + W_\beta + U_\beta, \end{aligned} \tag{3.20}$$

with the residual interaction

$$W_\beta = V_\beta\left(\zeta_\beta, \boldsymbol{r}_\beta\right) - U_\beta\left(r_\beta\right). \tag{3.21}$$

Then the Schrödinger equation (3.22) is now written by

$$\left[E_\beta - K_\beta - U_\beta\left(r_\beta\right)\right] \xi_\beta^{(+)}\left(\boldsymbol{r}_\beta\right) = \left\langle \psi_\beta \middle| W_\beta \middle| \Psi_\alpha^{(+)} \right\rangle. \tag{3.22}$$

The purpose of adding U_β is to make small the effect of the inhomogeneous from the right-hand-side of Eq. (3.22) compared to Eq. (3.2) by taking W_β as small as possible. The distorted wave $\chi_\beta^{(+)}$ describes the scattering due to the potential U_β with the Schrödinger equation

$$\left[E_\beta - K_\beta - U_\beta\left(r_\beta\right)\right] \chi_\beta^{(+)}\left(\boldsymbol{r}_\beta\right) = 0. \tag{3.23}$$

The proper choice of U_β is case by case. Explicit form of U_β in specific reactions is given in Sec. ChapTRForm2.

The formal solution of Eq. (3.22) can be expressed in terms of the solution $\chi_\beta^{(+)}$ for the homogeneous equation (3.23). From the similarity to Eq. (3.15), it is given by

$$\xi_\beta^{(+)}\left(\boldsymbol{r}_\beta\right) = \chi_\alpha^{(+)}\left(\boldsymbol{k}_\beta, \boldsymbol{r}_\beta\right)\delta_{\alpha\beta} - \frac{\mu_\beta}{2\pi\hbar^2}\int d\boldsymbol{r}'_\beta G_\beta^{(+)}\left(\boldsymbol{r}_\beta, \boldsymbol{r}'_\beta\right)\left\langle \psi_\beta \middle| W_\beta \middle| \Psi_\alpha^{(+)} \right\rangle, \tag{3.24}$$

where the Green's function $G_\beta^{(+)}$ propagates in the potential U_β. Therefore we obtain the T matrix

$$\begin{aligned} &T_{\beta\alpha}(\boldsymbol{k}_\beta, \boldsymbol{k}_\alpha) \\ &\quad = T_\beta^{(0)}(\boldsymbol{k}_\beta, \boldsymbol{k}_\alpha)\delta_{\beta\alpha} + \left\langle \chi_\beta^{(-)}\left(\boldsymbol{k}_\beta\right)\psi_\beta \middle| W_\beta \middle| \Psi_\alpha^{(+)}\left(\boldsymbol{k}_\alpha\right) \right\rangle. \\ &\quad = T_\beta^{(0)}(\boldsymbol{k}_\beta, \boldsymbol{k}_\alpha)\delta_{\beta\alpha} + \int d\zeta_\beta d\boldsymbol{r}_\beta \chi_\beta^{(-)}\left(\boldsymbol{k}_\beta, \boldsymbol{r}_\beta\right) V_\beta\left(\zeta_\beta, \boldsymbol{r}_\beta\right) - U_\beta\left(r_\beta\right)\Psi_\alpha^{(+)}\left(\boldsymbol{k}_\alpha\right), \end{aligned} \tag{3.25}$$

where $T_\beta^{(0)}$ defined by

$$T_\beta^{(0)}(\boldsymbol{k}_\beta, \boldsymbol{k}_\alpha) = \left\langle e^{i\boldsymbol{k}_\beta\cdot\boldsymbol{r}_\beta} \middle| U_\beta \middle| \chi_\beta^{(+)}\left(\boldsymbol{k}_\alpha\right) \right\rangle \tag{3.26}$$

describes the elastic scattering due to the potential U_β when $\beta = \alpha$. The incoming spherical wave $\chi_\gamma^{(-)}$ is defined as the time-reversal of the outgoing wave $\chi_\gamma^{(+)}$;

$$\chi_\gamma^{(-)}\left(\boldsymbol{k}_\gamma, \boldsymbol{r}_\gamma\right) = \chi_\gamma^{(+)*}\left(-\boldsymbol{k}_\gamma, \boldsymbol{r}_\gamma\right). \tag{3.27}$$

The second term of Eq. (3.25) is nothing but that it describes the transition from the α channel to β ($\neq \alpha$) channel. The transformation such as from Eqs. (3.20) to (3.25) with introducing the auxiliary potential U_β is known as the Gell-Mann, Goldberger transformation.

3.2.5 Post prior representation

From here we formulate with the post form representation, in which the T matrix involved the interaction in the final channel. There exist another one called the prior form. This is based on the idea that nuclear structures and reactions are the time-reversal invariant. Under this invariance, the transfer reaction $A(a,b)B$ is physically equivalent to the $b(B,a)A$ except for the phase factor;

$$T_{-\beta,-\alpha}(-\boldsymbol{k}_\beta,-\boldsymbol{k}_\alpha) = (-)^{\pi_{\beta\alpha}} T_{\beta\alpha}(\boldsymbol{k}_\beta,\boldsymbol{k}_\alpha). \tag{3.28}$$

The phase factor $\pi_{\beta\alpha}$ is related to the spins of particles. If we ignore the degree of spins, $\pi_{\beta\alpha}=0$. The T matrices corresponding to Eqs. (3.19) and (3.25) are respectively given by

$$T_{\beta\alpha}(\boldsymbol{k}_\beta,\boldsymbol{k}_\alpha) = \left\langle \Psi_\beta^{(-)}(\boldsymbol{k}_\beta) \middle| V_\alpha \middle| \psi_\alpha e^{i\boldsymbol{k}_\alpha\cdot\boldsymbol{r}_\alpha} \right\rangle \tag{3.29}$$

$$= T_\alpha^{(0)}(\boldsymbol{k}_\beta,\boldsymbol{k}_\alpha)\delta_{\beta\alpha} + \left\langle \Psi_\beta^{(-)}(\boldsymbol{k}_\beta) \middle| W_\alpha \middle| \psi_\alpha \chi_\alpha^{(+)}(\boldsymbol{k}_\alpha) \right\rangle. \tag{3.30}$$

The post and prior form of the T matrix is mathematically equivalent. However this equivalence may be broken when approximation is introduced to calculate the exact wave function $\Psi_\gamma^{(+)}$ or the distorted wave $\chi_\gamma^{(+)}$.

3.2.6 Lippmann-Schwinger equation and Born series

The Schrödinger equation (3.2) leads the Lippmann-Schwinger equation

$$\begin{aligned}\Psi_\alpha^{(\pm)} &= \psi_\alpha(\zeta_\alpha)\,\phi_\alpha(\boldsymbol{k}_\alpha,\boldsymbol{r}_\alpha) + \frac{1}{E_\alpha - K_\alpha - V_\alpha \pm i\varepsilon} V_\alpha \Psi_\alpha^{(\pm)} \\ &= \psi_\alpha(\zeta_\alpha)\,\phi_\alpha(\boldsymbol{k}_\alpha,\boldsymbol{r}_\alpha) + G_\alpha^{(\pm)} V_\alpha \Psi_\alpha^{(\pm)},\end{aligned} \tag{3.31}$$

where ϕ_α stands for the plane wave of the α channel, $\phi_\alpha(\boldsymbol{k}_\alpha,\boldsymbol{r}_\alpha) = e^{i\boldsymbol{k}_\alpha\cdot\boldsymbol{r}_\alpha}$, and $G_\alpha^{(\pm)}$ is the Green's function of the full Hamiltonian H;

$$G_\alpha^{(\pm)} = \frac{1}{E - h_\alpha - K_\alpha - V_\alpha \pm i\varepsilon}, \tag{3.32}$$

We can represent $G_\alpha^{(\pm)}$ with another expression by introducing the Green's function $G_{0\alpha}^{(\pm)}$,

$$G_{0\alpha}^{(\pm)} = \frac{1}{E - h_\alpha - K_\alpha \pm i\varepsilon}, \tag{3.33}$$

for the free Hamiltonian;

$$G_\alpha^{(\pm)} = G_{0\alpha}^{(\pm)} + G_{0\alpha}^{(\pm)} V_\alpha G_\alpha^{(\pm)}. \tag{3.34}$$

The formal solution of the Schrödinger equation (3.2) is obtained from Eq. (3.31);

$$\Psi_\alpha^{(\pm)} = \psi_\alpha(\zeta_\alpha)\,\phi_\alpha(\boldsymbol{k}_\alpha,\boldsymbol{r}_\alpha) + G_\alpha^{(\pm)} V_\alpha \psi_\alpha(\zeta_\alpha)\,\phi_\alpha(\boldsymbol{k}_\alpha,\boldsymbol{r}_\alpha). \tag{3.35}$$

By using Eq. (3.35), the T matrix for elastic scattering is given by

$$\begin{aligned} T(\boldsymbol{k}'_\alpha, \boldsymbol{k}_\alpha) &= \left\langle \psi_\alpha \phi \left(\boldsymbol{k}'_\alpha, \boldsymbol{r}_\alpha\right) \middle| V_\alpha \middle| \Psi^{(\pm)}_\alpha \right\rangle \\ &= \left\langle \phi \left(\boldsymbol{k}'_\alpha, \boldsymbol{r}_\alpha\right) \middle| V_\alpha + V_\alpha G^{(+)}_\alpha V_\alpha \middle| \phi \left(\boldsymbol{k}_\alpha, \boldsymbol{r}_\alpha\right) \right\rangle, \end{aligned} \tag{3.36}$$

where

$$k^2_\alpha = k'^2_\alpha = 2\mu_\alpha E/\hbar^2. \tag{3.37}$$

Equation (3.36) can be expressed with the Lippmann-Schwinger type;

$$T(\boldsymbol{k}'_\alpha, \boldsymbol{k}_\alpha) = V_\alpha + V_\alpha G^{(+)}_\alpha(E) V_\alpha \tag{3.38}$$

$$= V_\alpha + V_\alpha G^{(+)}_{0\alpha}(E) T(\boldsymbol{k}'_\alpha, \boldsymbol{k}_\alpha). \tag{3.39}$$

Here we explicitly put the argument E of the Green's functions. When Eq. (3.37) is satisfied, $T(\boldsymbol{k}'_\alpha, \boldsymbol{k}_\alpha)$ is called 'on-the-energy shell' or just 'on-shell'. For more complicated reactions such as multiple scattering, Eq. (3.37) may not be satisfied. This is said to be 'off-the-energy-shell' or 'off-shell'.

The Lippmann-Schwinger equation (3.31) can be rewritten as the Born series;

$$\Psi^{(+)}_\alpha = \left[1 + G^{(+)}_{0\alpha} V_\alpha + G^{(+)}_{0\alpha} V_\alpha G^{(+)}_{0\alpha} V_\alpha + \cdots\right] \phi_\alpha \left(\boldsymbol{k}_\alpha, \boldsymbol{r}_\alpha\right) \psi_\alpha \left(\zeta_\alpha\right). \tag{3.40}$$

Similarly for the residual interaction W_α defined by Eq. (3.21), we have

$$\Psi^{(+)}_\alpha = \left[1 + G^{(+)}_\alpha W_\alpha + G^{(+)}_\alpha W_\alpha G^{(+)}_\alpha W_\alpha + \cdots\right] \chi^{(+)}_\alpha \left(\boldsymbol{k}_\alpha, \boldsymbol{r}_\alpha\right) \psi_\alpha \left(\zeta_\alpha\right). \tag{3.41}$$

From these expression with the Born series, the T matrix for the $\beta \neq \alpha$ transition is given by

$$T_{\beta\alpha} = \left\langle e^{i\boldsymbol{k}_\beta \cdot \boldsymbol{r}_\beta} \psi_\beta \middle| V_\beta + V_\beta G^{(+)}_{0\alpha} V_\alpha + V_\beta G^{(+)}_{0\alpha} V_\alpha G^{(+)}_{0\alpha} V_\alpha + \cdots \middle| e^{i\boldsymbol{k}_\alpha \cdot \boldsymbol{r}_\alpha} \psi_\alpha \right\rangle \tag{3.42}$$

and

$$T_{\beta\alpha} = \left\langle \chi^{(-)}_\beta \psi_\beta \middle| W_\beta + W_\beta G^{(+)}_\alpha W_\alpha + W_\beta G^{(+)}_\alpha W_\alpha G^{(+)}_\alpha W_\alpha + \cdots \middle| \chi^{(+)}_\alpha \psi_\alpha \right\rangle. \tag{3.43}$$

If we choose only the first term of these series, the former gives the first Born approximation, or just the Born approximation;

$$T^{\mathrm{BA}}_{\beta\alpha}(\mathrm{post}) = \left\langle e^{i\boldsymbol{k}_\beta \cdot \boldsymbol{r}_\beta} \psi_\beta \middle| V_\beta \middle| e^{i\boldsymbol{k}_\alpha \cdot \boldsymbol{r}_\alpha} \psi_\alpha \right\rangle, \tag{3.44}$$

while the latter leads the T matrix of the distorted-wave Born approximation (DWBA);

$$T^{\mathrm{DWBA}}_{\beta\alpha}(\mathrm{post}) = \left\langle \chi^{(-)}_\beta \psi_\beta \middle| V_\beta - U_\beta \middle| \chi^{(+)}_\alpha \psi_\alpha \right\rangle. \tag{3.45}$$

Similarly T matrices of the prior form is given by

$$T^{\mathrm{BA}}_{\beta\alpha}(\mathrm{prior}) = \left\langle e^{i\boldsymbol{k}_\beta \cdot \boldsymbol{r}_\beta} \psi_\beta \middle| V_\alpha \middle| e^{i\boldsymbol{k}_\alpha \cdot \boldsymbol{r}_\alpha} \psi_\alpha \right\rangle, \tag{3.46}$$

$$T^{\mathrm{DWBA}}_{\beta\alpha}(\mathrm{prior}) = \left\langle \chi^{(-)}_\beta \psi_\beta \middle| V_\alpha - U_\alpha \middle| \chi^{(+)}_\alpha \psi_\alpha \right\rangle. \tag{3.47}$$

These are basic formalisms in order to describe transfer reactions; in particular DWBA is often adopted for analyses. However, in DWBA, higher order processes, for example the breakup effects of the projectile and the residual nucleus, are missing for the calculation of $\chi_\gamma^{(+)}$. Thus, in this work, we increase the accuracy of the model by formulating the coupled-channels Born approximation (CCBA), which includes the DWBA framework with a three-body model.

3.3 Coupled-channels Born approximation (CCBA) formalism

As a CCBA model, we explicitly take into account the breakup effects of the projectile and the residual nucleus by means of the method of the continuum-discretized coupled-channels (CDCC) in terms of a three-body model. Below the explicit form of the CDCC wave function with the partial wave expansion is given.

3.3.1 CDCC wave functions

In this subsection, we formulate the explicit form of the CDCC wave function with the partial wave expansion. An illustration of the stripping reaction, $a(x+b)+A \to b+B(x+A)$ is shown in Fig. 3.2. In our model it is assumed that the intrinsic spin of each of x, b, and A does not change through the scattering. Thus the degree of freedom of the intrinsic spin does not appear explicitly in the distorted wave. In addition the target nucleus A is assumed as structureless that vanishes ψ_A in this formulation.

In CDCC the three-body wave function in the initial channel $\Psi_\alpha^{(+)}$ is given by

$$\Psi_\alpha^{(+)}(\boldsymbol{r}_{xb}, \boldsymbol{r}_\alpha) \approx \sum_i \psi_{xb}^i(\boldsymbol{r}_{xb}) \chi_\alpha^{ii_0(+)}(\boldsymbol{r}_\alpha), \tag{3.48}$$

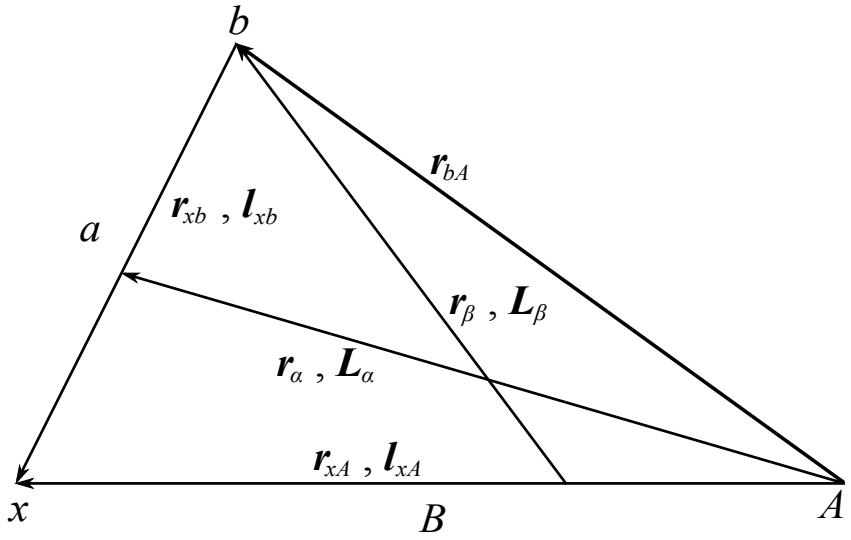

Figure 3.2: Coordinates for the transfer reaction $a(x+b)+A \to b+B(x+A)$.

which satisfies

$$[H_\alpha - E]\Psi_\alpha^{(+)}(\boldsymbol{r}_{xb}, \boldsymbol{r}_\alpha) = 0, \tag{3.49}$$

$$H_\alpha = K_{\boldsymbol{r}_\alpha} + h_{xb} + U_{xA}^{(\alpha)}(r_{xA}) + V_{xA}^{(\mathrm{C})}(r_{xA}) + U_{bA}^{(\alpha)}(r_{bA}) + V_{bA}^{(\mathrm{C})}(r_{bA}). \tag{3.50}$$

The coordinates for the transfer reaction are shown in Fig. 3.2 Eqs. (3.49) and (3.50) correspond to Eqs. (2.4) and (2.2), respectively. E is the total energy of the system and K_X is the kinetic energy regarding the coordinate X. The $U_{cA}^{(\gamma)}$ and $V_{cA}^{(\mathrm{C})}$ are, respectively, the nuclear distorting potential and Coulomb interaction between c ($= x$ or b) and A. Note that α and β respectively represent the initial and final channels. ψ_{xb}^i is the internal wave function of the projectile a with i its energy index; $i = i_0$ corresponds to the ground state of a and $i \neq i_0$ to the discretized continuum states of the x-b system. In this CCBA framework we adopt the pseudostate method given in Sec. 2.1.3 for the discretization because Gaussian basis functions used in the pseudostate method are applicable to CCBA, in which the radial part of ψ_{xb}^i has to be expanded with any function. The detail of the expansion of ψ_{xb}^i in CCBA is shown in Appx. C. Equation (2.8) for ψ_{xb}^i with the x-b internal Hamiltonian h_{xb} can be written as

$$\left(h_{xb} - \varepsilon_{xb}^i\right)\psi_{xb}^i(\boldsymbol{r}_{xb}) = 0, \tag{3.51}$$

$$h_{xb} = K_{\boldsymbol{r}_{xb}} + V_{xb}(r_{xb}) + V_{xb}^{(\mathrm{C})}(r_{xb}), \tag{3.52}$$

where ε_{xb}^i is the energy eigenvalue of the x-b system. V_{xb} is the nuclear binding potential, which reproduces the binding energy $\varepsilon_{xb}^{i_0}$ and $V_{xb}^{(\mathrm{C})}$ stands for the Coulomb interaction between x and b.

Similarly, the three-body wave function $\Psi_\beta^{(+)}$ in the final channel is given by

$$\Psi_\beta^{(+)}(\boldsymbol{r}_{xA}, \boldsymbol{r}_\beta) \approx \sum_j \psi_{xA}^j(\boldsymbol{r}_{xA})\chi_\beta^{jj_0(+)}(\boldsymbol{r}_\beta) \tag{3.53}$$

with the energy index j of the residual nucleus B, which corresponds to i in the initial channel. $\Psi_\beta^{(+)}$, satisfies

$$[H_\beta - E]\Psi_\beta^{(+)}(\boldsymbol{r}_{xA}, \boldsymbol{r}_\beta) = 0, \tag{3.54}$$

$$H_\beta = K_{\boldsymbol{r}_\beta} + h_{xA} + U_{bA}^{(\beta)}(r_{bA}) + V_{bA}^{(\mathrm{C})}(r_{bA}) + V_{xb}^{(\mathrm{C})}(r_{xb}), \tag{3.55}$$

where the x-A internal wave function ψ_{xA}^j satisfies following Schrödinger equation with the x-A internal Hamiltonian h_{xA};

$$\left(h_{xA} - \varepsilon_{xA}^j\right)\psi_{xA}^j(\boldsymbol{r}_{xA}) = 0, \tag{3.56}$$

$$h_{xA} = K_{\boldsymbol{r}_{xA}} + V_{xA}(r_{xA}) + V_{xA}^{(\mathrm{C})}(r_{xA}), \tag{3.57}$$

where ε_{xA}^j, V_{xA}, and $V_{xA}^{(\mathrm{C})}$ are respectively same as ε_{xb}^i, V_{xb}, and $V_{xb}^{(\mathrm{C})}$ but for the x-A system. Note that H_β does not contain the nuclear interaction between x and b that has been used as a transition interaction V_{xb} as shown below. This is noting but the fact that we choose the auxiliary potential in Eq. (3.21) so that only the interaction V_{xb} remains.

The partial waves of $\Psi_\alpha^{(+)}$ and $\Psi_\beta^{(+)}$ can be represented by

$$\Psi_\alpha^{(+)} = \sum_{l'_{xb}m'_{xb}} \sum_i \Phi^i_{a,l'_{xb}m'_{xb}} \chi^{ii_0(+)}_{m_{xb}m'_{xb}}(\boldsymbol{k}_\alpha, \boldsymbol{r}_\alpha), \tag{3.58}$$

$$\begin{aligned}\chi^{ii_0(+)}_{m_{xb}m'_{xb}}(\boldsymbol{k}_\alpha, \boldsymbol{r}_\alpha) = {} & \frac{4\pi}{k_\alpha r_\alpha} \sum_{JL_\alpha L'_\alpha} i^{L'_\alpha} \chi^{Jii_0}_{L_\alpha L'_\alpha l_{xb} l'_{xb}}(k_\alpha, r_\alpha) \\ & \times \sum_{\mu M_\alpha M'_\alpha} (l_{xb} m_{xb} L_\alpha M_\alpha | J\mu) \left(l'_{xb} m'_{xb} L'_\alpha M'_\alpha | J\mu\right) \\ & \times Y^*_{L_\alpha M_\alpha}(\hat{\boldsymbol{k}}_\alpha) Y_{L'_\alpha M'_\alpha}(\hat{\boldsymbol{r}}_\alpha),\end{aligned} \tag{3.59}$$

$$\Psi_\beta^{(+)} = \sum_{l'_{xA}m'_{xA}} \sum_j \Phi^j_{B,l'_{xA}m'_{xA}} \chi^{jj_0(+)}_{m_{xA}m'_{xA}}(\boldsymbol{k}_\beta, \boldsymbol{r}_\beta), \tag{3.60}$$

$$\begin{aligned}\chi^{jj_0(+)}_{m_{xA}m'_{xA}}(\boldsymbol{k}_\beta, \boldsymbol{r}_\beta) = {} & \frac{4\pi}{k_\beta r_\beta} \sum_{JL_\beta L'_\beta} i^{L'_\beta} \chi^{Jjj_0}_{L_\beta L'_\beta l_{xA} l'_{xA}}(k_\beta, r_\beta) \\ & \times \sum_{\mu M_\beta M'_\beta} (l_{xA} m_{xA} L_\beta M_\beta | J\mu) \left(l'_{xA} m'_{xA} L'_\beta M'_\beta | J\mu\right) \\ & \times Y^*_{L_\beta M_\beta}(\hat{\boldsymbol{k}}_\beta) Y_{L'_\beta M'_\beta}(\hat{\boldsymbol{r}}_\beta).\end{aligned} \tag{3.61}$$

Here, l_{xb} (L_α) is the orbital angular momentum between x and b (a and A) in the initial channel, while l_{xA} (L_β) stands for one between x and A (b and B) in the final channel, as shown in Fig. 3.2. m_{xc} and M_γ are respectively their z-components in each channel. Through the scattering process, the projectile's (residual nucleus') state can vary from its "incident" state owing to the interaction between a and A (b and B) in the initial (final) channel. Thus their quantum numbers can change to "prime" one due to the CC in the intermediate state, in which the particles interact each other. J (μ) is the total angular momentum (its z-component). The wave number regarding the coordinate $\boldsymbol{r}_\gamma$ of the γ channel is expressed by $\boldsymbol{k}_\gamma$.

The overlap $O_{\alpha\beta}$ defined by Eq. (3.10) is now

$$O_{\alpha\beta} = \int d\boldsymbol{r}_{xb} \psi^*_{xb}(\boldsymbol{r}_{xb}) \psi_{xA}(\boldsymbol{r}_{xA}), \tag{3.62}$$

where we assume $i = i_0$ and $j = j_0$, and they are omitted. From Fig. 3.2 we can see that the coordinate $\boldsymbol{r}_{xA}$ can be written as the linear combination of the coordinates $\boldsymbol{r}_{xb}$ and $\boldsymbol{r}_\alpha$ as $\boldsymbol{r}_{xA} = \boldsymbol{r}_\alpha + \frac{b}{a}\boldsymbol{r}_{xb}$. Thus $O_{\alpha\beta}$ is a function of $\boldsymbol{r}_\alpha$. However this nonorthogonality appears in the inner region regarding $\boldsymbol{r}_\alpha$. Now, since ψ_{xb} and ψ_{xA} decay exponentially owing to their bound states property, it is clear that $O_{\alpha\beta}(\boldsymbol{r}_\alpha)$ becomes zero for $\boldsymbol{r}_\alpha \to \infty$. This fact is physically reasonable because in the interior region, in which a and A can overlap, we cannot distinguish the system whether it should be represented as the a-A or b-B systems.

3.3.2 Transition matrix and cross section

In this subsection, by adopting CDCC, we formulate the transition matrix (T matrix) of the stripping reaction which includes the coupled-channels (CC) concerning the breakup states

of the projectile and the residual nucleus in both the initial and final channels, respectively. The T matrix in the post form is given by

$$\begin{aligned} T &= \mathscr{J} \left\langle \Psi^{(-)}_{\beta} \middle| V_{xb} \middle| \Psi^{(+)}_{\alpha} \right\rangle \\ &= \mathscr{J} \sum_{l'_{xA} l'_{xb} m'_{xA} m'_{xb}} \sum_{ij} \left\langle \Phi^{j}_{B,l'_{xA} m'_{xA}} \chi^{jj_0(-)}_{m_{xA} m'_{xA}} \middle| V_{xb} \middle| \Phi^{i}_{a,l'_{xb} m'_{xb}} \chi^{ii_0(+)}_{m_{xb} m'_{xb}} \right\rangle , \end{aligned} \tag{3.63}$$

the factor $\mathscr{J}$ is the Jacobian of the transformation from the integration variables $(\boldsymbol{r}_{xA}, \boldsymbol{r}_{xb})$ or $(\boldsymbol{r}_{xA}, \boldsymbol{r}_{bA})$ to the $(\boldsymbol{r}_{\alpha}, \boldsymbol{r}_{\beta})$ used in the present framework, which is given by

$$\mathscr{J} = \frac{\partial(\boldsymbol{r}_{xA}, \boldsymbol{r}_{xb})}{\partial(\boldsymbol{r}_{\alpha}, \boldsymbol{r}_{\beta})} = \left[\frac{aB}{x(a+A)} \right]^3 . \tag{3.64}$$

The reason why we choose the interaction V_{xb} as the residual interaction is, in general, the range of V_{xb} is expected to be the shortest in each subsystem. It means that we just have to calculate the T matrix in the range of the residual interaction. For example deuteron induced reactions, the interaction between p and n, which forms deuteron with the range of the nuclear interaction, is adopted.

In the exact form of Eq. (3.63), $\Psi^{(+)}_{\alpha}$ includes not only the a-A components, consisting of the elastic and breakup ones, but also rearrangement components such as Eq. (3.9). The latter is not explicitly taken into account in the present CCBA calculation. However, if we include large enough values of l_{xb}, the rearrangement channels can be described well [109, 117]. Furthermore, the transitions between the former and latter are shown to be weak [109, 117] (See also Appx. A).

Let us introduce the form factor in order to integrate the angular part of Eq. (3.63). As shown in Eq. (8) of Ref. [118], the form factor is given by

$$\left\langle \Phi^{j}_{B,l'_{xA} m'_{xA}} \middle| V_{xb} \middle| \Phi^{i}_{a,l'_{xb} m'_{xb}} \right\rangle = \sum_{lm} i^{-l} A_l \left(l m l'_{xb} m'_{xb} | l'_{xA} m'_{xA} \right) f^{ij}_{lm}(\boldsymbol{r}_{\beta}, \boldsymbol{r}_{\alpha}). \tag{3.65}$$

Here, l is the transferred angular momentum defined by

$$\boldsymbol{l} = \boldsymbol{l}_{xA} - \boldsymbol{l}_{xb} = \boldsymbol{l}'_{xA} - \boldsymbol{l}'_{xb}, \tag{3.66}$$

and it can vary in the range of

$$|l_{xb} - l_{xA}| \leq l \leq l_{xb} + l_{xA}, \tag{3.67}$$

$$\left|l'_{xb} - l'_{xA}\right| \leq l \leq l'_{xb} + l'_{xA}. \tag{3.68}$$

m is the z-component of l. The phase factor i^{-l} ensures time reversal properties. A_l is the spectroscopic amplitude and the form factor f^{ij}_{lm} can be given with the spherical harmonics expansion, Eq. (32) of Ref. [118], as follows;

$$f^{ij}_{lm}(\boldsymbol{r}_{\beta}, \boldsymbol{r}_{\alpha}) = \sum_{L_1 L_2 M_1 M_2} F^{ij}_{l L_1 L_2}(r_{\beta}, r_{\alpha}) \left(L_1 M_1 L_2 M_2 | l m \right) Y^{*}_{L_1 M_1}(\hat{\boldsymbol{r}}_{\beta}) Y^{*}_{L_2 M_2}(\hat{\boldsymbol{r}}_{\alpha}). \tag{3.69}$$

Explicit form of f^{ij}_{lm} in some cases is given in Appx. C. For example, when we expand ψ^i_{xb} and ψ^j_{xA} with Gaussian basis functions, the exact finite-range (FR) form of $F_{lL_\beta L_\alpha}$ is given by

$$F_{lL_\beta L_\alpha}(r_\beta, r_\alpha) = \sum_{\lambda_A \lambda_b L} \mathscr{R}^{ij}_{\lambda_A \lambda_b L}(r_\beta, r_\alpha) \mathscr{A}^{lL_\beta L_\alpha}_{\lambda_A \lambda_b L}, \tag{3.70}$$

$$\mathscr{R}^{ij}_{\lambda_A \lambda_b L}(r_\beta, r_\alpha) \equiv \frac{1}{4\pi} h_{\lambda_A}(r_\alpha, r_\beta) h_{\lambda_b}(r_\alpha, r_\beta) \sum_{i_A i_b} \tilde{g}^{ij}_{i_A i_b}(r_\alpha, r_\beta) \tilde{i}_L(\gamma^{ij}_{i_A i_b} r_\beta r_\alpha), \tag{3.71}$$

$$\begin{aligned}
\mathscr{A}^{lL_\beta L_\alpha}_{\lambda_A \lambda_b L} \equiv & \sum_{j_\alpha j_\beta} (-)^{j_\alpha + L_\alpha - L} \hat{L}^2 \hat{l}_{xA} \hat{l}_{xb} \hat{j}_\alpha \hat{j}_\beta \widehat{l_{xA} - \lambda_{xA}} \widehat{l_{xb} - \lambda_{xb}} \hat{\lambda}_{xA} \hat{\lambda}_{xb} \\
& \times (l_{xA} - \lambda_{xA}, 0, l_{xb} - \lambda_{xb}, 0 | j_\alpha 0) \, (\lambda_{xA} 0 \lambda_{xb} 0 | j_\beta 0) \\
& \times (j_\alpha 0 L 0 | L_\alpha 0) \, (j_\beta 0 L 0 | L_\beta 0) \\
& \times W(j_\alpha j_\beta L_\alpha L_\beta; l L) \begin{Bmatrix} l_{xA} - \lambda_{xA} & \lambda_{xA} & l_{xA} \\ l_{xb} - \lambda_{xb} & \lambda_{xb} & l_{xb} \\ j_\alpha & j_\beta & l \end{Bmatrix}.
\end{aligned} \tag{3.72}$$

Here the factor $W(j_\alpha j_\beta L_\alpha L_\beta; lL)$ is the Racah coefficient and the 3×3 matrix in the braces $\{\}$ is the 9-j symbol. Note that in this thesis an angular momentum with "hat", $\hat{L}$, stands for

$$\hat{L} = \sqrt{2L+1}. \tag{3.73}$$

The definitions of each variable in Eq. (3.70) are given in Appx. C.

To perform the angular integration we need to write down the time-reversal form of Eq. (3.61), $\chi^{jj_0(-)}_{m_{xA} m'_{xA}}$;

$$\begin{aligned}
\chi^{jj_0(-)*}_{m_{xA} m'_{xA}}(\boldsymbol{k}_\beta, \boldsymbol{r}_\beta) &= \chi^{jj_0(+)}_{-m_{xA}, -m'_{xA}}(-\boldsymbol{k}_\beta, \boldsymbol{r}_\beta) \\
&= (-)^{m_{xA} - m'_{xA}} \frac{4\pi}{k_\beta r_\beta} \sum_{J L_\beta L'_\beta} i^{L'_\beta} \chi^{Jjj_0}_{L_\beta L'_\beta l_{xA} l'_{xA}}(k_\beta, r_\beta) \\
&\times \sum_{\mu M_\beta M'_\beta} (l_{xA}, -m_{xA} L_\beta M_\beta | J \mu) \left(l'_{xA}, -m'_{xA} L'_\beta M'_\beta | J \mu\right) (-)^{L_\beta + M_\beta} \\
&\times Y_{L_\beta, -M_\beta}(\hat{\boldsymbol{k}}_\beta) Y_{L'_\beta M'_\beta}(\hat{\boldsymbol{r}}_\beta).
\end{aligned} \tag{3.74}$$

Inserting Eqs. (3.65), (3.69), and (3.74) to Eq. (3.63), we obtain

$$
\begin{aligned}
T = \mathscr{J} & \sum_{l'_{xA} l'_{xb} m'_{xA} m'_{xb}} \sum_{ij} \int d\boldsymbol{r}_\alpha \int d\boldsymbol{r}_\beta \\
& \times (-)^{m_{xA}-m'_{xA}} \frac{4\pi}{k_\beta r_\beta} \sum_{J L_\beta L'_\beta} i^{L'_\beta} \chi^{Jjj_0}_{L_\beta L'_\beta l_{xA} l'_{xA}}(k_\beta, r_\beta) \\
& \times \sum_{\mu M_\beta M'_\beta} (l_{xA}, -m_{xA} L_\beta M_\beta | J\mu) \left(l'_{xA}, -m'_{xA} L'_\beta M'_\beta | J\mu\right) \\
& \times (-)^{L_\beta + M_\beta} Y_{L_\beta, -M_\beta}(\hat{\boldsymbol{k}}_\beta) Y_{L'_\beta M'_\beta}(\hat{\boldsymbol{r}}_\beta) \\
& \times \sum_{lm} i^{-l} A_l \left(l m l'_{xb} m'_{xb} | l'_{xA} m'_{xA}\right) \\
& \times \sum_{L_1 L_2 M_1 M_2} F^{ij}_{l L_1 L_2}(r_\beta, r_\alpha) \left(L_1 M_1 L_2 M_2 | lm\right) Y^*_{L_1 M_1}(\hat{\boldsymbol{r}}_\beta) Y^*_{L_2 M_2}(\hat{\boldsymbol{r}}_\alpha) \\
& \times \frac{4\pi}{k_\alpha r_\alpha} \sum_{L_\alpha L'_\alpha} i^{L'_\alpha} \chi^{Jii_0}_{L_\alpha L'_\alpha l_{xb} l'_{xb}}(k_\alpha, r_\alpha) \\
& \times \sum_{M_\alpha M'_\alpha} (l_{xb} m_{xb} L_\alpha M_\alpha | J\mu) \left(l'_{xb} m'_{xb} L'_\alpha M'_\alpha | J\mu\right) Y^*_{L_\alpha M_\alpha}(\hat{\boldsymbol{k}}_\alpha) Y_{L'_\alpha M'_\alpha}(\hat{\boldsymbol{r}}_\alpha). \qquad (3.75)
\end{aligned}
$$

In Eq. (3.75), the angular integration can be done;

$$
\int d\hat{\boldsymbol{r}}_\alpha Y^*_{L_2 M_2}(\hat{\boldsymbol{r}}_\alpha) Y_{L'_\alpha M'_\alpha}(\hat{\boldsymbol{r}}_\alpha) = \delta_{L_2 L'_\alpha} \delta_{M_2 M'_\alpha}, \qquad (3.76)
$$

$$
\int d\hat{\boldsymbol{r}}_\beta Y^*_{L_1 M_1}(\hat{\boldsymbol{r}}_\beta) Y_{L'_\beta M'_\beta}(\hat{\boldsymbol{r}}_\beta) = \delta_{L_1 L'_\beta} \delta_{M_1 M'_\beta}. \qquad (3.77)
$$

The T matrix is then given by

$$
\begin{aligned}
T = 4\pi \mathscr{J} & \sum_{lJ} \sum_{l'_A L_\beta L'_\beta} \sum_{l'_b L_\alpha L'_\alpha} A_l I^{l l_{xA} l'_{xA} l_{xb} l'_{xb} ij}_{J L_\alpha L'_\alpha L_\beta L'_\beta} \\
& \times \sum_{m\mu} \sum_{m'_{xA} M_\beta M'_\beta} \sum_{m'_{xb} M_\alpha M'_\alpha} Y_{L_\beta, -M_\beta}(\hat{\boldsymbol{k}}_\beta) Y^*_{L_\alpha M_\alpha}(\hat{\boldsymbol{k}}_\alpha) (-)^{m_{xA}-m'_{xA}+L_\beta+M_\beta} i^{L'_\beta + L'_\alpha - l} \\
& \times (l_{xA}, -m_{xA} L_\beta M_\beta | J\mu) \left(l'_{xA}, -m'_{xA} L'_\beta M'_\beta | J\mu\right) \\
& \times \left(l m l'_{xb} m'_{xb} | l'_{xA} m'_{xA}\right) \left(L'_\beta M'_\beta L'_\alpha M'_\alpha | lm\right) \\
& \times (l_{xb}, m_{xb} L_\alpha M_\alpha | J\mu) \left(l'_{xb}, m'_{xb} L'_\alpha M'_\alpha | J\mu\right), \qquad (3.78)
\end{aligned}
$$

where the overlap integral $I^{l l_{xA} l'_{xA} l_{xb} l'_{xb} ij}_{J L_\alpha L'_\alpha L_\beta L'_\beta}$ is defined by

$$
\begin{aligned}
I^{l l_A l'_A l_b l'_b ij}_{J L_\alpha L'_\alpha L_\beta L'_\beta} \equiv \frac{4\pi}{k_\alpha k_\beta} \sum_{ij} & \int r_\alpha dr_\alpha \int r_\beta dr_\beta \\
& \times \chi^{Jjj_0}_{L_\beta L'_\beta l_A l'_A}(k_\beta, r_\beta) F^{ij}_{l L'_\beta L'_\alpha}(r_\beta, r_\alpha) \chi^{Jii_0}_{L_\alpha L'_\alpha l_b l'_b}(k_\alpha, r_\alpha). \qquad (3.79)
\end{aligned}
$$

If we take the z-axis to be parallel to the incident beam following the Madison conventions, the spherical harmonics becomes

$$Y^*_{L_\alpha M_\alpha}(0,0) = \delta_{M_\alpha 0}\hat{L}_\alpha(4\pi)^{-1/2}, \tag{3.80}$$

$$Y_{L_\beta,-M_\beta}(\theta,0) = (-)^{(|M_\beta|-M_\beta)/2}\hat{L}_\beta(4\pi)^{-1/2}\left[\frac{(L_\beta-|M_\beta|)!}{(L_\beta+|M_\beta|)!}\right]^{1/2} P_{L_\beta M_\beta}(\cos\theta). \tag{3.81}$$

Using Eq. (3.80) and (3.81), we obtain

$$\begin{aligned}
T = \mathscr{J}\sum_{lJ}\sum_{l'_{xA}L_\beta L'_\beta}\sum_{l'_{xb}L_\alpha L'_\alpha} & A_l I^{ll_{xA}l'_{xA}l_{xb}l'_{xb}ij}_{JL_\alpha L'_\alpha L_\beta L'_\beta}\hat{L}_\alpha\hat{L}_\beta \\
\times\sum_{m\mu}\sum_{m'_{xA}M_\beta M'_\beta}\sum_{m'_{xb}M'_\alpha} & (-)^{m_{xA}-m'_{xA}+L_\beta}(-)^{(|M_\beta|+M_\beta)/2}i^{L'_\beta+L'_\alpha-l} \\
\times & \left(l_{xA},-m_{xA}L_\beta M_\beta|J\mu\right)\left(l'_{xA},-m'_{xA}L'_\beta M'_\beta|J\mu\right) \\
\times & \left(lml'_{xb}m'_{xb}|l'_{xA}m'_{xA}\right)\left(L'_\beta M'_\beta L'_\alpha M'_\alpha|lm\right) \\
\times & \left(l_{xb}m_{xb}L_\alpha 0|J\mu\right)\left(l'_{xb}m'_{xb}L'_\alpha M'_\alpha|J\mu\right) \\
\times & \left[\frac{(L_\beta-|M_\beta|)!}{(L_\beta+|M_\beta|)!}\right]^{1/2} P_{L_\beta M_\beta}(\cos\theta).
\end{aligned} \tag{3.82}$$

The summation over m, m'_{xA}, m'_{xb}, M'_α, and M'_β in Eq. (3.82) results in

$$\begin{aligned}
\sum_{mm'_{xA}m'_{xb}M'_\alpha M'_\beta} & (-)^{-m'_{xA}}\left(l'_{xA},-m'_{xA}L'_\beta M'_\beta|J\mu\right)\left(lml'_{xb}m'_{xb}|l'_{xA}m'_{xA}\right) \\
& \times\left(L'_\beta M'_\beta L'_\alpha M'_\alpha|lm\right)\left(l'_{xb}m'_{xb}L'_\alpha M'_\alpha|J\mu\right) \\
& = \sum(-)^{-m'_{xA}}(-)^{l+l'_{xb}-l'_{xA}}\left(l'_{xb}m'_{xb}lm|l'_{xA}m'_{xA}\right)\left(l'_{xA},-m'_{xA}L'_\beta M'_\beta|J\mu\right) \\
& \times(-)^{L'_\beta+L'_\alpha-l}(-)^{L'_\beta+M'_\beta}\frac{\hat{l}}{\hat{L'_\alpha}}\left(l,-mL'_\beta M'_\beta|L'_\alpha,-M'_\alpha\right)\left(l'_{xb}m'_{xb}L'_\alpha M'_\alpha|J\mu\right) \\
& = (-)^{\mu}(-)^{L'_\alpha+l'_{xb}-l'_{xA}}\frac{\hat{l}}{\hat{L'_\alpha}} \\
& \times\sum\left(l'_{xb}m'_{xb}lm|l'_{xA}m'_{xA}\right)(-)^{l'_{xA}+L'_\beta-J}\left(l'_{xA}m'_{xA}L'_\beta,-M'_\beta|J,-\mu\right) \\
& \times(-)^{l+L'_\beta-L'_\alpha}\left(lmL'_\beta,-M'_\beta|L'_\alpha M'_\alpha\right)\left(l'_{xb}m'_{xb}L'_\alpha M'_\alpha|J\mu\right) \\
& = (-)^{\mu}(-)^{l'_{xb}+l-J}\frac{\hat{l}}{\hat{L'_\alpha}}\delta_{\mu 0}(-)^{l'_{xb}+l+L'_\beta+J}\hat{l'}_{xA}\hat{L'}_\alpha\begin{Bmatrix} l'_{xb} & l & l'_{xA} \\ L'_\beta & J & L'_\alpha\end{Bmatrix} \\
& = \hat{l}\hat{l'}_{xA}\delta_{\mu 0}(-)^{L'_\beta}\begin{Bmatrix} l'_{xb} & l & l'_{xA} \\ L'_\beta & J & L'_\alpha\end{Bmatrix},
\end{aligned} \tag{3.83}$$

where $\begin{Bmatrix} l'_{xb} & l & l'_{xA} \\ L'_\beta & J & L'_\alpha\end{Bmatrix}$ is the 6-j symbol and we have used the relation $(-)^{m'_{xA}-M'_\beta} = (-)^{-m'_{xA}+M'_\beta} = (-)^{\mu}$ ensured by properties of the Clebsch-Gordan coefficient $(l'_{xA},-m'_{xA}L'_\beta M'_\beta|J\mu)$.

Inserting Eq. (3.83) to Eq. (3.82), the T matrix becomes

$$
\begin{aligned}
T_{l_{xb}l_{xA}m_{xA}} = \mathscr{J} \sum_{lJ} \sum_{l'_{xA}L_\beta L'_\beta} \sum_{l'_{xb}L_\alpha L'_\alpha} & A_l I^{ll_{xA}l'_{xA}l_{xb}l'_{xb}ij}_{JL_\alpha L'_\alpha L_\beta L'_\beta} \hat{L}_\alpha \hat{L}_\beta \hat{l}\hat{l}'_{xA} \\
& \times \begin{Bmatrix} l'_{xb} & l & l'_{xA} \\ L'_\beta & J & L'_\alpha \end{Bmatrix} (-)^{L_\beta + L'_\beta} i^{L'_\beta + L'_\alpha - l} \\
& \times \sum_{\mu M_\beta} \delta_{\mu 0} (-)^{m_{xA}} (-)^{(|M_\beta| + M_\beta)/2} (l_{xA}, -m_{xA} L_\beta M_\beta | J\mu) (l_{xb} m_{xb} L_\alpha 0 | J\mu) \\
& \times \left[\frac{(L_\beta - |M_\beta|)!}{(L_\beta + |M_\beta|)!} \right]^{1/2} P_{L_\beta M_\beta}(\cos\theta). \qquad (3.84)
\end{aligned}
$$

Here we put the suffixes of T matrix, l_{xb}, l_{xA}, and m_{xA}, explicitly.

Next let us take the summation over μ as

$$
\begin{aligned}
& \sum_{\mu} \delta_{\mu 0} (l_{xA}, -m_{xA} L_\beta M_\beta | J\mu) (l_{xb} m_{xb} L_\alpha 0 | J\mu) \\
& \qquad = (l_{xA}, -m_{xA} L_\beta M_\beta | J0) (l_{xb} m_{xb} L_\alpha 0 | J0) \\
& \qquad = (l_{xA}, -m_{xA} L_\beta m_{xA} | J0) (l_{xb} 0 L_\alpha 0 | J0) \delta_{M_\beta m_{xA}} \delta_{m_{xb} 0}. \qquad (3.85)
\end{aligned}
$$

Then Eq. (3.84) becomes

$$
\begin{aligned}
T_{l_{xb}l_{xA}m_{xA}} = \mathscr{J} \sum_{lJ} \sum_{l'_{xA}L_\beta L'_\beta} \sum_{l'_{xb}L_\alpha L'_\alpha} & A_l I^{ll_{xA}l'_{xA}l_{xb}l'_{xb}ij}_{JL_\alpha L'_\alpha L_\beta L'_\beta} \hat{L}_\alpha \hat{L}_\beta \hat{l}\hat{l}'_{xA} \\
& \times (-)^{L_\beta + l'_{xA} + l'_{xb}} i^{L'_\beta - L'_\alpha - l} (-)^{(|m_{xA}| - m_{xA})/2} \\
& \times (l_{xA}, -m_{xA} L_\beta m_{xA} | J0) (l_{xb} 0 L_\alpha 0 | J0) W(l'_{xA} l'_{xb} L'_\beta L'_\alpha; lJ) \\
& \times \left[\frac{(L_\beta - |M_\beta|)!}{(L_\beta + |M_\beta|)!} \right]^{1/2} P_{L_\beta M_\beta}(\cos\theta). \qquad (3.86)
\end{aligned}
$$

If $m_{xA} \geq 0$, we can rewrite Eq. (3.86) by

$$
\begin{aligned}
T_{l_{xb}l_{xA}m_{xA}} = \mathscr{J} \sum_{lJ} \sum_{l'_{xA}L_\beta L'_\beta} \sum_{l'_{xb}L_\alpha L'_\alpha} & A_l I^{ll_{xA}l'_{xA}l_{xb}l'_{xb}ij}_{JL_\alpha L'_\alpha L_\beta L'_\beta} \hat{L}_\alpha \hat{L}_\beta \hat{l}\hat{l}'_{xA} \\
& \times (-)^{L_\beta + l'_{xA} + l'_{xb}} i^{L'_\beta - L'_\alpha - l} \\
& \times (l_{xA}, -m_{xA} L_\beta m_A | J0) (l_{xb} 0 L_\alpha 0 | J0) W(l'_{xA} l'_{xb} L'_\beta L'_\alpha; lJ) \\
& \times \left[\frac{(L_\beta - m_{xA})!}{(L_\beta + m_{xA})!} \right]^{1/2} P_{L_\beta m_{xA}}(\cos\theta), \qquad (3.87) \\
T_{l_{xb}l_{xA},-m_{xA}} = (-)^{l_{xA}+m_{xA}} \mathscr{J} \sum_{lJ} \sum_{l'_{xA}L_\beta L'_\beta} \sum_{l'_{xb}L_\alpha L'_\alpha} & A_l I^{ll_{xA}l'_{xA}l_{xb}l'_{xb}ij}_{JL_\alpha L'_\alpha L_\beta L'_\beta} \hat{L}_\alpha \hat{L}_\beta \hat{l}\hat{l}'_{xA} \\
& \times (-)^{L_\beta + l'_{xA} + l'_{xb}} i^{L'_\beta - L'_\alpha - l} \\
& \times (-)^{L_\beta - J} (l_{xA}, -m_{xA} L_\beta m_{xA} | J0) (l_{xb} 0 L_\alpha 0 | J0) W(l'_{xA} l'_{xb} L'_\beta L'_\alpha; lJ) \\
& \times \left[\frac{(L_\beta - m_{xA})!}{(L_\beta + m_{xA})!} \right]^{1/2} P_{L_\beta m_{xA}}(\cos\theta). \qquad (3.88)
\end{aligned}
$$

Eq. (3.88) can be expressed as

$$T_{l_{xb}l_{xA},-m_{xA}} = (-)^{l_{xA}+m_{xA}}\hat{\pi}_{\alpha\beta}T_{l_{xb}l_{xA}m_{xA}}, \tag{3.89}$$

where $\hat{\pi}_{\alpha\beta}$ is the operator which reproduces the phase factor $(-)^{L_\beta - J}$ in the L_β- and J-sums when $\pi_{\alpha\beta}$ operates $T_{l_{xb}l_{xA}m_{xA}}$ for $m_{xA} \geq 0$.

Then the transfer cross section is given by

$$\frac{d\sigma}{d\Omega} = \mathscr{S}\frac{\mu_\alpha\mu_\beta}{(2\pi\hbar^2)^2}\frac{k_\beta}{k_\alpha}\sum_{m_{xA}=-l_{xA}}^{l_{xA}}\left|T^l_{l_{xb}l_{xA}m_{xA}}\right|^2, \tag{3.90}$$

where μ_α and μ_β are the reduced masses for the initial and final channels, respectively. Equation (3.90) does not specify the z-components of particles' spins. Therefore it includes the spin factor $\mathscr{S}$ defined by

$$\mathscr{S} \equiv \frac{\hat{J}_B^2}{\hat{J}_A^2\hat{s}_x^2\hat{l}_{xA}^2}, \tag{3.91}$$

which comes out by taking an average over the initial spin orientations and a sum over them in the final channel. We only have to consider $\mathscr{S}$ as the spin dependent part, where s_X or J_X is the intrinsic spin of the particle X. The derivation of Eq. (3.91) is given in Appx. E. Note that l_{xb} is determined by the incident condition and also l_{xA} can be assumed from an observation condition.

Sometimes the zero-range (ZR) approximation is used for the overlap integral $I^{ll_{xA}l'_{xA}l_{xb}l'_{xb}ij}_{JL_\alpha L'_\alpha L_\beta L'_\beta}$. to save the computational cost. In the ZR approximation it is assumed that, in the form factor, the range of D^i_{xb} defined by

$$D^i_{xb}(\boldsymbol{r}_{xb}) = V_{xb}(\boldsymbol{r}_{xb})\psi^i_{xb}(\boldsymbol{r}_{xb}) \tag{3.92}$$

is short and it can be expressed by the δ-function, $D^i_{xb}(\boldsymbol{r}_{xb}) \sim \delta(\boldsymbol{r}_{xb})$. Equation (3.79) with the ZR approximation is rewritten as

$$\begin{aligned} I^{ll_{xA}l'_{xA}}_{JL_\beta L'_\beta} = {} & \frac{\sqrt{4\pi}}{k_\alpha k_\beta}\frac{B}{A}D^i_0\frac{\hat{J}\hat{L}'_\beta}{\hat{l}}\left(L'_\beta 0 J 0|l 0\right) \\ & \times\int dr_\alpha \chi^{Jjj_0}_{L_\beta L'_\beta l_A l'_{xA}}\left(k_\beta, \frac{A}{B}r_\alpha\right)\phi^{j*}_{l'_A}(r_\alpha)\chi^{Jii_0}_\alpha(k_\alpha, r_\alpha) \end{aligned} \tag{3.93}$$

with

$$D^i_0 = \int d\boldsymbol{r}_{xb}D^i_{xb}(\boldsymbol{r}_{xb}). \tag{3.94}$$

Note that in the ZR approximation the transition from non s-wave of ψ^i_{xb} is neglected because that components cannot be represented by the δ-function. See Appx. C for more detail.

3.3.3 Distorted-wave Born approximation (DWBA)

In this subsection we simplify the formula of the T matrix by neglectiing any CC effects, that is DWBA. For DWBA, the three-body wave function $\Psi_\alpha^{(+)}$ and $\Psi_\beta^{(+)}$ can be written by

$$\Psi_\alpha^{(+)} = \Phi_{a;l_{xb}m_{xb}}\chi^{(+)}_{m_{xb}}(\boldsymbol{k}_\alpha, \boldsymbol{r}_\alpha), \tag{3.95}$$

$$\chi^{(+)}_{m_{xb}}(\boldsymbol{k}_\alpha, \boldsymbol{r}_\alpha) = \frac{4\pi}{k_\alpha r_\alpha}\sum_{JL_\alpha} i^{L_\alpha}\chi^J_{L_\alpha}(k_\alpha, r_\alpha) \times \sum_{\mu M_\alpha}(l_{xb}m_{xb}L_\alpha M_\alpha|J\mu)\, Y^*_{L_\alpha M_\alpha}(\hat{\boldsymbol{k}}_\alpha)Y_{L_\alpha M_\alpha}(\hat{\boldsymbol{r}}_\alpha), \tag{3.96}$$

$$\Psi_\beta^{(+)} = \Phi_{B;l_{xA}m_{xA}}\chi^{(+)}_{m_{xA}}(\boldsymbol{k}_\beta, \boldsymbol{r}_\beta), \tag{3.97}$$

$$\chi^{(+)}_{m_{xA}}(\boldsymbol{k}_\beta, \boldsymbol{r}_\beta) = \frac{4\pi}{k_\beta r_\beta}\sum_{JL_\beta} i^{L_\beta}\chi^J_{L_\beta}(k_\beta, r_\beta) \times \sum_{\mu M_\beta}(l_{xA}m_{xA}L_\beta M_\beta|J\mu)\, Y^*_{L_\beta M_\beta}(\hat{\boldsymbol{k}}_\beta)Y_{L_\beta M_\beta}(\hat{\boldsymbol{r}}_\beta). \tag{3.98}$$

The T matrix with DWBA can be easily derived by following similar way as in CCBA. For $m_{xA} \geq 0$, we obtain

$$T_{l_{xb}l_{xA}m_{xA}} = \mathscr{J}\sum_{Jl L_\beta L_\alpha} A_l I^l_{JL_\alpha L_\beta}\hat{l}\hat{L}_\beta(-)^{l_{xb}+l_{xA}}i^{L_\alpha+L_\beta+l} \times W(l_{xA}l_{xb}L_\beta L_\alpha; lJ)\left[\frac{(L_\beta - m_{xA})!}{(L_\beta + m_{xA})!}\right]^{1/2} P_{L_\beta m_{xA}}(\cos\theta) \tag{3.99}$$

with the overlap integral $I^l_{JL_\alpha L_\beta}$ defined by

$$I^l_{JL_\alpha L_\beta} \equiv \frac{4\pi}{k_\alpha k_\beta}\int r_\alpha dr_\alpha \int r_\beta dr_\beta \chi^J_{L_\beta}(k_\beta, r_\beta)F_{lL_\beta L_\alpha}(r_\beta, r_\alpha)\chi^J_{L_\alpha}(k_\alpha, r_\alpha). \tag{3.100}$$

3.4 The ^{8}B(d,n)^{9}C reaction

3.4.1 Background

As a first application, we focus on the transfer reaction ^{8}B(d,n)^{9}C at 14.4 MeV/nucleon. The projectile d is loosely bound with its binding energy 2.22 MeV. In addition, the residual nucleus ^{9}C is a proton-rich unstable nucleus; its proton separation energy is 1.30 MeV. Thus to describe the transfer reaction precisely, one should take into account the breakup effects of d and ^{9}C and investigate how significant these effects on the transfer cross section.

The ^{8}B(d,n)^{9}C reaction has been paid attention with an astrophysical interest [108, 119]. Its cross section was measured [108] to indirectly determine the reaction rate of the proton capture reaction of ^{8}B, ^{8}B(p,γ)^{9}C. The ^{8}B(p,γ)^{9}C reaction in low-metallicity supermassive stars, is expected to lead the process called hot pp chain [119]:

$$^8\mathrm{B}(p,\gamma)^9\mathrm{C}(\alpha,p)^{12}\mathrm{N}(p,\gamma)^{13}\mathrm{O}(\beta^+\nu)^{13}\mathrm{N}(p,\gamma)^{14}\mathrm{O}. \tag{3.101}$$

The hot pp chain can be a possible alternative path to the synthesis of the CNO elements. Thus determination of the cross section $\sigma_{p\mathrm{B}}$ of the ^{8}B(p,γ)^{9}C reaction is important to understand the process. It is, however, difficult to measure $\sigma_{p\mathrm{B}}$ since the $\varepsilon_{p\mathrm{B}}$-dependence of $\sigma_{p\mathrm{B}}$ is quite strong, in particular, at low energy it has extremely small value. Therefore, instead of the cross section, the astrophysical factor,

$$S_{18}(\varepsilon_{p\mathrm{B}}) = \varepsilon_{p\mathrm{B}}\sigma_{p\mathrm{B}}(\varepsilon_{p\mathrm{B}})\exp[2\pi\eta], \tag{3.102}$$

which has weak energy dependence has been evaluated from several alternative measurements [108, 120, 121]. In particular S_{18} at zero energy, $S_{18}(0)$ is important to estimate since a typical stellar energy is extremely small. For example, the temperature of the sun at its center, 1.5×10^7 K, corresponds to around 1 keV. Here, η is the Sommerfeld parameter. Below, comparison of the calculated cross section and experimental data, and prospect to astrophysics are also given.

3.4.2 Numerical setting

In the ^{8}B(d,n)^{9}C reaction, p, n, and ^{8}B respectively corresponds to x, b, and A describe in Chap. 3.3. In this analysis $\psi^j_{p\mathrm{B}}$ is regarded as the overlap function of ^{9}C with the p-^{8}B(g.s.) configuration. Since the ground state of ^{9}C includes the component that cannot be described by the p-^{8}B(g.s.) configuration, $\psi^{j_0}_{p\mathrm{B}}$ has to be normalized by the square root of the spectroscopic factor $\mathcal{S}$. The breakup components $\psi^j_{p\mathrm{B}}$ ($j\neq j_0$) also have to be normalized by the same factor $\sqrt{\mathcal{S}}$, because

$$\begin{aligned}\Psi^{(+)}_\beta(\boldsymbol{r}_{p\mathrm{B}},\boldsymbol{r}_\beta) &= \lim_{\varepsilon\to+0}\frac{i\varepsilon}{E-H_\beta+i\varepsilon}e^{i\boldsymbol{k}_\beta\cdot\boldsymbol{r}_\beta}\sqrt{\mathcal{S}}\psi^{j_0}_{p\mathrm{B}}(\boldsymbol{r}_{p\mathrm{B}})\\ &= \sqrt{\mathcal{S}}\lim_{\varepsilon\to+0}\frac{i\varepsilon}{E-H_\beta+i\varepsilon}e^{i\boldsymbol{k}_\beta\cdot\boldsymbol{r}_\beta}\psi^{j_0}_{p\mathrm{B}}(\boldsymbol{r}_{p\mathrm{B}});\end{aligned} \tag{3.103}$$

note that the $\psi^j_{p\mathrm{B}}$ ($j \neq j_0$) are generated by the Mϕller wave operator $i\varepsilon/(E - H_\beta + i\varepsilon)$. Here, $\mathcal{S}$ has only one quantum number, i.e., $l_{p\mathrm{B}} = 1$ in the ground state of ^{9}C. This is due to the neglect of the intrinsic spin of each particle in the present study. Thus $\mathcal{S}$ is understood as an averaged value of the $\mathcal{S}$'s, each with a different value of the total angular momentum of the p-^{8}B(g.s.) system.

We adopt the one-range Gaussian interaction [122] for V_{pn}. The pseudo state method described in Sec. 2.1.3 with the real-range Gaussian basis functions [111] is used for obtaining the discretized-continuum states of d; we include the s- and d-states with neglecting the intrinsic spin of d. The number of the basis functions taken is 20, and the minimum (maximum) range parameter of Gaussian is 1.0 (30.0) fm. In CDCC we include the pseudostates with $\varepsilon^i_{pn} < 65$ MeV and $\varepsilon^i_{pn} < 80$ MeV for the s- and d-states, respectively. To obtain $\Psi^{(+)}_\alpha$, ψ^i_{pn} is calculated up to $r_{pn} = 100.0$ fm. The number of the partial waves for $\chi^{ii_0(+)}_\alpha$ and $\chi^{jj_0(-)}_\beta$ is 25. The maximum value of r_α and r_β for them are 25.0 and 20.0 fm, respectively. Thus for describing the transfer reaction, Eq. (3.63) is integrated over $\boldsymbol{r}_\alpha$ and $\boldsymbol{r}_\beta$ up to these values.

In the calculation of $\psi^j_{p\mathrm{B}}$ in the final channel, we adopt a Woods-Saxon central potential

$$V_{p\mathrm{B}}(r_{p\mathrm{B}}) = V_0 \left[1 + e^{(r_{p\mathrm{B}} - R_0)/a_0}\right]^{-1} \tag{3.104}$$

as $V_{p\mathrm{B}}$ with the radial parameter $R_0 = 1.25 \times 8^{1/3}$ fm and the diffuseness parameter $a_0 = 0.65$ fm. Its depth V_0 is determined to reproduce the proton separation energy of 1.30 MeV in the p-state. The interaction between a point charge and a uniformly charged sphere with the charge radius 2.5 fm is used as $V^{(\mathrm{C})}_{p\mathrm{B}}$, which is used also in the CDCC calculation in the initial channel. The pseudo state method is also used for the final channel. For the expansion of $\psi^j_{p\mathrm{B}}$ we take 20 Gaussian basis functions with the minimum (maximum) range parameter of 1.0 (20.0) fm. We take into account the s-, p-, d-, f-, and g-waves of

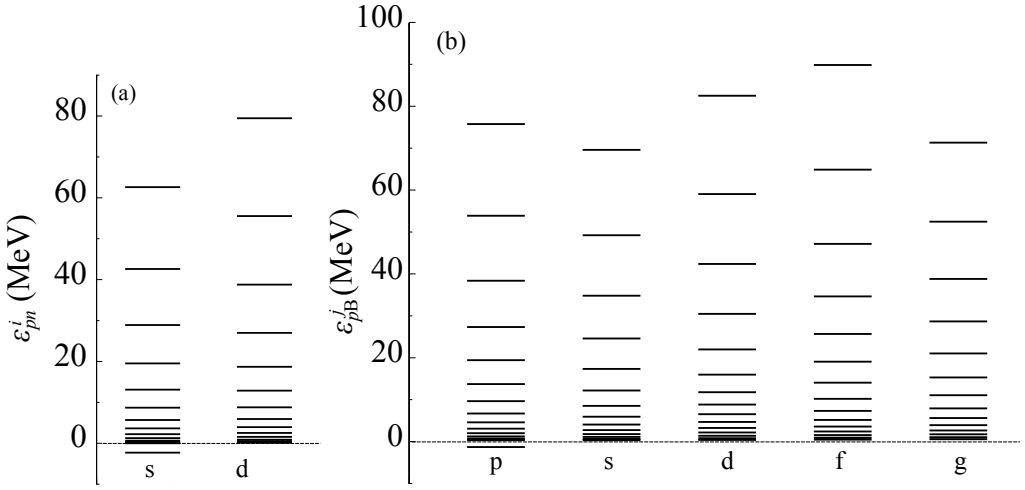

Figure 3.3: The eigenenergy of (a) ε^i_{pn} ((b) $\varepsilon^j_{p\mathrm{B}}$) for the each partial wave of ψ^i_{pn} ($\psi^j_{p\mathrm{B}}$).

$\psi^j_{p\mathrm{B}}$ with the maximum values of $\varepsilon^j_{p\mathrm{B}}$ of 70, 75, 85, 90, and 70 MeV, respectively. $\psi^j_{p\mathrm{B}}$ is calculated up to $r_{p\mathrm{B}} = 100.0$ fm. The Calculated energy spectra for ψ^i_{pn} and $\psi^j_{p\mathrm{B}}$ are shown in Fig. 3.3.

As for $U^{(\alpha)}_{p\mathrm{B}}$, $U^{(\alpha)}_{n\mathrm{B}}$, and $U^{(\beta)}_{n\mathrm{B}}$, we adopt the nucleon global optical potential for p-shell nuclei by Watson *et al.* [123] (WA). The non-local correction proposed by Timofeyuk and Johnson [124–126] (TJ) to the nucleon distorting potentials in the initial channel is used. Note that the TJ correction can effectively treat the non-locality of the deuteron optical potential, which consists of the nucleon optical potentials. The calculated energy shift [124–126] with the above mentioned p-n model is 17.8 MeV in the c.m. frame. The detail of the calculation of this energy shift is summarized in Appx. H. We thus evaluate $U^{(\alpha)}_{p\mathrm{B}}$ and $U^{(\alpha)}_{n\mathrm{B}}$ at 33.0 MeV in the laboratory frame, which is shifted from the incident energy of 14.4 MeV/nucleon. The non-local correction to $U^{(\beta)}_{n\mathrm{B}}$ is made following Perey and Buck [127] with the non-local parameter $\beta = 0.85$ fm.

We include only the s-states of ψ^i_{pn}, consisting of the ground and discretized-continuum states, in the calculation of the T matrix of the transfer process. It should be noted that the coupling between the s- and d-states of ψ^i_{pn} is taken into account in the calculation of $\Psi^{(+)}_\alpha$ with CDCC. It is found that D^i_{pn} defined below by Eq. (3.113) is negligibly small for the d-states of the deuteron, which justifies the neglect of them in the transfer process.

3.4.3 Breakup effects of d and ^{9}C on transfer cross section

We show in Fig. 3.4 the cross section of the transfer reaction ^{8}B(d,n)^{9}C at 14.4 MeV/nucleon as a function of the neutron emission angle in the c.m. frame. The thick (thin) solid line shows the cross section calculated with (without) the breakup states of both d and ^{9}C. Inclusion of the breakup channels gives large increase of about 58% in the cross section at 0°.

To see the breakup effects in more detail, we decompose the T matrix into

$$T_{\beta\alpha} = T_{\beta(\mathrm{el}),\alpha(\mathrm{el})} + T_{\beta(\mathrm{el}),\alpha(\mathrm{br})} + T_{\beta(\mathrm{br}),\alpha(\mathrm{el})} + T_{\beta(\mathrm{br}),\alpha(\mathrm{br})}, \tag{3.105}$$

$$T_{\beta(\mathrm{el}),\alpha(\mathrm{el})} \equiv \left\langle \psi^{j_0}_{p\mathrm{B}} \chi^{j_0 j_0(-)}_\beta \middle| V_{pn} \middle| \psi^{i_0}_{pn} \chi^{i_0 i_0(+)}_\alpha \right\rangle, \tag{3.106}$$

$$T_{\beta(\mathrm{el}),\alpha(\mathrm{br})} \equiv \left\langle \psi^{j_0}_{p\mathrm{B}} \chi^{j_0 j_0(-)}_\beta \middle| V_{pn} \middle| \sum_{i\neq i_0} \psi^{i}_{pn} \chi^{i i_0(+)}_\alpha \right\rangle, \tag{3.107}$$

$$T_{\beta(\mathrm{br}),\alpha(\mathrm{el})} \equiv \left\langle \sum_{j\neq j_0} \psi^{j}_{p\mathrm{B}} \chi^{j j_0(-)}_\beta \middle| V_{pn} \middle| \psi^{i_0}_{pn} \chi^{i_0 i_0(+)}_\alpha \right\rangle, \tag{3.108}$$

$$T_{\beta(\mathrm{br}),\alpha(\mathrm{br})} \equiv \left\langle \sum_{j\neq j_0} \psi^{j}_{p\mathrm{B}} \chi^{j j_0(-)}_\beta \middle| V_{pn} \middle| \sum_{i\neq i_0} \psi^{i}_{pn} \chi^{i i_0(+)}_\alpha \right\rangle. \tag{3.109}$$

The T matrix with the subscript $\gamma(\mathrm{el})$ and $\gamma(\mathrm{br})$ corresponds to the elastic transfer (ET) and the breakup transfer (BT) in the γ channel, respectively. A schematic picture of the ET and BT is shown in Fig. 3.5. $T_{\beta(\mathrm{el}),\alpha(\mathrm{el})}$ describes the transition from the ground channel in the

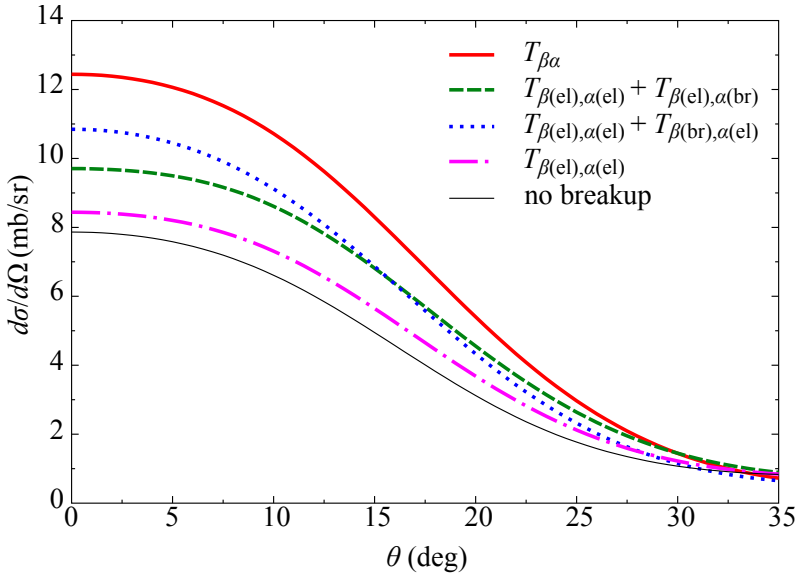

Figure 3.4: Breakup effects of d and ^{9}C on the cross section of ^{8}B(d,n)^{9}C at 14.4 MeV/nucleon as a function of the neutron emission angle in the c.m. frame. The thick solid and thin solid lines show, respectively, the results with and without the breakup states of both d and ^{9}C. The dashed (dotted) line represents the result with neglecting the breakup states of d (^{9}C) in the T matrix $T_{\beta\alpha}$. The cross section corresponding to the elastic transfer is shown by the dash-dotted line. See the text for detail.

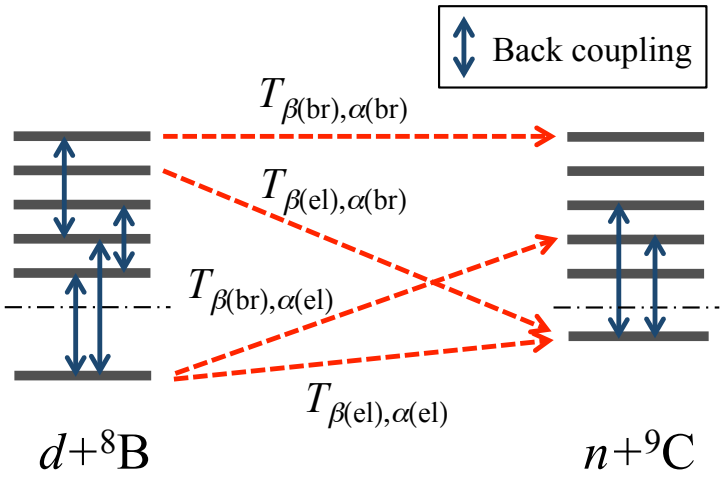

Figure 3.5: Illustration of the transfer processes. The transition from the initial channel (d+^{8}B) to the final channel (n+^{9}C) can be described by four T-matrix elements. See text for more detail.

initial channel (d+^{8}B system) to the ground channel in the final channel (n+^{9}C system), that is, the ET. Note that the ET includes the breakup effects through the back couplings, which is the channel couplings between the ground state and the discretized-continuum states in each channel. $T_{\beta(\mathrm{el}),\alpha(\mathrm{br})}$ $\left(T_{\beta(\mathrm{br}),\alpha(\mathrm{el})}\right)$ corresponds to the BT, which represents the transition from the breakup (ground) channel of d to the ground (breakup) channel of ^{9}C. The transfer process between the breakup channels in each channel is expressed by $T_{\beta(\mathrm{br}),\alpha(\mathrm{br})}$.

The dash-dotted line in Fig. 3.4 shows the cross section due to the ET, which includes the back couplings. The small difference between the thin solid line and the dash-dotted line indicates that those back-coupling effects are not significant in the present case. In other words, the ET can be described by the DWBA model because the small back-coupling effects are expected to be involved as the imaginary part of the optical potentials in the DWBA for the d-^{8}B and n-^{9}C systems. The dashed line shows the result including the breakup states of only d, which is by about 23% larger than the thin solid line at 0°. It is also found that the transfer cross section through the breakup states of d, which is calculated with only $T_{\beta(\mathrm{el}),\alpha(\mathrm{br})}$ is less than 1% of the dashed line. We thus conclude that the increase in the cross section caused by the breakup states of d is due to the interference between $T_{\beta(\mathrm{el}),\alpha(\mathrm{el})}$ and $T_{\beta(\mathrm{el}),\alpha(\mathrm{br})}$. This conclusion holds also for the role of the breakup states of ^{9}C; large interference between $T_{\beta(\mathrm{el}),\alpha(\mathrm{el})}$ and $T_{\beta(\mathrm{br}),\alpha(\mathrm{el})}$ increases the cross section by about 38% at 0° as shown by the dotted line. Furthermore, it is found numerically that the contribution of $T_{\beta(\mathrm{br}),\alpha(\mathrm{br})}$ on the cross section is negligibly small.

These properties of the numerical result can be understood as follows. If we make the adiabatic approximation [128–132] to $\Psi_\alpha^{(+)}$, we have

$$\Psi_\alpha^{(+)}(\boldsymbol{r}_{pn},\boldsymbol{r}_\alpha) \approx \psi_{pn}^{i_0}(\boldsymbol{r}_{pn})\chi_\alpha^{\mathrm{AD}(+)}(\boldsymbol{r}_{pn},\boldsymbol{r}_\alpha). \tag{3.110}$$

Note that in the adiabatic approximation, the eigenenergy ε_{pn}^i is replaced by the ground state energy $\varepsilon_{pn}^{i_0}$, and then $\boldsymbol{r}_{pn}$ is no longer the dynamical variable. The adiabatic wave function $\chi_\alpha^{\mathrm{AD}(+)}$ satisfies

$$\left[K_{\boldsymbol{r}_\alpha}+U_{p\mathrm{B}}^{(\alpha)}(r_{p\mathrm{B}})+U_{n\mathrm{B}}^{(\alpha)}(r_{n\mathrm{B}})-E_\alpha\right]\chi_\alpha^{\mathrm{AD}(+)}(\boldsymbol{r}_{pn},\boldsymbol{r}_\alpha)=0, \tag{3.111}$$

where $E_\alpha = E+\varepsilon_{pn}^{i_0}$. The $\boldsymbol{r}_{pn}$ dependence of $U_{N\mathrm{B}}^{(\alpha)}$ ($N=p$ or n) gives that of $\chi_\alpha^{\mathrm{AD}(+)}$. Consequently, $\Psi_\alpha^{(+)}$ contains not only the elastic-channel but also the breakup-channel components:

$$\chi_\alpha^{ii_0\mathrm{AD}(+)}(\boldsymbol{r}_\alpha) \equiv \langle\psi_{pn}^i(\boldsymbol{r}_{pn})|\psi_{pn}^{i_0}(\boldsymbol{r}_{pn})\chi_\alpha^{\mathrm{AD}(+)}(\boldsymbol{r}_{pn},\boldsymbol{r}_\alpha)\rangle. \tag{3.112}$$

The $\boldsymbol{r}_{pn}$ dependence of $U_{N\mathrm{B}}^{(\alpha)}$ is, however, quite weak within the range of V_{pn}. Then one can expect that for $\chi_\alpha^{ii_0\mathrm{AD}(+)}$ with $i\neq i_0$, the amplitude is quite smaller than that of $\chi_\alpha^{i_0i_0\mathrm{AD}(+)}$ because of $\langle\psi_{pn}^i|\psi_{pn}^{i_0}\rangle \sim 0$ and the phase is very similar to that of $\chi_\alpha^{i_0i_0\mathrm{AD}(+)}$ owing to $\langle\psi_{pn}^i|\psi_{pn}^{i_0}\rangle \sim 1$. The former is the reason for the very small contribution of the BT and the latter is that for the constructive interference between the ET and BT amplitudes.

These properties have been confirmed numerically. In Fig. 3.6, we show the moduli of the distorted wave $\chi_\alpha^{ii_0(+)}$ for the elastic component $i=i_0$ (thick solid line) and the

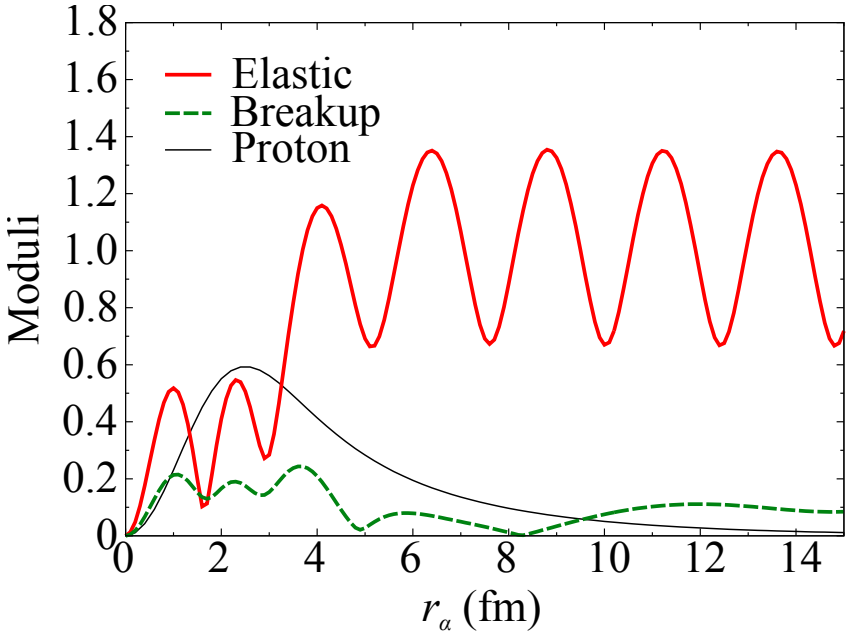

Figure 3.6: Moduli of the distorted wave $\chi_\alpha^{ii_0(+)}$ for the elastic component $i = i_0$ (thick solid line) and the breakup component $i \neq i_0$ (dashed line). The thick solid line is the proton-^{8}B wave function $\psi_{p\mathrm{B}}^{j_0}$. These moduli correspond to the $L_\alpha = 1$ partial wave, which is calculated within the ZR limit. See the text for more detail.

breakup component $i \neq i_0$ (dashed line). The former and latter are respectively defined by $\left|\chi_\alpha^{i_0 i_0(+)}\right|^2$ and $\left|\frac{D_{pn}^i}{D_{pn}^{i_0}}\chi_\alpha^{i_0 i_0(+)}\right|^2$, where D_i and D_i are respectively defined by Eqs. (3.92) and (3.94). The thin solid line is the proton single-particle wave function $\psi_{p\mathrm{B}}^{j_0}$. Note that we take only the $L_\alpha = 1$ partial wave for this moduli, for which the ZR approximation is adopted for simplicity. In the ZR limit, from Eq. (3.93), one can easily understand that the distorted wave only within the range of $\psi_{p\mathrm{B}}^{j_0}$ contributes to the transition amplitude. Therefore, if we see the region of r_α lower than around 8 fm, it can be seen that the phases of the solid and dashed lines are similar to each other and the latter has small amplitude compared to that of the former. This interpretation of the breakup effects can be applied to also $\Psi_\beta^{(-)}$ in the final channel. It should be noted that the adiabatic approximation [128–132] itself is found to work well; it makes the cross section smaller by about 6% (12%) when applied to $\Psi_\alpha^{(+)}$ $\left(\Psi_\beta^{(-)}\right)$.

The non-negligible BT component in each channel is opposite to what found in the analysis [106] of ^{13}C(^{6}Li,d)^{17}O below the Coulomb barrier energy, in which breakup effects of ^{6}Li ($= \alpha + d$) were investigated. Below we discuss the difference between the breakup properties of d and ^{6}Li in the two reactions. The origin of the difference can be understood from behavior of D_{pn}^i defined by

$$D_{pn}^i(r_{pn}) = V_{pn}(r_{pn})\phi_{pn}^i(r_{pn}), \tag{3.113}$$

where ϕ^i_{pn} is the radial part of ψ^i_{pn}. Eq. (3.113) is also defined for the α-d system:

$$D^i_{\alpha d}(r_{\alpha d}) = V_{\alpha d}(r_{\alpha d})\phi^i_{\alpha d}(r_{\alpha d}), \tag{3.114}$$

where the two-range Gaussian interaction $V_{\alpha d}$ given in Ref. [133] is adopted to generate the radial part $\phi^i_{\alpha d}$ of the s-wave eigenstate $\psi^i_{\alpha d}$. We show in panel (a) of Fig. 3.7 D^i_{pn} for some s-wave eigenstates of d; the eigenvalue ε^i_{pn} is given in the legend. Similarly, we plot $D^i_{\alpha d}$ in panel (b) of Fig. 3.7.

In panels (a) and (b) of Fig. 3.7, respectively, D^i_{pn} and $D^i_{\alpha d}$ for some eigenstates are plotted. One sees that the amplitude of D^i_{pn} for breakup states (the dashed and dotted lines) are comparable to that of $D^{i_0}_{pn}$ (solid line). On the other hand, $D^i_{\alpha d}$ for the breakup states are quite smaller than $D^{i_0}_{\alpha d}$, which is found to be due to the Coulomb interaction between α and d. Thus, difference in the BT components between the ^{8}B(d,n)^{9}C and ^{13}C(^{6}Li,d)^{17}O

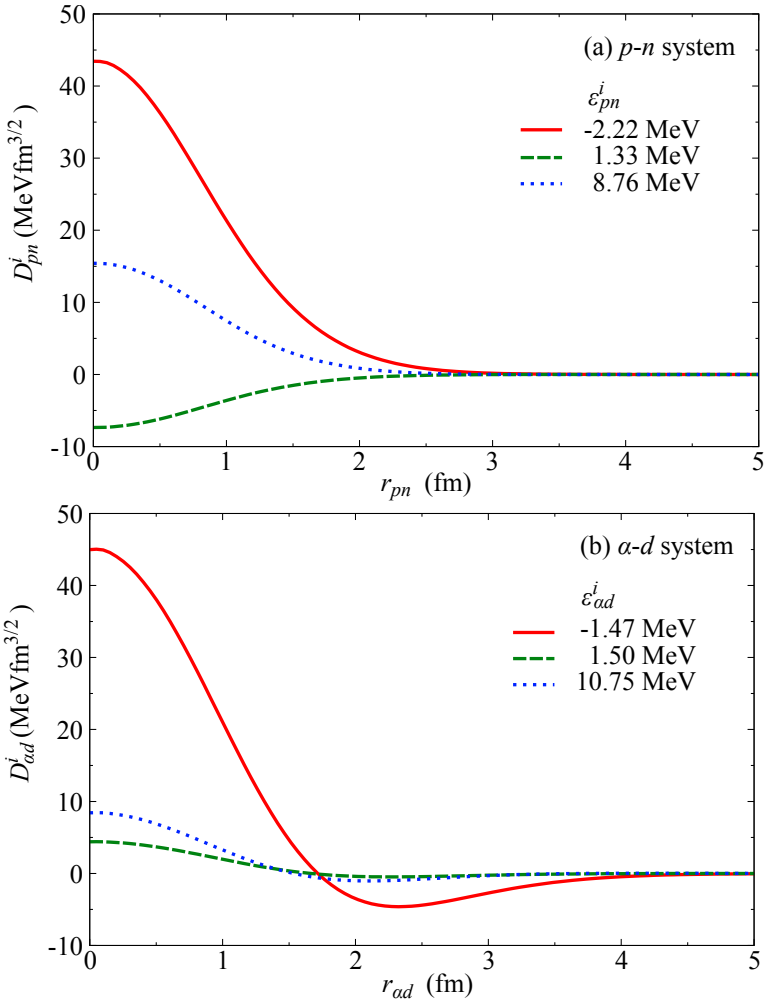

Figure 3.7: (a) D^i_{pn} for several ith states with the eigenenergy ε^i_{pn}. (b) Same as in panel (a) but for the α-d system.

reactions can be understood. It should be noted that a large value of D^i for a breakup state does not necessarily give a large BT cross section, because even in this case $\chi_\alpha^{ii_0}$ can be small as a result of the channel-couplings. Furthermore, the importance of the back-coupling effect depends on the reaction system in a non-trivial manner.

Another important finding is that the breakup channels in non p-state of ^{9}C play significant role on the transfer reaction. When we include the breakup states of $\psi^j_{p\mathrm{B}}$ with $l'_{p\mathrm{B}} \neq 1$, the transfer angular momentum of $l \neq 1$ can contributes to the transfer reaction. This is a quite interesting phenomenon, which has not been discussed so far. In usual DWBA analysis, if the projectile is an s-wave state, $l_{pn} = 0$, l is uniquely determined as $l = l_{p\mathrm{B}}$ from its definition of Eq. (3.67). However, l in the breakup states defined by Eq. (3.68) can be different even if $l_{pn} = l'_{pn} = 0$. It means that we have two sources of the transferred angular momentum. In fig. 3.8, the dotted and thin solid lines show the transfer cross section calculated with and without the breakup states of ^{9}C, respectively, when we include only the p-wave states of $\psi^j_{p\mathrm{B}}$. The breakup channels of the p-wave states increase the cross section by about 25% at 0°. This calculation corresponds to usual CCBA approach, in which l is uniquely determined to be 1. When we include the p-, s-, d-, f-, and g-waves, one obtains the solid line, which is about 25% larger than the dotted line. This enhancement of the cross section is due to the contribution of the d-wave in particular, as shown by the dashed line corresponding to the calculation with only the p- and d-waves. Thus, not only the $l = 1$ component but also the $l = 2$ one in the T matrix play an important role in the

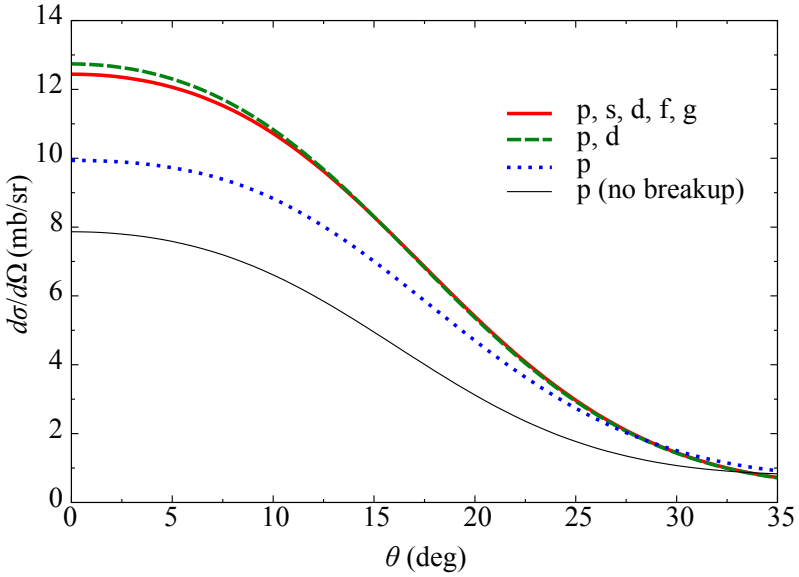

Figure 3.8: Contribution of the partial waves of $\psi^j_{p\mathrm{B}}$ on the cross section. The thick solid (dashed) line shows the cross section calculated with the p-, s-, d-, f-, g-waves (p-, and d-waves) of $\psi^j_{p\mathrm{B}}$. The cross section calculated with (without) the breakup states of ^{9}C in the only p-wave is shown by dashed (thin solid) line. The thick (thin) solid line is same as that in Fig. 3.4.

transfer reaction. This change of the transferred angular momentum l is brought from the channel couplings in the final channel. In other words, it is essential that $l_{p\mathrm{B}}$ couples to non p-waves in the intermediate state, described by Eq. (3.61).

This fact is expected to be due to the dynamical property of the present n-^{9}C system. We show, in Fig. 3.9, the partial breakup cross section (PBCS) of the ^{9}C on n at 22.1 MeV in the c.m. frame as a function of the n-^{9}C relative angular momentum L_β. The solid line is the total PBCS, which is defined by Eq.(2.52), while PBCSs defined by

$$\tilde{\sigma}_{\mathrm{bu}}^{j_0 l_{p\mathrm{B}};l'_{p\mathrm{B}}}(L_\beta) = \sum_j \tilde{\sigma}_{\mathrm{bu}}^{j_0 l_{p\mathrm{B}};jl'_{p\mathrm{B}}}(L_\beta), \tag{3.115}$$

for each partial wave $l_{p\mathrm{B}}$ of ^{9}C are plotted as other lines. Note that $\tilde{\sigma}_{\mathrm{bu}}^{j_0 l_{p\mathrm{B}};jl'_{p\mathrm{B}}}$ is defined by Eq. (2.53). Obviously the d-wave component (dash-dotted line) is dominant though the s-wave component (thick dotted line) has appreciable contribution. Other components, p (thick dotted line), f (thin dashed line), and g (thin dotted line), are negligibly small.

In Fig. 3.10, a simple picture of the breakup effects on the ^{8}B(d,n)^{9}C reaction, which enables us to correctly interpret the three-body dynamics of the present system, is illustrated. Important features of the transfer reaction are as follows:

1. The strong interferences between the ET and BT in each channel.
2. The weak back couplings and the small BT amplitude in each channel.

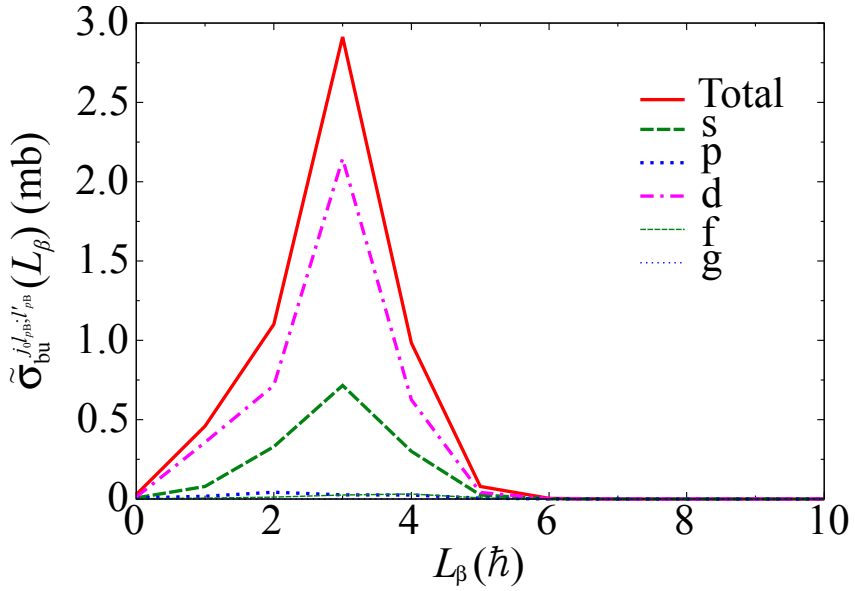

Figure 3.9: The partial breakup cross section for the n(^{9}C,p^8B) reaction at 22.1 MeV in the c.n. frame as a function of L_β. The solid line is the result of the total partial breakup cross section and the results for each partial wave $l_{p\mathrm{B}}$ of ^{9}C of $l_{p\mathrm{B}} = 0, 1, 2, 3,$ and 4 are respectively shown by the thick dashed, thick dotted, dash-dotted, thin dashed, and thin dotted lines.

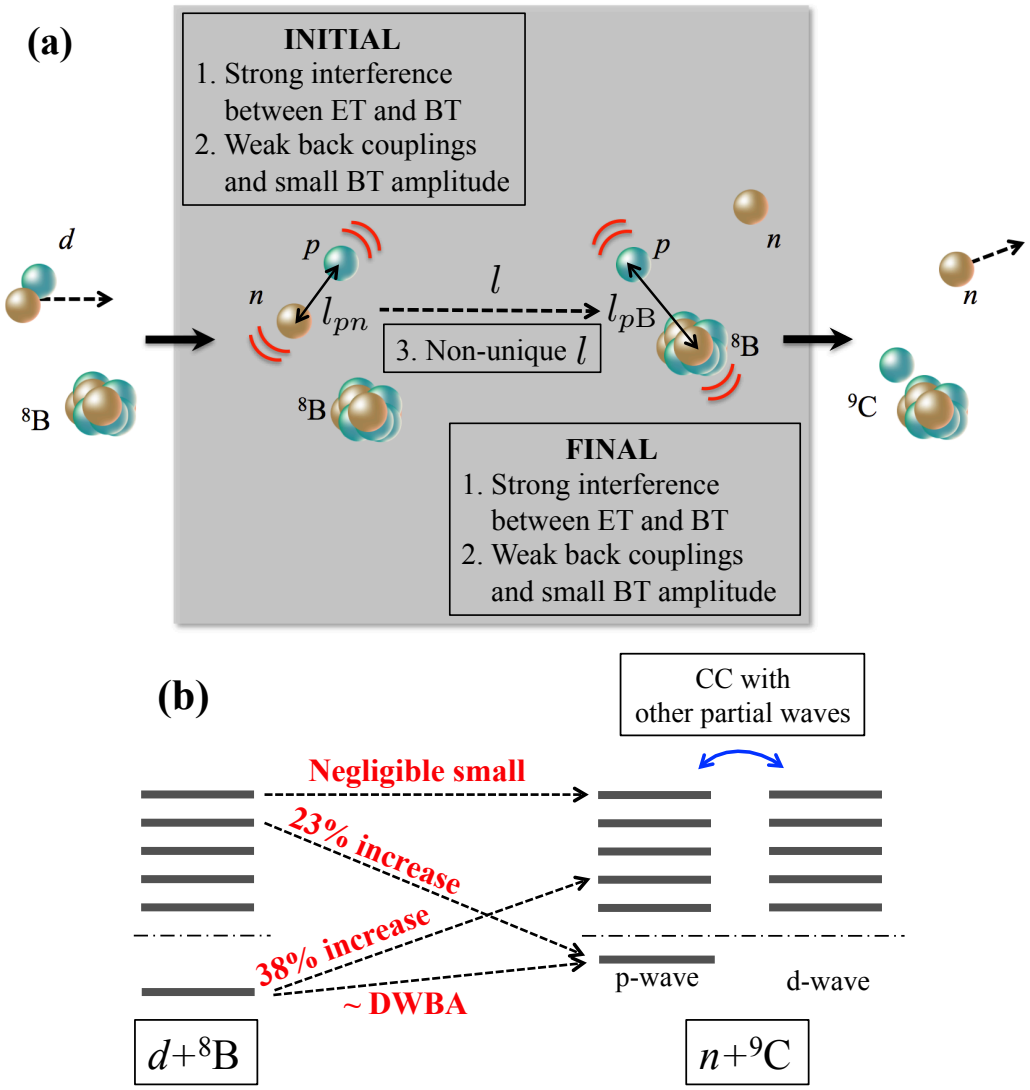

Figure 3.10: (a) The breakup effects of the transfer reaction in particular the contribution of the breakup channels and new feature such as the change of the transferred angular momentum are illustrated. (b) Schematic picture of the transfer process in the energy space is shown.

3. The change of l due to the channel couplings.

These features are completely different from the picture described by usual DWBA approach, in which any breakup effects are neglected and the proton is assumed to transfer into ^{8}B by a one-step process. We emphasize that the detail of the breakup effects of both the projectile and the residual nucleus is newly discussed by the present study.

3.4.4 Astrophysical study

In Fig. 3.11 the solid line shows the CCBA result. We have normalized the result to reproduce the experimental data [108] with multiplied by $\mathcal{S} = 0.361$. Note that from the present transfer reaction, $\mathcal{S}$ cannot be determined because the reaction is peripheral as confirmed below. Instead, the asymptotic normalization coefficient (ANC) [106, 134, 135] $C^{^9\mathrm{C}}_{p^8\mathrm{B}}$ for the overlap of the ^{9}C wave function with the p-^{8}B(g.s.) configuration is well determined. From $\mathcal{S}$ and the so-called single-particle ANC of $\psi^{j_0}_{p\mathrm{B}}$, one can obtain the ANC; $(C^{^9\mathrm{C}}_{p^8\mathrm{B}})^2 = 0.59$ fm^{-1}.

The uncertainty of the value of the ANC due to the distorting potential and peripherality of the reaction is examined in Ref. [136] By compiling the uncertainties due to peripherality (2%) and the optical potential (3%) as well as the experimental error of 22% [108], we obtain $(C^{^9\mathrm{C}}_{p^8\mathrm{B}})^2 = 0.59 \pm 0.02\ (\mathrm{theor.}) \pm 0.13\ (\mathrm{exp.})$ fm^{-1}, where (theor.) and (exp.) respectively stand for the theoretical and experimental uncertainties. Using the proportionality of $(C^{^9\mathrm{C}}_{p^8\mathrm{B}})^2$ to the astrophysical factor $S_{18}(0)$ defined by Eq. (3.102), we have

$$S_{18}(0) = 22 \pm 1\ (\mathrm{theor.}) \pm 5\ (\mathrm{exp.})\ \mathrm{eVb}. \tag{3.116}$$

Our resulting value of $S_{18}(0) = 22 \pm 6$ is by about 51% smaller than the result of the previous analysis evaluated from the same experimental data [108] with the DWBA analysis, which does not explicitly take into account the breakup states of nuclei. Thus, main reason of this discrepancy is expected to be due to the treatment of the breakup channels. As mentioned above, the back-coupling effects are found to be small in the present case. In fact, if we evaluate $C^{^9\mathrm{C}}_{p^8\mathrm{B}}$ and $S_{18}(0)$ from the thin solid line in Fig. 3.4, which ignore all of

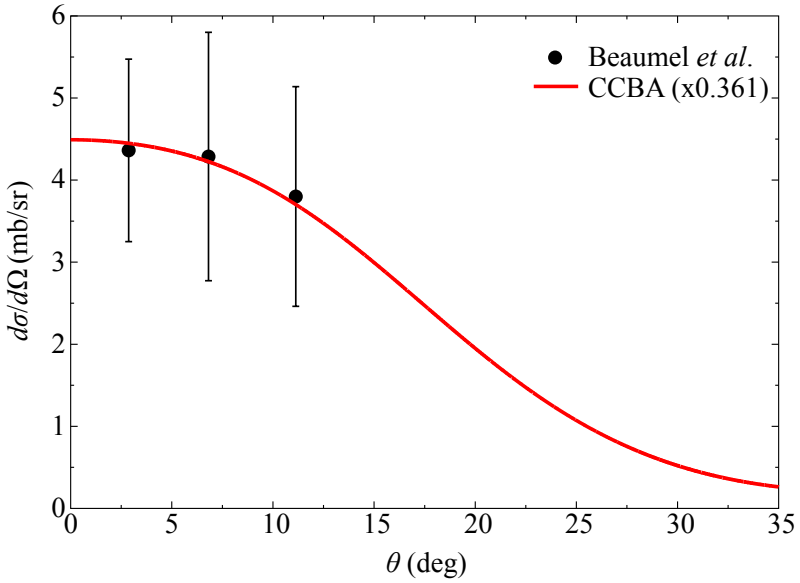

Figure 3.11: Cross section calculated with CCBA (solid line) is normalized to the experimental data [108].

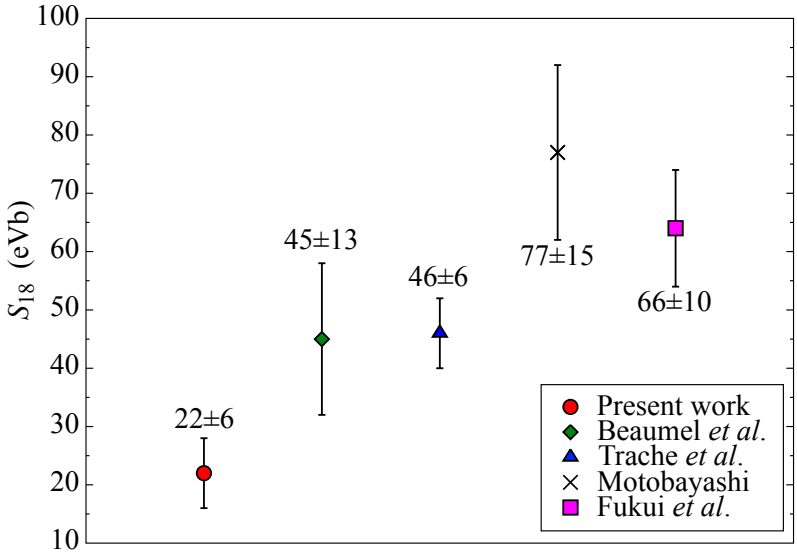

Figure 3.12: $S_{18}(0)$ in the present work (circle) is compared with the results evaluated from the ^{8}B(d,n)^{9}C reaction (diamond) [108] and values extracted from ^{9}C breakup reactions (triangle [120], cross [121], square [135]).

the breakup channels, we obtain $(C^{^9\mathrm{C}}_{p^8\mathrm{B}})^2 = 0.95$ fm^{-1} and $S_{18}(0) = 36$ eVb. This value is, within only about 2% difference, consistent with the result corresponding to the D1-N1 set for the distorting potentials, $(C^{^9\mathrm{C}}_{p^8\mathrm{B}})^2 = 0.97$ fm^{-1}, shown in Table 1 of Ref. [108]; the N1 corresponds to the WA potential. We have confirmed by our DWBA calculation that the result with the D1-N1 set agrees well with the thin solid line in Fig. 3.4. From these findings we conclude that inclusion of the breakup states of both d and ^{9}C is necessary to accurately describe the transfer reaction, which gives quite large increase in the cross section, that is, decrease in $S_{18}(0)$.

In fig 3.102, we compare our result of $S_{18}(0)$ with the previous results extracted from indirect measurements. As mentioned, we obtained a smaller $S_{18}(0)$ than that of Ref. [108] because of the contribution of d and ^{9}C breakup states. The present result is not consistent with the result of a three-body model analysis [135] of the inclusive [120] and exclusive [121] ^{9}C breakup reactions within 2σ. Further investigation is necessary to understand the reason for this discrepancy. Extension of the present framework to include breakup channels of ^{8}B as well as the three-body model description of ^{9}C will be important future work. Another possible reason for the discrepancy in $S_{18}(0)$ is the Pauli blocking effect on the transfer reaction [137, 138]. Antisymmetrization between a nucleon in d and that in ^{8}B in calculation of the d-^{8}B three-body wave function will be an important subject.

3.5 The ^{28}Si(d,p)^{29}Si reaction

3.5.1 Background

As another example we chose the ^{28}Si(d,p)^{29}Si. Since, the ground state of ^{29}Si can be regarded as an s-wave well bound nuclei with its n-^{28}Si binding energy of 7.69 MeV, we assume the breakup effects of ^{29}Si is negligible small and thus ignored. As a result shown below, the breakup effects are very different from them discussed in the previous section.

3.5.2 Numerical setting

In the ^{28}Si(d,p)^{29}Si reaction, n, p, and ^{28}Si can be treated as x, b, and A, respectively, describe in Chap. 3.3. The model of d is same as that for the ^{8}B(d,n)^{9}C reaction but we include only the s-wave of ψ^i_{pn}. The maximum energy of ε^i_{pn} is 33 MeV. $\chi^{ii_0(+)}_{\alpha}$ is calculated up to 15.0 fm with the maximum number of partial waves of 15. These values are adopted also for $\chi^{jj_0(+)}_{\beta}$.

As for the finial channel, we neglect any breakup channels of ^{29}Si. Thus, we approximate $\Psi^{(+)}_{\beta}$ as

$$\begin{aligned}\Psi^{(+)}_{\beta}(\boldsymbol{r}_{p\mathrm{Si}}, \boldsymbol{r}_{\beta}) &\sim \psi^{j_0}_{n\mathrm{Si}}(\boldsymbol{r}_{n\mathrm{Si}})\chi^{j_0 j_0(+)}_{\beta}(\boldsymbol{r}_{\beta}) \\ &\equiv \psi_{n\mathrm{Si}}(\boldsymbol{r}_{n\mathrm{Si}})\chi^{(+)}_{\beta}(\boldsymbol{r}_{\beta}).\end{aligned} \tag{3.117}$$

The distorted wave $\chi^{(+)}_{\beta}$ in the final channel satisfies

$$\left[K_{\boldsymbol{r}_\beta} + U^{(\beta)}_{p\mathrm{Si}}(r_\beta) + V^{(\mathrm{C})}_{p\mathrm{Si}}(r_\beta)\right]\chi^{(+)}_{\beta}(\boldsymbol{r}_{\beta}) = 0. \tag{3.118}$$

The Schrödinger equation for $\psi_{n\mathrm{Si}}$ is given as Eq. (3.56). The Woods-Saxon central potential (3.104) is adopted as $V_{n\mathrm{Si}}$ with radial parameter $R_0 = 1.16 \times 28^{1/3}$ fm and diffuseness parameter $a_0 = 0.78$ fm [139]. Its depth is adjusted to reproduce the neutron separation energy of 7.69 MeV in the s-state. $\psi_{p\mathrm{Si}}$ is expanded with 10 Gaussian functions. Their range parameters are taken from 0.1 fm to 11.0 fm. As for $U^{(\alpha)}_{p\mathrm{Si}}$, $U^{(\alpha)}_{n\mathrm{Si}}$, and $U^{(\beta)}_{p\mathrm{Si}}$, the nucleon global optical potential for sd-shell nuclei [140] is adopted.

3.5.3 Breakup effects of d on transfer cross section

In fig. 3.13 we show the cross section of the ^{28}Si(d,p)^{29}Si reaction at 18.75 MeV. The horizontal axis is the emitting angle of p in the c.m. frame. The thick solid line corresponds to the calculated cross section with CCBA, which explicitly includes the breakup states of ^{29}Si. When the CC of the breakup states is switched off, the thin solid line is obtained. At forward angles, the difference between two lines is small. On the other hand, at backward angles, the breakup effects is appreciable. By decomposing the T matrix, we can

investigate the BT and ET;

$$T = T_{\rm ET} + T_{\rm BT}, \tag{3.119}$$

$$T_{\rm ET} = \left\langle \psi_{n\rm Si}\chi_{\beta}^{(-)} \middle| V_{pn} \middle| \psi_{pn}^{i_0}\chi_{\alpha}^{i_0 i_0(+)} \right\rangle, \tag{3.120}$$

$$T_{\rm BT} = \left\langle \psi_{n\rm Si}\chi_{\beta}^{(-)} \middle| V_{pn} \middle| \sum_{i\neq i_0} \psi_{pn}^{i}\chi_{\alpha}^{i i_0(+)} \right\rangle. \tag{3.121}$$

The T-matrix elements $T_{\rm ET}$ and $T_{\rm BT}$ describe the ET and BT, respectively, in the initial channel. The calculated cross section with the former (latter) is shown by the dashed (dotted) line. The constructive interference between them can be seen in a whole region of θ, except that on the second peak of the cross section at about $\theta = 30^\circ$ the destructive interference exists. Note that in this calculation we assume the spectroscopic factor $\mathcal{S}$ is unity. Thus the calculations somewhat overestimate the experimental data [139].

As another finding, the significant difference between the dashed and thin solid lines can be seen. It indicates that there are strong back couplings between the elastic-breakup channels of d. Except for the second peak, the back couplings decrease the cross section.

These findings are very different from them for the ^{8}B(d,n)^{9}C reaction discussed in the previous section. Though the origin of this difference is not clarified, it is clear that the breakup effects strongly depend on system of reactions. Therefore a systematic study is important in order to investigate how the breakup effects change in each system.

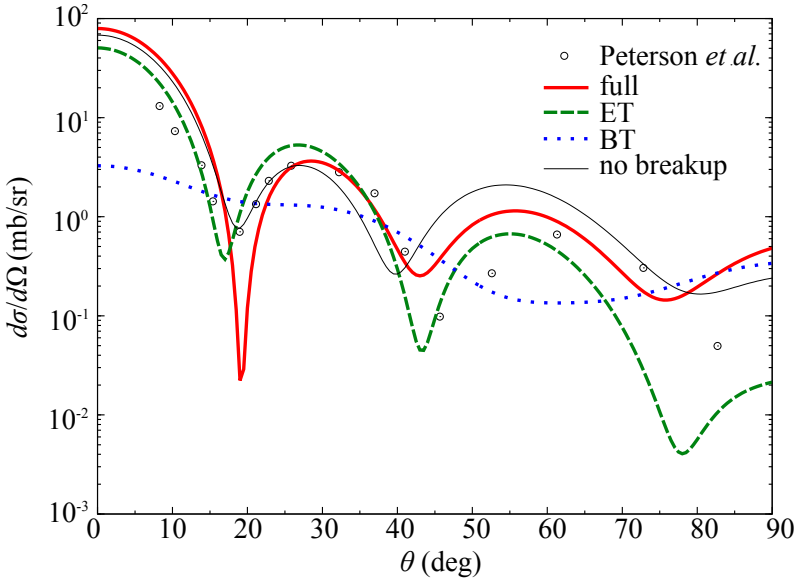

Figure 3.13: The cross section of the ^{28}Si(d,p)^{29}Si reaction at 18.75 MeV as a function of the emitting angle of p in the c.m. frame. The thick solid line is the CCBA result, which includes the CC effects of ^{29}Si. The elastic and breakup transfers in the initial channels are respectively shown as the dashed Thin solid line corresponds to the result without including the breakup channels. and dotted lines. Experimental data are taken from Ref. [139].

3.6 Summary

We formulate the CCBA framework that can explicitly take into account the CC of the breakup states of both the projectile and the residual nucleus.

In the ^{8}B(d,n)^{9}C reaction, the breakup effects of both d and ^{9}C are found to be significant on its cross section. In particular the strong interference of the ET and BT in each channel exists. By including the breakup channels of ^{9}C, which can have the different partial waves from that of the ground state, the change of the transferred angular momentum l involving the continuum states of ^{9}C is treated with in the present work. Different l components due to the dynamical CC play an important role as they significantly increase the cross section.

As for the ^{28}Si(d,p)^{29}Si reaction, it is found that at forward angles, the breakup effects of d is small. On the second peak of the cross section, the destructive interference between the ET and BT can be seen. It is also found that the back couplings are rather strong, and they seem to decrease the cross section except the second preak.

As a future work, a systematic study is demanded because the breakup effects can be different in each reaction, as shown in the Secs. 3.4 and 3.5. We would like to clarify how and why different the breakup effects are in each reaction. It is also interesting to investigate the four-body dynamics induced by a three-body loosely bound nuclei on the transfer reaction. For that purpose a two-nucleon transfer reaction could be one of subjects.

CHAPTER 4

Breakup Reaction of Loosely Bound System

Contents

4.1 Introduction

Let us consider the breakup reaction on a heavy ion target, for example, the dissociation of a charged nucleus by ^{208}Pb. In a naive description, the reaction process can be regarded as that a projectile breaks up into their fragments by the electric field generated by ^{208}Pb. As mentioned in Chap. 1, it is not easy to handle the Coulomb interaction because of its long-range property. Thus, a primitive reaction model, for example, the virtual photon theory (VPT) [12] is often used to describe the reaction simply. The VPT assumes that the breakup reaction proceeds with the one-step process caused by a virtual photon absorption. However, it is not trivial that the picture described by VPT is correct. The role of nuclear interaction and the multistep process, which are missing in VPT, should be investigated.

Recently the ^{15}C dissociation on the ^{208}Pb target is analyzed [17] by means of the dynamical eikonal approximation (DEA) [15, 16], in which the channel couplings of breakup states of ^{15}C due to the nuclear and Coulomb interaction is efficiently taken into account. Note that, in the eikonal approximation, it is assumed that the projectile-target distorted wave is not significant different from a corresponding plane wave [141]. By the analysis it is found that DEA is difficult to describe the Coulomb breakups precisely for a low incident energy case. Note that the Coulomb breakup stands for the breakup reaction dominated by Coulomb interaction and includes effects of nuclear interaction and the multistep

process. On the other hand, as formulated in Chap. 2, there is another reaction model based on the eikonal approximation; the eikonal continuum-discretized coupled-channels method (E-CDCC) [13, 14]. Thus, comparison of E-CDCC and DEA is expected to be important to describe the Coulomb breakups at low incident energy. After the comparison, the prescription to two models for the Coulomb breakups at low energy is proposed.

4.2 Formalism

4.2.1 The dynamical eikonal approximation (DEA)

We focus on the ^{15}C breakup reaction on the ^{208}Pb target at 20.0 MeV/nucleon and work with the three-body model ($n + ^{14}\mathrm{C} + ^{208}\mathrm{Pb}$). In the system, n, ^{14}C, and ^{208}Pb correspond to x, y, and A, respectively, as described in Chap. 2. In Fig. 4.1, the coordinate of the center-of-mass (c.m.) of ^{15}C relative to ^{208}Pb is denoted by $\boldsymbol{R}$, and $\boldsymbol{r}$ is the neutron-^{14}C relative coordinate. $\boldsymbol{R}_n$ and $\boldsymbol{R}_{14}$ are, respectively, the coordinates of neutron n and the c.m. of ^{14}C from ^{208}Pb. We assume both ^{14}C and ^{208}Pb to be inert nuclei. In this study we neglect the spin of n.

In the DEA, the three-body wave function is factorized following [15, 16]

$$\Psi(\boldsymbol{r}, \boldsymbol{R}) = \varphi\,(\boldsymbol{b}, z, \boldsymbol{r})\, e^{iK_0 z} e^{i\chi_{\mathrm{C}}(b,z)} e^{i\varepsilon_0 z/(\hbar v_0)}, \tag{4.1}$$

where we take the incident direction as z-axis of the cylindrical coordinate shown by Fig. 2.4 and $\boldsymbol{R} = (\boldsymbol{b}, z)$. The wave number K_0 between ^{15}C and ^{208}Pb is defined by Eq. (2.17) and ε_0 is the ground state energy of ^{15}C. The factor χ_{C} stands for the Coulomb phase that accounts for the Coulomb projectile-target scattering

$$\chi_{\mathrm{C}}(b, z) = -\frac{1}{\hbar v_0} \int_{-\infty}^{z} V_{\mathrm{C}}(R)\; dz', \tag{4.2}$$

where $v_0 = \hbar K_0/\mu$ is the initial velocity of the projectile with the Coulomb interaction V_{C} of the ^{15}C-^{208}Pb system defined by Eq. (2.77). Note that the phase $\exp\left[\varepsilon_0 z/(i\hbar v_0)\right]$ can

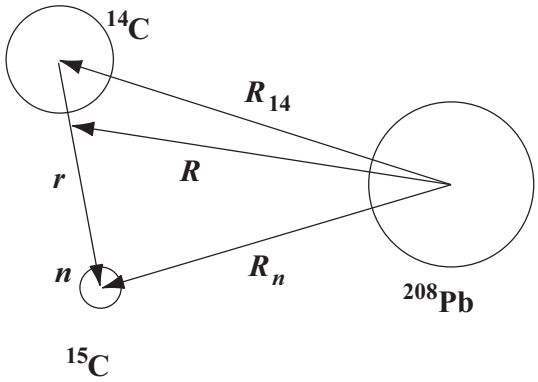

Figure 4.1: Schematic illustration of the $(^{14}\mathrm{C} + n) + ^{208}\mathrm{Pb}$ three-body system.

be ignored as it has no effect on physical observables [16]. φ describes the difference of the distorted wave from the plane wave.

From the factorization in Eq. (4.1), we obtain the DEA equation [15, 16]

$$i\hbar v_0 \frac{\partial}{\partial z}\varphi\left(\boldsymbol{b}, z, \boldsymbol{r}\right) = \left[h + U_{14}(\boldsymbol{R}_{14}) + U_n(\boldsymbol{R}_n) - \varepsilon_0 - V_{\rm C}(R)\right]\varphi\left(\boldsymbol{b}, z, \boldsymbol{r}\right), \tag{4.3}$$

where h is the internal Hamiltonian of the projectile. To simulate the interaction between n (^{14}C) and ^{208}Pb, we adopt the optical U_n (U_{14}). The initial condition for φ is given by

$$\lim_{z\to-\infty}\varphi\left(\boldsymbol{b}, z, \boldsymbol{r}\right) = \psi_{0\ell_0 m_0}(\boldsymbol{r}), \tag{4.4}$$

where $\psi_{0\ell_0 m_0}$ stands for the ground state of ^{15}C. Note that the eigenstate $\psi_{n\ell m}$ of the n-^{14}C system is specified by energy index n, the orbital angular momentum ℓ, and its z-component m for the system. When indices $\{n, \ell, m\} = \{0, \ell_0, m_0\}$, it stands for the initial state.

The DEA equation (4.3) is solved for all $\boldsymbol{b}$ with respect to z and $\boldsymbol{r}$ expanding the wave function φ on a three-dimensional mesh. This allows to include naturally all relevant states of ^{15}C, i.e., eigenenergies ε up to high values in the n-^{14}C continuum, and large angular momentum ℓ, and its z-component m. This resolution is performed assuming a constant projectile-target relative velocity $v = v_0$. It should be noted that this does not mean the adiabatic approximation, because in Eq. (4.3) the internal Hamiltonian h is explicitly included. The DEA thus treats properly the change in the eigenenergy of ^{15}C during the scattering process. However, it does not change the ^{15}C-^{208}Pb velocity accordingly, which is taken into account in E-CDCC as described by Eq. (2.84). This gives a violation of the conservation of the total energy of the three-body system. However, even at 20 MeV/nucleon, its effect is expected to be only a few percents as discussed below.

The calculation of physical observables requires the wave function Ψ of Eq. (4.1) at $z \to \infty$ [15, 16]. The corresponding Coulomb phase $\chi_{\rm C}$ reads [142]

$$\lim_{z\to\infty}\chi_{\rm C} = 2\eta_0 \ln(K_0 b), \tag{4.5}$$

where η_0 is the Sommerfeld parameter for the entrance channel given by Eq. (2.39).

4.2.2 Comparison between DEA and E-CDCC

To compare the DEA with the E-CDCC, we rewrite the DEA equation given by Eq. (4.3) in a coupled-channel (CC) representation. We expand φ as

$$\varphi\left(\boldsymbol{b}, z, \boldsymbol{r}\right) = \sum_{i\ell m}\xi_{n\ell m}(b, z)\psi_{n\ell m}(\boldsymbol{r})e^{\varepsilon_i z/(i\hbar v_0)}e^{i(m_0-m)\phi_R}. \tag{4.6}$$

Inserting Eq. (4.6) into Eq. (4.3), multiplied by $\psi_{n'\ell'm'}$ from the left, and integrating over $\boldsymbol{r}$, one gets

$$\frac{\partial}{\partial z}\xi_c(b, z) = \frac{1}{i\hbar v_0}\sum_{c'}\mathcal{F}_{cc'}(b, z)\xi_{c'}(b, z)e^{(\varepsilon_{n'}-\varepsilon_n)z/(i\hbar v_0)}, \tag{4.7}$$

which is nothing but the DEA equation (4.3) in its CC representation. Here we represent the channel indices $\{n, \ell, m\}$ as c. The coupling potential $\mathcal{F}_{cc'}$ is defined by Eq. (2.76).

The boundary condition Eq. (4.4) thus reads

$$\lim_{z\to-\infty} \xi_c(b,z) = \delta_{cc_0}, \tag{4.8}$$

which corresponds that of the E-CDCC given by Eq. (2.83). By inserting Eq. (4.6) into Eq. (4.1), the total wave function reads

$$\Psi(\boldsymbol{r},\boldsymbol{R}) \;=\; \sum_c \xi_c(b,z)\psi_c(\boldsymbol{r}) e^{(\varepsilon_n-\varepsilon_0)z/(i\hbar v_0)} e^{i(m_0-m)\phi_R} e^{iK_0 z} e^{i\chi_{\rm C}(b,z)}. \tag{4.9}$$

For comparison we rewrite the CC equation and three-body wave function within the E-CDCC, which are given in Chap. 2;

$$\frac{\partial}{\partial z}\bar{\xi}_c(b,z) = \frac{1}{i\hbar v_n(R)} \sum_{c'} \mathcal{F}_{cc'}(b,z)\bar{\xi}_{c'}(b,z) e^{i(K_{n'}-K_n)z} \mathcal{R}_{nn'}(b,z), \tag{4.10}$$

$$\Psi(\boldsymbol{r},\boldsymbol{R}) = \sum_c \bar{\xi}_c(b,z)\psi_c(\boldsymbol{r}) e^{iK_n z} e^{i(m_0-m)\phi_R} \phi_n^{\rm C}(R), \tag{4.11}$$

where the velocity v_n, the factor $\mathcal{R}_{nn'}$, and the approximate Coulomb incident wave $\phi_n^{\rm C}$ are defined by Eqs. (2.84), (2.85), and (2.81), respectively.

One may summarize the difference between Eqs. (4.7) and (4.10) as follows. First, the DEA uses the constant and channel-independent ^{15}C-^{208}Pb relative velocity v_0, whereas E-CDCC uses the velocity depending on both R and the channel n that ensures the total-energy conservation.

Second, whereas the right-hand side of Eq. (4.7) involves the phase $\exp\left[(\varepsilon_{n'}-\varepsilon_n)z/(i\hbar v_0)\right]$, the E-CDCC Eq. (4.10) includes the phase $\exp\left[i(K_{n'}-K_n)z\right]$. The former can be rewritten as

$$\frac{\varepsilon_{n'}-\varepsilon_n}{i\hbar v_0} z = \frac{\hbar^2(K_n^2-K_{n'}^2)\,\mu z}{2\mu\; i\hbar^2 K_0} = \frac{K_{n'}+K_n}{2K_0} i\left(K_{n'}-K_n\right) z. \tag{4.12}$$

If we can assume the semi-adiabatic approximation

$$\frac{K_{n'}+K_n}{2K_0} \approx 1, \tag{4.13}$$

the exponent Eq. (4.12) becomes the same as in E-CDCC. In the model space taken in the present study, Eq. (4.13) holds within 1.5% error at 20 MeV/nucleon of incident energy.

Third, E-CDCC equation contains $\mathcal{R}_{nn'}$ taking account of the channel dependence of the ^{15}C-^{208}Pb Coulomb wave function, which DEA neglects. Nevertheless, it should be noted that, as shown in Refs. [113, 114], the Coulomb wave functions in the initial and final channels involved in the transition matrix (T matrix) of E-CDCC eventually give a phase $2\eta_j \ln(K_j b)$, with j the energy index in the final channel. Thus, if Eq. (4.13) holds, the role of the Coulomb wave function in the evaluation of the T matrix in E-CDCC is expected to be the same as in DEA, since DEA explicitly includes the Coulomb eikonal phase, Eq. (4.5).

When the Coulomb interaction is absent, we have $\mathcal{R}_{ii'}(b,z)=1$ and no R dependence of the velocity. Therefore, it will be interesting to compare the results of DEA and E-CDCC with and without the Coulomb interaction separately. This correspondence of the two eikonal model is newly discussed by the present study [143].

4.3 Results and discussion

4.3.1 Model setting

We calculate the energy spectrum $d\sigma/d\varepsilon$ and the angular distribution $d\sigma/d\Omega$ of the breakup cross section of ^{15}C on ^{208}Pb at 20 MeV/nucleon, where ε is the relative energy between n and ^{14}C after breakup, and Ω is the scattering angle of the c.m. of the n-^{14}C system. We use the potential parameters shown in Table 5.1 for $U_{n\mathrm{C}}$ (the n-^{14}C interaction), U_{14}, and U_n [17]; the depth of $U_{n\mathrm{C}}$ for the d-wave is changed to 69.43 MeV to avoid a non-physical d resonance. The spin of the neutron is disregarded as mentioned earlier. We adopt Woods-Saxon potentials for the interactions:

$$\begin{aligned} U_x(R_x) &= -V_0 f(R_x,R_0,a_0) - iW_v f(R_x,R_w,a_w) \\ &\quad + iW_s \frac{d}{dR_x} f(R_x,R_w,a_w) \end{aligned} \tag{4.14}$$

with $f(R_x,\alpha,\beta)=(1+\exp[(R_x-\alpha)/\beta])^{-1}$; $R_x=r$, R_{14}, and R_n for $x=n\mathrm{C}$, 14, and n , respectively. The Coulomb interaction between ^{14}C and ^{208}Pb is described by assuming a uniformly charged sphere of radius R_{C}.

In E-CDCC, we take the maximum value of r to be 800 fm with the increment of 0.2 fm. When the Coulomb interaction is turned off, we take the n-^{14}C partial waves up to $\ell_{\max}=10$. For the discretization of ε, we adopt the average method given in Chap. 2. For each ℓ the continuum state is truncated at $k_{\max}=1.4$ fm^{-1} and discretized into 35 states with the equal spacing of $\Delta k=0.04$ fm^{-1}; k is the relative wave number between n and ^{14}C. The resulting number of coupled channels, N_{ch}, is 2311. The maximum values of z and b, $z_{\max}$ and $b_{\max}$, respectively, are both set to 50 fm. When the Coulomb interaction is included, we use $\ell_{\max}=6$, $k_{\max}=0.84$ fm^{-1}, $\Delta k=0.04$ fm^{-1}, $z_{\max}=1000$ fm, and $b_{\max}=150$ fm. We have $N_{\mathrm{ch}}=589$ in this case.

In the DEA calculations, we use the same numerical parameters as in Ref. [17]. In the purely nuclear case, the wave function φ is expanded over an angular mesh containing up to $N_\theta\times N_\phi=14\times 27$ points, a quasi-uniform radial mesh that extends up to 200 fm with

Table 4.1: Potential parameters for the pair interactions $U_{n\mathrm{C}}$, U_{14}, and U_n [17].

	V_0 (MeV)	R_0 (fm)	a_0 (fm)	W_v (MeV)	W_s (MeV)	R_w (fm)	a_w (fm)	R_{C} (fm)
$U_{n\mathrm{C}}$	63.02	2.651	0.600	—	—	—	—	—
U_{14}	50.00	9.844	0.682	50.00	—	9.544	0.682	10.84
U_n	44.82	6.932	0.750	2.840	21.85	7.466	0.580	—

200 points, $b_{\max} = 50$ fm, and $z_{\max} = 200$ fm (see Ref. [144] for details). In the charged case, the angular mesh contains up to $N_\theta \times N_\phi = 12 \times 23$ points, the radial mesh extends up to 800 fm with 800 points, $b_{\max} = 300$ fm, and $z_{\max} = 800$ fm.

4.3.2 Comparison without Coulomb interaction

In this subsection we would like to clarify the difference in the treatment of the Coulomb breakup between the E-CDCC and DEA. Thus we first check that both models agree when the Coulomb interaction is switched off. We show in Fig. 4.2 the results of $d\sigma/d\varepsilon$ calculated by DEA (solid line) and E-CDCC (dashed line). Note that, to obtain $d\sigma/d\varepsilon$, the integration in Eq. (2.50) is done for the scattering angle of the c.m. of the n-^{14}C system in the whole variable region. The two results agree very well with each other; the difference around the peak is below 3%.

In Fig. 4.3 the comparison in $d\sigma/d\Omega$ defined by Eq. (2.49) is shown. For the angular distribution, we integrate the double differential cross section Eq. (2.48) over ε up to 10 MeV. The agreement between the two models is excellent confirming that, when the Coulomb interaction is turned off, the DEA and E-CDCC solve the same equation and give the same result, as expected from the discussion at the end of Sec. 4.2.2. In particular this comparison indicates that Eq. (4.13) turns out to be satisfied with very high accuracy. It should be noted that the good agreement between the DEA and E-CDCC is obtained only when a very large model space is taken. In fact if we put $\ell_{\max} = 6$ in E-CDCC, we have 30% smaller $d\sigma/d\varepsilon$ than the converged value and, more seriously, even the shape cannot be reproduced. This result shows the importance of the higher partial waves of n-^{14}C for

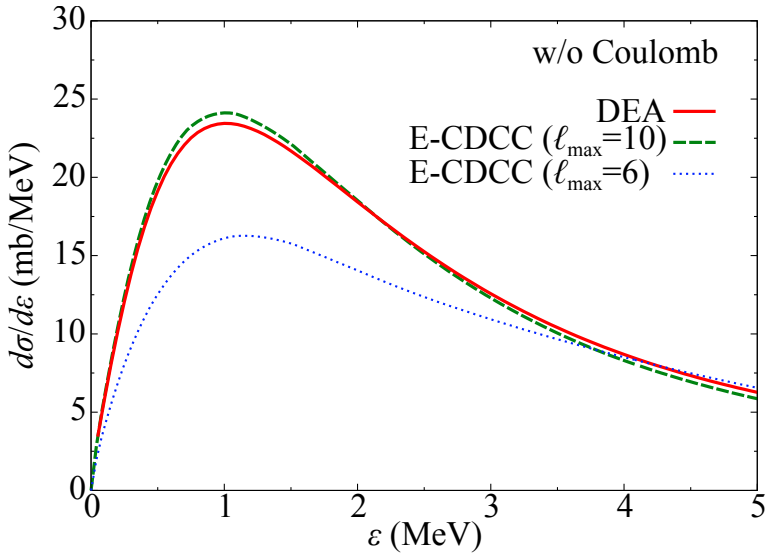

Figure 4.2: Energy spectrum of the ^{15}C breakup cross section on ^{208}Pb at 20 MeV/nucleon with the Coulomb interaction turned off. The solid and dashed lines show the results obtained by DEA and E-CDCC, respectively.

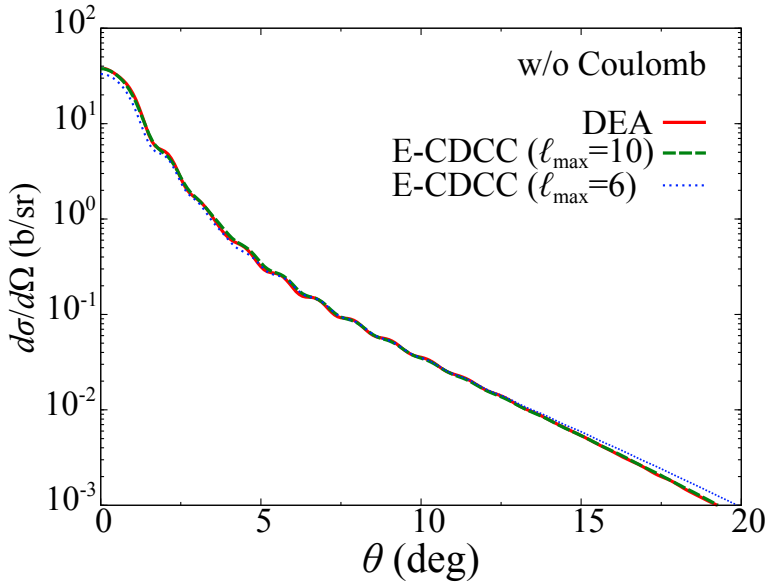

Figure 4.3: Same as Fig. 4.2 but for the angular distribution.

the nuclear breakup at 20 MeV/nucleon.

4.3.3 Comparison with Coulomb interaction

When the Coulomb interaction is switched on, DEA and E-CDCC no longer agree with each other. As seen in Fig. 4.4, the DEA energy spectrum (solid line) is much larger than the E-CDCC one (dashed line). Moreover none of them agrees with the full CDCC calculation (thin solid line): DEA is too high while E-CDCC is too low. The discrepancy of both models with the fully quantal calculation manifests itself even more clearly in the angular distribution. In Fig. 4.5 we see that not only do the DEA and E-CDCC cross sections differ in magnitude, but—as already seen in Ref. [17]—their oscillatory pattern is shifted to forward angle compared to the CDCC calculation. To understand where the problem comes from we analyze in Fig. 4.6 the contribution to the total breakup cross section of each projectile-target relative angular momentum L . As expected from Figs. 4.4 and 4.5, the DEA calculation is larger than the E-CDCC one, and this is observed over the whole L range. However, the most striking feature is to see that both models seem to be shifted to larger L compared to the full CDCC calculation. This shift is expected to be came from an insufficient description of projectile's trajectory due to the Coulomb deflection. To correct this, we replace in our calculations the transverse component of the projectile-target relative coordinate b by the empirical value [142, 145, 146]

$$b' = \frac{\eta_0}{K_0} + \sqrt{\frac{\eta_0^2}{K_0^2} + b^2}. \tag{4.15}$$

Equation (4.15) stands for the distance of closest approach in Rutherford scattering and is based on a concept that how we approximate the curved trajectory by straight line one. The

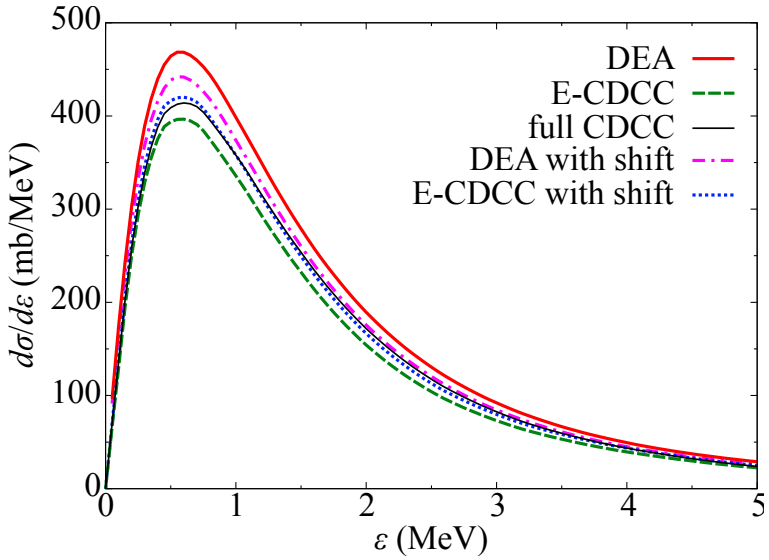

Figure 4.4: Energy spectrum of the ^{15}C breakup cross section on ^{208}Pb at 20 MeV/nucleon including the Coulomb interaction. The solid, dashed, and thin solid lines show the results obtained by DEA, E-CDCC, and full (QM) CDCC, respectively. The results obtained with the correction (4.15) are displayed with a dash-dotted line for DEA and a dotted line for E-CDCC.

Coulomb correction Eq. (4.15) make the impact parameter b and L larger, and hence the partial breakup cross section with the Coulomb correction is expected to shift toward lower L direction. The corresponding results are displayed in Figs. 4.4, 4.5 and 4.6 as dash-dotted lines for DEA and dotted lines for E-CDCC.

The correction Eq. (4.15) is very effective. It significantly reduces the shift observed in the L contributions to the breakup cross section (see Fig. 4.6). Accordingly, it brings both DEA and E-CDCC energy spectra closer to the full CDCC one (see Fig. 4.4). Note that for this observable the correction seems better for E-CDCC than for DEA: even with the shift, the latter still exhibits a non-negligible enhancement with respect to CDCC at low energy ε. More impressive result is the improvement of the behavior of the shift in the angular distribution observed in Ref. [17] and in Fig. 4.5. In particular, the shifted DEA cross section is now very close to the CDCC one, but at forward angles, where DEA overestimates CDCC. Once shifted, E-CDCC still underestimates slightly the full CDCC calculation. However, its oscillatory pattern is now in phase with that of the CDCC cross section, which is a big achievement in itself. This shows that the lack of Coulomb deflection observed in Ref. [17] for eikonal-based calculations can be efficiently corrected by the simple shift Eq. (4.15) suggested long ago [142, 145].

Albeit efficient, the correction Eq. (4.15) is not perfect. This is illustrated by the enhanced (shifted) DEA cross section observed in the low-energy peak in Fig. 4.4 and at forward angles in Fig. 4.5. Both problems can be related to the same root because the forward-angle part of the angular distribution is dominated by low-energy contributions.

As shown in Ref. [16], that part of the cross section is itself dominated by large b's, at which the correction Eq. (4.15) is not fully sufficient. As shown in Fig. 4.6, the shifted DEA remains slightly larger than the full CDCC. Future works may suggest a better way

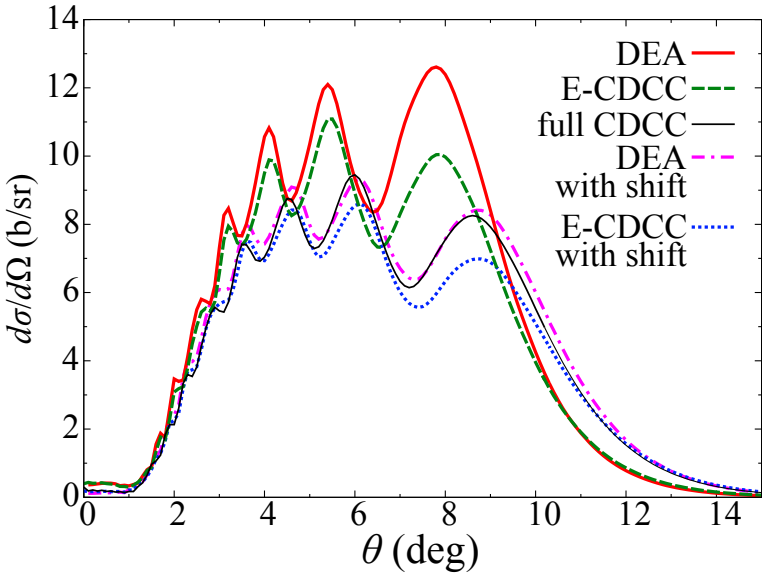

Figure 4.5: Same as Fig. 4.4 but for the angular distribution.

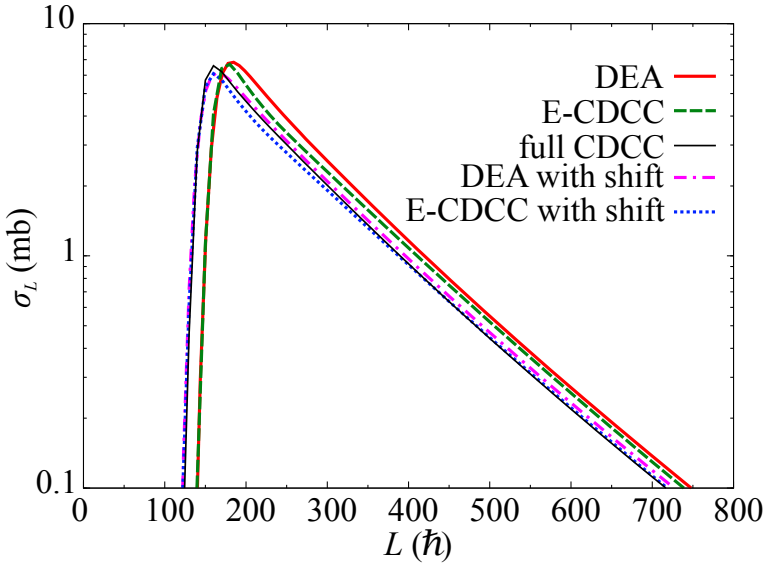

Figure 4.6: Contribution to the total breakup cross section per projectile-target angular momentum L. Neglecting the Coulomb deflection, DEA and E-CDCC are shifted to large L compared to the full CDCC. The correction Eq. (4.15) significantly reduces this shift for both models.

to handle this shift than the empirical correction Eq. (4.15). Nevertheless, these results show that this correction provides a simple, elegant, and cost-effective way to account for Coulomb deflection in eikonal-based models. This fact suggests that the concept of the "trajectory" is well held even though complicated processes exist, for example the interference of the nuclear and Coulomb interactions and the multistep process.

The underestimation of the full CDCC angular distribution by E-CDCC comes most likely from a convergence problem within that reaction model. This is illustrated in Fig. 4.7, showing the L-contribution to the total breakup cross section. The thin solid line corresponds to the (converged) CDCC calculation, whereas the other lines correspond to (shifted) E-CDCC calculations with bin widths of $\Delta k = 0.02$ (solid line), 0.03 (dashed line), and 0.04 fm^{-1} (dotted line). As can be seen, below $L \approx 500\ \hbar$, no convergence can be obtained, although CDCC has fully converged. We cannot expect this model to provide accurate breakup cross sections. The results displayed in Figs. 4.4 and 4.5 are therefore unexpectedly good. Note that the present ill-behavior of E-CDCC occurs only when the Coulomb interaction involved is strong and the incident energy is low; no such behavior was observed in previous studies [6, 113, 114, 147, 148]. Interestingly, DEA does not exhibit such a convergence issue. This is reminiscent of the work of Dasso *et al.* [149], where it was observed that reaction calculations converge faster by expanding the wave function upon a mesh rather than by discretization of the continuum.

The aforementioned results indicate that the shift Eq. (4.15) corrects efficiently for the Coulomb deflection, which is expected to play a significant role at large L. At small L, we believe the nuclear projectile-target interaction will induce significant couplings between various partial waves, which cannot be accounted for by that simple correction. To include these couplings, the hybrid solution between E-CDCC and the full CDCC has been

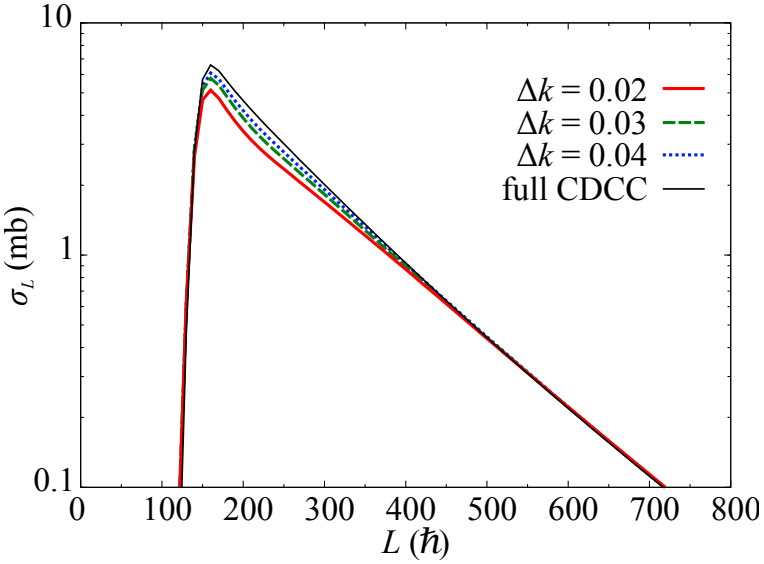

Figure 4.7: Convergence problem observed in (shifted) E-CDCC calculations: cross sections computed with different bin widths do not converge towards the CDCC calculation.

suggested [113, 114] and described as Eq. (2.104). At low L a usual CDCC calculation is performed, which fully accounts for the strong coupling expected from the nuclear interaction between the projectile and the target. At larger L, these couplings are expected to become negligible, which implies that a (shifted) E-CDCC calculation should be reliable. As explained in Refs. [113, 114], the transition angular momentum L_{C} above which E-CDCC is used is an additional parameter of the model space that has to be determined in the convergence analysis. Depending on the beam energy and the system studied, usual values of L_{C} are in the range 400–1000 $\hbar$. In the present case, due to the convergence issue observed in E-CDCC, the value $L_{\mathrm{C}} = 500\ \hbar$ is chosen.

The cross sections calculated with this hybrid solution are barely visible as they are superimposed to the full CDCC results for both the angular distribution (Fig. 4.8(a)) and the energy spectrum (Fig. 4.8(b)). The coupling of the hybrid solution to the Coulomb shift Eq. (4.15) enables us to reproduce exactly the CDCC calculations at a much lower computational cost since the computational time for each b with E-CDCC is about 1/60 of that for each L with full CDCC. In addition, it solves the convergence problem of E-CDCC.

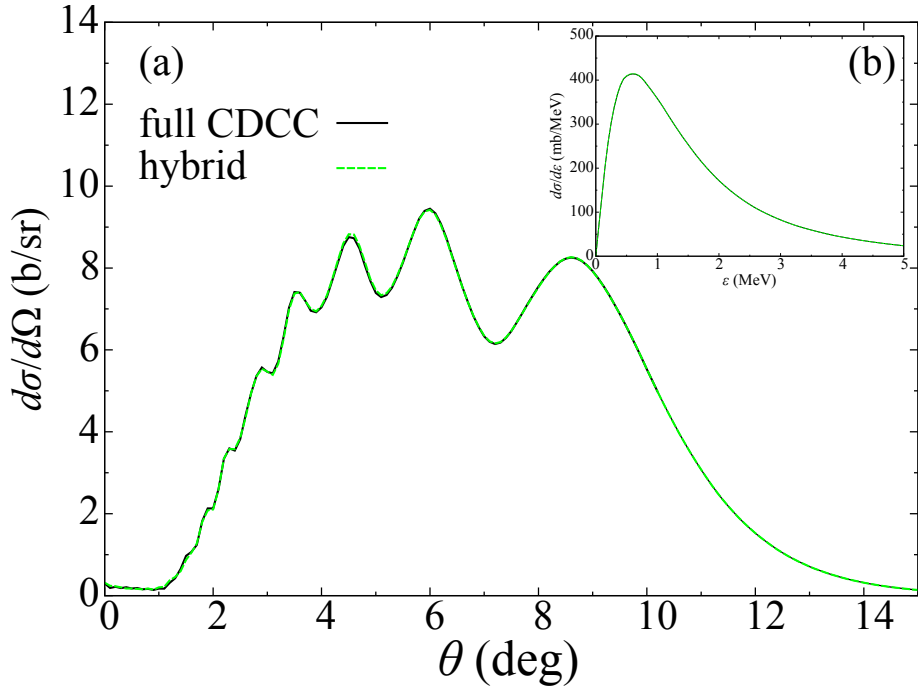

Figure 4.8: Comparison of the full quantum calculation (solid line) and the hybrid calculation (dashed line) on (a) the angular distribution and (b) the energy spectrum.

4.4 Summary

The eikonal approximation is known to be an efficient procedure to describe breakup reactions. However, at a low incident energy, it was reported [17] that a model based on the eikonal approximation, that is the dynamical eikonal approximation (DEA), cannot reproduce the result obtained from more rigorous calculation with the method of the continuum-discretized coupled-channels (CDCC). As another reaction model based on the eikonal approximation, there exists the hybrid version of the CDCC method with the eikonal approximation (E-CDCC). To solve this discrepancy, we have compared the E-CDCC with the DEA. It have been shown that two models solve essentially same Schrödinger equation when the Coulomb interaction is absent.

We have focused on the same test case as in Ref. [17], i.e., the breakup of ^{15}C on ^{208}Pb at 20 MeV/nucleon. For this reaction Eq. (4.13) holds within 1.5% error. When the Coulomb interaction is artificially turned off, DEA and E-CDCC are found to give the same result within 3% difference for both the energy spectrum and the angular distribution. This supports the equivalence of the two models for describing the breakup process due purely to nuclear interactions as expected.

Next we make a comparison including the Coulomb interaction. In this case, DEA and E-CDCC no longer agree with each other and they both disagree with the full CDCC calculation. In particular both angular distributions are focused at too forward an angle, as reported in Ref. [17]. This lack of Coulomb deflection of the eikonal approximation can be solved using the empirical shift Eq. (4.15). Using this shift the agreement with CDCC improves significantly. This suggests that, for the low energy breakup reaction, the concept of the "trajectory" is held even though the reaction process includes complicated features such as the interference of the nuclear and Coulomb interactions and the multistep process.

It has been found that the quantum mechanical (QM) correction to the E-CDCC proposed in Ref. [113, 114] works well. In the QM correction, the partial wave calculated by E-CDCC with a lower orbital angular momentum is replaced by that obtained from the full CDCC. It would be important to find a efficient QM correction to the DEA. Moreover, it will be interesting to apply the eikonal approximation with the corrections proposed here for transfer reactions, in which generally a low incident energy is adopted.

CHAPTER 5

Cluster-Investigation via Observables

Contents

5.1 Introduction

The clustering phenomena, which is the separately localization of some particles, have been predicted by theoretical studies that several states of unstable nuclei or of sd-shell nuclei have a cluster structure [150]. However, there is no direct measurement of the cluster structure except for resonance states decaying into constituent clusters. Therefore, it is desirable to establish how to extract the quantitative information on the clustering from observables.

In theoretical studies it is known that the α-cluster state develops in the surface region of nuclei. In this work we focus on ^{20}Ne as a typical nucleus having an α-^{16}O cluster structure, though it is well bound nucleus. The purpose of the present study is to extract the probability of the α-clustering in the surface region from the α-transfer reaction, ^{16}O(^{6}Li,d)^{20}Ne.

Furthermore, at excited states of nuclei, if they populate near thresholds, cluster structures are expected to develop and loosely bound state. Thus, for the investigation of these cluster structures by using nuclear reactions, it is needed to consider the dynamics of loosely bound system, in particular the breakup effects of nuclei into their constituent clusters. However, at this moment, the inclusion of these effects in our model is out of our scope. First, in this paper, we aim to show how to identify the cluster structure regarding the well-bound stable nucleus, ^{20}Ne, from observables. Then, as future works, it will come

out that the cluster-investigation of loosely bound systems such as unstable nuclei with taking into account their breakup effects.

5.2 Theoretical framework

5.2.1 Microscopic description of cluster wave function

As for the relative wave function between α and ^{16}O, we adopt a microscopic cluster model. The total wave function of ^{20}Ne with the resonating group method (RGM) [151–154] for the α-^{16}O configuration is given by

$$|\Psi_{\rm Ne}\rangle = \frac{1}{\sqrt{20!}}\mathcal{A}\left[\chi_l(r)Y_{l0}(\hat{\boldsymbol{r}})\phi(\alpha)\phi({\rm Ne})\right], \tag{5.1}$$

where r is the relative coordinate between α and ^{16}O, $\mathcal{A}$ stands for the antisymmetrization operator, and $\phi(C)$ is the intrinsic wave function of the nucleus C. χ_l can be expanded by the orthonormal set R_{nl} of the radial wave function of the harmonic oscillator (HO) as

$$\chi_l(r) = \sum_n a_n R_{nl}(r), \tag{5.2}$$

$$a_n = \int r^2 dr R_{nl}(r)\chi_l(r). \tag{5.3}$$

Here, n and l correspond to the principal quantum number and the orbital angular momentum of the HO, respectively. The relative wave function is defined by

$$u_l(r) = \sum_n a_n\sqrt{\mu_{nl}}R_{nl}(r) \tag{5.4}$$

with the eigenvalue μ_{nl} of the RGM norm kernel [155]. For a normalized cluster wave function satisfying $\langle\Psi|\Psi\rangle = 1$, the relative wave function u_l is normalized to unity. Details of the formulation of the microscopic cluster model are given in Ref. [156]

5.2.2 Distorted-wave Born Approximation (DWBA) formalism

In this work the α-transfer reaction ^{16}O(^{6}Li,d)^{12}C is described with the post form distorted wave Born Approximation (DWBA) approach expressed in Sec. 3.3.3. The coordinates for the reaction system are illustrated in Fig. 5.1. The transition matrix for the α-transfer reaction is given by

$$T^{\rm (post)}_{\rm DWBA} = \left\langle \Psi_f^{(-)} \middle| V_{\alpha d} \middle| \Psi_i^{(+)} \right\rangle, \tag{5.5}$$

where the α-d interaction $V_{\alpha d}$ in the final channel is adopted as the transition interaction, which causes the transition from the initial channel i to the final channel f. The total wave functions $\Psi_i^{(+)}$ and $\Psi_f^{(-)}$ for the initial and final channels, respectively, are written as

$$\Psi_i^{(+)}(\boldsymbol{r}_{\alpha d}, \boldsymbol{r}_i) = \psi_{\alpha d}(\boldsymbol{r}_{\alpha d})\chi_i^{(+)}(\boldsymbol{r}_i), \tag{5.6}$$

$$\Psi_f^{(-)}(\boldsymbol{r}_{\alpha {\rm O}}, \boldsymbol{r}_f) = \psi_{\alpha {\rm O}}(\boldsymbol{r}_{\alpha {\rm O}})\chi_f^{(-)}(\boldsymbol{r}_f), \tag{5.7}$$

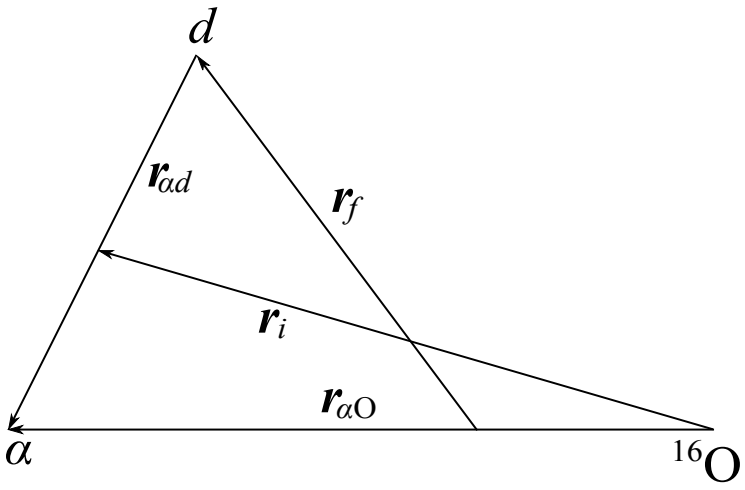

Figure 5.1: Illustration of the three-body system.

where $\psi_{\alpha d}$ ($\psi_{\alpha O}$) is the relative wave function of the α-d (α-^{16}O) system and the distorted wave between ^{6}Li and ^{16}O (d and ^{20}Ne) is represented by $\chi_i^{(+)}$ ($\chi_f^{(-)}$). The superscript $(+)$ and $(-)$ represents the outgoing and incoming boundary conditions, respectively, on the scattering wave function. We adopt the cluster wave function defined by Eq. (5.4) for u_l, the radial part of $\psi_{\alpha O}$. Thus $\psi_{\alpha d}$ is given by

$$\psi_{\alpha d}(\boldsymbol{r}_{\alpha d}) = u_l(r_{\alpha d})Y_{lm}(\hat{\boldsymbol{r}}_{\alpha d}), \tag{5.8}$$

where m is the projection of $\boldsymbol{l}$ onto the z-axis.

5.3 Result

5.3.1 Numerical inputs

We adopt the Volkov No. 2 effective interaction with the Majorana parameter $m = 0.62$ [157] to calculate the α-^{16}O relative wave function u_l. The width parameter $\nu = 0.16$ fm^{-2} is used for both α and ^{16}O. $\psi_{\alpha d}$ is calculated with a two-range Gaussian interaction $V_{\alpha d}$ [133].

We consider the ^{16}O(^{6}Li,d)^{20}Ne reaction at four incident energies: 20, 38, 42, and 75 MeV. At 20 and 38 MeV, we adopt phenomenological distorting potentials of a Woods-Saxon form given in Ref. [158] for calculating $\chi_i^{(+)}$ and $\chi_f^{(-)}$. At 42 (75) MeV, potential parameters are taken from Ref. [159] (Ref. [160]) and Ref. [161] (set 2 of Ref. [162]) for the initial and final channels, respectively.

5.3.2 α distribution on transfer cross section

To investigate the role of the α-cluster distribution in the transfer reaction ^{16}O(^{6}Li,d)^{20}Ne, the cross sections are calculated with the ^{20}Ne wave functions of the cluster model (CM),

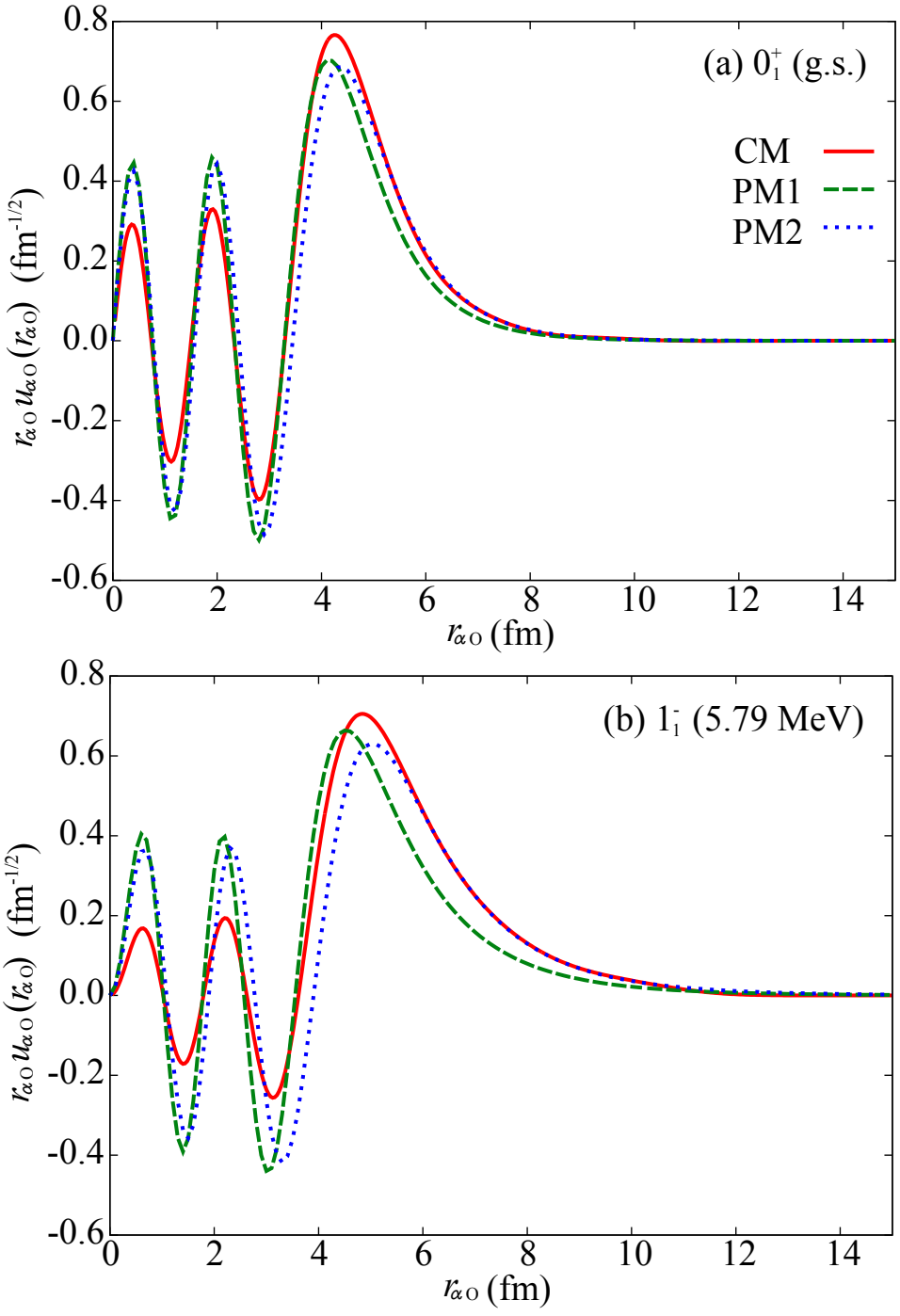

Figure 5.2: (a) The α-^{16}O relative wave functions for the 0_1^+ state calculated with CM (solid line) and two parameter sets of PM: PM1 (dashed line) and PM2 (dotted line). (b) Same as in (a) but for the 1_1^- state.

Eq. (5.4), and of the potential model (PM). In PM the α-^{16}O relative wave function is simply calculated with the Woods-Saxon potential $V_{\alpha\mathrm{O}}$ between α and ^{16}O: $V_{\alpha\mathrm{O}} = -V_0/[1+\exp\{(r_{\alpha\mathrm{O}}-r_0)/a\}]$. The parameters of $V_{\alpha\mathrm{O}}$ are listed in Table 5.1. Figures 5.2(a) and 5.2(b) show the α-^{16}O relative wave functions of the 0^+_1 (ground state) and the 1^-_1 state (5.79 MeV), respectively. For the 1^-_1 state we use a bound state approximation to calculate the relative wave function, taking the binding energy to be 0.2 MeV. By changing the parameter a, the PM wave function (PM2) can reproduce the behavior of the CM wave function in the surface region ($r_{\alpha\mathrm{O}} \gtrsim 5$ fm).

The transfer cross sections of ^{16}O(^{6}Li,d)^{20}Ne(0^+_1) as a function of the neutron emitting angle θ in the center-of-mass frame are compared with the experimental data [158,160,163] in Fig. 5.3. One sees the result with CM (solid line) agrees well with that with PM2 (dotted line) up to the third maximum at all energies. On the other hand, the result with PM1 (dashed line) deviates from the other two significantly. As shown in Fig. 5.2, CM and PM1 gives the same distribution in the surface region but are different from each other in the inner region. Whereas the two sets of PM show a difference only in the surface region. Thus, the results of Fig. 5.3 suggest that the transfer cross section is not sensitive to the inner part of the structure of ^{20}Ne but it probes the α-^{16}O radial wave function in the surface region. , where a clustering structure is known to make u_l show a characteristic behavior.

It should be noted that the radial wave functions used here are normalized to unity. Nevertheless, PM1 gives a significantly different absolute value of the cross section from the results with other two models. This strongly suggests that an accurate determination of a spectroscopic factor (SF) from a transfer reaction is very difficult. Another important remark is that the surface region in this study means about 5–8 fm in the relative distance of α and ^{16}O, i.e., still within a range of the nuclear interaction between the two clusters. Thus, the transfer process considered here is not governed by the asymptotic normalization coefficient (ANC). The α-clustering probability in the surface region will be a third alternative to the SF and the ANC for nuclear structural information to be extracted from reaction observables.

Unfortunately, however, agreement of the calculations with CM and PM with the experimental data is not satisfactorily well. One of the reasons for this will be ambiguity of the distorting potentials, those for ^{6}Li in particular. We will fix this possible problem by adopting an $\alpha + d + {}^{16}$O three-body model in describing the transfer reaction. In this case we need the α-^{16}O and d-^{16}O distorting potentials, for which some global parameterizations

Table 5.1: Potential parameters for $V_{\alpha\mathrm{O}}$ in fm. The depth V_0 of $V_{\alpha\mathrm{O}}$ is determined so as to reproduce the binding energy 4.73 MeV and 0.20 MeV for 0^+_1 and 1^-_1 states, respectively.

	0^+_1		1^-_1	
	r_0	a	r_0	a
PM1	$1.25\times16^{1/3}$	0.65	$1.25\times16^{1/3}$	0.65
PM2	$1.25\times16^{1/3}$	0.76	$1.25\times16^{1/3}$	0.83

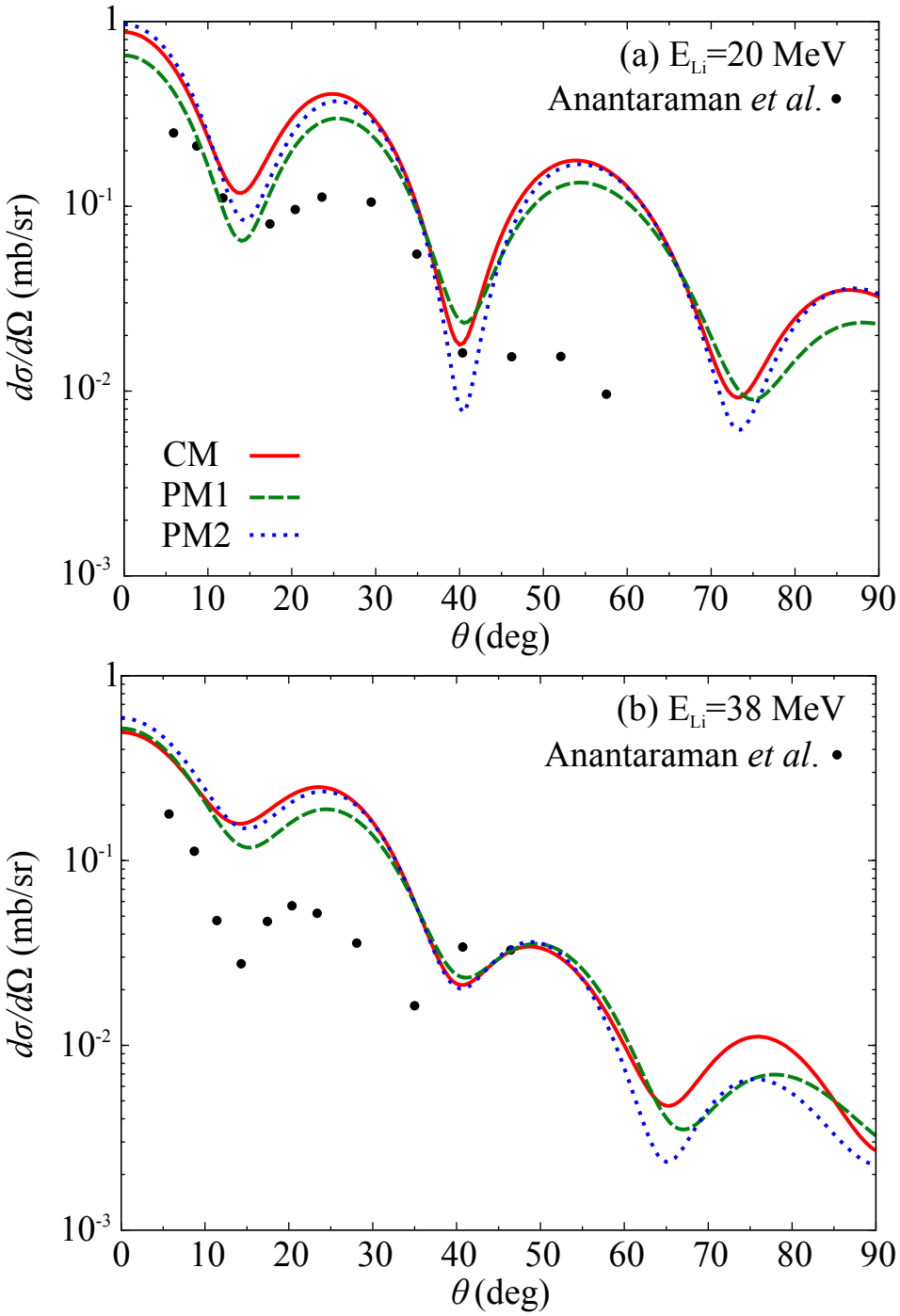
(a) E_Li=20 MeV
Anantaraman et al. •
CM
PM1
PM2
dσ/dΩ (mb/sr)
θ (deg)
(b) E_Li=38 MeV
Anantaraman et al. •
dσ/dΩ (mb/sr)
θ (deg)

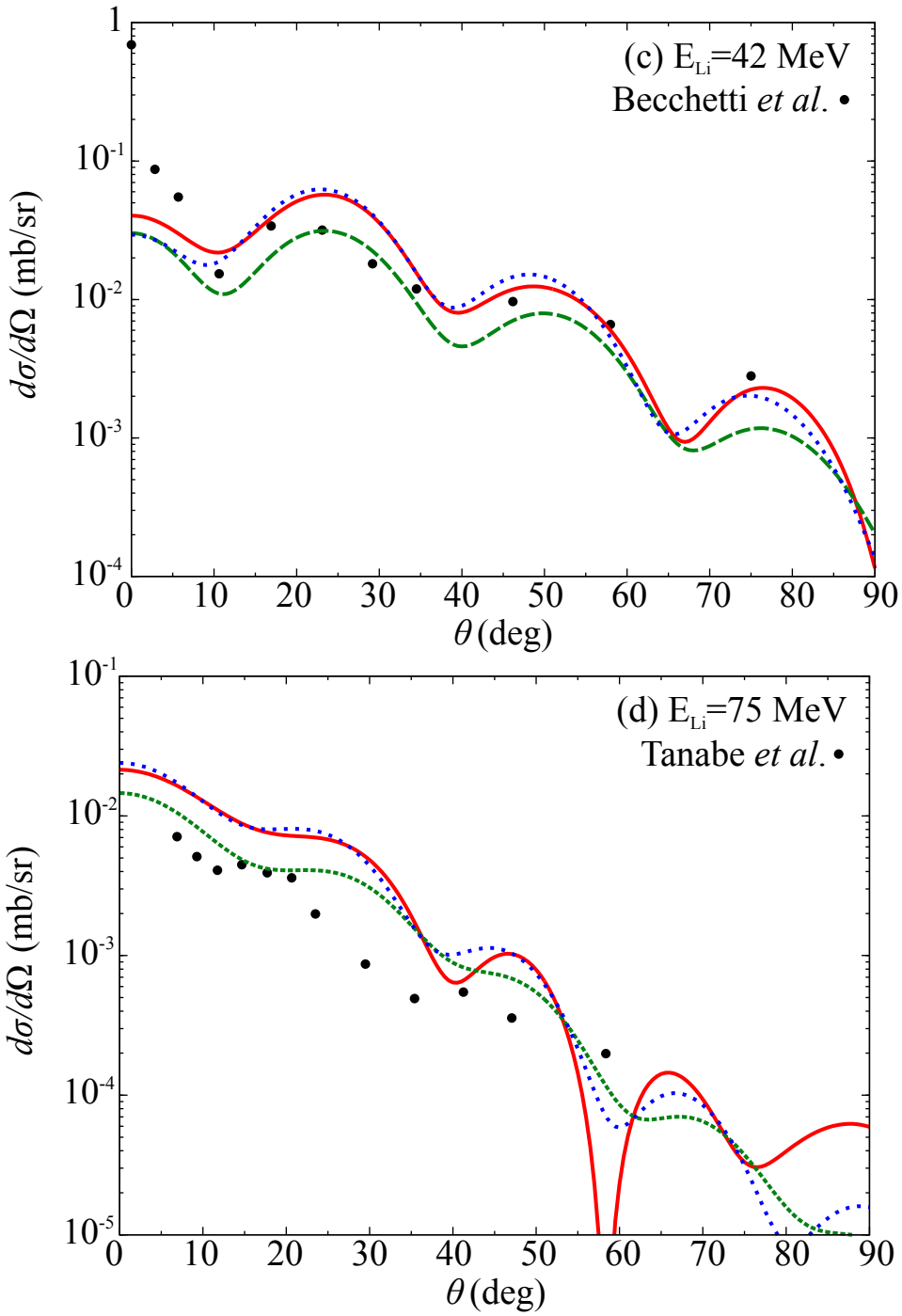

Figure 5.3: Transfer cross sections of ^{16}O(^{6}Li,d)^{20}Ne(0^{+}_{1}) at (a) 20 MeV, (b) 38 MeV, (c) 42 MeV, and (d) 75 MeV. In each panel, the solid line shows the calculation with the CM wave function. Results with PM1 and PM2 wave function are shown by the dashed and dotted lines, respectively. Experimental data are taken from Ref. [158, 160, 163].

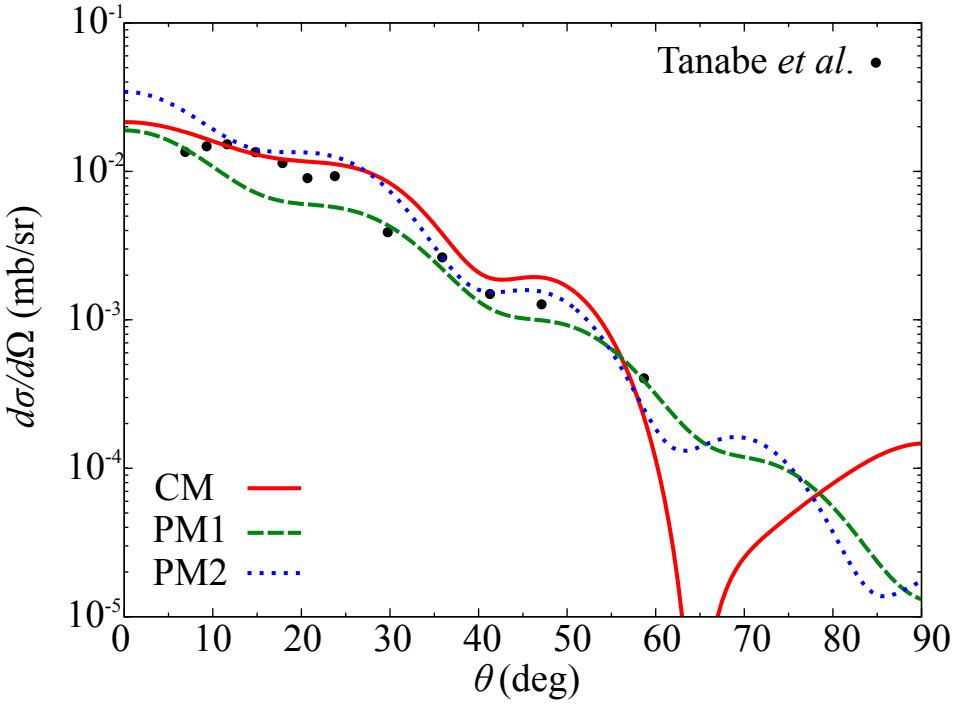

Figure 5.4: Same as in Fig. 5.3 but for the transfer cross section to the 1^-_1 state of ^{20}Ne.

can be used.

Figure 5.4 shows the transfer cross section populating the 1^-_1 state of ^{20}Ne. One may draw a similar conclusion on this result to that for the transfer to the 0^+_1 state. It implies a possibility to probe a cluster structure also in a resonance state of a nucleus. This will be one of the advantages to use transfer reactions for the study of clustering phenomena.

5.4 Summary

We have analyzed the transfer reaction ^{16}O(^{6}Li,d)^{20}Ne to investigate the radial dependence of the α-cluster probability. The α-^{16}O relative wave function calculated microscopically are adopted in the DWBA analysis. We have found that the angular distribution of the transfer cross section is a good probe to see the radial dependence of the α-clustering probability. The procedure proposed in the present study can be useful and applicable to probe the cluster structure via observables in general systems such as unstable nuclei and sd-shell nuclei. As future work, to take into account the breakup channels of ^{6}Li with an $\alpha + d$+^{16}O three-body model by means of the continuum-discretized coupled-channels method (CDCC) [3,5,6] will be important. This will also minimize ambiguity of distorting potentials required in reaction calculations.

CHAPTER 6

Conclusion and Prospect

In this thesis, a three-body dynamics induced by loosely bound nuclei is studied. When a system consists of a projectile, which is loosely bound system of a two-body, and a target nucleus, the projectile can break up into its constituents in the intermediate state of scattering. Thus we have focused on a role of the breakup states of a projectile and it has been investigated by means of the method of the continuum-discretized coupled-channels (CDCC). By using the CDCC method, one can explicitly take into account the channel-couplings among ground and breakup channels of nuclei. An analysis with CDCC enables us to understand a three-body dynamics correctly.

In Chap. 2, the formulation of CDCC has been given. In CDCC a three-body wave function of the system is expanded with projectile's eigenfunctions, which include infinite number of states. It is difficult to handle this wave function, we truncate the momentum space at a certain value. Then its discretization is done in a finite space with using one of two procedures of the discretization. One is the average method, in which the projectile's wave function is taken as an average in momentum "bin" state. The other is the pseudostate method, in which the projectile's wave function is expanded with basis functions and the internal Hamiltonian of the projectile is diagonalized with them. The former is adopted for breakup reactions in Chap. 4, while the latter is used for transfer reactions discussed in Chap. 3. Moreover, the CDCC framework with the eikonal approximation, in which the deviation of the projectile-target distorted wave from a plane wave is assumed to be small, is formulated, that is the eikonal-CDCC (E-CDCC). The E-CDCC can be performed as a coupled-channels calculation with a minimal computational cost compared to a full quantum calculation.

In Chap. 3, we have formulated the coupled-channel Born approximation (CCBA) model, which explicitly takes into account the breakup states of both a projectile and a residual nucleus in the initial and final channels, respectively. As a first application, the ^{8}B(d,n)^{9}C reaction at 14.4 MeV/nucleon has been analyzed with the CCBA model. It has been found that there exists a strong interference between the elastic transfer (ET) and the breakup transfer (BT) in each channel. Note that the former is the transfer process from the ground state in the initial channel to the ground state in the final channel, and includes the back couplings, which is the channel-couplings between the ground and breakup states in each channel. The latter is the transfer process from or into breakup states in each channel. It has also been pointed out that the back couplings are weak in each channel and the BT between breakup channels is negligibly small. Furthermore the transferred angular momentum l can change through the channel-couplings with non ground state's partial waves of ^{9}C. This dynamical change of l enhances the cross section by about 25% at forward

angles, and the importance of that involving the continuum states of ^{9}C has been newly discussed by our study. Thus it has been found that the picture of the ^{8}B(d,n)^{9}C reaction is different from that described by a conventional distorted-wave Born approximation (DWBA), in which the breakup channels of both d and ^{9}C are neglected. Next, the CCBA calculation has been performed for the ^{28}Si(d,p)^{29}Si reaction. For this reaction, it has been found that there is a strong back couplings in the initial channel and it decreases the cross section. This fact is very different from that for the ^{8}B(d,n)^{9}C reaction. Therefore it is needed to systematically investigate breakup effects on transfer reactions in order to clarify how that effects change in each reaction.

A discussion on breakup reactions has been given in Chap. 4. In particular, we have focused on a case with heavy ion target at a low incident energy, for example ^{208}Pb(^{15}C,n^{14}C) at 20.0 MeV/nucleon. For such a case, it has been expected to be difficult to precisely describe the reaction due to Coulomb interactions by means of the eikonal approximation. In the eikonal approximation, a Schrödinger equation to be solved is reduced to a first-order differential equation and it is much easier to solve compared to that in a full quantum case. First, we have compared two reaction models, which are based on the eikonal approximation, one is the eikonal CDCC (E-CDCC) and the other is the dynamical eikonal approximation (DEA). It has been found that two models solve essentially same equations when Coulomb interactions are absent. In this artificial case, the cross sections calculated with two models agree with each other. When Coulomb interactions exist, a situation is changed. Both models have not been able to reproduce results obtained from a full quantum calculation. To solve this problem, we have adopted the distance of closest approach in Rutherford scattering. This corresponds to the Coulomb correction that the curved trajectory is approximated by the straight line one, and it has worked well. Two models with the correction have reproduced well the full quantum results. It suggests that a concept of a "trajectory" is efficient in order to describe breakup reactions with strong Coulomb interactions.

The presence of the α-cluster states in nuclei has been investigated from the analysis of α-transfer reactions. Since cluster states develop at near threshold energy for decaying into their fragment, their structure is expected to be loosely bound system. In particular, for unstable nuclei, it may appear in their ground state. As a first application, the search for the α-cluster state of ^{20}Ne with the α-^{16}O configuration in its ground state, though it is not loosely bound state, has been done by using the α-transfer reaction, ^{16}O(^{6}Li,d)^{20}Ne. For the description of the α-transfer reaction, the wave function of ^{20}Ne calculated from the microscopic cluster model is adopted. Whereas, the DWBA model has been used for the description of the reaction process. It has been found that the transfer cross section is sensitive to evaluate the relative position of α particle to the ^{16}O core. We call the amplitude of the cluster wave function at this position as the α-clustering probability. Since this probability is involving the information of radii of clusters, which are not discussed in several studies to see spectroscopic factors, this probability could be a new indicator to argue the presence of α-cluster structures in nuclei. Furthermore it can be determined by comparing the experimental data, i.e., our framework is corroborative study, which exists out of conventional works that only bring theoretical predictions. For the future work it is needed to take into account the breakup states of ^{6}Li be means of CDCC in

the CCBA analysis of the α-transfer reaction. Though it is interesting to consider the continuum states of the residual nucleus, ^{20}Ne in this case, for the CCBA calculation, they cannot be calculated by the microscopic cluster model at this moment. After we buildup the procedure to prove the cluster structure of ^{20}Ne, the systematic investigation of the clustering in several nuclei, for example, well-known light nuclei with cluster structure, sd-shell nuclei, which do not have the α-cluster in their ground state, and unstable nuclei, will come out.

APPENDIX A

The Continuum-Discretized Coupled-Channels Method as Approximate Faddeev Formulation with Angular Momentum Truncation

The method of the continuum-discretized coupled-channels (CDCC) is discussed in Ref. [109] as an approximate calculation of three-body systems with a truncation of a Faddeev formulation [164, 165] in angular momentum space. We consider the $d+A$ scattering with the $p+n+A$ three-body model. The total wave function Ψ of the system satisfies the Schrödinger equation

$$[E - K - V(r) - U_p(r_p) - U_n(r_n)]\,\Psi = 0, \tag{A.1}$$

where E is the total energy and K stands for the kinetic energy operator of the system. We assume that the p-n interaction V is rotationally invariant and the interaction potentials between the nucleons in d and A are U_p and U_n. Coordinates of the system is shown in Fig. A.1.

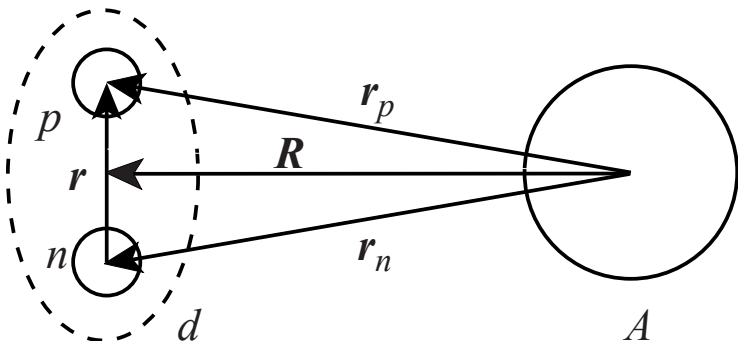

Figure A.1: Coordinates of the $p+n+A$ three-body system.

Here we introduce the projection operator P defined by

$$P = \int d\hat{\boldsymbol{r}} \sum_{l=0}^{l_m} \sum_{m} Y_{lm}\left(\hat{\boldsymbol{r}}\right) Y_{lm}^{*}\left(\hat{\boldsymbol{r}}\right), \tag{A.2}$$

which only selects the low angular momentum l regarding the p-n system up to a maximum value l_m. Then we can define

$$Q \equiv 1 - P, \tag{A.3}$$
$$P^2 = P, \tag{A.4}$$
$$Q^2 = Q, \tag{A.5}$$
$$PQ = QP = 0. \tag{A.6}$$

The partial wave functions $P\Psi$ and $Q\Psi$ are orthogonal. Furthermore they consist of the Faddeev components; $\Psi = \Psi_d + \Psi_p + \Psi_n$, where the each components are defined by the standard Faddeev equations [164, 165]

$$\left[E - K - V\right] \Psi_d = V\left(\Psi_p + \Psi_n\right), \tag{A.7}$$
$$\left[E - K - U_p\right] \Psi_p = U_p\left(\Psi_d + \Psi_n\right), \tag{A.8}$$
$$\left[E - K - U_n\right] \Psi_n = U_n\left(\Psi_d + \Psi_p\right). \tag{A.9}$$

As we can see from Eqs. (A.7) to (A.9), the deuteron component Ψ_d corresponds to the state when p and n construct d. Whereas the proton (neutron) component Ψ_p (Ψ_n) expresses the channel for the proton (neutron) scattering state toward the n-A (p-A) subsystem, which can be both bound and continuum states.

By multiplying Eq. (A.1) by P and Q from the left, we have the following coupled equations respectively;

$$\left[E - K - V - PU\right] P\Psi = PUQ\Psi, \tag{A.10}$$
$$\left[E - K - V - QU\right] Q\Psi = QUP\Psi, \tag{A.11}$$

where $U = U_p + U_n$. When one sets the right-hand side (RHS) of Eq. (A.10) as 0, it becomes

$$\left[E - K - V - PUP\right] P\Psi = 0. \tag{A.12}$$

Thus the CDCC approximation $\Psi^{\mathrm{CDCC}} \approx P\Psi$ leads

$$\left[E - K - V - PUP\right] \Psi^{\mathrm{CDCC}} = 0. \tag{A.13}$$

The elimination of the coupling term $PUQ\Psi$ in Eq. (A.10) is based on the argument that $PUQ\Psi$ is expected to be small (a) because U has small matrix element if l significantly changes between the P and Q spaces, and (b) because, when l_m is taken to be a large value, U only connects $l \sim l'$ states in each space.

To make clear the difference between the CDCC approach and the complete theory, we look the distorted Faddeev equations

$$[E - K - V - PUP]\,\hat{\Psi}_d = V\left(\hat{\Psi}_p + \hat{\Psi}_n\right), \tag{A.14}$$

$$[E - K - U_p]\,\hat{\Psi}_p = (U_p - PU_pP)\,\hat{\Psi}_d + U_p\hat{\Psi}_n, \tag{A.15}$$

$$[E - K - U_n]\,\hat{\Psi}_n = (U_n - PU_nP)\,\hat{\Psi}_d + U_n\hat{\Psi}_p, \tag{A.16}$$

in which the three-body distorting potentials are inserted. It was pointed out [110] that the distorted Faddeev equations (A.14) to (A.16) still hold the mathematical properties of the standard Faddeev equations (A.7) to (A.9). When Eqs. (A.14) to (A.16) are added, the original Schrödinger equation (A.1) is recovered.

By adding only Eqs. (A.15) and (A.16), one obtains

$$[E - K - U_p - U_n]\left(\hat{\Psi}_p + \hat{\Psi}_n\right) = (U - PUP)\,\hat{\Psi}_d. \tag{A.17}$$

The subtraction of PUP in Eq. (A.17) is expected to weaken the coupling between Ψ_d and $\Psi_p + \Psi_n$.

Since, from Eq. (A.14), $QV\left(\hat{\Psi}_p + \hat{\Psi}_n\right) = VQ\left(\hat{\Psi}_p + \hat{\Psi}_n\right) \sim 0$, we can approximate that the deuteron component $\hat{\Psi}_d$ has only the P-space contribution;

$$\hat{\Psi}_d \approx P\hat{\Psi}_d. \tag{A.18}$$

Then the insertion of Eq. (A.18) into Eq. (A.17) leads

$$[E - K - U_p - U_n]\left(\hat{\Psi}_p + \hat{\Psi}_n\right) \approx QUP\hat{\Psi}_d. \tag{A.19}$$

Here we use

$$\begin{aligned}(U - PUP)\,\hat{\Psi}_d &\approx (U - PUP)\,P\hat{\Psi}_d \\ &= [U - (1-Q)\,U\,(1-Q)]\,P\hat{\Psi}_d \\ &= (PUQ + QUQ + QUP)\,P\hat{\Psi}_d \\ &= QUP\hat{\Psi}_d. \end{aligned} \tag{A.20}$$

Within the approximation Eq. (A.18), each component of Ψ is calculated by solving the simultaneous equations associated with Eqs. (A.14) and (A.19). The amplitude of $\hat{\Psi}_p + \hat{\Psi}_n$ extracted from Eq. (A.19) is expected to be small owing to the projection operator Q. Furthermore, since the short-ranged V suppresses the magnitude of $\hat{\Psi}_p + \hat{\Psi}_n$ within its range in Eq. (A.14), the Q components from Eq. (A.19) do not contribute to the calculation.

One can insert the CDCC wave function Ψ^{CDCC} into Eq. (A.19) as a zeroth order approximation for $\hat{\Psi}_d$. Then Eq. (A.14) is solved as an inhomogeneous differential equation. In the calculation the P-space part of $\hat{\Psi}_p + \hat{\Psi}_n$ should be considered because V is the short ranged interaction. This is the justification of CDCC as a truncation of the Faddeev formalism in the space of l.

This fact can also be understood from that, first we adopt $\Psi^{\rm CDCC}$ as the zeroth order solution of Eq. (A.14) when the RHS is set to be zero. Then $\hat{\Psi}_d$ is inserted as the source term in the RHS of Eq. (A.19). As mentioned above, the component $QUP\hat{\Psi}_d$, which is expected to be small if l_m is taken to be large enough, produces a small amplitudes of $\hat{\Psi}_p + \hat{\Psi}_n$ in Eq. (A.19). Therefore, we can regard $\Psi^{\rm CDCC}$ as an approximate solution of Eq. (A.14). These formulations that elucidate the good agreement between CDCC and the distorted Faddeev formulation is sometimes called the Austern-Yahiro-Kawai theorem.

Before establishing the Austern-Yahiro-Kawai theorem, CDCC was criticized [166, 167] for (I) how to define the asymptotic behavior of coupled-channel distorted wave, (II) whether CDCC calculations provide converged results regarding their model space parameters such as the maximum values of the p-n orbital angular momenta and the p-n relative momenta, and (III) the justification of the results if they converge. The problem (I) was resolved in Ref. [5] by the l-truncation that enables to reduce the asymptotic form of coupling potentials to proper one. Then, for the task (II), it was numerically proved that results obtained by CDCC calculations does converge [168–170]. Finally the formulation of CDCC was authorized to be an good approximation of the Faddeev exact solution for three-body scattering with the idea based on the l-truncation [109, 117].

APPENDIX B

Coupling Potential

Contents

In this appendix, the derivations of Eqs. (2.68) and (2.71) are given.

B.1 Derivation of Z factor

The integral in Eq. (2.67) can be done by using the Wigner-Eckart theorem as follows;

$$
\begin{aligned}
&\left\langle \left[Y_{\ell'}(\hat{\boldsymbol{r}}) \otimes Y_{L'}(\hat{\boldsymbol{R}})\right]_{JM} \middle| \left[Y_{\lambda}(\hat{\boldsymbol{r}}) \otimes Y_{\lambda}(\hat{\boldsymbol{R}})\right]_{00} \middle| \left[Y_{\ell}(\hat{\boldsymbol{r}}) \otimes Y_{L}(\hat{\boldsymbol{R}})\right]_{JM} \right\rangle \\
&= \left\langle \left[Y_{\ell'}(\hat{\boldsymbol{r}}) \otimes Y_{L'}(\hat{\boldsymbol{R}})\right]_{J} \middle|\middle| \left[Y_{\lambda}(\hat{\boldsymbol{r}}) \otimes Y_{\lambda}(\hat{\boldsymbol{R}})\right]_{0} \middle|\middle| \left[Y_{\ell}(\hat{\boldsymbol{r}}) \otimes Y_{L}(\hat{\boldsymbol{R}})\right]_{J} \right\rangle \frac{1}{\hat{J}} \left(JMJ00|JM\right) \\
&= \hat{J} \begin{Bmatrix} \ell & L & J \\ \lambda & \lambda & 0 \\ \ell' & L' & J \end{Bmatrix} \left\langle Y_{\ell'} \,||Y_{\lambda}||\, Y_{\ell} \right\rangle \left\langle Y_{L'} \,||Y_{\lambda}||\, Y_{L} \right\rangle \\
&= \hat{J} \begin{Bmatrix} \ell' & L' & J \\ \ell & L & J \\ \lambda & \lambda & 0 \end{Bmatrix} (-)^{\lambda} \frac{\hat{\ell}'\hat{\lambda}}{\sqrt{4\pi}} \left(\ell'0\lambda0|\ell0\right) (-)^{\lambda} \frac{\hat{L}'\hat{\lambda}}{\sqrt{4\pi}} \left(L'0\lambda0|L0\right) .
\end{aligned}
\tag{B.1}
$$

Here, for the third line of Eq. (B.1), we have used the relation of the reduced matrix element with the 9-j symbol given by

$$
\begin{aligned}
&\left\langle \left[Y_{\ell_1}(\hat{\boldsymbol{r}}) \otimes Y_{L_1}(\hat{\boldsymbol{R}})\right]_{J_1} \middle|\middle| \left[Y_{l_2}(\hat{\boldsymbol{r}}) \otimes Y_{l_2}(\hat{\boldsymbol{R}})\right]_{J_2} \middle|\middle| \left[Y_{\ell_3}(\hat{\boldsymbol{r}}) \otimes Y_{L_3}(\hat{\boldsymbol{R}})\right]_{J_3} \right\rangle \\
&= \hat{J}_1\hat{J}_2\hat{J}_3 \begin{Bmatrix} \ell_3 & L_3 & J_3 \\ \ell_2 & L_2 & J_2 \\ \ell_1 & L_1 & J_1 \end{Bmatrix} \left\langle Y_{\ell_1} \,||Y_{\ell_2}||\, Y_{\ell_3} \right\rangle \left\langle Y_{L_1} \,||Y_{L_2}||\, Y_{L_3} \right\rangle ,
\end{aligned}
\tag{B.2}
$$

To obtain the fourth line of Eq. (B.1), we have used Eq. (K.186).

The 9-j symbol including 0 component can be expressed by the Racah coefficient as

follows;

$$
\begin{aligned}
&\left\langle \left[Y_{\ell'}(\hat{\boldsymbol{r}}) \otimes Y_{L'}(\hat{\boldsymbol{R}})\right]_{JM} \middle| \left[Y_{\lambda}(\hat{\boldsymbol{r}}) \otimes Y_{\lambda}(\hat{\boldsymbol{R}})\right]_{00} \middle| \left[Y_{\ell}(\hat{\boldsymbol{r}}) \otimes Y_{L}(\hat{\boldsymbol{R}})\right]_{JM} \right\rangle \\
&= \hat{J} \begin{Bmatrix} \ell' & \ell & \lambda \\ L' & L & \lambda \\ J & J & 0 \end{Bmatrix} \frac{\hat{\ell}'\hat{L}'\hat{\lambda}^2}{4\pi} \left(\ell' 0 \lambda 0 | \ell 0\right) \left(L' 0 \lambda 0 | L 0\right) \\
&= \hat{J} \frac{(-)^{\ell+L'+\lambda+J}}{\hat{\lambda}\hat{J}} \begin{Bmatrix} \ell' & \ell & \lambda \\ L & L' & J \end{Bmatrix} \frac{\hat{\ell}'\hat{L}'\hat{\lambda}^2}{4\pi} \left(\ell' 0 \lambda 0 | \ell 0\right) \left(L' 0 \lambda 0 | L 0\right) \\
&= (-)^{\ell+L'+\lambda+J} \begin{Bmatrix} \ell & \ell' & \lambda \\ L' & L & J \end{Bmatrix} \frac{\hat{\ell}'\hat{L}'\hat{\lambda}}{4\pi} \left(\ell' 0 \lambda 0 | \ell 0\right) \left(L' 0 \lambda 0 | L 0\right) \\
&= (-)^{\ell+L'+\lambda+J} (-)^{\ell+\ell'+L+L'} W(\ell, \ell', L, L'; \lambda, J) \frac{\hat{\ell}'\hat{L}'\hat{\lambda}}{4\pi} \left(\ell' 0 \lambda 0 | \ell 0\right) \left(L' 0 \lambda 0 | L 0\right) \\
&= (-)^{\ell'+L+\lambda+J} W(\ell, \ell', L, L'; \lambda, J) \frac{\hat{\ell}'\hat{L}'\hat{\lambda}}{4\pi} (-)^{\ell'} \frac{\hat{\ell}}{\hat{\lambda}} \left(\ell' 0 \ell 0 | \lambda 0\right) (-)^{L'} \frac{\hat{L}}{\hat{\lambda}} \left(L' 0 L 0 | \lambda 0\right) \\
&= (-)^{L+L'+\lambda+J} \frac{\hat{\ell}\hat{\ell}'\hat{L}\hat{L}'}{4\pi\hat{\lambda}} \left(\ell' 0 \ell 0 | \lambda 0\right) \left(L' 0 L 0 | \lambda 0\right) W(\ell, \ell', L, L'; \lambda, J)
\end{aligned} \tag{B.3}
$$

Thus, by inserting Eq. (B.3) into Eq. (2.67), we obtain the Z factor

$$
\begin{aligned}
Z(\ell' L' \ell L; \lambda J) = i^{\ell+\ell'+L+L'} (-)^{L+L'+J} &\frac{\hat{\ell}\hat{\ell}'\hat{L}'\hat{L}'}{\hat{\lambda}^2} \\
&\times \left(\ell' 0 \ell 0 | \lambda 0\right) \left(L' 0 L 0 | \lambda 0\right) W(\ell \ell' L L'; \lambda J).
\end{aligned} \tag{B.4}
$$

B.2 Derivation of Coulomb coupling potential

Since the Coulomb interaction is well known, its form of the multipole expansion is also known. $V_x^{\lambda(\mathrm{C})}$ defined by Eq. (2.62) can be decompose into two terms;

$$
V_x^{\lambda(\mathrm{C})}(\alpha r, R) \equiv X_x^{\lambda}(R) + W_x^{\lambda}(r, R), \tag{B.5}
$$

where X_x^{λ} (W_x^{λ}) does not (does) depend on r. As follows we see X_x^{λ} for each case, which is divided by the magnitude relation of r_x and R_{C}. R_{C} is the Coulomb radius of a uniformly charged sphere,

$$
V^{(\mathrm{C})}(\rho) = \begin{cases} \frac{Z_x Z_y e^2}{2R_{\mathrm{C}}} \left(3 - \frac{\rho^2}{R_{\mathrm{C}}}^2\right) & \text{for } \rho \le R_{\mathrm{C}}, \\ \frac{Z_x Z_y e^2}{\rho} & \text{for } \rho > R_{\mathrm{C}}. \end{cases} \tag{B.6}
$$

1. $r_x \le R_{\mathrm{C}}$ for every w
   In this case we have

$$
\begin{aligned}
V_x^{(\mathrm{C})}(r_x) &= \frac{Z_x Z_y e^2}{2R_{\mathrm{C}}} \left(3 - \frac{r_x^2}{R_{\mathrm{C}}^2}\right) \\
&= \frac{Z_x Z_y e^2}{2R_{\mathrm{C}}} \left(3 - \frac{R^2 + \alpha^2 r^2}{R_{\mathrm{C}}^2}\right) - \frac{Z_x Z_y e^2}{2R_{\mathrm{C}}} . \frac{\alpha R r w}{R_{\mathrm{C}}^2}
\end{aligned} \tag{B.7}
$$

Thus from Eq. (2.62) we obtain

$$V_x^{\lambda(\mathrm{C})}(\alpha r, R) = \frac{\hat{\lambda}^2}{2}\int_{-1}^{1}\left[\frac{Z_x Z_y e^2}{2R_\mathrm{C}}\left(3-\frac{R^2+\alpha^2 r^2}{R_\mathrm{C}^2}\right)-\frac{Z_x Z_y e^2}{2R_\mathrm{C}}\frac{\alpha R r w}{R_\mathrm{C}^2}\right]P_\lambda(w)dw$$
$$= \begin{cases} \dfrac{Z_x Z_y e^2}{2R_\mathrm{C}}\left(3-\dfrac{R^2+\alpha^2 r^2}{R_\mathrm{C}^2}\right) & \lambda = 0, \\ -\dfrac{Z_x Z_y e^2}{2R_\mathrm{C}}\dfrac{\alpha R r}{R_\mathrm{C}^2} & \lambda = 1, \\ 0 & \lambda \geq 2 \end{cases} \tag{B.8}$$

Here $P_0(w) = 1$, $P_1(w) = w$, and

$$\int_{-1}^{1} w^n P_\lambda(w)dw = 0 \quad \text{for} \quad n = 0, 1, \cdots, \lambda - 1, \tag{B.9}$$

are used. Therefore $X_{x,i}^{\lambda}$ is calculated by

$$X_{x,1}^{\lambda}(r_x) = \begin{cases} \dfrac{Z_x Z_y e^2}{2R_\mathrm{C}}\left(3-\dfrac{R^2}{R_\mathrm{C}^2}\right) & \lambda = 0, \\ 0 & \lambda \geq 1 \end{cases} \tag{B.10}$$

2. $r_x \geq R_\mathrm{C}$ for every w
   In this case we have following relation:

$$\frac{1}{r_x} = \frac{1}{\sqrt{R^2+\alpha^2 r^2+2\alpha R r w}} = \begin{cases} \dfrac{1}{R}\displaystyle\sum_\ell \left(\frac{\alpha r}{R}\right)^\ell P_\ell(w) & R \geq \alpha r, \\ \dfrac{1}{\alpha r}\displaystyle\sum_\ell \left(\frac{R}{\alpha r}\right)^\ell P_\ell(w) & R \leq \alpha r \end{cases} \tag{B.11}$$

Thus $V_x^{\lambda(\mathrm{C})}$ is

$$V_x^{\lambda(\mathrm{C})}(\alpha r, R) = \frac{\hat{\lambda}^2}{2}\int_{-1}^{1}\frac{Z_x Z_y e^2}{r_x}P_\lambda(w)dw$$
$$= \begin{cases} Z_x Z_y e^2 \dfrac{(\alpha r)^\lambda}{R^{\lambda+1}}P_\ell(w) & R \geq \alpha r, \\ Z_x Z_y e^2 \dfrac{R^\lambda}{(\alpha r)^{\lambda+1}}P_\ell(w) & R \leq \alpha r \end{cases} \tag{B.12}$$

Here ℓ aligns to λ in Eq. (B.12) since we use the orthogonal condition Eq. (2.60). Therefore $X_{x,ii}^{\lambda}$ is finite only when $\lambda = 0$ and $R > \alpha r$:

$$X_{x,2}^{\lambda}(r_x) = \frac{Z_x Z_y e^2}{R}, \tag{B.13}$$

and any other cases $X_{x,2}^{\lambda} = 0$.

3. Exception of 1 and 2
   $V_x^{\lambda(\mathrm{C})}$ can be written as

$$V_x^{\lambda(\mathrm{C})}(\alpha r, R) = \frac{\hat{\lambda}^2}{2}\left(\int_{-1}^{w_0} \frac{Z_x Z_y e^2}{r_x} P_\lambda(w)dw + \int_{w_0}^{1} \frac{Z_x Z_y e^2}{R_\mathrm{C}}\left(3 - \frac{r_x^2}{R_\mathrm{C}^2}\right) P_\lambda(w)dw\right), \tag{B.14}$$

   where w_0, which express that at $w = w_0$ $r_x = R_\mathrm{C}$, is defined by

$$w_0 = \frac{R_\mathrm{C}^2 - R^2 - \alpha^2 r^2}{2\alpha R r}. \tag{B.15}$$

   We can obtain $X_{x,3}^\lambda$ from Eq. (B.14).

Therefore X_x^λ and $W_x^\lambda = V_x^{\lambda(\mathrm{C})} - X_x^\lambda$ can be evaluated. When $R \leq R_\mathrm{C}$, $f_x^{(\mathrm{C})}$ in Eq. (2.70) is written by

$$\begin{aligned} f^{(\mathrm{C})}_{x,n'\ell' n\ell\lambda}(R) &= \int_0^\infty \hat{\phi}^*_{n'\ell'}(r) V_x^{\lambda(\mathrm{C})}(\alpha r, R)\hat{\phi}_{n\ell}(r)dr \\ &= \int_0^{\frac{R_\mathrm{C}-R}{\alpha}} \hat{\phi}^*_{n'\ell'}(r)\left(X^\lambda_{x,1}(R) + W^\lambda_{x,1}(r,R)\right)\hat{\phi}_{n\ell}(r)dr \\ &+ \int_{\frac{R_\mathrm{C}-R}{\alpha}}^{\frac{R_\mathrm{C}+R}{\alpha}} \hat{\phi}^*_{n'\ell'}(r)\left(X^\lambda_{x,3}(R) + W^\lambda_{x,3}(r,R)\right)\hat{\phi}_{n\ell}(r)dr \\ &+ \int_{\frac{R_\mathrm{C}+R}{\alpha}}^\infty \hat{\phi}^*_{n'\ell'}(r)\left(X^\lambda_{x,2}(R) + W^\lambda_{x,2}(r,R)\right)\hat{\phi}_{n\ell}(r)dr. \end{aligned} \tag{B.16}$$

On the other hand for $R \geq R_\mathrm{C}$ we obtain

$$\begin{aligned} f^{(\mathrm{C})}_{x,n'\ell' n\ell\lambda}(R) &= \int_0^{\frac{R-R_\mathrm{C}}{\alpha}} \hat{\phi}^*_{n'\ell'}(r)\left(X^\lambda_{x,2}(R) + W^\lambda_{x,2}(r,R)\right)\hat{\phi}_{n\ell}(r)dr \\ &+ \int_{\frac{R-R_\mathrm{C}}{\alpha}}^{\frac{R+R_\mathrm{C}}{\alpha}} \hat{\phi}^*_{n'\ell'}(r)\left(X^\lambda_{x,3}(R) + W^\lambda_{x,3}(r,R)\right)\hat{\phi}_{n\ell}(r)dr \\ &+ \int_{\frac{R+R_\mathrm{C}}{\alpha}}^\infty \hat{\phi}^*_{n'\ell'}(r)\left(X^\lambda_{x,1}(R) + W^\lambda_{x,1}(r,R)\right)\hat{\phi}_{n\ell}(r)dr. \end{aligned} \tag{B.17}$$

Here let's focus on the case of $R > R_\mathrm{C}$. In the case, only the first term of Eq. (B.17) has an amplitude. We write the term, which contains X_x^λ,

$$\begin{aligned} &\int_0^{\frac{R-R_\mathrm{C}}{\alpha}} \hat{\phi}^*_{n'\ell'}(r) X^0_{x,2}(R)\hat{\phi}_{n\ell}(r)dr \\ &\quad= \frac{Z_x Z_y e^2}{R}\left(\int_0^\infty \hat{\phi}^*_{n'\ell'}(r)\hat{\phi}_{n\ell}(r)dr - \int_{\frac{R-R_\mathrm{C}}{\alpha}}^\infty \hat{\phi}^*_{n'\ell'}(r)\hat{\phi}_{n\ell}(r)dr\right) \\ &\quad= \frac{Z_x Z_y e^2}{R}\left(\delta_{n'n}\delta_{\ell'\ell} - \int_{\frac{R-R_\mathrm{C}}{\alpha}}^\infty \hat{\phi}^*_{n'\ell'}(r)\hat{\phi}_{n\ell}(r)dr\right). \end{aligned} \tag{B.18}$$

Here we use Eqs. (2.13) and (B.12). In CDCC Eq. (B.18) is integrated up to $r = r_{\max}$ as follows.

$$\begin{aligned}
&\int_0^{\frac{R-R_{\rm C}}{\alpha}} \hat{\phi}^*_{n'\ell'}(r) X^0_{x,2}(R) \hat{\phi}_{n\ell}(r) dr \\
&\qquad \approx \frac{Z_x Z_y e^2}{R} \left(\int_0^{r_{\max}} \hat{\phi}^*_{n'\ell'}(r) \hat{\phi}_{n\ell}(r) dr - \int_{\frac{R-R_{\rm C}}{\alpha}}^{r_{\max}} \hat{\phi}^*_{n'\ell'}(r) \hat{\phi}_{n\ell}(r) dr \right) \\
&\qquad \approx \frac{Z_x Z_y e^2}{R} \left(\delta_{n'n}\delta_{\ell'\ell} - \int_{\frac{R-R_{\rm C}}{\alpha}}^{r_{\max}} \hat{\phi}^*_{n'\ell'}(r) \hat{\phi}_{n\ell}(r) dr \right). \qquad \text{(B.19)}
\end{aligned}$$

Note that $r_{\max}$ should be taken as the orthogonal condition Eq. (2.13) can be satisfied. The second term of Eq. (B.19) appears when $r_{\max} \geq \frac{R-R_{\rm C}}{\alpha}$. Thus we obtain the same form as Eq. (B.17):

$$\begin{aligned}
f^{\rm (C)}_{x,n'\ell'n\ell\lambda}(R) = \frac{Z_x Z_y e^2}{R} &\left[\delta_{n'n}\delta_{\ell'\ell} - \int_{\frac{R-R_{\rm C}}{\alpha}}^{r_{\max}} \hat{\phi}^*_{n'\ell'}(r) \hat{\phi}_{n\ell}(r) dr \theta\left(r_{\max} - (R-R_{\rm C})/\alpha\right) \right] \\
&+ \int_0^{\frac{R-R_{\rm C}}{\alpha}} \hat{\phi}^*_{n'\ell'}(r) + W^\lambda_{x,2}(r,R) \hat{\phi}_{n\ell}(r) dr \\
&+ \int_{\frac{R-R_{\rm C}}{\alpha}}^{\frac{R+R_{\rm C}}{\alpha}} \hat{\phi}^*_{n'\ell'}(r) \left(X^\lambda_{x,3}(R) + W^\lambda_{x,3}(r,R) \right) \hat{\phi}_{n\ell}(r) dr \theta\left(r_{\max} - (R-R_{\rm C})/\alpha\right) \\
&+ \int_{\frac{R+R_{\rm C}}{\alpha}}^{r_{\max}} \hat{\phi}^*_{n'\ell'}(r) \left(X^\lambda_{x,1}(R) + W^\lambda_{x,1}(r,R) \right) \hat{\phi}_{n\ell}(r) dr \theta\left(r_{\max} - (R-R_{\rm C})/\alpha\right), \qquad \text{(B.20)}
\end{aligned}$$

where $\theta(r_1 - r_2)$ is the step function defined by

$$\theta(r_1 - r_2) = \begin{cases} 0 & r_1 < r_2 \\ 1 & r_1 \geq r_2. \end{cases} \qquad \text{(B.21)}$$

APPENDIX C

Calculation of Form Factor

Contents

C.1 Finite-range Form factor

C.1.1 Gaussian expansion

The form factor defined by Eq. (3.69) with the exact finite-range (FR) integration of Eq. (3.79) can be rewritten with using Eqs. (3.76) and (3.77) by

$$\begin{aligned} f_{lm}(\boldsymbol{r}_\beta, \boldsymbol{r}_\alpha) &= \sum_{L_\alpha L_\beta M_\alpha M_\beta} F_{l L_\beta L_\alpha}(r_\beta, r_\alpha)\, (L_\beta M_\beta L_\alpha M_\alpha | lm)\, Y^*_{L_\beta M_\beta}(\hat{\boldsymbol{r}}_\beta) Y^*_{L_\alpha M_\alpha}(\hat{\boldsymbol{r}}_\alpha) \\ &= \sum_{L_\alpha L_\beta} (-)^{L_\beta + L_\alpha - l} F_{l L_\beta L_\alpha}(r_\beta, r_\alpha)\, \left[Y_{L_\alpha}(\hat{\boldsymbol{r}}_\alpha) \otimes Y_{L_\beta}(\hat{\boldsymbol{r}}_\beta) \right]^*_{lm}. \end{aligned} \tag{C.1}$$

The form factor f_{lm} can be also written by definition,

$$f_{lm}(\boldsymbol{r}_\beta, \boldsymbol{r}_\alpha) \equiv \sum_{m_A m_b} (-)^{m_b}\, (l_A m_A l_b, -m_b | lm)\, \psi^*_{xA}(\boldsymbol{r}_{xA}) D_{xb}(\boldsymbol{r}_{xb}), \tag{C.2}$$

where,

$$D_{xb}(\boldsymbol{r}_{xb}) \equiv V_{xb}(r_{xb}) \psi_{xb}(\boldsymbol{r}_{xb}). \tag{C.3}$$

Here we assume the interaction $V_{xb}(r_{xb})$ between x and b is scalar, and ψ_{xc} is the relative wave function between x and c.

To express the Eq. (3.65) with the set of coordinates $(\boldsymbol{r}_\beta, \boldsymbol{r}_\alpha)$, we expand the radial part of Eq. (3.65) with Gaussian. Thus ψ_{xA} and D_{xb} can be written as

$$\psi_{xA}(\boldsymbol{r}_{xA}) = \frac{\phi_{l_A}(r_{xA})}{r^{l_A}_{xA}} r^{l_A}_{xA} Y_{l_A m_A}(\hat{\boldsymbol{r}}_{xA}), \tag{C.4}$$

$$D_{xb}(\boldsymbol{r}_{xb}) = \frac{d_{l_b}(r_{xb})}{r^{l_b}_{xb}} r^{l_b}_{xb} Y_{l_b m_b}(\hat{\boldsymbol{r}}_{xb}). \tag{C.5}$$

The radial parts of Eq. (C.4) and Eq. (C.5) are expanded:

$$\frac{\phi_{l_A}(r_{xA})}{r_{xA}^{l_A}} = \sum_{i_A} C_{i_A} \exp(-\nu_{i_A} r_{xA}^2), \tag{C.6}$$

$$\frac{d_{l_b}(r_{xb})}{r_{xb}^{l_b}} = \sum_{i_b} C_{i_b} \exp(-\nu_{i_b} r_{xb}^2). \tag{C.7}$$

Using Eq. (C.6) and (C.7), we obtain

$$\begin{aligned} f_{lm}(\boldsymbol{r}_\beta, \boldsymbol{r}_\alpha) = &\sum_{i_A i_b} g_{i_A i_b}(r_\alpha, r_\beta) \exp(\gamma_{i_A i_b} \boldsymbol{r}_\beta \cdot \boldsymbol{r}_\alpha) \\ &\times \sum_{m_A m_b} (-)^{m_b} (l_A m_A l_b, -m_b | lm)\, r_{xA}^{l_A} Y_{l_A m_A}^*(\hat{\boldsymbol{r}}_{xA}) r_{xb}^{l_b} Y_{l_b m_b}(\hat{\boldsymbol{r}}_{xb}), \end{aligned} \tag{C.8}$$

where

$$g_{i_A i_b}(r_\alpha, r_\beta) \equiv C_{i_A} C_{i_b} \exp(-\alpha_{i_A i_b} r_\alpha^2) \exp(-\beta_{i_A i_b} r_\beta^2), \tag{C.9}$$

and coordinates are written by $\boldsymbol{r}_{xA} = s\boldsymbol{r}_\alpha + t\boldsymbol{r}_\beta$ and $\boldsymbol{r}_{xb} = p\boldsymbol{r}_\alpha + q\boldsymbol{r}_\beta$ with

$$\begin{aligned} s &\equiv \frac{B}{x}\frac{a}{a+A}, \quad t \equiv -\frac{B}{x}\frac{b}{b+B}, \\ p &\equiv \frac{a}{x}\frac{A}{a+A}, \quad q \equiv -\frac{a}{x}\frac{B}{b+B}, \end{aligned} \tag{C.10}$$

then α, β, and γ are defined by

$$\begin{aligned} \alpha_{i_A i_b} &= \nu_{i_A} s^2 + \nu_{i_b} p^2, \\ \beta_{i_A i_b} &= \nu_{i_A} t^2 + \nu_{i_b} q^2, \\ \gamma_{i_A i_b} &= -2(\nu_{i_A} st + \nu_{i_b} pq) > 0. \end{aligned} \tag{C.11}$$

Gaussian, $\exp(\gamma_{i_A i_b} \boldsymbol{r}_\beta \cdot \boldsymbol{r}_\alpha)$, can be expanded with modified Bessel function i_L,

$$\exp(\gamma_{i_A i_b} \boldsymbol{r}_\beta \cdot \boldsymbol{r}_\alpha) = 4\pi \sum_L (-)^L \hat{L} i_L(\gamma_{i_A i_b} r_\beta r_\alpha) \left[Y_L(\hat{\boldsymbol{r}}_\alpha) \otimes Y_L(\hat{\boldsymbol{r}}_\beta)\right]_{00}. \tag{C.12}$$

Since coordinates can be expressed by $\boldsymbol{r}_{xA} = s\boldsymbol{r}_\alpha + t\boldsymbol{r}_\beta$ and $\boldsymbol{r}_{xb} = p\boldsymbol{r}_\alpha + q\boldsymbol{r}_\beta$ in spherical harmonics with $\hat{\boldsymbol{r}}_\alpha$ $\hat{\boldsymbol{r}}_\beta$, the spherical harmonics converts,

$$r_{xA}^{l_A} Y_{l_A, m_A}^*(\hat{\boldsymbol{r}}_{xA}) = \sum_{\lambda_A}^{l_A} h_{\lambda_A}(r_\alpha, r_\beta) \left[Y_{l_A - \lambda_A}(\hat{\boldsymbol{r}}_\alpha) \otimes Y_{\lambda_A}(\hat{\boldsymbol{r}}_\beta)\right]^*_{l_A m_A}, \tag{C.13}$$

$$r_{xb}^{l_b} Y_{l_b, m_b}(\hat{\boldsymbol{r}}_{xb}) = \sum_{\lambda_b}^{l_b} h_{\lambda_b}(r_\alpha, r_\beta) \left[Y_{l_b - \lambda_b}(\hat{\boldsymbol{r}}_\alpha) \otimes Y_{\lambda_b}(\hat{\boldsymbol{r}}_\beta)\right]_{l_b m_b}, \tag{C.14}$$

where

$$h_{\lambda_A}(r_\alpha, r_\beta) \equiv \frac{\sqrt{4\pi}}{\hat{\lambda}_A} \sqrt{{}_{2l_A+1}C_{2\lambda_A}} (sr_\alpha)^{l_A - \lambda_A} (tr_\beta)^{\lambda_A}, \tag{C.15}$$

$$h_{\lambda_b}(r_\alpha, r_\beta) \equiv \frac{\sqrt{4\pi}}{\hat{\lambda}_b} \sqrt{{}_{2l_b+1}C_{2\lambda_b}} (pr_\alpha)^{l_b - \lambda_b} (qr_\beta)^{\lambda_b}, \tag{C.16}$$

and

$$ {}_{2l_c+1}C_{2\lambda_c} = \frac{(2l_c+1)!}{(2l_c+1-2\lambda_c)!(2\lambda_c)!} \tag{C.17} $$

is the binomial coefficient.

The radial part $F_{lL_\beta L_\alpha}$ of Eq. (C.1) can be calculated by

$$ F_{lL_\beta L_\alpha}(r_\beta, r_\alpha) = (-)^{L_\beta+L_\alpha-l} \int d\hat{\boldsymbol{r}}_\alpha d\hat{\boldsymbol{r}}_\beta \left[Y_{L_\alpha}(\hat{\boldsymbol{r}}_\alpha) \otimes Y_{L_\beta}(\hat{\boldsymbol{r}}_\beta)\right]_{lm} f_{lm}(\boldsymbol{r}_\beta, \boldsymbol{r}_\alpha). \tag{C.18} $$

Inserting Eq. (C.8), (C.12), (C.13), and (C.14) to Eq. (C.18), we obtain

$$ \begin{aligned} F_{lL_\beta L_\alpha}(r_\beta, r_\alpha) = & \sum_{i_A i_b} g_{i_A i_b}(r_\alpha, r_\beta) \sum_{\lambda_A \lambda_b} h_{\lambda_A}(r_\alpha, r_\beta) h_{\lambda_b}(r_\alpha, r_\beta) 4\pi \sum_L (-)^L \hat{L} i_L(\gamma_{i_A i_b} r_\beta r_\alpha) \\ & \times (-)^{L_\beta+L_\alpha-l} \int d\hat{\boldsymbol{r}}_\alpha d\hat{\boldsymbol{r}}_\beta \sum_{m_A m_b} (-)^{m_b} \left(l_A m_A l_b, -m_b | lm\right) \\ & \times \left[Y_{l_A-\lambda_A}(\hat{\boldsymbol{r}}_\alpha) \otimes Y_{\lambda_A}(\hat{\boldsymbol{r}}_\beta)\right]^*_{l_A m_A} \left[Y_{l_b-\lambda_b}(\hat{\boldsymbol{r}}_\alpha) \otimes Y_{\lambda_b}(\hat{\boldsymbol{r}}_\beta)\right]_{l_b m_b} \\ & \times \left[Y_L(\hat{\boldsymbol{r}}_\alpha) \otimes Y_L(\hat{\boldsymbol{r}}_\beta)\right]_{00} \left[Y_{L_\alpha}(\hat{\boldsymbol{r}}_\alpha) \otimes Y_{L_\beta}(\hat{\boldsymbol{r}}_\beta)\right]_{lm}. \end{aligned} \tag{C.19} $$

Here we convert the spherical harmonics in the vector coupling in order to align its arguments as follows:

$$ \begin{aligned} & \sum_{m_A m_b} (-)^{m_b} \left(l_A m_A l_b, -m_b | lm\right) \left[Y_{l_A-\lambda_A}(\hat{\boldsymbol{r}}_\alpha) \otimes Y_{\lambda_A}(\hat{\boldsymbol{r}}_\beta)\right]^*_{l_A m_A} \left[Y_{l_b-\lambda_b}(\hat{\boldsymbol{r}}_\alpha) \otimes Y_{\lambda_b}(\hat{\boldsymbol{r}}_\beta)\right]_{l_b m_b} \\ & \quad = \left[\left[Y_{l_A-\lambda_A}(\hat{\boldsymbol{r}}_\alpha) \otimes Y_{\lambda_A}(\hat{\boldsymbol{r}}_\beta)\right]_{l_A m_A} \otimes \left[Y_{l_b-\lambda_b}(\hat{\boldsymbol{r}}_\alpha) \otimes Y_{\lambda_b}(\hat{\boldsymbol{r}}_\beta)\right]_{l_b m_b}\right]^*_{lm} \\ & \quad = \sum_{j_\alpha j_\beta} \hat{l}_A \hat{l}_b \hat{j}_\alpha \hat{j}_\beta \begin{Bmatrix} l_A - \lambda_A & \lambda_A & l_A \\ l_b - \lambda_b & \lambda_b & l_b \\ j_\alpha & j_\beta & l \end{Bmatrix} \\ & \quad \times \left[\left[Y_{l_A-\lambda_A}(\hat{\boldsymbol{r}}_\alpha) \otimes Y_{l_b-\lambda_b}(\hat{\boldsymbol{r}}_\alpha)\right]_{j_\alpha} \otimes \left[Y_{\lambda_A}(\hat{\boldsymbol{r}}_\beta) \otimes Y_{\lambda_b}(\hat{\boldsymbol{r}}_\beta)\right]_{j_\beta}\right]^*_{lm}. \end{aligned} \tag{C.20} $$

Then the angular integration of Eq. (C.19) can be done using the Wigner-Eckart theorem:

$$ \begin{aligned} & \int d\hat{\boldsymbol{r}}_\alpha d\hat{\boldsymbol{r}}_\beta \left[\left[Y_{l_A-\lambda_A}(\hat{\boldsymbol{r}}_\alpha) \otimes Y_{l_b-\lambda_b}(\hat{\boldsymbol{r}}_\alpha)\right]_{j_\alpha} \otimes \left[Y_{\lambda_A}(\hat{\boldsymbol{r}}_\beta) \otimes Y_{\lambda_b}(\hat{\boldsymbol{r}}_\beta)\right]_{j_\beta}\right]^*_{lm} \\ & \quad \times \left[Y_L(\hat{\boldsymbol{r}}_\alpha) \otimes Y_L(\hat{\boldsymbol{r}}_\beta)\right]_{00} \left[Y_{L_\alpha}(\hat{\boldsymbol{r}}_\alpha) \otimes Y_{L_\beta}(\hat{\boldsymbol{r}}_\beta)\right]_{lm} \\ & \quad = \Big\langle \Big[\left[Y_{l_A-\lambda_A}(\hat{\boldsymbol{r}}_\alpha) \otimes Y_{l_b-\lambda_b}(\hat{\boldsymbol{r}}_\alpha)\right]_{j_\alpha} \otimes \left[Y_{\lambda_A}(\hat{\boldsymbol{r}}_\beta) \otimes Y_{\lambda_b}(\hat{\boldsymbol{r}}_\beta)\right]_{j_\beta}\Big]^*_{lm} \\ & \quad \times \left|\left[Y_L(\hat{\boldsymbol{r}}_\alpha) \otimes Y_L(\hat{\boldsymbol{r}}_\beta)\right]_{00}\right| \left[Y_{L_\alpha}(\hat{\boldsymbol{r}}_\alpha) \otimes Y_{L_\beta}(\hat{\boldsymbol{r}}_\beta)\right]_{lm} \Big\rangle \\ & \quad = \frac{1}{\hat{l}} \left(lm00|lm\right) \left\langle j_\alpha j_\beta l \,\|LL0\|\, L_\alpha L_\beta l \right\rangle. \end{aligned} \tag{C.21} $$

The reduced matrix element can be calculate with 9-j and 6-j symbol

$$\begin{aligned}
\langle j_\alpha j_\beta l \,\|LL0\|\, L_\alpha L_\beta l\rangle &= \hat{l}^2 \begin{Bmatrix} j_\alpha & j_\beta & l \\ L_\alpha & L_\beta & l \\ L & L & 0 \end{Bmatrix} \langle j_\alpha \,\|L\|\, L_\alpha\rangle \langle j_\beta \,\|L\|\, L_\beta\rangle \\
&= \hat{l}^2 \frac{(-)^{-j_\beta-l-L_\alpha-L}}{\hat{l}\hat{L}} \begin{Bmatrix} j_\alpha & j_\beta & l \\ L_\beta & L_\alpha & L \end{Bmatrix} \\
&\times \left\langle [Y_{l_A-\lambda_A}(\hat{\boldsymbol{r}}_\alpha) \otimes Y_{l_b-\lambda_b}(\hat{\boldsymbol{r}}_\alpha)]_{j_\alpha} \,\|Y_L(\hat{\boldsymbol{r}}_\alpha)\|\, Y_{L_\alpha}(\hat{\boldsymbol{r}}_\alpha)\right\rangle \\
&\times \left\langle [Y_{\lambda_A}(\hat{\boldsymbol{r}}_\beta) \otimes Y_{\lambda_b}(\hat{\boldsymbol{r}}_\beta)]_{j_\beta} \,\|Y_L(\hat{\boldsymbol{r}}_\beta)\|\, Y_{L_\beta}(\hat{\boldsymbol{r}}_\beta)\right\rangle \\
&= \hat{l}^2 \frac{(-)^{-j_\beta-l-L_\alpha-L}}{\hat{l}\hat{L}} \begin{Bmatrix} j_\alpha & j_\beta & l \\ L_\beta & L_\alpha & L \end{Bmatrix} \\
&\times \frac{1}{\sqrt{4\pi}} \frac{\widehat{l_A-\lambda_A}\widehat{l_b-\lambda_b}}{\hat{j}_\alpha} (l_A-\lambda_A, 0, l_b-\lambda_b, 0|j_\alpha 0) \\
&\times \frac{1}{\sqrt{4\pi}} \frac{\hat{\lambda}_A\hat{\lambda}_b}{\hat{j}_\beta} (\lambda_A 0 \lambda_b 0|j_\beta 0) \\
&\times \langle Y_{j_\alpha}(\hat{\boldsymbol{r}}_\alpha) \,\|Y_L(\hat{\boldsymbol{r}}_\alpha)\|\, Y_{L_\alpha}(\hat{\boldsymbol{r}}_\alpha)\rangle \left\langle Y_{j_\beta}(\hat{\boldsymbol{r}}_\beta) \,\|Y_L(\hat{\boldsymbol{r}}_\beta)\|\, Y_{L_\beta}(\hat{\boldsymbol{r}}_\beta)\right\rangle \\
&= \frac{\hat{l}}{\hat{L}}(-)^{-j_\beta-l-L_\alpha-L} \begin{Bmatrix} j_\alpha & j_\beta & l \\ L_\beta & L_\alpha & L \end{Bmatrix} \\
&\times \frac{\widehat{l_A-\lambda_A}\widehat{l_b-\lambda_b}\hat{\lambda}_A\hat{\lambda}_b}{4\pi\hat{j}_\alpha\hat{j}_\beta} (l_A-\lambda_A, 0, l_b-\lambda_b, 0|j_\alpha 0) (\lambda_A 0\lambda_b 0|j_\beta 0) \\
&\times (-)^L \frac{\hat{j}_\alpha\hat{L}}{\sqrt{4\pi}} (j_\alpha 0 L 0|L_\alpha 0) (-)^L \frac{\hat{j}_\beta\hat{L}}{\sqrt{4\pi}} (j_\beta 0 L 0|L_\beta 0) \\
&= \frac{1}{(4\pi)^2}(-)^{-j_\beta-l-L_\alpha-L}(-)^{j_\alpha+j_\beta+L_\alpha+L_\beta}\hat{l}\hat{L}\widehat{l_A-\lambda_A}\widehat{l_b-\lambda_b}\hat{\lambda}_A\hat{\lambda}_b \\
&\times W(j_\alpha j_\beta L_\alpha L_\beta; lL) (l_A-\lambda_A, 0, l_b-\lambda_b, 0|j_\alpha 0) (\lambda_A 0\lambda_b 0|j_\beta 0) \\
&\times (j_\alpha 0 L 0|L_\alpha 0) (j_\beta 0 L 0|L_\beta 0)\,. \qquad \text{(C.22)}
\end{aligned}$$

Inserting Eq. (C.21) to Eq. (C.19) using Eq. (C.22), we obtain following formula with a few transformations,

$$F_{lL_\beta L_\alpha}(r_\beta, r_\alpha) = \sum_{\lambda_A\lambda_b L} \mathscr{R}_{\lambda_A\lambda_b L}(r_\beta, r_\alpha)\mathscr{A}^{lL_\beta L_\alpha}_{\lambda_A\lambda_b L}, \qquad \text{(C.23)}$$

$$\mathscr{R}_{\lambda_A\lambda_b L}(r_\beta, r_\alpha) \equiv \frac{1}{4\pi} h_{\lambda_A}(r_\alpha, r_\beta) h_{\lambda_b}(r_\alpha, r_\beta) \sum_{i_A i_b} \tilde{g}_{i_A i_b}(r_\alpha, r_\beta)\tilde{i}_L(\gamma_{i_A i_b} r_\beta r_\alpha), \qquad \text{(C.24)}$$

$$\begin{aligned}
\mathscr{A}^{lL_\beta L_\alpha}_{\lambda_A\lambda_b L} &\equiv \sum_{j_\alpha j_\beta} (-)^{j_\alpha+L_\alpha-L}\hat{L}^2\hat{l}_A\hat{l}_b\hat{j}_\alpha\hat{j}_\beta\widehat{l_A-\lambda_A}\widehat{l_b-\lambda_b}\hat{\lambda}_A\hat{\lambda}_b \\
&\times (l_A-\lambda_A, 0, l_b-\lambda_b, 0|j_\alpha 0) (\lambda_A 0\lambda_b 0|j_\beta 0) (j_\alpha 0 L 0|L_\alpha 0) (j_\beta 0 L 0|L_\beta 0) \\
&\times W(j_\alpha j_\beta L_\alpha L_\beta; lL) \begin{Bmatrix} l_A-\lambda_A & \lambda_A & l_A \\ l_b-\lambda_b & \lambda_b & l_b \\ j_\alpha & j_\beta & l \end{Bmatrix}, \qquad \text{(C.25)}
\end{aligned}$$

where we transform the product of Gaussian and the modified Bessel function as follows;

$$(-)^L g_{i_A i_b}(r_\alpha, r_\beta) i_L(\gamma_{i_A i_b} r_\beta r_\alpha) = \tilde{g}_{i_A i_b}(r_\alpha, r_\beta) \tilde{i}_L(\gamma_{i_A i_b} r_\beta r_\alpha), \tag{C.26}$$

$$\tilde{g}_{i_A i_b}(r_\alpha, r_\beta) = C_{i_A} C_{i_b} \exp\left[-\nu_{i_A}(s r_\alpha + t r_\beta)^2\right] \exp\left[-\nu_{i_b}(p r_\alpha + q r_\beta)^2\right], \tag{C.27}$$

$$\tilde{i}_L(\gamma_{i_A i_b} r_\beta r_\alpha) = (-)^L \exp(-\gamma_{i_A i_b} r_\beta r_\alpha) i_L(\gamma_{i_A i_b} r_\beta r_\alpha). \tag{C.28}$$

The "reduced" modified Bessel function $\tilde{i}_L(\gamma_{i_A i_b} r_\beta r_\alpha)$ is calculated by the subroutine BESSI [171] in our CCBA code FRANTIC. The details of the clculation for $\tilde{i}_L(\gamma_{i_A i_b} r_\beta r_\alpha)$ is discussed in Appx. I.

C.1.2 Multipole expansion

If the bound state wave functions are expanded with the multipole expansion method instead of Gaussian, the representation of the form factor will be changed. In this method, we expand the product of $\phi^*_{l_{xA}}(r_{xA})/r^{l_{xA}}_{xA}$ and $d_{l_b}(r_{xb})/r^{l_b}_{xb}$, it means,

$$\begin{aligned} Q(r_{xA}, r_{xb}) &\equiv \frac{\phi^*_{l_A}(r_{xA})}{r^{l_A}_{xA}} \frac{d_{l_b}(r_{xb})}{r^{l_b}_{xb}} \\ &= \sum_k \tilde{Q}_k(r_\alpha, r_\beta) P_k(w), \end{aligned} \tag{C.29}$$

$$\tilde{Q}_k(r_\alpha, r_\beta) = \frac{\hat{k}^2}{2} \int_{-1}^{1} Q(r_{xA}, r_{xb}) P_k(w) dw, \tag{C.30}$$

where $w = \cos\theta_{\alpha\beta}$ with the angle $\theta_{\alpha\beta}$ between $\boldsymbol{r}_\alpha$ and $\boldsymbol{r}_\beta$.

Then we can obtain the form factor

$$\begin{aligned} f_{lm}(\boldsymbol{r}_\beta, \boldsymbol{r}_\alpha) &= \sum_k \tilde{Q}_k(r_\alpha, r_\beta) P_k(w) \sum_{m_{xA} m_{xb}} (-)^{m_{xb}} (l_{xA} m_{xA} l_{xb}, -m_{xb} | lm) \\ &= r^{l_A}_{xA} Y^*_{l_A m_A}(\hat{\boldsymbol{r}}_{xA}) r^{l_b}_{xb} Y_{l_b m_b}(\hat{\boldsymbol{r}}_{xb}) \\ &= \frac{1}{\sqrt{4\pi}} \sum_k \tilde{Q}_k(r_\alpha, r_\beta) \frac{4\pi}{\hat{k}} (-)^k \left[Y_k(\hat{\boldsymbol{r}}_\alpha) \otimes Y_k(\hat{\boldsymbol{r}}_\beta)\right]_{00} \\ &\times \sum_{m_A m_b} (-)^{m_b} (l_A m_A l_b, -m_b | lm) \\ &= \left[Y_{l_A - \lambda_A}(\hat{\boldsymbol{r}}_\alpha) \otimes Y_{\lambda_A}(\hat{\boldsymbol{r}}_\beta)\right]^*_{l_A m_A} \left[Y_{l_b - \lambda_b}(\hat{\boldsymbol{r}}_\alpha) \otimes Y_{\lambda_b}(\hat{\boldsymbol{r}}_\beta)\right]_{l_b m_b} \end{aligned} \tag{C.31}$$

Because the term which relates to the sums of m_A and m_b is completely same as Eq. (C.20), we just have to calculate the angular integration same as Eq. (C.21) and (C.22) except that L in the Gaussian expansion is equivalent to k in the multipole expansion.

Therefore the radial part of Eq. (C.31) is given by

$$
\begin{aligned}
F_{lL_\beta L_\alpha}(r_\beta, r_\alpha) &= \sum_{\lambda_A \lambda_b k} \mathscr{R}_{\lambda_A \lambda_b k}(r_\beta, r_\alpha) \mathscr{A}^{lL_\beta L_\alpha}_{\lambda_A \lambda_b k}, \\
\mathscr{R}_{\lambda_A \lambda_b k}(r_\beta, r_\alpha) &\equiv \frac{1}{4\pi} h_{\lambda_A}(r_\alpha, r_\beta) h_{\lambda_b}(r_\alpha, r_\beta) \tilde{Q}_k(r_\alpha, r_\beta), \\
\mathscr{A}^{lL_\beta L_\alpha}_{\lambda_A \lambda_b L} &\equiv \sum_{j_\alpha j_\beta} (-)^{j_\alpha + L_\alpha} \hat{l}_A \hat{l}_b \hat{j}_\alpha \hat{j}_\beta \widehat{l_A - \lambda_A} \widehat{l_b - \lambda_b} \hat{\lambda}_A \hat{\lambda}_b \\
&\quad \times (l_A - \lambda_A, 0, l_b - \lambda_b, 0 | j_\alpha 0)\, (\lambda_A 0 \lambda_b 0 | j_\beta 0) \\
&\quad \times (j_\alpha 0 k 0 | L_\alpha 0)\, (j_\beta 0 k 0 | L_\beta 0) \\
&\quad \times W(j_\alpha j_\beta L_\alpha L_\beta; l k) \begin{Bmatrix} l_A - \lambda_A & \lambda_A & l_A \\ l_b - \lambda_b & \lambda_b & l_b \\ j_\alpha & j_\beta & l \end{Bmatrix},
\end{aligned}
\tag{C.32}
$$

C.2 Zero-range form factor

In the zero-range (ZR) limit, we do not have to expand the wave functions of the projectile and the residual nucleus. The form factor with the ZR approximation is given,

$$
\begin{aligned}
f_{lm}(\boldsymbol{r}_\beta, \boldsymbol{r}_\alpha) &\equiv \psi^*_{xA}(\boldsymbol{r}_{xA}) D_{xb}(\boldsymbol{r}_{xb}) \\
&\approx \psi^*_{xA}(\boldsymbol{r}_{xA}) D_0 \delta(\boldsymbol{r}_{xb}) \\
&= \psi^*_{xA}(\boldsymbol{r}_\alpha) D_0 \delta\left(\boldsymbol{r}_\beta - \frac{A}{B}\boldsymbol{r}_\alpha\right),
\end{aligned}
\tag{C.33}
$$

where D_{xb} is defined by Eq. (C.3). We can understand from Fig. C.1 that $\boldsymbol{r}_{xA}$ becomes equal to $\boldsymbol{r}_\alpha$ and $\delta(\boldsymbol{r}_{xb}) = \delta\left(\boldsymbol{r}_\beta - \frac{A}{B}\boldsymbol{r}_\alpha\right)$ because $\boldsymbol{r}_{xb} = p\boldsymbol{r}_\alpha + q\boldsymbol{r}_\beta$. Eq. (C.33) means that $\psi_{xb}(\boldsymbol{r}_{xb})$ is the s-wave because so is δ-function.

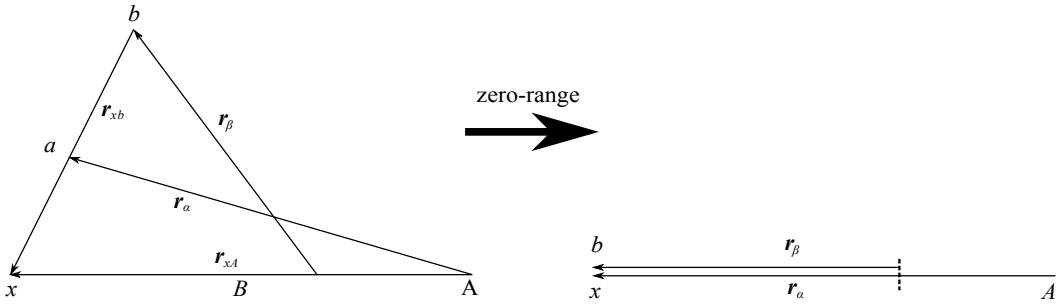

Figure C.1: illustration of the ZR approximation.

The radial part of Eq. (C.33) can be derive with same way as that of Eq. (3.70),

$$\begin{aligned}
F_{lL_\beta L_\alpha}(r_\beta, r_\alpha) &= (-)^{L_\beta+L_\alpha-l} \int d\hat{\boldsymbol{r}}_\alpha d\hat{\boldsymbol{r}}_\beta \left[Y_{L_\alpha}(\hat{\boldsymbol{r}}_\alpha) \otimes Y_{L_\beta}(\hat{\boldsymbol{r}}_\beta)\right]_{lm} f_{lm}(\boldsymbol{r}_\beta, \boldsymbol{r}_\alpha) \\
&= (-)^{L_\beta+L_\alpha-l} \phi^*_{l_A}(r_\alpha) D_0 \frac{\delta\left(r_\beta - \frac{A}{B} r_\alpha\right)}{\left(\frac{A}{B} r_\alpha\right)^2} \\
&\times \int d\hat{\boldsymbol{r}}_\alpha \int d\hat{\boldsymbol{r}}_\beta \delta\left(\hat{\boldsymbol{r}}_\beta - \hat{\boldsymbol{r}}_\alpha\right) \left[Y_{L_\alpha}(\hat{\boldsymbol{r}}_\alpha) \otimes Y_{L_\beta}(\hat{\boldsymbol{r}}_\beta)\right]_{lm} Y^*_{lm}(\hat{\boldsymbol{r}}_\alpha) \\
&= (-)^{L_\beta+L_\alpha-l} \phi^*_{l_A}(r_\alpha) D_0 \frac{\delta\left(r_\beta - \frac{A}{B} r_\alpha\right)}{\left(\frac{A}{B} r_\alpha\right)^2} \\
&\times \int d\hat{\boldsymbol{r}}_\alpha \left[Y_{L_\alpha}(\hat{\boldsymbol{r}}_\alpha) \otimes Y_{L_\beta}(\hat{\boldsymbol{r}}_\alpha)\right]_{lm} Y^*_{lm}(\hat{\boldsymbol{r}}_\alpha) \\
&= \phi^*_{l_A}(r_\alpha) D_0 \frac{\delta\left(r_\beta - \frac{A}{B} r_\alpha\right)}{\left(\frac{A}{B} r_\alpha\right)^2} \frac{1}{\sqrt{4\pi}} \frac{\hat{L}_\alpha \hat{L}_\beta}{\hat{l}} \left(L_\beta 0 L_\alpha 0 | l 0\right) \int d\hat{\boldsymbol{r}}_\alpha Y_{lm}(\hat{\boldsymbol{r}}_\alpha) Y^*_{lm}(\hat{\boldsymbol{r}}_\alpha) \\
&= \phi^*_{l_A}(r_\alpha) D_0 \frac{\delta\left(r_\beta - \frac{A}{B} r_\alpha\right)}{\left(\frac{A}{B} r_\alpha\right)^2} \frac{1}{\sqrt{4\pi}} \frac{\hat{L}_\alpha \hat{L}_\beta}{\hat{l}} \left(L_\beta 0 L_\alpha 0 | l 0\right). \qquad \text{(C.34)}
\end{aligned}$$

Then we can calculate the overlap integral, $I^{l l_A l'_A}_{J L_\beta L'_\beta}$, with the assumption, $l_b = l'_b = 0$,

$$\begin{aligned}
I^{l l_A l'_A}_{J L_\beta L'_\beta} &= \frac{4\pi}{k_\alpha k_\beta} D_0 \frac{1}{\sqrt{4\pi}} \frac{\hat{J}\hat{L}'_\beta}{\hat{l}} \left(L'_\beta 0 J 0 | l 0\right) \\
&\times \int r_\alpha dr_\alpha \int r_\beta dr_\beta \chi^J_{L_\beta L'_\beta l_A l'_A}(k_\beta, r_\beta) \phi^*_{l'_A}(r_\alpha) \frac{\delta\left(r_\beta - \frac{A}{B} r_\alpha\right)}{\left(\frac{A}{B} r_\alpha\right)^2} \chi^J_\alpha(k_\alpha, r_\alpha) \\
&= \frac{\sqrt{4\pi}}{k_\alpha k_\beta} \frac{B}{A} D_0 \frac{\hat{J}\hat{L}'_\beta}{\hat{l}} \left(L'_\beta 0 J 0 | l 0\right) \int dr_\alpha \chi^J_{L_\beta L'_\beta l_A l'_A}\left(k_\beta, \frac{A}{B} r_\alpha\right) \phi^*_{l'_A}(r_\alpha) \chi^J_\alpha(k_\alpha, r_\alpha). \qquad \text{(C.35)}
\end{aligned}$$

The strength of the δ-function, D_0, can be calculated by definition,

$$D_0 = \int d\boldsymbol{r}_{xb} D_{xb}(\boldsymbol{r}_{xb}). \qquad \text{(C.36)}$$

This integration can be done easily if ψ_{xb} is the s-wave. Otherwise we have to do a special treatment to this integration, for example it is mentioned in Ref. [172]. Thus the assumption, $l_b = l'_b = 0$, requires the alignment of L_α and J in Eq. (C.35). It should not, however, be applied the ZR approximation for the case of the non s-wave projectile, because the range of D_{xb} could be much larger than that of the s-wave function. Therefore the ZR approximation may be bad for describing the precise form factor.

Note that the wave function of a bound state should be real, it means $\phi^*_{l_A} = \phi_{l_A}$. As for the transfer amplitude and the cross section, we can use same formulae as in the case of the FR framework. Therefore inserting Eq. (C.35) to Eqs. (3.87) and (3.88), we obtain the transfer amplitude and then can calculate the cross section with Eq. (3.90).

APPENDIX D

Finite-Range Correction (FRC) to Zero-Range (ZR) Form Factor

Contents

D.1 FRC formalism with Distorted-wave Born approximation (DWBA)

D.1.1 Formulation

We consider the transfer reaction, $a(x+b)+A \to b+B(x+A)$. The transition matrix of the stripping reaction with the distorted-wave Born approximation (DWBA) is given by

$$T_{\beta\alpha}^{\mathrm{DWBA}} = \left\langle \chi_{\beta}^{(-)}(\boldsymbol{r}_{\beta}) \left| \mathscr{F}(\boldsymbol{r}_{xb}, \boldsymbol{r}_{xA}) \right| \chi_{\alpha}^{(+)}(\boldsymbol{r}_{\alpha}) \right\rangle_{\boldsymbol{r}_{\alpha}, \boldsymbol{r}_{xb}}, \tag{D.1}$$

where the form factor $\mathscr{F}$, which is not represented by the angular momentum expression, is defined by

$$\mathscr{F}(\boldsymbol{r}_{xb}, \boldsymbol{r}_{xA}) \equiv \psi_{xA}^{*}(\boldsymbol{r}_{xA}) D_{xb}(\boldsymbol{r}_{xb}), \tag{D.2}$$

$$D_{xb}(\boldsymbol{r}_{xb}) \equiv V_{xb}(r_{xb}) \psi_{xb}(\boldsymbol{r}_{xb}), \tag{D.3}$$

with a scalar interaction $V_{xb}(r_{xb})$ between x and b. $\chi_{\gamma}^{(\pm)}$ is the distorted wave corresponds to γ channel. And also we ignore intrinsic spins so as to simplify the discussion. Arguments of the distorted waves shown in Fig. 3.2, can be written as

$$\boldsymbol{r}_{\alpha} = \boldsymbol{r}_{xA} - \sigma \boldsymbol{r}_{xb}, \tag{D.4}$$

$$\boldsymbol{r}_{\beta} = \tau^{-1} \boldsymbol{r}_{xA} - \boldsymbol{r}_{xb}, \tag{D.5}$$

with $\sigma = b/a$ and $\tau = B/A$. Here we will rewrite distorted waves χ_α and χ_β with Taylor expansion around $\boldsymbol{r}_\alpha = \boldsymbol{r}_{xA}$ and $\tau\boldsymbol{r}_\beta = \boldsymbol{r}_{xA}$, respectively, that is,

$$\chi_\alpha^{(+)}(\boldsymbol{r}_{xA} - \sigma\boldsymbol{r}_{xb}) = e^{-\sigma\nabla_{\boldsymbol{r}_\alpha}\cdot\boldsymbol{r}_{xb}}\chi_\alpha^{(+)}(\boldsymbol{r}_{xA}), \tag{D.6}$$

$$\chi_\beta^{(-)*}(\tau^{-1}\boldsymbol{r}_{xA} - \boldsymbol{r}_{xb}) = e^{-\tau\nabla_{\boldsymbol{r}_\beta}\cdot\boldsymbol{r}_{xb}}\chi_\beta^{(-)*}(\tau^{-1}\boldsymbol{r}_{xA}). \tag{D.7}$$

Then Eq. (D.1) becomes

$$T_{\beta\alpha}^{\mathrm{DWBA}} = \int d\boldsymbol{r}_{xb} D_{xb}(\boldsymbol{r}_{xb}) e^{-(\tau\nabla_{\boldsymbol{r}_\beta} + \sigma\nabla_{\boldsymbol{r}_\alpha})\cdot\boldsymbol{r}_{xb}} \times \int d\boldsymbol{r}_{xA}\chi_\beta^{(-)*}(\tau^{-1}\boldsymbol{r}_{xA})\psi_{xA}^*(\boldsymbol{r}_{xA})\chi_\alpha^{(+)}(\boldsymbol{r}_{xA}), \tag{D.8}$$

where we use $d\boldsymbol{r}_\alpha = d\boldsymbol{r}_{xA}$.

Since the $\boldsymbol{r}_{xb}$ integration part of Eq. (D.8) has a short range function, D_{xb}, we expand the exponential of this term as follows:

$$\int d\boldsymbol{r}_{xb} D_{xb}(\boldsymbol{r}_{xb}) e^{-(\tau\nabla_{\boldsymbol{r}_\beta} + \sigma\nabla_{\boldsymbol{r}_\alpha})\cdot\boldsymbol{r}_{xb}} = \int d\boldsymbol{r}_{xb} D_{xb}(\boldsymbol{r}_{xb}) \left[1 + \frac{1}{6}(\tau\nabla_{\boldsymbol{r}_\beta} + \sigma\nabla_{\boldsymbol{r}_\alpha})^2\boldsymbol{r}_{xb}^2 + \dots\right]. \tag{D.9}$$

This expansion is based on Ref. [2, 172], where it is formulated the expansion of the operator, $\exp(\boldsymbol{r}\cdot\boldsymbol{O})$, that is,

$$e^{\boldsymbol{r}\cdot\boldsymbol{O}} = 4\pi\sum_{nlm} c_{nl} r^{2n+l} Y_{lm}^*(\hat{\boldsymbol{r}}) O^{2n+l} Y_{lm}(\hat{\boldsymbol{O}}),. \tag{D.10}$$

$$c_{nl} = \frac{(n+l)!2^l}{n!(2n+2l+1)!}. \tag{D.11}$$

In Eq. (D.10) the first order of the series can appear, but it will vanish because of the symmetry of the odd function integration over whole region if we adopt the s-wave as D_{xb}. The formulation of this kind of the finite-range correction (FRC) for the non s-wave case is developed in Ref. [172], but I do not mention the detail of that here.

Anyway when we see up to only second order term of Eq. (D.10), in the transition matrix we have

$$\begin{aligned}
&(\tau\nabla_{\boldsymbol{r}_\beta} + \sigma\nabla_{\boldsymbol{r}_\alpha})^2\chi_\beta^{(-)*}(\tau^{-1}\boldsymbol{r}_{xA})\psi_{xA}^*(\boldsymbol{r}_{xA})\chi_\alpha^{(+)}(\boldsymbol{r}_{xA}) \\
&= \left[(\tau^2 - \sigma\tau)\nabla_{\boldsymbol{r}_\beta}^2 + (\sigma^2 - \sigma\tau)\nabla_{\boldsymbol{r}_\alpha}^2 + \sigma\tau(\nabla_{\boldsymbol{r}_\beta} + \nabla_{\boldsymbol{r}_\alpha})^2\right] \\
&\times \chi_\beta^{(-)*}(\tau^{-1}\boldsymbol{r}_{xA})\psi_{xA}^*(\boldsymbol{r}_{xA})\chi_\alpha^{(+)}(\boldsymbol{r}_{xA}) \\
&= (\tau^2 - \sigma\tau)\left\{\nabla_{\boldsymbol{r}_\beta}^2\chi_\beta^{(-)*}(\tau^{-1}\boldsymbol{r}_{xA})\right\}\psi_{xA}^*(\boldsymbol{r}_{xA})\chi_\alpha^{(+)}(\boldsymbol{r}_{xA}) \\
&+ (\sigma^2 - \sigma\tau)\chi_\beta^{(-)*}(\tau^{-1}\boldsymbol{r}_{xA})\psi_{xA}^*(\boldsymbol{r}_{xA})\left\{\nabla_{\boldsymbol{r}_\alpha}^2\chi_\alpha^{(+)}(\boldsymbol{r}_{xA})\right\} \\
&+ \sigma\tau(\nabla_{\boldsymbol{r}_\beta} + \nabla_{\boldsymbol{r}_\alpha})^2\chi_\beta^{(-)*}(\tau^{-1}\boldsymbol{r}_{xA})\psi_{xA}^*(\boldsymbol{r}_{xA})\chi_\alpha^{(+)}(\boldsymbol{r}_{xA}).
\end{aligned} \tag{D.12}$$

The part of the first term of Eq. (D.12) can be

$$\begin{aligned}\nabla^2_{\boldsymbol{r}_\beta}\chi^{(-)*}_\beta(\tau^{-1}\boldsymbol{r}_{xA}) &= \nabla^2_{\boldsymbol{r}_{xA}}\chi^{(-)*}_\beta(\tau^{-1}\boldsymbol{r}_{xA}) \\ &= \frac{1}{\tau^2}\nabla^2_{\tau^{-1}\boldsymbol{r}_{xA}}\chi^{(-)*}_\beta(\tau^{-1}\boldsymbol{r}_{xA}),\end{aligned} \tag{D.13}$$

because $d\boldsymbol{r}_{xA} = \tau d\left(\tau^{-1}\boldsymbol{r}_{xA}\right)$ and $\nabla^2_{\boldsymbol{r}_{xA}} = 1/\tau^2\nabla^2_{\tau^{-1}\boldsymbol{r}_{xA}}$. As for the third term of Eq. (D.12), we can derive

$$\begin{aligned}&(\nabla_{\boldsymbol{r}_\beta} + \nabla_{\boldsymbol{r}_\alpha})^2\chi^{(-)*}_\beta(\tau^{-1}\boldsymbol{r}_{xA})\psi^*_{xA}(\boldsymbol{r}_{xA})\chi^{(+)}_\alpha(\boldsymbol{r}_{xA}) \\ &\quad= \left\{\nabla_{\boldsymbol{r}_{xA}}\left(\chi^{(-)*}_\beta(\tau^{-1}\boldsymbol{r}_{xA})\chi^{(+)}_\alpha(\boldsymbol{r}_{xA})\right)\psi^*_{xA}(\boldsymbol{r}_{xA})\right\} \\ &\quad= \chi^{(-)*}_\beta(\tau^{-1}\boldsymbol{r}_{xA})\chi^{(+)}_\alpha(\boldsymbol{r}_{xA})\left\{\nabla^2_{\boldsymbol{r}_{xA}}\psi^*_{xA}(\boldsymbol{r}_{xA})\right\}.\end{aligned} \tag{D.14}$$

To obtain Eq. (D.14) we perform the partial integration, $\int$(D.14) $d\boldsymbol{r}_{xA}$, and use the nature of wave functions, that is, $\chi^{(\pm)}_\gamma(\boldsymbol{r}_\gamma = 0) \to 0$ and $\psi^*_{xA}(\boldsymbol{r}_{xA} = \infty) \to 0$. Then Eq. (D.12) can be written by

$$\begin{aligned}\text{(D.12)} &= (1-\frac{\sigma}{\tau})\left\{\nabla^2_{\tau^{-1}\boldsymbol{r}_{xA}}\chi^{(-)*}_\beta(\tau^{-1}\boldsymbol{r}_{xA})\right\}\psi^*_{xA}(\boldsymbol{r}_{xA})\chi^{(+)}_\alpha(\boldsymbol{r}_{xA}) \\ &+ (\sigma^2-\sigma\tau)\chi^{(-)*}_\beta(\tau^{-1}\boldsymbol{r}_{xA})\psi^*_{xA}(\boldsymbol{r}_{xA})\left\{\nabla^2_{\boldsymbol{r}_\alpha}\chi^{(+)}_\alpha(\boldsymbol{r}_{xA})\right\} \\ &+ \sigma\tau\chi^{(-)*}_\beta(\tau^{-1}\boldsymbol{r}_{xA})\left\{\nabla^2_{\boldsymbol{r}_{xA}}\psi^*_{xA}(\boldsymbol{r}_{xA})\right\}\chi^{(+)}_\alpha(\boldsymbol{r}_{xA}) \\ &= \sigma\left[(\frac{1}{\sigma}-\frac{1}{\tau})\left\{\nabla^2_{\tau^{-1}\boldsymbol{r}_{xA}}\chi^{(-)*}_\beta(\tau^{-1}\boldsymbol{r}_{xA})\right\}\psi^*_{xA}(\boldsymbol{r}_{xA})\chi^{(+)}_\alpha(\boldsymbol{r}_{xA})\right. \\ &+ (\sigma-\tau)\chi^{(-)*}_\beta(\tau^{-1}\boldsymbol{r}_{xA})\psi^*_{xA}(\boldsymbol{r}_{xA})\left\{\nabla^2_{\boldsymbol{r}_\alpha}\chi^{(+)}_\alpha(\boldsymbol{r}_{xA})\right\} \\ &+ \left.\tau\chi^{(-)*}_\beta(\tau^{-1}\boldsymbol{r}_{xA})\left\{\nabla^2_{\boldsymbol{r}_{xA}}\psi^*_{xA}(\boldsymbol{r}_{xA})\right\}\chi^{(+)}_\alpha(\boldsymbol{r}_{xA})\right].\end{aligned} \tag{D.15}$$

Now we have following relationship,

$$\frac{1}{\sigma}-\frac{1}{\tau} = \frac{a}{b}-\frac{A}{B} = \frac{aB-Ab}{bB} = \frac{(b+x)B-(B-x)b}{bB} = \frac{x(b+B)}{bB} = \frac{x}{\mu_\beta}, \tag{D.16}$$

$$\sigma-\tau = \frac{b}{a}-\frac{B}{A} = \frac{Ab-aB}{aA} = \frac{-x(B+b)}{aA} = -\frac{x(a+A)}{aA} = -\frac{x}{\mu_\alpha}, \tag{D.17}$$

$$\tau = \frac{B}{A} = x\frac{A+x}{xA} = \frac{x}{\mu_x}. \tag{D.18}$$

where μ is the reduced masses of corresponding systems. If the distorted waves are generated by potentials U, [1] then from the Schrödinger equation we have

$$\nabla^2_{\boldsymbol{r}_\alpha}\chi^{(+)}_\alpha(\boldsymbol{r}_{xA}) = \frac{2\mu_\alpha}{\hbar^2}\left[U_\alpha(r_{xA}) - E_\alpha\right]\chi^{(+)}_\alpha(\boldsymbol{r}_{xA}), \tag{D.19}$$

$$\nabla^2_{\tau^{-1}\boldsymbol{r}_{xA}}\chi^{(-)*}_\beta(\tau^{-1}\boldsymbol{r}_{xA}) = \frac{1}{\tau^2}\frac{2\mu_\beta}{\hbar^2}\left[U_\beta(\tau^{-1}r_{xA}) - E_\beta\right]\chi^{(-)*}_\beta(\tau^{-1}\boldsymbol{r}_{xA}). \tag{D.20}$$

[1] This U should consists of the nuclear potential and the Coulomb potential. We can see lately from Eq. (D.25) that the Coulomb part will be canceled out in the term of $V_{xA} + U_\beta - U_\alpha$ for the (d,p) reaction. Because the product of the proton numbers of two charged particles might be same, that is, Z_1Z_2 in U_α equals to that in U_β for the (d,p) reaction. As for the (d,n) reaction Z_1Z_2 in U_α equals to that in V_{xA}. Note that, however, the cancellation will be bad for general transfer reactions, for example (^{6}Li,d) reaction.

This is corresponded to the local energy approximation (LEA), that is, the operator ∇_γ is replaced by a local momentum or a local energy. As for the wave function of the residual nucleus, it leads

$$\nabla^2_{\boldsymbol{r}_{xA}}\psi^*_{xA}(\boldsymbol{r}_{xA}) = \frac{2\mu_a}{\hbar^2}\left[V_{xA}(r_{xA}) - E_{xA}\right]\psi^*_{xA}(\boldsymbol{r}_{xA}), \tag{D.21}$$

where $\mu_a = xb/a$ is the reduced mass of the projectile a, $a = x + b$ and V_{xA} is the binding potential between x and A (it might be real). So, inserting Eqs. from (D.16) to (D.21), into Eq. (D.15), we have

$$\begin{aligned}(\text{D.15}) &= \frac{2\mu_a}{\hbar^2}\left[U_\beta(\tau^{-1}r_{xA}) - E_\beta + V_{xA}(r_{xA}) - E_{xA} - U_\alpha(r_{xA}) + E_\alpha\right] \\ &\quad\times \chi^{(-)*}_\beta(\tau^{-1}\boldsymbol{r}_{xA})\psi^*_{xA}(\boldsymbol{r}_{xA})\chi^{(+)}_\alpha(\boldsymbol{r}_{xA}) \\ &= \frac{2\mu_a}{\hbar^2}\left[V_{xA}(r_{xA}) + U_\beta(\tau^{-1}r_{xA}) - U_\alpha(r_{xA}) - (E_{xA} + E_\beta - E_\alpha)\right] \\ &\quad\times \chi^{(-)*}_\beta(\tau^{-1}\boldsymbol{r}_{xA})\psi^*_{xA}(\boldsymbol{r}_{xA})\chi^{(+)}_\alpha(\boldsymbol{r}_{xA}).\end{aligned} \tag{D.22}$$

From the energy conservation, it is trivial that

$$E_{xA} + E_\beta - E_\alpha = -B_a, \tag{D.23}$$

where B_a is the binding energy of x in the projectile a (positive value). Then we obtain the transition matrix by inserting Eq. (D.9) and (D.22) to Eq. (D.8),

$$T^{\text{DWBA}}_{\beta\alpha} = D_0\int d\boldsymbol{r}\chi^{(-)*}_\beta(\tau^{-1}\boldsymbol{r})\psi^*_{xA}(\boldsymbol{r})F_{\text{corr}}(r)\chi^{(+)}_\alpha(\boldsymbol{r}), \tag{D.24}$$

$$F_{\text{corr}}(r) \equiv 1 + \frac{\rho^2}{6}\frac{2\mu_a}{\hbar^2}\left[V_{xA}(r) + U_\beta\left(\frac{A}{B}r\right) - U_\alpha(r) + B_a\right] \tag{D.25}$$

where

$$\begin{aligned}D_0 &= \int d\boldsymbol{r}_{xb}D_{xb}(\boldsymbol{r}_{xb}) \\ &= \sqrt{4\pi}\int dr_{xb}r^2_{xb}d_{xb}(r_{xb}),\end{aligned} \tag{D.26}$$

with the product of the the projectile wave function, ϕ_{xb}, and a scalar interaction between x and b, $V_{xb}(r_{xb})$, that is, $d_{xb}(r_{xb}) = V_{xb}(r_{xb})\phi_{xb}(r_{xb})$. ρ, which is defined by [2]

$$\rho = \frac{\sqrt{\int d\boldsymbol{r}_{xb}\boldsymbol{r}^2_{xb}D_{xb}(\boldsymbol{r}_{xb})}}{\sqrt{\int d\boldsymbol{r}_{xb}D_{xb}(\boldsymbol{r}_{xb})}}. \tag{D.27}$$

Now we can see the pretty important thing that if we include only first term of F_{corr}, it corresponds to the zero-range (ZR) limit, that is,

$$D_{xb}(\boldsymbol{r}_{xb}) = D_0\delta(\boldsymbol{r}_{xb}). \tag{D.28}$$

Therefore the second term of F_{corr} acts as a correction of the ZR to the exact finite-range (FR) calculation. So, this framework is the second order correction.

[2] ρ is the input parameter named FNRNG in the computer code RANA developed by Y. Iseri. Please note that FNRNG $= \rho/\sqrt{6}$. This is due to the difference between the definition of this note and that of RANA.

D.1.2 Application

We perform the DWBA calculation to see the FR effects on the ^{13}C(^{6}Li,d)^{17}O at 3.6 MeV, which is analyzed with the ZR approximation in Ref. [106]. In this calculation for the distorted wave $\chi_\alpha^{(+)}$ ($\chi_\beta^{(-)}$), we adopt the phenomenological optical potential [173] ([174, 175]) for the ^{6}Li-^{13}C (d-^{17}O) system. The detail of the numerical settings except for the optical potentials are given in Ref. [106]. Figure D.1 shows that the transfer cross section of the ^{13}C(^{6}Li,d)^{17}O at 3.6 MeV as a function of the deuteron emitting angle. At backward angle there is about 32% difference between the results of the FR (solid line) and ZR (dotted line) calculation. The FRC (dashed line) overestimates the FR result at most region of θ. This can be understood by looking Fig. D.2 in which $F_{\rm corr}(r)$ and the distorted waves, $\chi_\alpha^{(+)}$ and $\chi_\beta^{(-)}$ are plotted. In panel (a) we show the real and imaginary parts $F_{\rm corr}$ by the solid and dashed lines, respectively. In the interior region $F_{\rm corr}$ behaves with a nontrivial manner. However this parts does not affect the cross section since the reaction is peripheral [106]. In panel (b) the real part of the s-wave components of the partial wave for $\chi_\alpha^{(+)}$ and $\chi_\beta^{(-)}$ are respectively plotted as the solid and dashed lines. The distorted waves in the region lesser than about 5 fm have very small amplitude. Thus it can be understood that the real part of $F_{\rm corr}$ increase the cross section.

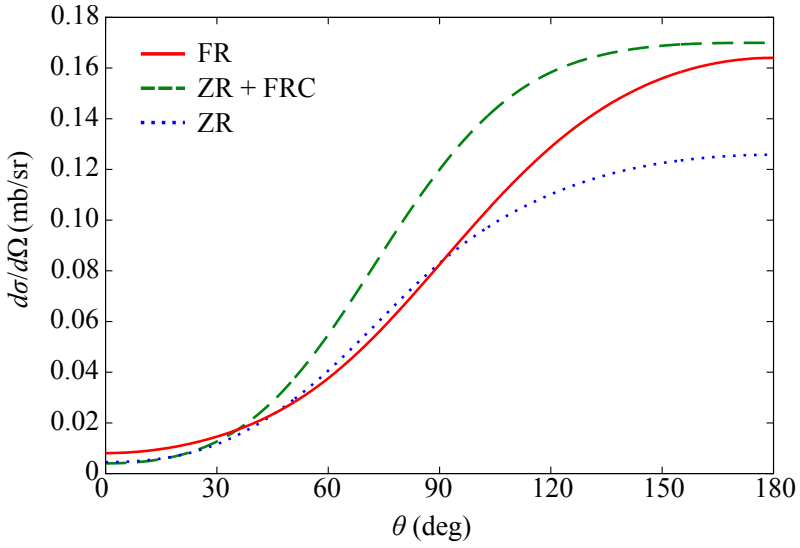

Figure D.1: The cross section of the ^{13}C(^{6}Li,d)^{17}O at 3.6 MeV/nucleon obtained by DWBA of the FR calculation (solid line), the ZR calculation (dotted line), and the ZR calculation with the FRC (dashed line).

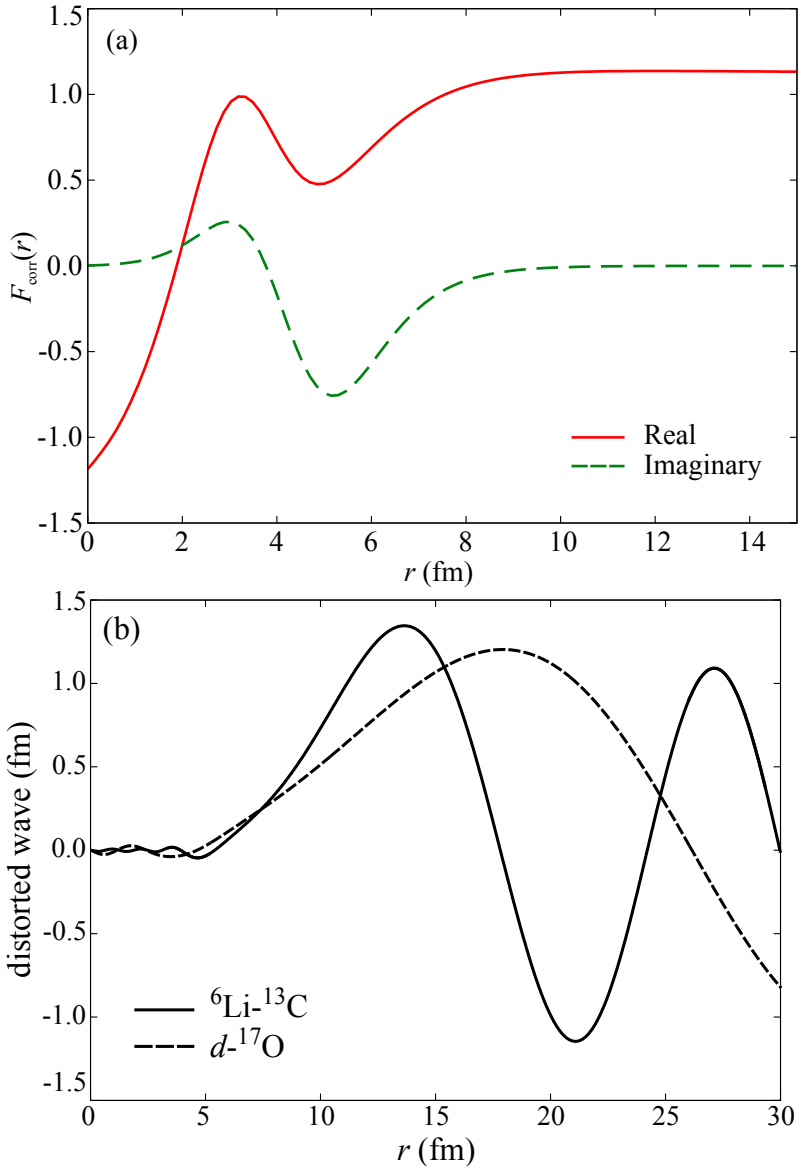

Figure D.2: (a) The real (imaginary) part of $F_{\rm corr}$ is shown by the solid (dashed) line. (b) The solid (dashed) line corresponds to the real part of the s-wave component of the partial wave for $\chi_\alpha^{(+)}$ ($\chi_\beta^{(-)}$) in the initial (final) channel.

As another example we choose the $^{28}(d,p)^{29}$Si reaction discussed in Chap. 3. In fig. D.3 we show the cross section of the transfer reaction at (a) 17.85 MeV and (b) 50.00 MeV. In each panel the lines correspond to them in Fig. D.1. Note that in panel (a), the calculations does not reproduce the experimental data [139], because we assume the spectroscopic factor $\mathcal{S} = 1$ for the n-^{28}Si configuration. For both the incident energies the FR effects are very small and the FRCs well reproduce the FR results.

On the $^{28}(d,p)^{29}$Si reaction, the FR effects decrease the cross section, which is opposite

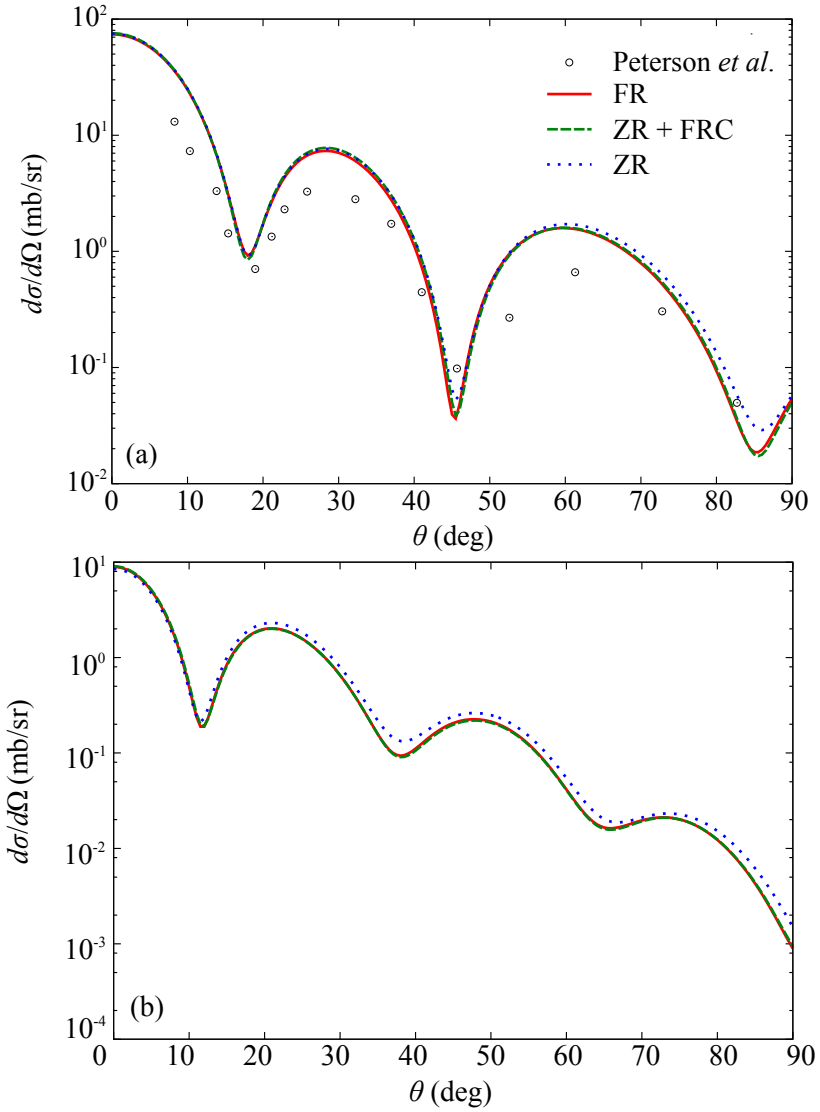

Figure D.3: Same as that in Fig. D.1 but for the the $^{28}(d,p)^{29}$Si reaction at (a) 17.85 MeV and (b) 50.00 MeV. The available experimental data for 17.85 MeV is taken from Ref. [139].

on the peripheral ^{13}C(^{6}Li,d)^{17}O reaction. This indicates that the $F_{\rm corr}$ at the interior region affects the cross section since the incident energies are much higher than the Coulomb barrier height of the d-^{28}Si. The behaviors of two $F_{\rm corr}$s for each incident energy are very similar. This is due to the good cancellation in Eq. (D.25) even though the optical potentials [140, 176] we adopt have an energy dependence.

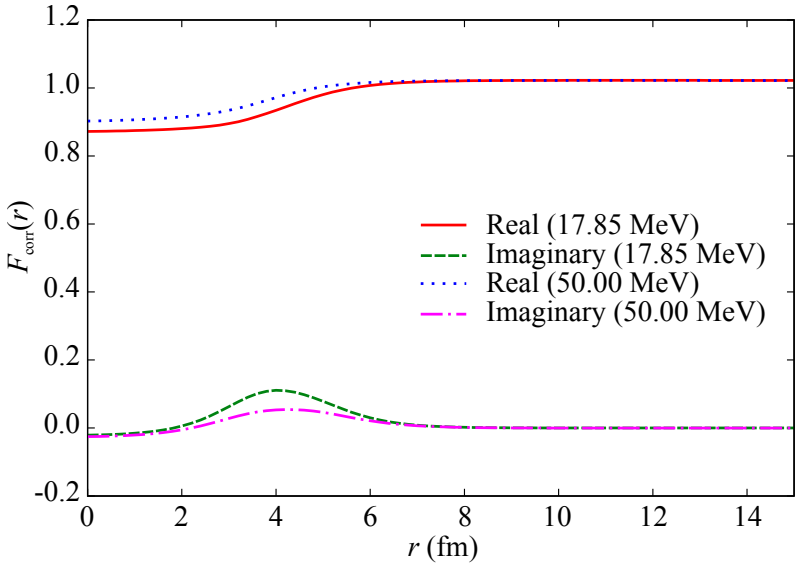

Figure D.4: The real and imaginary parts of $F_{\rm corr}$ at 18.75 MeV (50.00 MeV) are respectively shown as the solid (dashed) and dotted (dash-dotted) lines.

D.2 FRC formalism with coupled-channels Born approximation (CCBA)

D.2.1 Formulation

We work with the three-body ($x+b+A$) model to formulate the FRC under the coupled-channels Born Approximation (CCBA). The general expression of the transition matrix based on the post form can be written by

$$\begin{aligned} T_{\beta\alpha} &= \left\langle \Psi^{(-)}_{\beta} \left| V_{xb} \right| \Psi^{(+)}_{\alpha} \right\rangle_{\boldsymbol{r}_\alpha, \boldsymbol{r}_{xb}} \\ &= \int d\boldsymbol{r}_{xb} d\boldsymbol{r}_\alpha \Psi^{(-)}_{\beta}(\boldsymbol{r}_{xA}, \boldsymbol{r}_\beta) V_{xb}(\boldsymbol{r}_{xb}) \Psi^{(+)}_{\alpha}(\boldsymbol{r}_{xb}, \boldsymbol{r}_\alpha), \end{aligned} \tag{D.29}$$

where $\Psi^{(+)}_{\alpha}$ ($\Psi^{(+)}_{\beta}$) is the exact three-body wave function in the initial (final) channel. These wave functions satisfy following Schödinger equations:

$$\left[K_{\boldsymbol{r}_\alpha} + U^{(\alpha)}_{xA}(\boldsymbol{r}_{xA}) + U^{(\alpha)}_{bA}(\boldsymbol{r}_{bA}) + h_{xb} - E \right] \Psi^{(+)}_{\alpha}(\boldsymbol{r}_{xb}, \boldsymbol{r}_\alpha) = 0, \tag{D.30}$$

$$\left[K_{\boldsymbol{r}_\beta} + U^{(\beta)}_{bA}(\boldsymbol{r}_{bA}) + h_{xA} - E \right] \Psi^{(-)}_{\beta}(\boldsymbol{r}_{xA}, \boldsymbol{r}_\beta) = 0. \tag{D.31}$$

Here we ignore the intrinsic spins of each particles. $K_{\boldsymbol{r}_\gamma}$ is the kinetic operator related to the coordinate $\boldsymbol{r}_\gamma$, and h_{xc} is the internal Hamiltonian for the x-c system.

For the final channel, we adopt the countinuum-discretized coupled channels (CDCC)

method [3,5,6]:

$$\Psi_\beta^{(+)}(\boldsymbol{r}_{xA},\boldsymbol{r}_\beta) \approx \sum_i \psi_{xA}^i(\boldsymbol{r}_{xA})\chi_\beta^{ii_0(+)}(\boldsymbol{r}_\beta), \tag{D.32}$$

$$\left[h_{xA} - \varepsilon_i^{(\beta)}\right]\psi_{xA}^i = 0. \tag{D.33}$$

ψ_{xA}^i stands for the x-A relative wave function, and the distorted wave of ejectile b is represented by $\chi_\beta^{ii_0(+)}$. Here we use i as the energy index specifying a discretized continuum state of B, and i_0 corresponds to the ground state of B. One may obtain $\chi_\beta^{ii_0(+)}$ by solving standard CDCC equations [3,5,6].

Arguments of the final state wave functions, $\boldsymbol{r}_{xA}$ and $\boldsymbol{r}_\beta$ shown in Fig. 3.2, can be written as

$$\boldsymbol{r}_{xA} = \boldsymbol{r}_\alpha + \sigma\boldsymbol{r}_{xb}, \tag{D.34}$$

$$\begin{aligned}\boldsymbol{r}_\beta &= \tau^{-1}\boldsymbol{r}_{xA} - \boldsymbol{r}_{xb}\\ &= \tau^{-1}\boldsymbol{r}_\alpha + \xi\boldsymbol{r}_{xb},\end{aligned} \tag{D.35}$$

with $\xi = \sigma/\tau - 1$. Then we will rewrite ψ_{xA}^i and $\chi_\beta^{ii_0(+)}$ with Taylor expansion around $\boldsymbol{r}_{xA} = \boldsymbol{r}_\alpha$ and $\tau\boldsymbol{r}_\beta = \boldsymbol{r}_\alpha$, respectively, that is,

$$\psi_{xA}^i(\boldsymbol{r}_\alpha + \sigma\boldsymbol{r}_{xb}) = e^{\sigma\nabla_{\boldsymbol{r}_{xA}}\cdot\boldsymbol{r}_{xb}}\psi_{xA}^i(\boldsymbol{r}_\alpha), \tag{D.36}$$

$$\chi_\beta^{ii_0(+)}(\tau^{-1}\boldsymbol{r}_\alpha + \xi\boldsymbol{r}_{xb}) = e^{\tau\xi\nabla_{\boldsymbol{r}_\beta}\cdot\boldsymbol{r}_{xb}}\chi_\beta^{ii_0(+)}(\tau^{-1}\boldsymbol{r}_\alpha), \tag{D.37}$$

where $\nabla_{\boldsymbol{r}_{xA}}$ and $\nabla_{\boldsymbol{r}_\beta}$ operates to only ψ_{xA}^i and $\chi_\beta^{ii_0(+)}$, respectively. Then Eq. (D.29) becomes

$$\begin{aligned}T_{\beta\alpha} = \sum_i \int d\boldsymbol{r}_{xb}d\boldsymbol{r}_\alpha e^{(\sigma\nabla_{\boldsymbol{r}_{xA}}+\tau\xi\nabla_{\boldsymbol{r}_\beta})\cdot\boldsymbol{r}_{xb}}\\ \times \chi_\beta^{ii_0(-)*}(\tau^{-1}\boldsymbol{r}_\alpha)\psi_{xA}^{i*}(\boldsymbol{r}_\alpha)V_{xb}(\boldsymbol{r}_{xb})\Psi_\alpha^{(+)}(\boldsymbol{r}_{xb},\boldsymbol{r}_\alpha).\end{aligned} \tag{D.38}$$

As similar way to that of DWBA case, we adopt the LEA for the final and the initial channels, respectively;

$$\begin{aligned}\sum_i \left[\frac{\hbar^2}{2\mu_\beta}\nabla^2_{\tau^{-1}\boldsymbol{r}_\alpha} + \frac{\hbar^2}{2\mu_x A}\nabla^2_{\boldsymbol{r}_{xA}}\right]\chi_\beta^{ii_0(-)*}(\tau^{-1}\boldsymbol{r}_\alpha)\psi_{xA}^{i*}(\boldsymbol{r}_\alpha)\\ = \left[U_{xA}^{(\beta)}(\boldsymbol{r}_{xA}) + U_{bA}^{(\beta)}(\boldsymbol{r}_{bA}) - E\right]\chi_\beta^{ii_0(-)*}(\tau^{-1}\boldsymbol{r}_\alpha)\psi_{xA}^{i*}(\boldsymbol{r}_\alpha),\end{aligned} \tag{D.39}$$

$$\nabla^2_{\boldsymbol{r}_\alpha}\Psi_\alpha^{(+)}(\boldsymbol{r}_{xb},\boldsymbol{r}_\alpha) = \frac{2\mu_\alpha}{\hbar^2}\left[U_{xA}^{(\alpha)}(\boldsymbol{r}_{xA}) + U_{bA}^{(\alpha)}(\boldsymbol{r}_{bA}) + h_{xb} - E\right]\Psi_\alpha^{(+)}(\boldsymbol{r}_{xb},\boldsymbol{r}_\alpha). \tag{D.40}$$

Here we used $K_\gamma = -\hbar^2\nabla^2_{\boldsymbol{r}_\gamma}/(2\mu_\gamma)$. To obtain Eqs. (D.39) and (D.40) we perform the partial integration, which corresponds to the $\boldsymbol{r}_\alpha$-integration of Eq. (D.14) in DWBA, and

use the nature of wave functions, that is, $\chi_\beta^{ii_0(-)*}(\boldsymbol{r}_\beta = 0) \to 0$ and $\psi_{xA}^{i*}(\boldsymbol{r}_{xA} = \infty) \to 0$ [3].

Then the transition matrix becomes

$$\begin{aligned} T_{\beta\alpha} = \sum_i \int d\boldsymbol{r}_{xb} d\boldsymbol{r}_\alpha \chi_\beta^{ii_0(-)*}(\tau^{-1}\boldsymbol{r}_\alpha)\psi_{xA}^{i*}(\boldsymbol{r}_\alpha)V_{xb}(\boldsymbol{r}_{xb}) \\ \times \left(1 + \frac{1}{6}\boldsymbol{r}_{xb}^2 \frac{2\mu_a}{\hbar^2}\left[U_{xA}^{(\beta)}(\boldsymbol{r}_{xA}) + U_{bA}^{(\beta)}(\boldsymbol{r}_{bA}) - U_{xA}^{(\alpha)}(\boldsymbol{r}_{xA}) - U_{bA}^{(\alpha)}(\boldsymbol{r}_{bA}) - h_{xb}\right]\right) \\ \times \Psi_\alpha^{(+)}(\boldsymbol{r}_{xb}, \boldsymbol{r}_\alpha). \end{aligned} \tag{D.41}$$

Let's focus on the potentials $U_{xA}^{(\gamma)}(\boldsymbol{r}_{xA})$ and $U_{bA}^{(\gamma)}(\boldsymbol{r}_{bA})$. These can be written by followings with Taylor expansion around $\boldsymbol{r}_{xA} = \boldsymbol{r}_\alpha$ and $\boldsymbol{r}_{bA} = \boldsymbol{r}_\alpha$, respectively,

$$\begin{aligned} U_{xA}^{(\gamma)}(\boldsymbol{r}_{xA}) &= U_{xA}^{(\gamma)}(\boldsymbol{r}_\alpha + \sigma\boldsymbol{r}_{xb}) \\ &= U_{xA}^{(\gamma)}(\boldsymbol{r}_\alpha) + \left[\nabla_{\boldsymbol{r}_\alpha} U_{xA}^{(\gamma)}(\boldsymbol{r}_\alpha)\right] \cdot \sigma\boldsymbol{r}_{xb} + \left[\nabla_{\boldsymbol{r}_\alpha}^2 U_{xA}^{(\gamma)}(\boldsymbol{r}_\alpha)\right] \cdot \frac{(\sigma\boldsymbol{r}_{xb})^2}{2} + \ldots, \end{aligned} \tag{D.42}$$

$$\begin{aligned} U_{bA}^{(\gamma)}(\boldsymbol{r}_{bA}) &= U_{bA}^{(\gamma)}(\boldsymbol{r}_\alpha - \eta\boldsymbol{r}_{xb}) \\ &= U_{bA}^{(\gamma)}(\boldsymbol{r}_\alpha) - \left[\nabla_{\boldsymbol{r}_\alpha} U_{bA}^{(\gamma)}(\boldsymbol{r}_\alpha)\right] \cdot \eta\boldsymbol{r}_{xb} + \left[\nabla_{\boldsymbol{r}_\alpha}^2 U_{bA}^{(\gamma)}(\boldsymbol{r}_\alpha)\right] \cdot \frac{(\eta\boldsymbol{r}_{xb})^2}{2} + \ldots, \end{aligned} \tag{D.43}$$

where $\eta = x/a$ and we use $\nabla_{\boldsymbol{r}_{xA}} = \nabla_{\boldsymbol{r}_{bA}} = \nabla_{\boldsymbol{r}_\alpha}$. If U_{bA} satisfies

$$\begin{aligned} U_{bA}(\boldsymbol{r}_\alpha) &\sim \frac{b}{x} U_{xA}(\boldsymbol{r}_\alpha) \\ &= \frac{\sigma}{\eta} U_{xA}(\boldsymbol{r}_\alpha), \end{aligned} \tag{D.44}$$

the first order term of $\boldsymbol{r}_{xb}$ in Eqs. (D.42) and (D.43) can be canceled out. The term larger than second order of $\boldsymbol{r}_{xb}$ may be negligible because the product of $\boldsymbol{r}_{xb}^2$ in Eq. (D.42) or Eq. (D.43) and that of Eq. (D.41), $\boldsymbol{r}_{xb}^4$, might be very small. Therefore Eq. (D.41) transforms

$$\begin{aligned} T_{\beta\alpha} = \int d\boldsymbol{r}_{xb} d\boldsymbol{r}_\alpha \chi_\beta^{ii_0(-)*}(\tau^{-1}\boldsymbol{r}_\alpha)\psi_{xA}^{i*}(\boldsymbol{r}_\alpha)V_{xb}(\boldsymbol{r}_{xb}) \\ \times \left(1 + \frac{1}{6}\boldsymbol{r}_{xb}^2 \frac{2\mu_a}{\hbar^2}\left[U_{xA}^{(\beta)}(\boldsymbol{r}_\alpha) + U_{bA}^{(\beta)}(\boldsymbol{r}_\alpha) - U_{xA}^{(\alpha)}(\boldsymbol{r}_\alpha) - U_{bA}^{(\alpha)}(\boldsymbol{r}_\alpha) - h_{xb}\right]\right) \\ \times \Psi_\alpha^{(+)}(\boldsymbol{r}_{xb}, \boldsymbol{r}_\alpha). \end{aligned} \tag{D.45}$$

Next we apply the CDCC framework also for $\Psi_\alpha^{(+)}$, that is,

$$\Psi_\alpha^{(+)}(\boldsymbol{r}_{xb}, \boldsymbol{r}_\alpha) \approx \sum_i \psi_{xb}^i(\boldsymbol{r}_{xb})\chi_\alpha^{ii_0(+)}(\boldsymbol{r}_\alpha), \tag{D.46}$$

[3] In principle ψ_{xA}^{i*} must oscillate even in the asymptotic region. However in the frame work of the CDCC we can reduce this oscillation with the concept that we see only the observables that is affected by ψ_{xA}^{i*} with a certain finite range of $\boldsymbol{r}_{xA}$.

The x-b wave function ψ^i_{xb} satisfies

$$\left(h_{xb} - \varepsilon^{(\alpha)}_i\right)\psi^i_{xb} = 0. \tag{D.47}$$

Using Eqs. (D.46) and (D.47), we obtain

$$T_{\beta\alpha} = \sum_{ij} D^i_0 \int d\boldsymbol{r}\chi^{jj_0(-)*}_\beta(\tau^{-1}\boldsymbol{r})\psi^j_{xA}(\boldsymbol{r})F^i_{\rm corr}(\boldsymbol{r})\chi^{ii_0(+)}_\alpha(\boldsymbol{r}), \tag{D.48}$$

$$F^i_{\rm corr}(\boldsymbol{r}) \equiv 1 + \frac{\rho_i^2}{6}\frac{2\mu_a}{\hbar^2}\left[U^{(\beta)}_{xA}(\boldsymbol{r}) - U^{(\beta)}_{bA}(\boldsymbol{r}) + U^{(\alpha)}_{xA}(\boldsymbol{r}) - U^{(\alpha)}_{bA}(\boldsymbol{r}) - \varepsilon^{(\alpha)}_i\right], \tag{D.49}$$

where

$$D^i_0 = \int d\boldsymbol{r}_{xb} D^i_{xb}(\boldsymbol{r}_{xb}), \tag{D.50}$$

with

$$D^i_{xb}(\boldsymbol{r}_{xb}) = V_{xb}(\boldsymbol{r}_{xb})\psi^i_{xb}(\boldsymbol{r}_{xb}). \tag{D.51}$$

The integration of Eq. (D.50) can be done easily if ψ^i_{xb} is the s-wave. Otherwise we have to do a special treatment to this integration, for example it is mentioned in Ref. [172]. ρ_i, which is defined by

$$\rho_i = \frac{\sqrt{\int d\boldsymbol{r}_{xb}\boldsymbol{r}^2_{xb}D^i_{xb}(\boldsymbol{r}_{xb})}}{\sqrt{\int d\boldsymbol{r}_{xb}D^i_{xb}(\boldsymbol{r}_{xb})}}. \tag{D.52}$$

If $U^{(\alpha)}_{xA} = U^{(\beta)}_{xA}$ and $U^{(\alpha)}_{bA} = U^{(\beta)}_{bA}$, $F^i_{\rm corr}$ becomes

$$F^i_{\rm corr}(\boldsymbol{r}) = 1 - \frac{\rho_i^2}{6}\frac{2\mu_a}{\hbar^2}\varepsilon_i. \tag{D.53}$$

We can see from Eq. (D.53) that the elastic transfer (transfer process form the ground state of a, that is, $i = i_0$) increases the cross section because $\varepsilon_{i_0} < 0$. On the other hand, the breakup transfer (transfer process from continuum states of a) decreases it since $\varepsilon_{i\neq i_0} > 0$ (in general). It should be noted that the correction factor $F^i_{\rm corr}$ depends only on i, the energy index of the initial channel, not on j, that of the final channel.

In summarize the approximations to the potentials which we use in this framework.

1. $U^{(\gamma)}_{bA}(\boldsymbol{r}_\alpha) \sim (b/x)U^{(\gamma)}_{xA}(\boldsymbol{r}_\alpha)$
   This is the assumption that the optical potential is proportional to the mass ratio.
2. $U^{(\alpha)}_{xA} = U^{(\beta)}_{xA}$
   If we adopt the same x-A interaction for both initial and finial channel, the optical potential of initial channel $U^{(\alpha)}_{xA}$ might be real which is due to be consistent with the final channel binding potential $U^{(\beta)}_{xA}$. Therefore $U^{(\beta)}_{xA} - U^{(\alpha)}_{xA}$ is canceled out in Eq. (D.49). However if $U^{(\alpha)}_{xA} \neq U^{(\beta)}_{xA}$, it is not trivial that the assumption of Eq. (D.44) is reasonable or not.

D.2.2 Application

We chose the transfer reaction ^{8}B(d,n)^{9}C at 14.4 MeV/nucleon, which is analyzed in Chap. 3 to see the FR effects on the cross section. Numerical settings are mentioned in Chap. 3.4.2. We show in Fig. D.5 the results obtained by the FR calculation (solid line), the ZR calculation (dotted line), and the ZR calculation with the FRC described by Eqs. (D.48) and (D.49) (dashed line). One finds the FR effect gives about 20% increase in the cross section at $\theta = 0^\circ$. The FRC works well qualitatively but not sufficient to get good agreement with the solid line. This suggests the FR effect found in ^{8}B(d,n)^{9}C at 14.4 MeV/nucleon contains a higher-order component that cannot be included in the present procedure.

The correction function $F^i_{\rm LEA}$ of Eq. (D.49) is plotted in Fig. D.6; panel (a) and (b) correspond to the real and imaginary parts of $F^i_{\rm LEA}$, respectively. It is found that $F^i_{\rm LEA}$ has a nontrivial behavior in the interior region, say, $r_\alpha \lesssim 6$ fm. As clarified in Chap. 3, however, the ^{8}B(d,n)^{9}C reaction at 14.4 MeV/nucleon is peripheral with respect to $r_{p\rm B}$ that is the same as r_α in the ZR limit. Thus, the contribution of $F^i_{\rm LEA}$ in the interior region to the T matrix is expected to be very small. In this case, a simple estimation of the FR effect based on Eq. (D.53) works well. At higher incident energies, where we have less peripherality, the FR effect can change significantly.

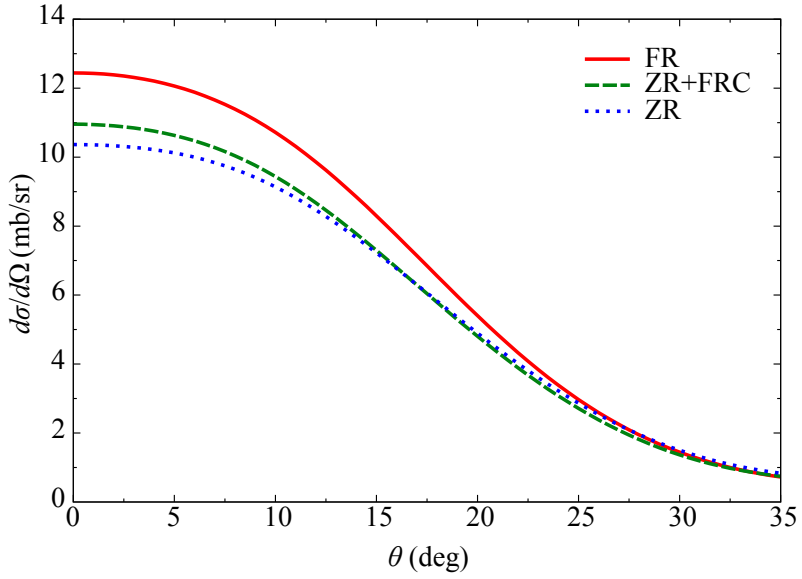

Figure D.5: Same as them in Fig. D.1 but for the ^{8}B(d,n)^{9}C at 14.4 MeV/nucleon described with CCBA.

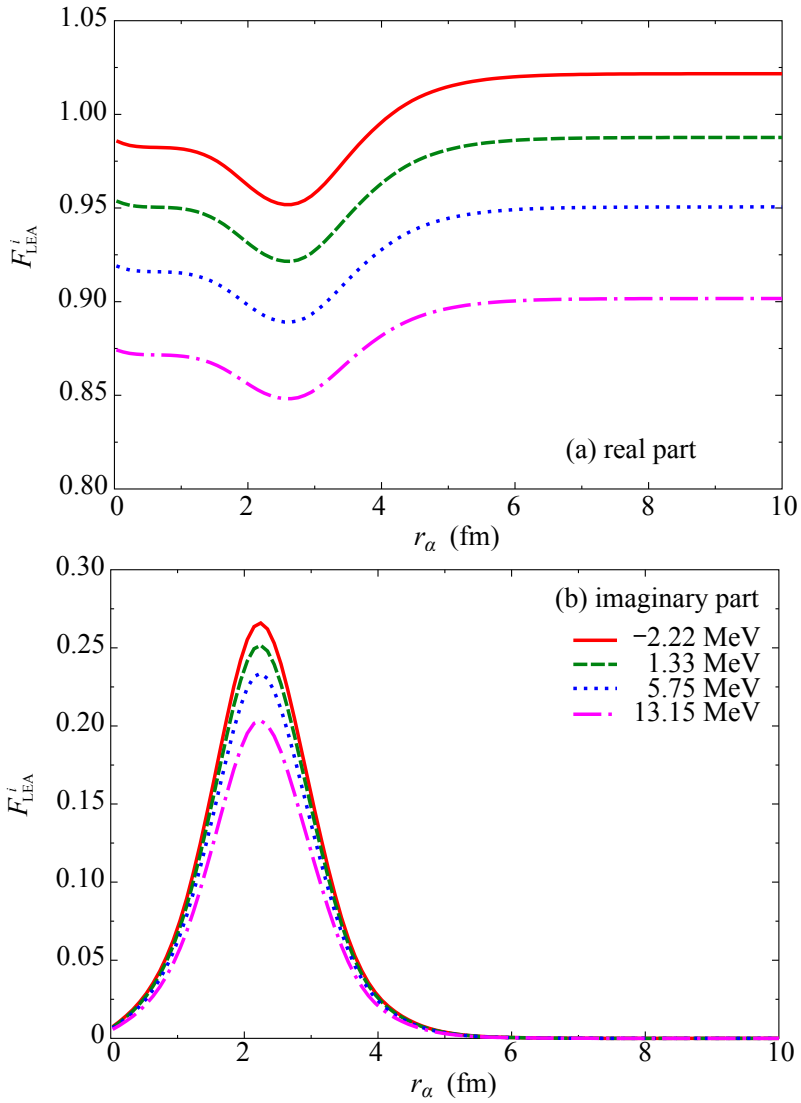

Figure D.6: Panels (a) and (b) are respectively the real and imaginary parts of the correction function $F^i_{\rm LEA}$ defined by Eq. (D.49). Each lines correspond to the result with ε^i_{pn} specified in the legends.

APPENDIX E

Treatment of Spins for Transfer Cross Section

Let's consider the transfer reaction, $a(x+b)+A \to b+B(x+A)$. The transfer cross section which does not specify the z-components of particles' spins in question must be taken an average over the initial spin orientations and a sum over their final things. Therefore the cross section is given by

$$\frac{d\sigma}{d\Omega} = \frac{1}{\hat{s}_a^2 \hat{J}_A^2} \sum_{m_a M_A m_b M_B} \frac{\mu_\alpha \mu_\beta}{(2\pi\hbar^2)^2} \frac{k_\beta}{k_\alpha} |T|^2 , \tag{E.1}$$

where μ_α (μ_β) and k_α (k_β) are the reduced mass and the wave number for the initial (final) channel, respectively. s_c or J_c is the intrinsic spins of particle c and its z-component is m_c or M_c. The transition matrix T is defined by

$$T = \left\langle \Psi_\beta^{(-)} \middle| \hat{V} \middle| \Psi_\alpha^{(+)} \right\rangle . \tag{E.2}$$

Here we don't mind whether T is the post or prior form. The total wave functions $\Psi_\alpha^{(+)}$ for the initial channel and $\Psi_\beta^{(+)}$ for the final channel can be written by

$$\Psi_\alpha^{(+)} = \Phi_{s_a m_a}^{(a)} \Phi_{J_A M_A}^{(A)} \chi_\alpha^{(+)}(\boldsymbol{k}_\alpha, \boldsymbol{r}_\alpha), \tag{E.3}$$

$$\Psi_\beta^{(-)*} = \Phi_{s_b m_b}^{(b)*} \Phi_{J_B M_B}^{(B)*} \chi_\beta^{(-)*}(\boldsymbol{k}_\beta, \boldsymbol{r}_\beta), \tag{E.4}$$

where $\Phi^{(c)}$ is the wave function of particle c and $\chi_\gamma^{(\pm)}$ is the distorted wave of the γ channel. The coordinates $\boldsymbol{r}_\alpha$ and $\boldsymbol{r}_\beta$ are shown in Fig. 3.2. $\Phi^{(a)}$ and $\Phi^{(B)}$ can be expanded with the relative wave function of consisting particles, $\psi^{(a)}$ or $\psi^{(B)}$, respectively, that is,

$$\begin{aligned} \Phi_{s_a m_a}^{(a)} = & \sum_{m_x M_{xb} m_{xb}} (s_x m_x s_b m_b | S_{xb} M_{xb}) \, (S_{xb} M_{xb} l_{xb} m_{xb} | s_a m_a) \\ & \times \psi_{l_{xb} m_{xb}}^{(a)} \Phi_{s_x m_x}^{(x)} \Phi_{s_b m_b}^{(b)}, \end{aligned} \tag{E.5}$$

$$\begin{aligned} \Phi_{J_B M_B}^{(B)} = & \sum_{m_x M_{xA} m_{xA}} (s_x m_x J_A M_A | S_{xA} M_{xA}) \, (S_{xA} M_{xA} l_{xA} m_{xA} | J_B M_B) \\ & \times \psi_{l_{xA} m_{xA}}^{(B)} \Phi_{s_x m_x}^{(x)} \Phi_{J_A M_A}^{(A)}, \end{aligned} \tag{E.6}$$

where S_{xc} (l_{xc}) and M_{xc} (m_{xc}) are the channel spins (relative angular momenta) between x and c, and its z-component.

We assume that the transition interaction $\hat{V}$ dose not operate onto $\Phi^{(c)}$, it means $\hat{V}$ is commutable to $\Phi^{(c)}$. Using this assumption, we obtain the transition matrix by inserting Eqs. from (E.3) to (E.6) into Eq. (E.2) as

$$\begin{aligned}
T = & \sum_{m_{xb}m_{xA}} \left\langle \chi^{(-)}_{\beta} \psi^{(B)}_{l_{xA}m_{xA}} \middle| \hat{V} \middle| \psi^{(a)}_{l_{xb}m_{xb}} \chi^{(+)}_{\alpha} \right\rangle \\
& \times \sum_{\substack{m_x M_{xb} \\ m'_x M_{xA}}} \left(s_x m_x s_b m_b | S_{xb} M_{xb}\right) \left(S_{xb} M_{xb} l_{xb} m_{xb} | s_a m_a\right) \\
& \qquad \times \left(s_x m'_x J_A M_A | S_{xA} M_{xA}\right) \left(S_{xA} M_{xA} l_{xA} m_{xA} | J_B M_B\right) \\
& \qquad \times \left\langle \Phi^{(x)}_{s_x m'_x} \Phi^{(b)}_{s_b m_b} \Phi^{(A)}_{J_A M_A} \middle| \Phi^{(x)}_{s_x m_x} \Phi^{(b)}_{s_b m_b} \Phi^{(A)}_{J_A M_A} \right\rangle \\
= & \sum_{m_{xb}m_{xA}} \tilde{T}_{m_{xb}m_{xA}} \sum_{m_x M_{xb} M_{xA}} \left(s_x m_x s_b m_b | S_{xb} M_{xb}\right) \left(S_{xb} M_{xb} l_{xb} m_{xb} | s_a m_a\right) \\
& \qquad \times \left(s_x m_x J_A M_A | S_{xA} M_{xA}\right) \left(S_{xA} M_{xA} l_{xA} m_{xA} | J_B M_B\right),
\end{aligned} \tag{E.7}$$

where

$$\tilde{T}_{m_{xb}m_{xA}} \equiv \left\langle \chi^{(-)}_{\beta} \psi^{(B)}_{l_{xA}m_{xA}} \middle| \hat{V} \middle| \psi^{(a)}_{l_{xb}m_{xb}} \chi^{(+)}_{\alpha} \right\rangle, \tag{E.8}$$

and we used

$$\left\langle \Phi^{(x)}_{s_x m'_x} \Phi^{(b)}_{s_b m_b} \Phi^{(A)}_{J_A M_A} \middle| \Phi^{(x)}_{s_x m_x} \Phi^{(b)}_{s_b m_b} \Phi^{(A)}_{J_A M_A} \right\rangle = \delta_{m_x m'_x}. \tag{E.9}$$

In order to insert Eq. (E.7) to Eq. (E.1), we have to calculate following z-component summation,

$$\begin{aligned}
\sum_{\substack{m_a M_A \\ m_b M_B}} |T|^2 = & \sum_{\substack{m_a M_A \\ m_b M_B}} \sum_{\substack{m_{xb} m_{xA} \\ m'_{xb} m'_{xA}}} \tilde{T}_{m_{xb}m_{xA}} \tilde{T}^*_{m'_{xb}m'_{xA}} \\
& \times \sum_{\substack{m_x M_{xb} \\ M_{xA} m'_x \\ M'_{xb} M'_{xA}}} \left(s_x m_x s_b m_b | S_{xb} M_{xb}\right) \left(s_x m'_x s_b m_b | S_{xb} M'_{xb}\right) \\
& \qquad \times \left(S_{xb} M_{xb} l_{xb} m_{xb} | s_a m_a\right) \left(S_{xb} M'_{xb} l_{xb} m'_{xb} | s_a m_a\right) \\
& \qquad \times \left(s_x m_x J_A M_A | S_{xA} M_{xA}\right) \left(s_x m'_x J_A M_A | S_{xA} M'_{xA}\right) \\
& \qquad \times \left(S_{xA} M_{xA} l_{xA} m_{xA} | J_B M_B\right) \left(S_{xA} M'_{xA} l_{xA} m'_{xA} | J_B M_B\right).
\end{aligned} \tag{E.10}$$

For simplicity we assume $l_{xb} = m_{xb} = m'_{xb} = 0$. This would be reasonable for the case of the s-wave dominant projectile, such as the deuteron induced transfer reaction. Then we have

$$\begin{aligned}
\left(S_{xb} M_{xb} 00 | s_a m_a\right) &= \delta_{S_{xb} S_a} \delta_{M_{xb} m_a}, \\
\left(S_{xb} M'_{xb} 00 | s_a m_a\right) &= \delta_{S_{xb} S_a} \delta_{M'_{xb} m_a}.
\end{aligned} \tag{E.11}$$

Therefore

$$\sum_{m_a m_b M_{xb} M'_{xb}} (s_x m_x s_b m_b | S_{xb} M_{xb}) \left(s_x m'_x s_b m'_b | S_{xb} M'_{xb}\right) \delta_{S_{xb} S_a} \delta_{M_{xb} m_a} \delta_{M'_{xb} m_a}$$
$$= \frac{\hat{s}_a^2}{\hat{s}_x^2} \sum_{m_a m_b} (s_a, -m_a s_b m_b | s_x, -m_x) \left(s_a, -m_a s_b m_b | s_x, -m'_x\right) \delta_{S_{xb} S_a}$$
$$= \frac{\hat{s}_a^2}{\hat{s}_x^2} \delta_{S_{xb} S_a} \delta_{m_x m'_x}. \tag{E.12}$$

Using Eq. (E.12) we obtain

$$\sum_{m_x m'_x M_A} (s_x m_x J_A M_A | S_{xA} M_{xA}) \left(s_x m'_x J_A M_A | S_{xA} M'_{xA}\right) \delta_{m_x m'_x} = \delta_{M_{xA} M'_{xA}}. \tag{E.13}$$

Then we can sum over remaining components

$$\sum_{M_{xA} M'_{xA} M_B} (S_{xA} M_{xA} l_{xA} m_{xA} | J_B M_B) \left(S_{xA} M'_{xA} l_{xA} m'_{xA} | J_B M_B\right) \delta_{S_{xb} S_a} \delta_{M_{xb} m_a} \delta_{M_{xA} M'_{xA}}$$
$$= \frac{\hat{J}_B^2}{\hat{l}_{xA}^2} \sum_{M_{xA} M_B} (S_{xA} M_{xA} J_B, -M_B | l_{xA}, -m_{xA}) \left(S_{xA} M_{xA} J_B, -M_B | l_{xA}, -m'_{xA}\right)$$
$$= \frac{\hat{J}_B^2}{\hat{l}_{xA}^2} \delta_{m_{xA} m'_{xA}}. \tag{E.14}$$

Finally Eq. (E.10) becomes

$$\sum_{m_a M_A m_b M_B} |T|^2 = \frac{\hat{s}_a^2 \hat{J}_B^2}{\hat{s}_x^2 \hat{l}_{xA}^2} \sum_{m_{xA}} \left|\tilde{T}_{m_{xA}}\right|^2, \tag{E.15}$$

and we obtain the cross section formula

$$\frac{d\sigma}{d\Omega} = \mathscr{S} \frac{\mu_\alpha \mu_\beta}{(2\pi\hbar^2)^2} \frac{k_\beta}{k_\alpha} \sum_{m_{xA}} \left|\tilde{T}_{m_{xA}}\right|^2, \tag{E.16}$$

$$\mathscr{S} \equiv \frac{\hat{J}_B^2}{\hat{J}_A^2 \hat{s}_x^2 \hat{l}_{xA}^2}. \tag{E.17}$$

Eq. (E.16) means that we only have to multiply the "spinless" cross section , which is calculated with $\tilde{T}_{m_{xA}}$, by the spin factor $\mathscr{S}$.

APPENDIX F

Plane Wave Limit on Transfer Reaction

Contents

The formulation of the transfer cross section in the plane wave limit is useful to check the coding. In this note the projectile is assumed to be an s-wave nucleus. The degree of spins is neglected.

F.1 Case for transfer angular momentum l=0

F.1.1 Integration over coordinates of bound state nuclei

First let's consider the transfer angular momentum $\boldsymbol{l}$ is equal to zero. It means that the residual nucleus B in the transfer reaction $a(x+b)+A \to b+B(x+A)$ is an s-wave state. In the plane wave limit the transition matrix for this reaction can be written by

$$T^{\mathrm{PW}} = \int d\boldsymbol{r}_{xb} d\boldsymbol{r}_{xA} e^{-i\boldsymbol{k}_\beta \cdot \boldsymbol{r}_\beta} \psi_{xA}(\boldsymbol{r}_{xA}) V_{xb}(r_{xb}) \psi_{xb}(\boldsymbol{r}_{xb}) e^{i\boldsymbol{k}_\alpha \cdot \boldsymbol{r}_\alpha}, \tag{F.1}$$

where we assume the interaction $V_{xb}(r_{xb})$ between x and b is scalar, and ψ_{xc} is the relative wave function between x and c. Coordinates are shown in Fig. 3.2. $\boldsymbol{k}_\alpha$ ($\boldsymbol{k}_\beta$) is the relative wave number for the a-A (b-B) system.

If the radial parts of ψ_{xA} and $D_{xb} = V_{xb}\psi_{xb}$ are respectively expressed with Gaussian;

$$D_{xb}(\boldsymbol{r}_{xb}) = \frac{C_b}{\sqrt{4\pi}} \exp(-\nu_b r_{xb}^2), \tag{F.2}$$

$$\psi_{xA}(\boldsymbol{r}_{xA}) = \frac{C_A}{\sqrt{4\pi}} \exp(-\nu_A r_{xA}^2), \tag{F.3}$$

Eq. (F.1) can be written as

$$T^{\rm PW} = \frac{C_b C_A}{4\pi} \int d\boldsymbol{r}_{xb} \exp(-\nu_b r_{xb}^2) e^{-i\boldsymbol{q}_{xb}\cdot\boldsymbol{r}_{xb}} \int d\boldsymbol{r}_{xA} \exp(-\nu_A r_{xA}^2) e^{-i\boldsymbol{q}_{xA}\cdot\boldsymbol{r}_{xA}}, \quad \text{(F.4)}$$

$$\boldsymbol{q}_{xb} = c_1 \boldsymbol{k}_\alpha - d_2 \boldsymbol{k}_\beta, \quad \text{(F.5)}$$
$$\boldsymbol{q}_{xA} = c_2 \boldsymbol{k}_\alpha - d_2 \boldsymbol{k}_\beta. \quad \text{(F.6)}$$

Here we use

$$\boldsymbol{r}_\alpha = c_1 \boldsymbol{r}_{xb} + c_2 \boldsymbol{r}_{xA}, \quad \text{(F.7)}$$
$$\boldsymbol{r}_\beta = d_1 \boldsymbol{r}_{xb} + d_2 \boldsymbol{r}_{xA}, \quad \text{(F.8)}$$

$$\begin{aligned} c_1 &\equiv -\frac{t}{qs-pt}, \quad c_2 \equiv \frac{q}{qs-pt}, \\ d_1 &\equiv \frac{s}{qs-pt}, \quad d_2 \equiv -\frac{p}{qs-pt}. \end{aligned} \quad \text{(F.9)}$$

Coordinates Eq. (F.9) are defined by

$$\boldsymbol{r}_{xA} = s\boldsymbol{r}_\alpha + t\boldsymbol{r}_\beta, \quad \text{(F.10)}$$
$$\boldsymbol{r}_{xb} = p\boldsymbol{r}_\alpha + q\boldsymbol{r}_\beta, \quad \text{(F.11)}$$

$$\begin{aligned} s &\equiv \frac{B}{x}\frac{a}{a+A}, \quad t \equiv -\frac{B}{x}\frac{b}{b+B}, \\ p &\equiv \frac{a}{x}\frac{A}{a+A}, \quad q \equiv -\frac{a}{x}\frac{B}{b+B}. \end{aligned} \quad \text{(F.12)}$$

By using the formula for the Fourier transformation of the Gaussian,

$$\int d\boldsymbol{x}\; e^{i\boldsymbol{p}\cdot\boldsymbol{x}} e^{-a(\boldsymbol{x}\pm\boldsymbol{y})^2} = \int d\boldsymbol{x}'\; e^{i\boldsymbol{p}\cdot(\boldsymbol{x}'\mp\boldsymbol{y})} e^{-ax'^2} = \left(\frac{\pi}{a}\right)^{3/2} e^{-p^2/(4a)} e^{\mp i\boldsymbol{p}\cdot\boldsymbol{y}}, \quad \text{(F.13)}$$

the integration in Eq. (F.4) can be done. Thus we obtain

$$T^{\rm PW} = \frac{C_b C_A}{4\pi} \left(\frac{\pi}{\nu_b}\right)^{3/2} e^{-q_{xb}^2/(4\nu_b)} \left(\frac{\pi}{\nu_A}\right)^{3/2} e^{-q_{xA}^2/(4\nu_A)}. \quad \text{(F.14)}$$

If D_{xb} and ψ_{xA} is expanded by the superposition of many Gaussian bases,

$$D_{xb}(\boldsymbol{r}_{xb}) = \sum_{i_b} \frac{C_{i_b}}{\sqrt{4\pi}} \exp(-\nu_{i_b} r_{xb}^2), \quad \text{(F.15)}$$

$$\psi_{xA}(\boldsymbol{r}_{xA}) = \sum_{i_A} \frac{C_{i_A}}{\sqrt{4\pi}} \exp(-\nu_{i_A} r_{xA}^2), \quad \text{(F.16)}$$

Eq. (F.14) can be written as

$$T^{\rm PW} = \frac{1}{4\pi} \sum_{i_b} C_{i_b} \left(\frac{\pi}{\nu_{i_b}}\right)^{3/2} e^{-q_{xb}^2/(4\nu_{i_b})} \sum_{i_A} C_{i_A} \left(\frac{\pi}{\nu_{i_A}}\right)^{3/2} e^{-q_{xA}^2/(4\nu_{i_A})}. \quad \text{(F.17)}$$

F.1.2 Integration over coordinates of plane waves

Let's convert the integration variables $(\boldsymbol{r}_{xb}, \boldsymbol{r}_{xA})$ into $(\boldsymbol{r}_\alpha, \boldsymbol{r}_\beta)$ in Eq. (F.1). Eq. (F.1) is now

$$T^{\mathrm{PW}} = \mathscr{J} \int d\boldsymbol{r}_\alpha d\boldsymbol{r}_\beta e^{-i\boldsymbol{k}_\beta\cdot\boldsymbol{r}_\beta} f(\boldsymbol{r}_\alpha, \boldsymbol{r}_\beta) e^{i\boldsymbol{k}_\alpha\cdot\boldsymbol{r}_\alpha}, \tag{F.18}$$

$$\begin{aligned} f(\boldsymbol{r}_\alpha, \boldsymbol{r}_\beta) &= \psi_{xA}(\boldsymbol{r}_{xA}) D_{xb}(\boldsymbol{r}_{xb}) \\ &= \frac{C_b C_A}{4\pi} e^{-\alpha r_\alpha^2} e^{-\beta r_\beta^2} e^{\gamma \boldsymbol{r}_\alpha\cdot\boldsymbol{r}_\beta}. \end{aligned} \tag{F.19}$$

Here we use Eqs. (F.2) and (F.3) in Eq. (F.19) and then α, β, and γ are defined by

$$\alpha = \nu_A s^2 + \nu_b p^2, \tag{F.20}$$

$$\beta = \nu_A t^2 + \nu_b q^2, \tag{F.21}$$

$$\gamma = -2(\nu_A st + \nu_b pq) > 0. \tag{F.22}$$

$\mathscr{J}$ is the Jacobian of the transformation from the variables $(\boldsymbol{r}_{xA}, \boldsymbol{r}_{xb})$ to the $(\boldsymbol{r}_\alpha, \boldsymbol{r}_\beta)$. The $\boldsymbol{r}_\alpha$-integration in Eq. (F.18) can be done by the following procedure;

$$\begin{aligned} \int d\boldsymbol{r}_\alpha e^{-\alpha r_\alpha^2} e^{\gamma \boldsymbol{r}_\alpha\cdot\boldsymbol{r}_\beta} e^{i\boldsymbol{k}_\alpha\cdot\boldsymbol{r}_\alpha} &= e^{\alpha\varepsilon^2 r_\beta^2} \int d\boldsymbol{r}_\alpha e^{-\alpha(\boldsymbol{r}_\alpha - \varepsilon\boldsymbol{r}_\beta)^2} e^{i\boldsymbol{k}_\alpha\cdot\boldsymbol{r}_\alpha} \\ &= e^{\alpha\varepsilon^2 r_\beta^2} \left(\frac{\pi}{\alpha}\right)^{3/2} e^{-k_\alpha^2/(4\alpha)} e^{i\varepsilon\boldsymbol{k}_\alpha\cdot\boldsymbol{r}_\beta}, \end{aligned} \tag{F.23}$$

$$\varepsilon \equiv \frac{\gamma}{2\alpha}. \tag{F.24}$$

To obtain Eq. (F.23) we use Eq. (F.13). Then we have

$$\begin{aligned} T^{\mathrm{PW}} &= \frac{\mathscr{J}}{4\pi} C_b C_A \left(\frac{\pi}{\alpha}\right)^{3/2} e^{-k_\alpha^2/(4\alpha)} \int d\boldsymbol{r}_\beta e^{i(\varepsilon\boldsymbol{k}_\alpha - \boldsymbol{k}_\beta)\cdot\boldsymbol{r}_\beta} e^{-(\beta-\varepsilon^2\alpha)r_\beta^2} \\ &= \frac{\mathscr{J}}{4\pi} C_b C_A \left(\frac{\pi}{\alpha}\right)^{3/2} e^{-k_\alpha^2/(4\alpha)} \left(\frac{\pi}{\bar{\beta}}\right)^{3/2} e^{-K^2/(4\bar{\beta})}, \end{aligned} \tag{F.25}$$

$$\boldsymbol{K} = \varepsilon\boldsymbol{k}_\alpha - \boldsymbol{k}_\beta, \tag{F.26}$$

$$\bar{\beta} = \beta - \varepsilon^2\alpha. \tag{F.27}$$

If we adopt Eqs. (F.15) and (F.16) instead of Eqs. (F.2) and (F.3), Eq. (F.25) leads to

$$T^{\mathrm{PW}} = \frac{\mathscr{J}}{4\pi} \sum_{i_b} C_{i_b} \sum_{i_A} C_{i_A} \left(\frac{\pi}{\alpha_{i_A i_b}}\right)^{3/2} e^{-k_\alpha^2/(4\alpha_{i_A i_b})} \left(\frac{\pi}{\bar{\beta}_{i_A i_b}}\right)^{3/2} e^{-K_{i_A i_b}^2/(4\bar{\beta}_{i_A i_b})}, \tag{F.28}$$

$$\boldsymbol{K}_{i_A i_b} = \varepsilon_{i_A i_b}\boldsymbol{k}_\alpha - \boldsymbol{k}_\beta, \tag{F.29}$$

$$\bar{\beta}_{i_A i_b} = \beta_{i_A i_b} - \varepsilon_{i_A i_b}^2 \alpha_{i_A i_b}, \tag{F.30}$$

$$\varepsilon_{i_A i_b} \equiv \frac{\gamma_{i_A i_b}}{2\alpha_{i_A i_b}}, \tag{F.31}$$

$$\alpha_{i_A i_b} = \nu_{i_A} s^2 + \nu_{i_b} p^2, \tag{F.32}$$

$$\beta_{i_A i_b} = \nu_{i_A} t^2 + \nu_{i_b} q^2, \tag{F.33}$$

$$\gamma_{i_A i_b} = -2(\nu_{i_A} st + \nu_{i_b} pq) > 0. \tag{F.34}$$

To prove that Eqs. (F.17) and (F.25) are equivalent to each other, we transform some variables. First, from the definition of $\bar{\beta}$, Eq. (F.27), we obtain

$$\begin{aligned}\bar{\beta} &= \beta - \varepsilon^2\alpha \\ &= \beta - \frac{\gamma^2}{4\alpha} \\ &= \nu_A t^2 + \nu_b q^2 - \frac{(\nu_A st + \nu_b pq)^2}{\nu_A s^2 + \nu_b p^2} \\ &= \frac{(qs-pt)^2\nu_A\nu_b}{\nu_A s^2 + \nu_b p^2},\end{aligned} \tag{F.35}$$

and then

$$\alpha\bar{\beta} = (qs-pt)^2\nu_A\nu_b. \tag{F.36}$$

Second, the argument of the exponential function in Eq. (F.25) can be rewritten by

$$\begin{aligned}\frac{k_\alpha^2}{\alpha} + \frac{K^2}{\bar{\beta}} &= \left(\frac{1}{\alpha} + \frac{\varepsilon^2}{\bar{\beta}}\right)k_\alpha^2 + \frac{1}{\bar{\beta}}k_\beta^2 - 2\frac{\varepsilon}{\bar{\beta}}k_\alpha k_\beta\cos\theta \\ &= \frac{\nu_A t^2 + \nu_b q^2}{(qs-pt)^2\nu_A\nu_b}k_\alpha^2 + \frac{\nu_A s^2 + \nu_b p^2}{(qs-pt)^2\nu_A\nu_b}k_\beta^2 \\ &\times \frac{-2(\nu_A s^2 + \nu_b p^2)}{(qs-pt)^2\nu_A\nu_b}\frac{-2(\nu_A st + \nu_b pq)}{2(\nu_A s^2 + \nu_b p^2)}k_\alpha k_\beta\cos\theta \\ &= \frac{1}{\alpha\bar{\beta}}\left(\beta k_\alpha^2 + \alpha k_\beta^2 - \gamma k_\alpha k_\beta\cos\theta\right).\end{aligned} \tag{F.37}$$

By inserting Eqs. (F.36) and (F.37) into Eq. (F.25) we get

$$T^{\mathrm{PW}} = \frac{C_b C_A}{4\pi}C_b C_A\left(\frac{\pi^2}{\nu_A\nu_b}\right)^{3/2}\exp\left[-\frac{1}{4\alpha\bar{\beta}}\left(\beta k_\alpha^2 + \alpha k_\beta^2 - \gamma k_\alpha k_\beta\cos\theta\right)\right]. \tag{F.38}$$

Here we use the property of $\mathscr{J}$, a 6×6 matrix, indicated symbolically by,

$$\mathscr{J} = \frac{\partial(\boldsymbol{r}_{xA},\boldsymbol{r}_{xb})}{\partial(\boldsymbol{r}_\alpha,\boldsymbol{r}_\beta)} = \begin{vmatrix}\frac{\partial\boldsymbol{r}_{xA}}{\partial\boldsymbol{r}_\alpha} & \frac{\partial\boldsymbol{r}_{xb}}{\partial\boldsymbol{r}_\alpha} \\ \frac{\partial\boldsymbol{r}_{xA}}{\partial\boldsymbol{r}_\beta} & \frac{\partial\boldsymbol{r}_{xb}}{\partial\boldsymbol{r}_\beta}\end{vmatrix}^3 = \begin{vmatrix}s & p \\ t & q\end{vmatrix}^3 = (sq-pt)^3 = \left[\frac{aB}{x(a+A)}\right]^3, \tag{F.39}$$

where we do not care about sign of $\mathscr{J}$ because the cross section contains the only square of $\mathscr{J}$.

Next, we focus on the argument of the exponential function in Eq. (F.14). It can be rewritten by

$$\begin{aligned}\frac{q_{xb}^2}{\nu_b} + \frac{q_{xA}^2}{\nu_A} &= \frac{1}{(qs-pt)^2}\left\{\left(\frac{t^2}{\nu_b} + \frac{q^2}{\nu_A}\right)k_\alpha^2 + \left(\frac{s^2}{\nu_b} + \frac{p^2}{\nu_A}\right)k_\beta^2 + 2\left(\frac{st}{\nu_b} + \frac{pq}{\nu_A}\right)k_\alpha k_\beta\cos\theta\right\} \\ &= \frac{1}{\alpha\bar{\beta}}\left(\beta k_\alpha^2 + \alpha k_\beta^2 - \gamma k_\alpha k_\beta\cos\theta\right).\end{aligned} \tag{F.40}$$

By inserting Eq. (F.40) into Eq. (F.14), we get Eq. (F.38).

F.2 Case for transfer angular momentum $l \neq 0$

F.2.1 Integration over coordinates of bound state nuclei

Eq. (F.14) can be easily extended in the case with a finite value of $\boldsymbol{l}$. Now we assume that the projectile is an s-wave, and hence, the orbital angular momentum of the partial wave of ψ_{xA} is aligned to $\boldsymbol{l}$. Thus ψ_{xA} is expanded by

$$\psi_{xA}(\boldsymbol{r}_{xA}) = \phi_l(r_{xA})Y_{lm}(\hat{\boldsymbol{r}}_{xA}), \tag{F.41}$$

$$\phi_l(r_{xA}) = \sum_{i_A} C_{i_A} r_{xA}^l \exp(-\nu_{i_A} r_{xA}^2), \tag{F.42}$$

where m is the z-component of $\boldsymbol{l}$. For $\boldsymbol{r}_{xA}$-integration in Eq. (F.1), the following formula is useful:

$$\int d\boldsymbol{x}\, e^{i\boldsymbol{p}\cdot\boldsymbol{x}} e^{-ax^2} x^l Y_{lm}(\hat{\boldsymbol{x}}) = \left(\frac{\pi}{a}\right)^{3/2} \left(\frac{ip}{2a}\right)^l Y_{lm}(\hat{\boldsymbol{p}}). \tag{F.43}$$

Inserting Eqs. (F.15) and from (F.41) to (F.43) into Eq. (F.1),

$$\begin{aligned} T_m^{\rm PW} = &\sum_{i_b} \frac{C_{i_b}}{\sqrt{4\pi}} \left(\frac{\pi}{\nu_{i_b}}\right)^{3/2} e^{-q_{xb}^2/(4\nu_{i_b})} \\ &\times \sum_{i_A} C_{i_A} \left(\frac{\pi}{\nu_{i_A}}\right)^{3/2} e^{-q_{xA}^2/(4\nu_{i_A})} \left(\frac{iq_{xA}}{2\nu_{i_A}}\right)^l Y_{lm}(\hat{\boldsymbol{q}}_{xA}). \end{aligned} \tag{F.44}$$

The unpolarized cross section is given by

$$\begin{aligned} \frac{d\sigma}{d\Omega} &= \mathscr{S} \frac{\mu_\alpha \mu_\beta}{(2\pi\hbar^2)^2} \frac{k_\beta}{k_\alpha} \sum_m |T_m^{\rm PW}|^2 \\ &= \mathscr{S} \frac{\mu_\alpha \mu_\beta}{(2\pi\hbar^2)^2} \frac{k_\beta}{k_\alpha} \frac{\hat{l}^2}{4\pi} \\ &\times \left| \sum_{i_b} \frac{C_{i_b}}{\sqrt{4\pi}} \left(\frac{\pi}{\nu_{i_b}}\right)^{3/2} e^{-q_{xb}^2/(4\nu_{i_b})} \sum_{i_A} C_{i_A} \left(\frac{\pi}{\nu_{i_A}}\right)^{3/2} e^{-q_{xA}^2/(4\nu_{i_A})} \left(\frac{q_{xA}}{2\nu_{i_A}}\right)^l \right|^2, \end{aligned} \tag{F.45}$$

$$\mathscr{S} \equiv \left(\frac{\hat{J}_B}{\hat{J}_A \hat{s}_x \hat{l}}\right)^2, \tag{F.46}$$

where μ_α (μ_β) is the reduced mass of the a-A (b-B) system. In Eq. (F.45) we use

$$\sum_m Y_{lm}^*(\hat{\boldsymbol{q}}_{xA}) Y_{lm}(\hat{\boldsymbol{q}}_{xA}) = \frac{\hat{l}^2}{4\pi} P_l(\cos 0) = \frac{\hat{l}^2}{4\pi}. \tag{F.47}$$

F.3 Zero-range approximation

If we adopt the zero-range (ZR) approximation,

$$D_{xb}(\boldsymbol{r}_{xb}) \sim D_0\delta(\boldsymbol{r}_{xb}), \tag{F.48}$$

the $\boldsymbol{r}_{xb}$-integration of Eq. (F.43) can be easily done:

$$\int d\boldsymbol{r}_{xb} D_{xb}(\boldsymbol{r}_{xb}) e^{i\boldsymbol{q}_{xb}\cdot\boldsymbol{r}_{xb}} = D_0. \tag{F.49}$$

Here we still assume that ψ_{xb} is an s-wave state. Then Eq. (F.44) and Eq.(F.45), respectively, become

$$T_m^{\rm PW} = D_0 \sum_{i_A} C_{i_A} \left(\frac{\pi}{\nu_{i_A}}\right)^{3/2} e^{-q_{xA}^2/(4\nu_{i_A})} \left(\frac{iq_{xA}}{2\nu_{i_A}}\right)^l Y_{lm}(\hat{\boldsymbol{q}}_{xA}), \tag{F.50}$$

$$\frac{d\sigma}{d\Omega} = \mathscr{S}\frac{\mu_\alpha\mu_\beta}{(2\pi\hbar^2)^2}\frac{k_\beta}{k_\alpha}\frac{\hat{l}^2}{4\pi}D_0^2 \left|\sum_{i_A} C_{i_A} \left(\frac{\pi}{\nu_{i_A}}\right)^{3/2} e^{-q_{xA}^2/(4\nu_{i_A})} \left(\frac{q_{xA}}{2\nu_{i_A}}\right)^l\right|^2. \tag{F.51}$$

In the ZR approximation if we formulate the T matrix by integrating over only the angular part of $\boldsymbol{r}_{xA}$, it is useful to estimate the numerical convergence of the radial integration of the overlap function such as Eq. (C.35). In the ZR limit the transition matrix with remaining the $\boldsymbol{r}_{xA}$-integration is given by

$$T_m^{\rm PW} = D_0 \int d\boldsymbol{r}_{xA} \sum_{i_A} C_{i_A} r_{xA}^l \exp(-\nu_{xA} r_{xA}^2) Y_{lm}(\hat{\boldsymbol{r}}_{xA}) e^{-i\boldsymbol{q}_{xA}\cdot\boldsymbol{r}_{xA}}. \tag{F.52}$$

By expanding the plane wave $e^{-i\boldsymbol{q}_{xA}\cdot\boldsymbol{r}_{xA}}$ with Rayleigh formula,

$$e^{-i\boldsymbol{q}_{xA}\cdot\boldsymbol{r}_{xA}} = 4\pi\sum_{LM}(-)^L i^L j_L(q_{xA}r_{xA}) Y_{LM}^*(\hat{\boldsymbol{r}}_{xA}) Y_{LM}^*(\hat{\boldsymbol{q}}_{xA}), \tag{F.53}$$

we can easily derive the formula. Here $j_L(q_{xA}r_{xA})$ is the spherical Bessel function. From Eqs. (F.53) and (F.52), we have

$$\begin{aligned} T_m^{\rm PW} &= D_0 \int_0^\infty dr_{xA} r_{xA}^2 \sum_{i_A} C_{i_A} r_{xA}^l \exp(-\nu_{xA} r_{xA}^2) 4\pi \sum_{LM}(-)^L i^L j_L(q_{xA}r_{xA}) Y_{LM}^*(\hat{\boldsymbol{q}}_{xA}) \\ &\times \int d\hat{\boldsymbol{r}}_{xA} Y_{LM}^*(\hat{\boldsymbol{r}}_{xA}) Y_{lm}(\hat{\boldsymbol{r}}_{xA}) \\ &= 4\pi D_0 (-)^l i^l \sum_{i_A} C_{i_A} \int_0^\infty dr_{xA} r_{xA}^{l+2} \exp(-\nu_{xA} r_{xA}^2) j_L(q_{xA}r_{xA}) Y_{LM}^*(\hat{\boldsymbol{q}}_{xA}). \end{aligned} \tag{F.54}$$

To obtain Eq. (F.55) we use the orthogonal condition of the spherical harmonics,

$$\int d\hat{\boldsymbol{r}}_{xA} Y_{LM}^*(\hat{\boldsymbol{r}}_{xA}) Y_{lm}(\hat{\boldsymbol{r}}_{xA}) = \delta_{Ll}\delta_{Mm}. \tag{F.55}$$

Thus the cross section is given by

$$\frac{d\sigma}{d\Omega} = 4\pi\mathscr{S}\frac{\mu_\alpha\mu_\beta}{(2\pi\hbar^2)^2}\frac{k_\beta}{k_\alpha}\hat{l}^2 D_0^2\left|\sum_{i_A} C_{i_A}\int_0^\infty dr_{xA} r_{xA}^{l+2}\exp(-\nu_{xA}r_{xA}^2)j_L(q_{xA}r_{xA})\right|^2. \tag{F.56}$$

As an example, we compare the cross sections calculated by Eqs. (F.51) and (F.56) for the ^{8}B(d,n)^{9}C reaction at 14.4 MeV/nucleon. In fig. F.1 the thick solid line shows the cross section calculated with Eq. (F.51). The dashed and the dotted lines correspond the result obtained from Eq. (F.56) by integrating over r_{xA} up to 25.0 and 15.0 fm, respectively. The dashed line reproduces well the thick solid line. However the difference between the thick solid line and the dotted line is appreciable at forward angle in the linear scale. While one sees the oscillation of the dotted line at backward angle in the logarithmic scale. This suggests that the radial integration of Eq. (F.56) converge with the maximum value of r_{xA}

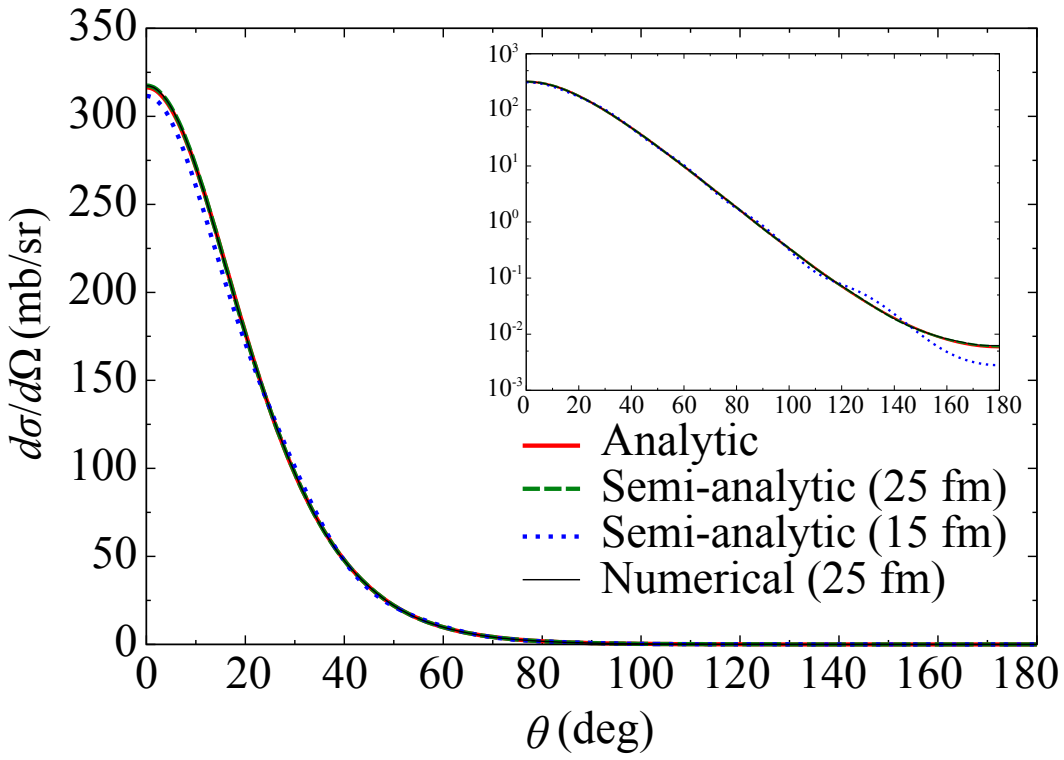

Figure F.1: The transfer cross section of ^{8}B(d,n)^{9}C reaction at 14.4 MeV/nucleon when we switch off any distorting potentials in the ZR limit. Thick solid line is the result obtained from Eq. (F.51). The dashed (dotted) line shows the cross section calculated with Eq. (F.56) by integrating over r_{xA} up to 25.0 (15.0) fm. If we numerically integrate the overlap function of Eq. (C.35), the thick solid line is obtained. In the small window the results in the logarithmic scale are shown.

of 25.0 fm. If we calculate the cross section from Eq. (C.35), where it is integrated over r_{xA} up to 25.0 fm without any distorted potentials, the thin solid line is obtained, which is identical with the thick solid line. Thus, Eq. (F.56) is useful to naively understand how large the model space describes the system.

APPENDIX G

Adiabatic Approximation on Transfer Reactions

Contents

G.1 Formulation

Let us consider the stripping reaction $a(x+b)+A \to b+B(x+A)$. For simplicity we ignore all of the intrinsic spins of each particle and all of the Coulomb interactions for the subsystems x-A, b-A, and b-B. Here we discuss the adiabatic (AD) approximation to the wave function $\Psi_\beta^{(+)}$ in the final channel on the reaction. Following Ref. [177], $\Psi_\beta^{(+)}$ with the AD approximation, that is, $\Psi_\beta^{\mathrm{AD}(+)}$ can be described by

$$\Psi_\beta^{\mathrm{AD}(+)}(\boldsymbol{r}_{xA}, \boldsymbol{r}_\beta) = \tilde{\chi}_\beta^{\mathrm{AD}(+)}(\boldsymbol{r}_{bA})\psi_{xA}(\boldsymbol{r}_{xA}) \exp\left(-i\alpha \boldsymbol{k}_\beta \cdot \boldsymbol{r}_{xA}\right), \tag{G.1}$$

$$\alpha \equiv \frac{m_x}{m_B}, \tag{G.2}$$

where the coordinates are shown in Fig. 3.2 and the relative wave number $\boldsymbol{k}_\beta$ is calculated from the outgoing energy of the system. The wave function ψ_{xA} describes the relative motion of the x-A system and m_X is the mass of the particle X. The b-B distorted wave $\tilde{\chi}_\beta^{\mathrm{AD}(+)}$ satisfies

$$\left[\frac{\hbar^2}{2\mu_\beta}\nabla^2_{\boldsymbol{r}_\beta} + U_{bA}(\boldsymbol{r}_{bA}) - (E - \varepsilon_{xA})\right] \tilde{\chi}_\beta^{\mathrm{AD}(+)}(\boldsymbol{r}_{bA}) = 0, \tag{G.3}$$

with the boundary condition

$$\tilde{\chi}_\beta^{\mathrm{AD}(+)}(\boldsymbol{r}_{bA}) \xrightarrow{\text{asymp.}} \exp\left(i\alpha \boldsymbol{k}_\beta \cdot \boldsymbol{r}_{bA}\right) + (\text{outgoing wave}). \tag{G.4}$$

Here μ_β is the reduced mass of the b-B system and the optical potential U_{bA} between b and A describes the distortion of the system. Owing to the AD approximation, the internal Hamiltonian h_{xA} in the Schrödinger equation is replaced by the ground state energy ε_{xA} of the residual nucleus B. The total energy is expressed by E.

If we adopt the zero-range (ZR) approximation expressed by Chap. 3 and Appx.D, the coordinates become

$$\boldsymbol{r}_{bA} \xrightarrow{\text{ZR}} \boldsymbol{r}_{xA}, \tag{G.5}$$

$$\boldsymbol{r}_{\beta} \xrightarrow{\text{ZR}} \mu \boldsymbol{r}_{xA}, \tag{G.6}$$

where$\mu = m_A/m_B$. Thus, within the ZR limit, we have

$$\begin{aligned}\Psi_{\beta}^{\text{AD}(+)}(\boldsymbol{r}_{xA}, \boldsymbol{r}_{\beta}) &\xrightarrow{\text{ZR}} \tilde{\chi}_{\beta}^{\text{AD}(+)}(\boldsymbol{r}_{xA})\psi_{xA}(\boldsymbol{r}_{xA}) \exp\left(-i\alpha \boldsymbol{k}_{\beta} \cdot \boldsymbol{r}_{xA}\right), \\ &\equiv \Psi_{\beta}^{\text{ZRAD}(+)}(\boldsymbol{r}_{xA}).\end{aligned} \tag{G.7}$$

One easily finds that the AD wave function with the ZR approximation has the proper asymptotic form, i.e., the plane wave regarding the coordinate $\boldsymbol{r}_{\beta}$;

$$\begin{aligned}&\Psi_{\beta}^{\text{ZRAD}(+)}(\boldsymbol{r}_{xA}) \\ &\quad\xrightarrow{\text{asymp.}} \exp\left(i\boldsymbol{k}_{\beta} \cdot \boldsymbol{r}_{xA}\right) \psi_{xA}(\boldsymbol{r}_{xA}) \exp\left(-i\alpha \boldsymbol{k}_{\beta} \cdot \boldsymbol{r}_{xA}\right) + (\text{outgoing wave}), \\ &\quad= \exp\left(i\mu \boldsymbol{k}_{\beta} \cdot \boldsymbol{r}_{xA}\right) \psi_{xA}(\boldsymbol{r}_{xA}) + (\text{outgoing wave}).\end{aligned} \tag{G.8}$$

From here, we discuss the partial wave expansion of $\Psi_{\beta}^{\text{ZRAD}(+)}$. First, we expand the distorted wave $\tilde{\chi}_{\beta}^{\text{AD}(+)}$ as

$$\tilde{\chi}_{\beta}^{\text{AD}(+)}(\boldsymbol{r}_{xA}) = \frac{4\pi}{k_{\beta} r_{xA}} \sum_{L} (-)^L i^L \hat{L} \chi_L(k_{\beta}, r_{xA}) \left[Y_L\left(\hat{\boldsymbol{k}}_{\beta}\right) \otimes Y_L\left(\hat{\boldsymbol{r}}_{xA}\right)\right]_{00}. \tag{G.9}$$

Similarly the plane wave in Eq. (G.7) is expanded by following the Rayleigh's relation as

$$\exp\left(-i\alpha \boldsymbol{k}_{\beta} \cdot \boldsymbol{r}_{xA}\right) = 4\pi \sum_{L'} i^{L'} \hat{L}' j_{L'}(\alpha k_{\beta} r_{xA}) \left[Y_{L'}\left(\hat{\boldsymbol{k}}_{\beta}\right) \otimes Y_{L'}\left(\hat{\boldsymbol{r}}_{xA}\right)\right]_{00}, \tag{G.10}$$

where $j_{L'}$ is the spherical Bessel function. Thus we obtain

$$\begin{aligned}\Psi_{\beta}^{\text{ZRAD}(+)}(\boldsymbol{r}_{xA}) = \;& \psi_{xA}(\boldsymbol{r}_{xA}) \frac{4\pi}{k_{\beta} r_{xA}} \sum_{L} (-)^L i^L \hat{L} \chi_L(k_{\beta}, r_{xA}) \left[Y_L\left(\hat{\boldsymbol{k}}_{\beta}\right) \otimes Y_L\left(\hat{\boldsymbol{r}}_{xA}\right)\right]_{00} \\ &\times 4\pi \sum_{L'} i^{L'} \hat{L}' j_{L'}(\alpha k_{\beta} r_{xA}) \left[Y_{L'}\left(\hat{\boldsymbol{k}}_{\beta}\right) \otimes Y_{L'}\left(\hat{\boldsymbol{r}}_{xA}\right)\right]_{00} \\ =\; & \psi_{xA}(\boldsymbol{r}_{xA}) \frac{4\pi}{k_{\beta} r_{xA}} \sum_{LL'} (-)^L i^{L+L'} \hat{L}^2 \hat{L}'^2 \chi_L(k_{\beta}, r_{xA}) j_{L'}(\alpha k_{\beta} r_{xA}) \\ &\times \sum_{\lambda\mu} \frac{1}{\hat{\lambda}} \left(\lambda, -\mu\lambda\mu | 00\right) \left(L0L'0 | \lambda 0\right) \left(L0L'0 | \lambda 0\right) \\ &\times Y_{\lambda,-\mu}\left(\hat{\boldsymbol{k}}_{\beta}\right) Y_{\lambda\mu}\left(\hat{\boldsymbol{r}}_{xA}\right).\end{aligned} \tag{G.11}$$

Here we used the following relations;

$$\begin{aligned}
&\left[Y_L\left(\hat{\boldsymbol{k}}_\beta\right)\otimes Y_L\left(\hat{\boldsymbol{r}}_{xA}\right)\right]_{00}\left[Y_{L'}\left(\hat{\boldsymbol{k}}_\beta\right)\otimes Y_{L'}\left(\hat{\boldsymbol{r}}_{xA}\right)\right]_{00}\\
&\quad=\left[\left[Y_L\left(\hat{\boldsymbol{k}}_\beta\right)\otimes Y_L\left(\hat{\boldsymbol{r}}_{xA}\right)\right]_0\otimes\left[Y_{L'}\left(\hat{\boldsymbol{k}}_\beta\right)\otimes Y_{L'}\left(\hat{\boldsymbol{r}}_{xA}\right)\right]_0\right]_{00}\\
&\quad=\sum_\lambda\hat{\lambda}^2\begin{Bmatrix}L & L & 0\\ L' & L' & 0\\ \lambda & \lambda & 0\end{Bmatrix}\left[\left[Y_L\left(\hat{\boldsymbol{k}}_\beta\right)\otimes Y_{L'}\left(\hat{\boldsymbol{k}}_\beta\right)\right]_\lambda\otimes\left[Y_L\left(\hat{\boldsymbol{r}}_{xA}\right)\otimes Y_{L'}\left(\hat{\boldsymbol{r}}_{xA}\right)\right]_\lambda\right]_{00}\\
&\quad=\sum_{\lambda\mu}\frac{\hat{\lambda}}{\hat{L}\hat{L}'}\left(\lambda,-\mu\lambda\mu|00\right)\left[Y_L\left(\hat{\boldsymbol{k}}_\beta\right)\otimes Y_{L'}\left(\hat{\boldsymbol{k}}_\beta\right)\right]_{\lambda,-\mu}\left[Y_L\left(\hat{\boldsymbol{r}}_{xA}\right)\otimes Y_{L'}\left(\hat{\boldsymbol{r}}_{xA}\right)\right]_{\lambda\mu},
\end{aligned}\tag{G.12}$$

$$\left[Y_L\left(\hat{\boldsymbol{k}}_\beta\right)\otimes Y_{L'}\left(\hat{\boldsymbol{k}}_\beta\right)\right]_{\lambda,-\mu}=\frac{\hat{L}\hat{L}'}{\sqrt{4\pi}\hat{\lambda}}\left(L0L'0|\lambda0\right)Y_{\lambda,-\mu}\left(\hat{\boldsymbol{k}}_\beta\right),\tag{G.13}$$

$$\left[Y_L\left(\hat{\boldsymbol{r}}_{xA}\right)\otimes Y_{L'}\left(\hat{\boldsymbol{r}}_{xA}\right)\right]_{\lambda\mu}=\frac{\hat{L}\hat{L}'}{\sqrt{4\pi}\hat{\lambda}}\left(L0L'0|\lambda0\right)Y_{\lambda\mu}\left(\hat{\boldsymbol{r}}_{xA}\right).\tag{G.14}$$

Now we have the relation

$$\left(\lambda,-\mu\lambda\mu|00\right)Y_{\lambda,-\mu}\left(\hat{\boldsymbol{k}}_\beta\right)=\frac{(-)^\lambda}{\hat{\lambda}}Y^*_{\lambda\mu}\left(\hat{\boldsymbol{k}}_\beta\right),\tag{G.15}$$

the wave function becomes

$$\begin{aligned}
\Psi_\beta^{\mathrm{ZRAD}(+)}(\boldsymbol{r}_{xA})=\psi_{xA}(\boldsymbol{r}_{xA})\frac{4\pi}{k_\beta r_{xA}}\sum_{\lambda\mu}\sum_{LL'}(-)^{L+\lambda}i^{L+L'}\frac{\hat{L}^2\hat{L}'^2}{\hat{\lambda}^2}\left(L0L'0|\lambda0\right)^2\\
\times\chi_L(k_\beta,r_{xA})j_{L'}(\alpha k_\beta r_{xA})Y^*_{\lambda\mu}\left(\hat{\boldsymbol{k}}_\beta\right)Y_{\lambda\mu}\left(\hat{\boldsymbol{r}}_{xA}\right).
\end{aligned}\tag{G.16}$$

When the arguments $\lambda,\ \mu,\ L,$ and L' regarding the summations are replaced into

$$(\lambda,\mu)\to(L,M),\tag{G.17}$$

$$L'\to\lambda,\tag{G.18}$$

$$L\to L',\tag{G.19}$$

Eq. (G.16) can be written as

$$\begin{aligned}
\Psi_\beta^{\mathrm{ZRAD}(+)}(\boldsymbol{r}_{xA})=\psi_{xA}(\boldsymbol{r}_{xA})\frac{4\pi}{k_\beta r_{xA}}\sum_{LM}\sum_{\lambda L'}(-)^{L+L'}i^{\lambda+L'}\frac{\hat{L}'^2\hat{\lambda}^2}{\hat{L}^2}\left(L'0\lambda0|L0\right)^2\\
\times\chi_{L'}(k_\beta,r_{xA})j_\lambda(\alpha k_\beta r_{xA})Y^*_{LM}\left(\hat{\boldsymbol{k}}_\beta\right)Y_{LM}\left(\hat{\boldsymbol{r}}_{xA}\right).
\end{aligned}\tag{G.20}$$

Meanwhile, $\Psi_\beta^{\mathrm{ZRAD}(+)}$ can be straightforwardly expanded as

$$\Psi_\beta^{\mathrm{ZRAD}(+)}(\boldsymbol{r}_{xA})=\psi_{xA}(\boldsymbol{r}_{xA})\frac{4\pi}{k_\beta r_{xA}}\sum_{LM}i^L\tilde{\chi}_L(k_\beta,r_{xA})Y^*_{LM}\left(\hat{\boldsymbol{k}}_\beta\right)Y_{LM}\left(\hat{\boldsymbol{r}}_{xA}\right).\tag{G.21}$$

Therefore, by comparing Eqs. (G.20) and (G.21), the partial wave $\tilde{\chi}_{L'}$, which should be adopted in the AD approximation, is explicitly written down by

$$\begin{aligned}\tilde{\chi}_L(k_\beta, r_{xA}) &= \sum_{\lambda L'} (-)^{L+L'} i^{\lambda+L'-L} \frac{\hat{L}'^2 \hat{\lambda}^2}{\hat{L}^2} \left(L'0\lambda 0|L0\right)^2 \chi_{L'}(k_\beta, r_{xA}) j_\lambda(\alpha k_\beta r_{xA}) \\ &= \sum_{\lambda L'} (-)^{L+L'} i^{\lambda+L'-L} \hat{\lambda}^2 \left(L0\lambda 0|L'0\right)^2 \chi_{L'}(k_\beta, r_{xA}) j_\lambda(\alpha k_\beta r_{xA}) \\ &= \sum_{\lambda} \hat{\lambda}^2 j_\lambda(\alpha k_\beta r_{xA}) \sum_{L'} (-)^{(L'-L-\lambda)/2} \left(L0\lambda 0|L'0\right)^2 \chi_{L'}(k_\beta, r_{xA}),\end{aligned} \tag{G.22}$$

where we used the property that $L+\lambda+L'$ is even, which is ensured by the Clebsch-Gordan coefficient. The maximum value of L' is determined from L if the maximum value of λ is given. Thus the range of the summation over λ has to be determined from the convergence of the cross section.

Note that, in Eq. (G.22), one finds the argument (k_β, r_{xA}) of $\tilde{\chi_L}$ and $\chi_{L'}$ is different from that in the usual ZR approximation, $(k_\beta, \mu r_{xA})$ as shown in Eq. (3.93). Due to this vanishing of the factor μ from the argument, $\tilde{\chi_L}$ must be normalized with multiplying by μ so that it has a proper asymptotic form.

Also it should be noted that, if there is the Coulomb interaction, in order to obtain Eq. (G.22), the Coulomb interaction between x and b has to be replaced by that between b and A. Because the validity of this prescription is not ensured, we have to be careful to adopt the present procedure for the charged particle system. If there is no Coulomb interaction in the final channel, for instance, the (d, n) reaction, it is expected to work well within the ZR approximation.

G.2 Application

As an application, we chose the ^{8}B(d,n)^{9}C reaction at 14.4 MeV/nucleon. The numerical setups are same as that mentioned in Sec. 3.4.2. In this calculation we adopt the ZR approximation. The breakup effects of d in the initial channel are explicitly taken into account by means of CDCC as described in Chap. 3. On the other hand, them of ^{9}C in the final channel are treated with some procedures. The solid line in Fig. G.1 is the ZR-CCBA result with adopting CDCC as well as the initial channel. This result is same as the dotted line in Fig. D.5. The dashed line is the result obtained from the conventional AD approximation, or so-called the Johnson-Soper (JS) approximation [128–132]. The good agreement between the solid and dashed lines are already mentioned in Chap. 3 even though it is the finite-range (FR) case there. On the other hand, the dotted line, which is obtained from the AD approximation proposed by Timofeyuk and Johnson [177], i.e., formulated in this Appendix, is about 50% larger than the solid line at 0°. For the calculate Eq. (G.22), λ is taken up to 11. Though more detailed analysis is needed to clarify this discrepancy, it can be said that the Timofeyuk-Johnson AD approximation seems to excessively take into account the breakup effects of ^{9}C in the transfer reaction compared to the conventional AD approximation.

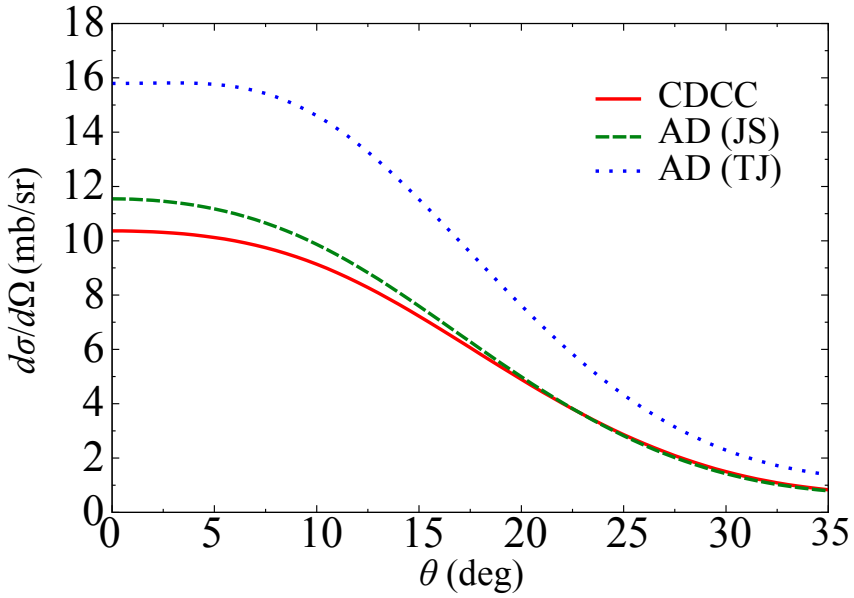

Figure G.1: Comparison of the cross section of the ^{8}B(d,n)^{9}C at 14.4 MeV/nucleon obtained by adopting CDCC (solid line), the conventional AD approximation (dashed line), and the new AD approximation described this section (dotted line) for the calculation of the wave function in the final channel. See the text for more detail.

APPENDIX H

Non-local Correction for Nucleon Optical Potential for Transfer Reactions

Contents

H.1 Energy shift

In usual theoretical approach with the three-body (p+n+A) model for the transfer reaction $A(d,p)B$, the d-A optical potential is assumed as a sum of neutron and proton optical potentials taken at energy

$$E_N = \frac{E_d}{2}. \tag{H.1}$$

Here E_N is the energy of a nucleon optical potential in the c.m. frame and E_d is the deuteron incident energy in the c.m. frame. Equation (H.1) stands for that the nucleons in deuteron are equally sharing the energy. However, the legitimacy of this assumption has not yet been ensured. Instead of explicitly treating the energy dependence of nucleon optical potentials, a non-local N-A potential can be alternative.

It is not easy to use non-local potentials, the prescription of the treatment of the non-locality was proposed [124–126] for the so-called equivalent local potential. Following Refs. [124–126], the non-locality can be easily treated by taking the energy E_N as

$$E_N = \frac{E_d}{2} + \Delta E, \tag{H.2}$$

where the energy shift ΔE is defined by

$$\Delta E = \frac{1}{2} \langle T_{pn} \rangle , \tag{H.3}$$

$$\langle T_{pn} \rangle = \frac{\hbar^2}{M_N} \int d\boldsymbol{r} \phi_1(\boldsymbol{r}) \nabla_r^2 \phi_0(\boldsymbol{r}). \tag{H.4}$$

Here the M_N is the nucleon mass and ϕ_0 is the p-n relative wave function in the ground state of deuteron. The relative distance between nucleons is represented by $\boldsymbol{r}$ and ϕ_1 is defined with the p-n interaction V_{pn};

$$\phi_1(\boldsymbol{r}) = \frac{V_{pn}(\boldsymbol{r})\phi_0(\boldsymbol{r})}{\langle\phi_0 \left|V_{pn}\right| \phi_0\rangle}. \tag{H.5}$$

The wave function ϕ_0 satisfies the Schrödinger equation

$$\left[\frac{\hbar^2}{2\mu}\nabla_r^2 + V_{pn}(\boldsymbol{r}) - \varepsilon_0\right]\phi_0(\boldsymbol{r}) = 0, \tag{H.6}$$

where $\mu = M_N^2/(2M_N)$ and $\varepsilon_0 = -2.22$ MeV is the ground state energy of deuteron. Equation (H.4) stands for the expectation value of the p-n kinetic energy $T_{pn} = \frac{\hbar^2}{2\mu}\nabla_r^2$ averaged over the range of V_{pn}. The energy shift ΔE must be positive that is ensured by Eq. (H.3). It means that the nucleon energy E_N always becomes higher than original one. Therefore the real part of nucleon optical potentials goes shallow and it effectively contains the effect that the potential becomes shallower due to the non-locality.

By using Eqs. (H.5) and (H.6), $\langle T_{pn}\rangle$ becomes

$$\begin{aligned}
\langle T_{pn}\rangle &= \frac{\hbar^2}{M_N}\int d\boldsymbol{r}\phi_1(\boldsymbol{r})\frac{2\mu}{\hbar^2}\left[\varepsilon_0 - V_{pn}(\boldsymbol{r})\right]\phi_0(\boldsymbol{r}) \\
&= \frac{2\mu}{M_N}\left[\varepsilon_0\frac{\langle\phi_0 \left|V_{pn}\right| \phi_0\rangle}{\langle\phi_0 \left|V_{pn}\right| \phi_0\rangle} - \frac{\left\langle\phi_0 \left|V_{pn}^2\right| \phi_0\right\rangle}{\langle\phi_0 \left|V_{pn}\right| \phi_0\rangle}\right] \\
&= \varepsilon_0 - \left\langle V_{pn}^2\right\rangle, \qquad \text{(H.7)} \\
\left\langle V_{pn}^2\right\rangle &\equiv \langle\phi_1 \left|V_{pn}\right| \phi_0\rangle \\
&= \frac{\left\langle\phi_0 \left|V_{pn}^2\right| \phi_0\right\rangle}{\langle\phi_0 \left|V_{pn}\right| \phi_0\rangle} < 0. \qquad \text{(H.8)}
\end{aligned}$$

Here we used $\frac{2\mu}{M_N} = \frac{2M_N^2/(2M_N)}{M_N} = 1$. One sees, from Eqs. (H.7) and (H.8), that the energy shift ΔE can be calculated if the deuteron model, i.e., V_{pn} and ϕ_0, is determined.

H.2 Specific model of deuteron

H.2.1 Hultén potential

As a simple model of deuteron, the Hultén potential [178] is often used. In this model V_{pn} is given by

$$V_{pn}(r) = -\frac{V_0^{(\mathrm{H})}}{e^{(\gamma-\kappa)r} - 1}, \tag{H.9}$$

$$V_0^{(\mathrm{H})} = \frac{\hbar^2}{2\mu}\left(\gamma^2 - \kappa^2\right), \tag{H.10}$$

where $\kappa = 0.232\ \mathrm{fm}^{-1}$ and $\gamma = 6.255\kappa$. Using this potential, the wave function ϕ_0 is analytically obtained as

$$\phi_0(\boldsymbol{r}) = \frac{u_0(r)}{r} Y_{00}\left(\hat{\boldsymbol{r}}\right), \tag{H.11}$$

$$u_0(r) = \mathcal{N}\left(e^{-\kappa r} - e^{-\gamma r}\right), \tag{H.12}$$

$$\mathcal{N} = \frac{\sqrt{2\kappa\gamma\left(\kappa+\gamma\right)}}{\gamma - \kappa}. \tag{H.13}$$

Then the energy shift can be analytically calculated;

$$\begin{aligned}
\left\langle \phi_0 \left| V_{pn} \right| \phi_0 \right\rangle &= 4\pi \int dr r^2 \phi_0(\boldsymbol{r}) V_{pn}(r) \phi_0(\boldsymbol{r}) \\
&= \int dr u_0^2(r) V_{pn}(r) \\
&= -\frac{\hbar^2}{2\mu}\kappa\left(\kappa+\gamma\right), \qquad \text{(H.14)} \\
\left\langle V_{pn}^2 \right\rangle &= \frac{\int dr u_0^2(r) V_{pn}^2(r)}{\left\langle \phi_0 \left| V_{pn} \right| \phi_0 \right\rangle} \\
&= \frac{\left(\mathcal{N} V_0^{(\mathrm{H})}\right)^2}{\left\langle \phi_0 \left| V_{pn} \right| \phi_0 \right\rangle} \int_0^\infty dr e^{-2\gamma r} \\
&= \frac{\hbar^2}{2\mu}\left(\gamma+\kappa\right)^2, \qquad \text{(H.15)} \\
\left\langle T_{pn} \right\rangle &= \varepsilon_0 - \frac{\hbar^2}{2\mu}\left(\gamma+\kappa\right)^2. \qquad \text{(H.16)}
\end{aligned}$$

Thus we have

$$\begin{aligned}
\Delta E &= \frac{1}{2}\left(\varepsilon_0 - \frac{\hbar^2}{2\mu}\left(\gamma+\kappa\right)^2\right) \\
&\sim 57\ \mathrm{MeV}. \qquad \text{(H.17)}
\end{aligned}$$

H.2.2 Ohmura potential and Gaussian basis functions

If we adopt the Ohmura potential [122],

$$V_{pn}(r) = -V_0^{(\mathrm{O})} e^{-\left(\frac{r}{r_0}\right)^2}, \tag{H.18}$$

$V_0^{(\mathrm{O})} = 72.15$ MeV, $r_0 = 1.484$ fm, it is convenient to expand ϕ_0 in terms of the Gaussian basis functions;

$$\phi_0(\boldsymbol{r}) = \frac{u_0(r)}{r} Y_{00}\left(\hat{\boldsymbol{r}}\right), \tag{H.19}$$

$$u_0(r) = \sum_i C_i r e^{-\mu_i r^2}, \tag{H.20}$$

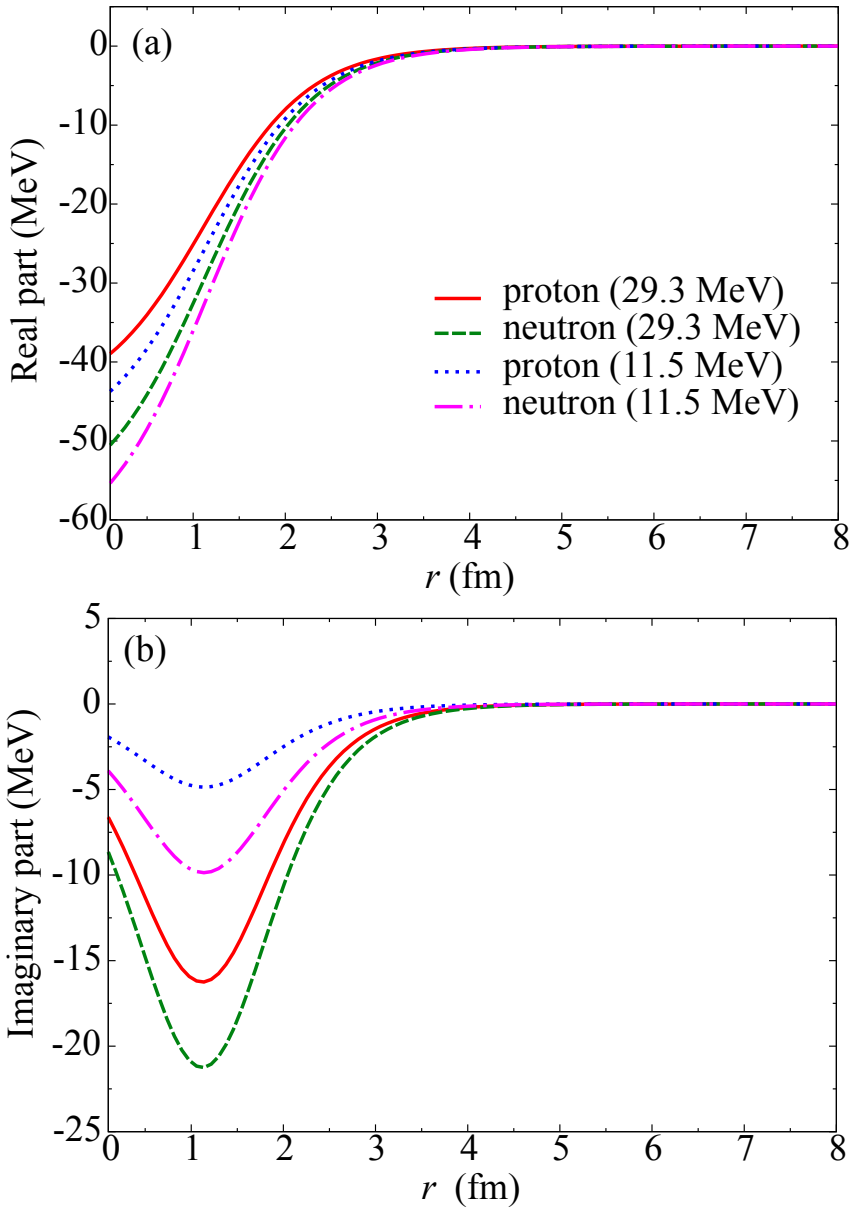

Figure H.1: Nucleon optical potential of the d-^{8}B system for (a) the real and (b) imaginary parts at 29.3 MeV for proton (solid line) and neutron (dashed line), and 11.5 MeV for proton (dotted line) and neutron (dash-dotted line).

where we assumed that ϕ_0 is the s-wave. How to calculate the expansion coefficients C_i is shown in Appx. J.

Now, because every functions are written with Gaussian functions, the energy shift can

be calculated analytically;

$$\begin{aligned}
\langle \phi_0 | V_{pn} | \phi_0 \rangle &= 4\pi \int dr r^2 \phi_0(\boldsymbol{r}) V_{pn}(r) \phi_0(\boldsymbol{r}) \\
&= \int dr u_0^2(r) V_{pn}(r) \\
&= -V_0^{(\mathrm{O})} \sum_{ij} C_i C_j \int_0^\infty dr r^2 \exp\left[-\left(\mu_i + \mu_j + \frac{1}{r_0} \right) r^2 \right] \\
&= -\frac{\sqrt{\pi}}{4} V_0^{(\mathrm{O})} \sum_{ij} \frac{C_i C_j}{\left(\mu_i + \mu_j + \frac{1}{r_0} \right)^{3/2}}, \qquad \text{(H.21)} \\
\left\langle V_{pn}^2 \right\rangle &= \frac{\int dr u_0^2(r) V_{pn}^2(r)}{\langle \phi_0 | V_{pn} | \phi_0 \rangle} \\
&= \frac{\left(V_0^{(\mathrm{O})} \right)^2}{\langle \phi_0 | V_{pn} | \phi_0 \rangle} \sum_{ij} C_i C_j \int_0^\infty dr r^2 \exp\left[-\left(\mu_i + \mu_j + \frac{2}{r_0} \right) r^2 \right] \\
&= \frac{\sqrt{\pi}}{4} \frac{\left(V_0^{(\mathrm{O})} \right)^2}{\langle \phi_0 | V_{pn} | \phi_0 \rangle} \sum_{ij} \frac{C_i C_j}{\left(\mu_i + \mu_j + \frac{2}{r_0} \right)^{3/2}}, \qquad \text{(H.22)}
\end{aligned}$$

When we use setups shown in Sec. 3.4.2, the energy shift ΔE is calculated to be 17.8 MeV.

The effects of this energy shift on the potential is shown in Fig. H.1 for the

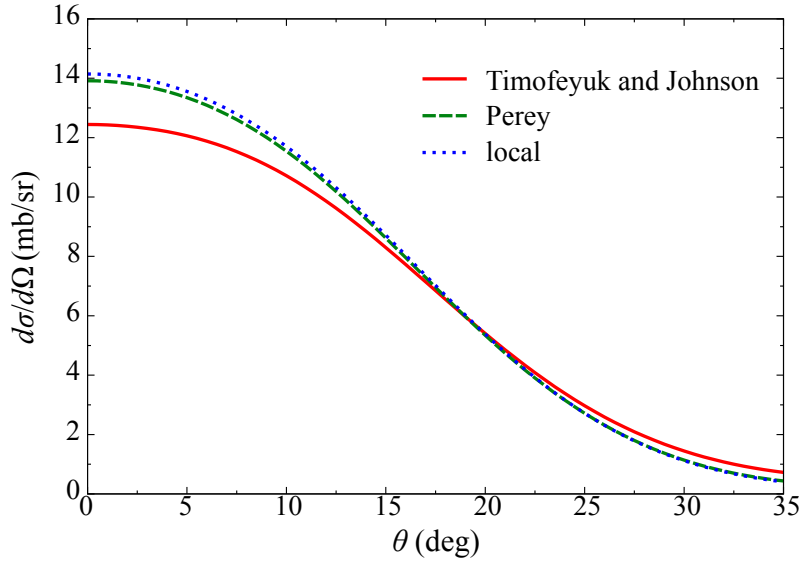

Figure H.2: Non-locality of the nucleon-^{8}B potential for the ^{8}B(d,n)^{9}C reaction at 14.4 MeV/nucleon. The cross section calculated with the equivalent local potential obtained from the present prescription (solid line), the conventional procedure (dashed line), and the local potential without the non-local correction (dotted line) are shown.

nucleon-^{8}B system at 14.4 MeV/nucleon in the laboratory frame, which corresponds to 11.5 MeV/nucleon in the c.m. frame. The parameters of the local optical potential are taken from Ref. [123]. As we can see in Fig. H.1(a), the real parts of the energy-shifted potentials for proton (solid line) and neutron (dashed line) are going to be shallow compared to them at original energy of 11.5 MeV of the former (dotted line) and the latter (dash-dotted line). Whereas the behavior of the imaginary parts of them shown in Fig. H.1(b) is opposite.

Thus these tendency of the potentials is expected to decrease the elastic cross section and also the transfer cross section since the amplitude of the distorted wave, which is generated by these energy-shifted potentials, become smaller compared with that by the default ones. In fact, as shown in Fig. H.2, the transfer cross section of the ^{8}B(d,n)^{9}C reaction calculated with the equivalent local potential obtained from the present prescription (solid line) is about 12% smaller than the result without the non-local correction (dotted line), in which no energy-shift is adopted. Note that these calculation is based on CCBA described in Chap. 3, i.e., the breakup effects of d and ^{9}C are explicitly taken into account by means of the CDCC method.

Conventionally the Perey factor $f_{\rm NL}$ [127] defined by

$$f_{\rm NL}(r_\alpha) = \left[1 - \frac{\mu\beta^2}{2\hbar^2} U_{\rm L}(r_\alpha)\right]^{-1/2} \tag{H.23}$$

has been used for the non-local correction by multiplying distorted waves by $f_{\rm NL}$. Here $U_{\rm L}$ is the energy-dependent local potential and the non-local parameter $\beta = 0.85$ fm for nucleon and 0.54 fm for deuteron is often used. The coordinate r_α is the relative distance between d and ^{8}B. Since, $f_{\rm NL}$ is less than unity only in the range of $U_{\rm L}$, the amplitude of distorted waves with $f_{\rm NL}$ becomes small in the interior region. In CDCC, there has not been established well how to calculate the Perey factor, that is, it is not trivial what we should adopt as $U_{\rm L}$. In the present work, $f_{\rm NL}$ is calculated with $U_{\rm L}$ assumed by the coupling potential in the ground state of d;

$$U_{\rm L}(r_\alpha) \approx \langle \phi_0 \left| U_p + U_n \right| \phi_0 \rangle \,, \tag{H.24}$$

where we adopt the N-^{8}B optical potential [123] as U_N and $\beta = 0.54$ fm. The cross section calculated with the Perey factor is shown by the dashed line in Fig. H.2. In the present system, the non-local effects described by the Perey factor is found to be small.

APPENDIX I

Manipulation of Modified Bessel Function

Contents

I.1 Reduced modified Bessel function

Let us consider a Gaussian function $f(r)$ defined by

$$f(r) = e^{-\nu r^2}, \tag{I.1}$$

where ν is the range of Gaussian. If the argument $\boldsymbol{r}$ is expressed by

$$\boldsymbol{r} = a\boldsymbol{x} + b\boldsymbol{y}, \tag{I.2}$$

Eq. (I.1) is rewritten as

$$\begin{aligned} f(r) &= e^{-\nu(a\boldsymbol{x}+b\boldsymbol{y})^2} \\ &= e^{-\nu a^2 x^2} e^{-\nu b^2 y^2} e^{-2\nu ab\boldsymbol{x}\cdot\boldsymbol{y}}. \end{aligned} \tag{I.3}$$

The factor $e^{-2\nu ab\boldsymbol{x}\cdot\boldsymbol{y}}$ can be expanded by using the modified Bessel function i_L as follows,

$$e^{-2\nu ab\boldsymbol{x}\cdot\boldsymbol{y}} = \sum_L (-)^L \hat{L}^2 i_L(z) P_L(w), \tag{I.4}$$

$$z \equiv 2\nu abxy, \tag{I.5}$$

where P_L is the Legendre polynomial and $w = \cos(\theta)$ with the angle θ between $\boldsymbol{x}$ and $\boldsymbol{y}$. Eqs. (I.3) and (I.4) correspond to Eqs. (C.8) and (C.12), respectively.

In the subroutine BESSI [171], the "reduced" modified Bessel function $\tilde{i}_L$ is calculated instead of i_L in order to eliminate divergence, which appears in a process of calculation of i_L. Here $\tilde{i}_L$ is defined by

$$\tilde{i}_L(z) \equiv (-)^L i_L(z) e^{-z}. \tag{I.6}$$

Then Eq. (I.4) becomes

$$e^{-2\nu ab\boldsymbol{x}\cdot\boldsymbol{y}} = e^z \sum_L \hat{L}^2 \tilde{i}_L(z) P_L(w). \tag{I.7}$$

Thus we have

$$\begin{aligned} f(r) &= e^{-\nu a^2 x^2} e^{-\nu b^2 y^2} e^z \sum_L \hat{L}^2 \tilde{i}_L(z) P_L(w) \\ &= e^{-\nu(ax-by)^2} \sum_L \hat{L}^2 \tilde{i}_L(z) P_L(w). \end{aligned} \tag{I.8}$$

I.2 Asymptotic form

The modified Bessel function i_L is defined by

$$i_L(z) \equiv (-)^L j_L(iz) \quad \text{for} \quad z \in \mathbb{R}, \tag{I.9}$$

where j_L is the spherical Bessel function, which has the asymptotic form,

$$j_L(z) \to \frac{1}{z} \sin\left(z - \frac{\pi L}{2}\right). \tag{I.10}$$

We extend this asymptotic form to the complex value:

$$j_L(z) \to \frac{1}{z2i}\left[e^{i\left(z-\frac{\pi L}{2}\right)} - e^{-i\left(z-\frac{\pi L}{2}\right)}\right]. \tag{I.11}$$

Thus we obtain

$$\begin{aligned} i_L(z) &\to (-)^L \frac{1}{iz2i}\left[e^{i\left(iz-\frac{\pi L}{2}\right)} - e^{-i\left(iz-\frac{\pi L}{2}\right)}\right] \\ &= \frac{1}{2z}\left[e^z - (-)^L e^{-z}\right]. \end{aligned} \tag{I.12}$$

For the reduced modified Bessel function, its asymptotic form is given by

$$\begin{aligned} \tilde{i}_L(z) &\to (-)^L \frac{1}{2z}\left[e^z - (-)^L e^{-z}\right] e^{-z} \\ &= \frac{1}{2z}\left[(-)^L - e^{-2z}\right]. \end{aligned} \tag{I.13}$$

One sees that in Eq. (I.13), L only acts as the parity factor $(-)^L$.

Note that by a numerical test it is found that the accuracy of the asymptotic form of Eq. (I.13) depends on L and it goes worse as L increases. For example when $L = 10$ and $z = 2000$, the ambiguity of Eq. (I.13) is about 3%. In Eq. (C.24) we calculate

$$\tilde{i}_L(z) = \tilde{i}_L(\gamma r_\alpha r_\beta) \tag{I.14}$$

by using the definition Eq. (I.6) up to $z \leq 1000$, and for z greater than 1000, Eq. (I.13) is adopted in our CCBA code named FRANTIC. It should be noted that typically γ has a value in the range of $0.1\ \text{fm}^2 < \gamma < 100\ \text{fm}^2$. We evaluate the accuracy of Eq. (I.13) on the cross section of the ^{28}Si(d,p)^{29}Si reaction at 18.75 MeV is at most less than 1% at 0° of the emitting angle of p. For this reaction, the integration in for the T matrix is performed over both r_α and r_β up to 15.0 fm. The maximum value 15 $\hbar$ of L is adopted. Therefore for the cross section, it does not matter the accuracy of the asymptotic form Eq. (I.13).

APPENDIX J

Gaussian Expansion Method

As discussed in Chaps. 2 and 3, a wave function is expanded with Gaussian basis functions. Here the details of the procedure for the expansion are given. We consider any function $f(r)$ defined for $r \geq 0$, and expand it with the real Gaussian basis of n the number of the bases;

$$f(r) = \sum_i^n c_i N_i r^l \exp\left[-\nu_i r^2\right]. \tag{J.1}$$

Here $\nu_i = 1/\rho_i^2$ and the range ρ_i of the Gaussian is given by the geometric series,

$$\rho_i = \rho_{\min} a^{i-1}, \tag{J.2}$$

$$a = \left(\frac{\rho_{\max}}{\rho_{\min}}\right)^{1/(n-1)}, \tag{J.3}$$

where $\rho_{\min}$ ($\rho_{\max}$) stands for the first (final) term of the series. If $f(r)$ is the radial function of a partial wave with an orbital angular momentum l, $f(r)$ behaves $f(r) \sim r^l$ around $r \sim 0$. The factor r^l is introduced so that the behavior of $f(r)$ around $r \sim 0$ is reproduced. Each ith basis function is normalized to unity as

$$\int \left(N_i r^l \exp\left[-\nu_i r^2\right]\right)^2 r^2 dr = 1. \tag{J.4}$$

The integration in the left-hand-side of Eq. (J.4) can be done by using the Gauss integration;

$$\begin{aligned}\int \left(N_i r^l \exp\left[-\nu_i r^2\right]\right)^2 r^2 dr &= N_i^2 \int r^{2(l+1)} \exp\left[-\nu_i r^2\right] r^2 dr \\ &= N_i^2 \frac{(2l+1)!!}{2^{l+2}} \sqrt{\frac{\pi}{(2\nu_i)^{2l+3}}}.\end{aligned} \tag{J.5}$$

Thus the normalization coefficient N_i is given by

$$N_i = \sqrt{\frac{2^{l+2}}{(2l+1)!!}} \left(\frac{(2\nu_i)^{2l+3}}{\pi}\right)^{1/4}. \tag{J.6}$$

The expansion coefficient c_i is obtained as follows. If we integrate Eq. (J.1) with multiplied by $N_j r^l \exp\left[-\nu_j r^2\right]$ over r, we have

$$\begin{aligned}\int f(r) N_j r^l \exp\left[-\nu r^2\right] r^2 dr &= \sum_i c_i N_i N_j \int r^{2(l+1)} \exp\left[-\left(\nu_i + \nu_j\right) r^2\right] \\ &= \sum_i c_i N_i N_j \frac{(2l+1)!!}{2^{l+2}} \sqrt{\frac{\pi}{\left(\nu_i + \nu_j\right)^{2l+3}}} \\ &= \sum_i c_i \left(\frac{2\sqrt{\nu_i \nu_j}}{\nu_i + \nu_j}\right)^{(2l+3)/2}. \end{aligned} \tag{J.7}$$

Thus c_i is obtained as a solution of the simultaneous equation

$$\left(\mathcal{A}_{ij}\right)\left(c_i\right) = \left(\mathcal{B}_i\right), \tag{J.8}$$

where $\mathcal{A}_{ij}$ and $\mathcal{B}_j$ are given by

$$\mathcal{A}_{ij} = \left(\frac{2\sqrt{\nu_i \nu_j}}{\nu_i + \nu_j}\right)^{(2l+3)/2} \tag{J.9}$$

$$\mathcal{B}_i = \int f(r) N_i r^l \exp\left[-\nu_i r^2\right] r^2 dr. \tag{J.10}$$

APPENDIX K

Angular Momentum Algebra

Contents

Angular momentum algebra is summarized here. Reference [179] is helpful for the algebra.

K.1 Spherical harmonics and related functions

K.1.1 Definition

The spherical harmonics $Y_{lm}(\theta, \phi)$, which are components of some irreducible tensor of rank l, are defined by the commutation relations

$$[L_\mu, Y_{lm}(\theta,\phi)] = \sqrt{l(l+1)}\,(lm1\mu|l, m+\mu)\,Y_{lm}(\theta,\phi), \tag{K.1}$$

where L_μ ($\mu = \pm 1, 0$) is a spherical component of the angular momentum operator $\boldsymbol{L}$ and it is defined by

$$L_1 = -\frac{1}{\sqrt{2}} e^{i\phi}\left\{\frac{\partial}{\partial\theta} + i\cot\theta\frac{\partial}{\partial\phi}\right\}, \tag{K.2}$$

$$L_0 = -i\frac{\partial}{\partial\phi}, \tag{K.3}$$

$$L_{-1} = -\frac{1}{\sqrt{2}} e^{i\phi}\left\{\frac{\partial}{\partial\theta} - i\cot\theta\frac{\partial}{\partial\phi}\right\}. \tag{K.4}$$

Three commutation relations for each μ generate

$$L_{\pm1}Y_{lm}(\theta,\phi) = \mp\sqrt{\frac{l(l+1) - m(m\pm1)}{2}}\,Y_{l,m\pm1}(\theta,\phi) \tag{K.5}$$

$$L_0 Y_{lm}(\theta,\phi) = mY_{lm}(\theta,\phi) \tag{K.6}$$

K.1.2 Deferential equations

The spherical harmonics $Y_{lm}(\theta,\phi)$ is the eigenfunction of the operators $\boldsymbol{L}$ and L_z as follows;

$$\boldsymbol{L}^2 Y_{lm}(\theta,\phi) = l(l+1)\hbar^2 Y_{lm}(\theta,\phi), \tag{K.7}$$
$$L_z Y_{lm}(\theta,\phi) = m\hbar Y_{lm}(\theta,\phi). \tag{K.8}$$

Thus, $Y_{lm}(\theta,\phi)$ satisfies

$$\left[\frac{1}{\sin\theta}\frac{\partial}{\partial\theta}\left(\sin\theta\frac{\partial}{\partial\theta}\right) + \frac{1}{\sin^2\theta}\frac{\partial^2}{\partial\phi^2} + l(l+1)\right] Y_{lm}(\theta,\phi) = 0, \tag{K.9}$$

$$\left[i\frac{\partial}{\partial\phi} + m\right] Y_{lm}(\theta,\phi) = 0. \tag{K.10}$$

K.1.3 Orthonormality

$$\int_0^{2\pi} d\phi \int_0^{\pi} d\theta \sin\theta Y^*_{lm}(\theta,\phi) Y_{l'm'}(\theta,\phi) = \delta_{ll'}\delta_{mm'}, \tag{K.11}$$
$$\sum_{lm} Y^*_{lm}(\theta',\phi') Y_{lm}(\theta,\phi) = \delta(\theta'-\theta)\delta(\phi'-\phi). \tag{K.12}$$

K.1.4 Phase

In this thesis, we chose the phase of $Y^*_{lm}(\theta,\phi)$ as [1]

$$Y^*_{lm}(\theta,\phi) = Y_{lm}(\theta,-\phi) = (-)^m Y_{l,-m}(\theta,\phi). \tag{K.15}$$

K.1.5 Symmetric properties

1. **Replacement $\theta \to \pi - \theta$ and $\phi = \pi + \phi$**

$$Y_{lm}(\pi-\theta,\phi) = (-)^{l-m} Y_{lm}(\theta,\phi), \tag{K.16}$$
$$Y_{lm}(\theta,\pi+\phi) = (-)^m Y_{lm}(\theta,\phi), \tag{K.17}$$
$$Y_{lm}(\pi-\theta,\pi+\phi) = (-)^l Y_{lm}(\theta,\phi). \tag{K.18}$$

[1] Note that another phase convention is sometimes adopted in other paper;

$$\tilde{Y}_{lm}(\theta,\phi) = i^l Y_{lm}(\theta,\phi), \tag{K.13}$$
$$\tilde{Y}^*_{lm}(\theta,\phi) = (-)^{l+m} Y_{l,-m}(\theta,\phi). \tag{K.14}$$

2. **Change of argument sign**

$$Y_{lm}(-\theta,\phi) = (-)^m Y_{lm}(\theta,\phi), \tag{K.19}$$
$$Y_{lm}(\theta,-\phi) = (-)^m Y_{l,-m}(\theta,\phi), \tag{K.20}$$
$$Y_{lm}(-\theta,-\phi) = Y_{l,-m}(\theta,\phi). \tag{K.21}$$

3. **The periodicity in θ and ϕ**

$$Y_{lm}(\theta \pm n\pi,\phi) = \begin{cases} (-)^l Y_{lm}(\theta,\phi) & \text{if } n \text{ is odd,} \\ Y_{lm}(\theta,\phi) & \text{if } n \text{ is even,} \end{cases} \tag{K.22}$$
$$Y_{lm}(\theta,\phi \pm n\pi) = \begin{cases} (-)^m Y_{lm}(\theta,\phi) & \text{if } n \text{ is odd,} \\ Y_{lm}(\theta,\phi) & \text{if } n \text{ is even.} \end{cases} \tag{K.23}$$

K.1.6 Useful relations

$$\int d\Omega Y_{l_1m_1}(\Omega)Y_{l_2m_2}(\Omega)Y^*_{l_3m_4}(\Omega) = \frac{1}{\sqrt{4\pi}}\frac{\hat{l}_1\hat{l}_2}{\hat{l}_3}\left(l_1m_1l_2m_2|l_3m_3\right)\left(l_10l_20|l_30\right). \tag{K.24}$$
$$\begin{aligned}\left[Y_{l_1}(\Omega)\otimes Y_{l_2}(\Omega)\right]_{LM} &\equiv \sum_{m_1m_2}\left(l_1m_1l_2m_2|LM\right)Y_{l_1m_1}(\Omega)Y_{l_2m_2}(\Omega) \\ &= \frac{1}{\sqrt{4\pi}}\frac{\hat{l}_1\hat{l}_2}{\hat{L}}\left(l_10l_20|L0\right)Y_{LM}(\Omega).\end{aligned} \tag{K.25}$$
$$\int d\Omega\left[Y_{l_1}(\Omega)\otimes Y_{l_2}(\Omega)\right]_{LM} = (-)^{l_1}\hat{l}_1\delta_{l_1l_2}\delta_{L0}\delta_{M0}. \tag{K.26}$$
$$Y_{lm}(\Omega)Y_{l'm'}(\Omega) = \frac{\hat{l}\hat{l}'}{\sqrt{4\pi}}\sum_k\left(l'0l0|k0\right)\left(l'm'lm|k,m'+m\right)\frac{1}{\hat{k}}Y_{k,m'+m}(\Omega). \tag{K.27}$$
$$Y_{ll}(\Omega) = (-)^l\sqrt{\frac{(2l+1)!}{2}}\frac{1}{2^ll!}\sin^l\theta\frac{1}{\sqrt{2\pi}}e^{il\phi}. \tag{K.28}$$
$$Y_{lm}(0,\phi) = \frac{\hat{l}}{\sqrt{4\pi}}\delta_{m0}. \tag{K.29}$$
$$r^lY_{lm}(\hat{\boldsymbol{r}}) = \sum_{\lambda=0}^{l}\frac{\sqrt{4\pi}}{\hat{\lambda}}\sqrt{{}_{2l+1}C_{2\lambda}}(ax)^{l-\lambda}(by)^\lambda\left[Y_{l-\lambda}(\hat{\boldsymbol{x}})\otimes Y_\lambda(\hat{\boldsymbol{y}})\right]_{lm}, \tag{K.30}$$
$$\boldsymbol{r} = a\boldsymbol{x} + b\boldsymbol{y}, \tag{K.31}$$
$${}_{2l+1}C_{2\lambda} = \frac{(2l+1)!}{(2l+1-2\lambda)!(2\lambda)!}. \tag{K.32}$$

where $\Omega \equiv \hat{\boldsymbol{r}} \equiv (\theta,\phi)$. Note that, in this thesis, the "hat" on the angular momentum stands for

$$\hat{L} = \sqrt{2L+1}. \tag{K.33}$$

K.1.7 Relations with other functions

1. **Legendre polynomial** $P_l(w)$ **(**$w \equiv \cos\theta$**)**

$$Y_{l0}(\Omega) = \frac{\hat{l}}{\sqrt{4\pi}} P_l(w). \tag{K.34}$$

$$\int_{-1}^{1} P_l(w) P_{l'}(w) dw = \frac{2}{\hat{l}^2} \delta_{ll'}. \tag{K.35}$$

$$\sum_l \frac{\hat{l}^2}{2} P_l(w) P_l(w') = \delta(w - w'), \qquad w' \equiv \cos\theta', \tag{K.36}$$

$$\begin{aligned} P_l(w_{12}) &= \frac{4\pi}{\hat{l}^2} \sum_m Y^*_{lm}(\hat{\boldsymbol{r}}_1) Y_{lm}(\hat{\boldsymbol{r}}_2) \\ &= \frac{4\pi}{\hat{l}^2} \sum_m Y_{lm}(\hat{\boldsymbol{r}}_1) Y^*_{lm}(\hat{\boldsymbol{r}}_2) \\ &= \frac{4\pi}{\hat{l}} (-)^l \left[Y_l(\hat{\boldsymbol{r}}_1) \otimes Y_l(\hat{\boldsymbol{r}}_2) \right]_{00}, \end{aligned} \tag{K.37}$$

where $w_{12} \equiv \cos\theta_{12}$ with the angle θ_{12} between two vectors $\boldsymbol{r}_1$ and $\boldsymbol{r}_2$.

2. **Legendre function** $P_{lm}(w)$

$$Y_{lm}(\Omega) = (-)^{(|m|+m)/2} \sqrt{\frac{\hat{l}^2}{4\pi} \frac{(l-|m|)!}{(l+|m|)!}} P_{lm}(w) e^{im\phi}. \tag{K.38}$$

$$P_{lm}(w) = (1-w^2)^{|m|/2} \frac{d^{|m|}}{dw^{|m|}} P_l(w). \tag{K.39}$$

$$P_{l,-m}(w) = P_{lm}(w). \tag{K.40}$$

$$P_{l0}(w) = P_l(w). \tag{K.41}$$

$$\int_{-1}^{1} P_{lm}(w) P_{l'm} dw = \frac{2}{\hat{l}^2} \frac{(l-|m|)!}{(l+|m|)!} \delta_{ll'}. \tag{K.42}$$

K.1.8 Explicit forms

1. **The spherical harmonics**

$$Y_{00}(\Omega) = \frac{1}{\sqrt{4\pi}}. \tag{K.43}$$

$$Y_{10}(\Omega) = \sqrt{\frac{3}{4\pi}}\cos\theta, \quad Y_{1\pm1}(\Omega) = \mp\sqrt{\frac{3}{8\pi}}\sin\theta e^{\pm i\phi}. \tag{K.44}$$

$$\begin{aligned} Y_{20}(\Omega) &= \sqrt{\frac{15}{16\pi}}\left(3\cos^3\theta - 1\right), \quad Y_{2\pm1}(\Omega) = \mp\sqrt{\frac{15}{8\pi}}\sin\theta\cos\theta e^{\pm i\phi}, \\ Y_{2\pm2}(\Omega) &= \sqrt{\frac{15}{32\pi}}\sin^2\theta e^{\pm 2i\phi}. \end{aligned} \tag{K.45}$$

$$\begin{aligned} Y_{30}(\Omega) &= \sqrt{\frac{7}{16\pi}}\cos\theta\left(5\cos^2\theta - 3\cos\theta\right), \\ Y_{3\pm1}(\Omega) &= \mp\sqrt{\frac{21}{64\pi}}\sin\theta\left(5\cos^2\theta - 1\right)e^{\pm i\phi}, \\ Y_{3\pm2}(\Omega) &= \sqrt{\frac{105}{32\pi}}\sin^2\theta\cos\theta e^{\pm 2i\phi}, \quad Y_{3\pm3}(\Omega) = \mp\sqrt{\frac{35}{64\pi}}\sin^3\theta e^{\pm 3i\phi}. \end{aligned} \tag{K.46}$$

2. **The Legendre polynomial**

$$P_0(w) = 1, \quad P_1(w) = w, \quad P_2(w) = \frac{3}{2}w^2 - \frac{1}{2}, \quad P_3(w) = \frac{5}{2}w^3 - \frac{3}{2}w. \tag{K.47}$$

$$P_l(1) = 1, \quad P_l(-w) = (-)^l P_l(w). \tag{K.48}$$

$$P_{2n-1}(0) = 0, \quad n = 1, 2, 3, \cdots, \tag{K.49}$$

$$P_{2n}(0) = (-)^n \frac{(2n-1)!!}{(2n)!!}, \quad n = 1, 2, 3, \cdots. \tag{K.50}$$

3. **The Legendre function**

$$P_{l0}(w) = P_l(w), \quad P_{l,-m}(w) = P_{lm}(w). \tag{K.51}$$

$$P_{11}(w) = (1 - w^2)^{1/2}. \tag{K.52}$$

$$P_{21}(w) = 3(1 - w^2)^{1/2}w, \quad P_{22}(w) = 3(1 - w^2). \tag{K.53}$$

$$\begin{aligned} P_{31}(w) &= \frac{3}{2}(1 - w^2)^{1/2}\left(5w^2 - 1\right), \quad P_{32}(w) = 15(1 - w^2)w, \\ P_{33}(w) &= 15(1 - w^2)^{3/2}. \end{aligned} \tag{K.54}$$

$$P_{lm}(\pm1) = 0 \quad (m > 0), \tag{K.55}$$

$$P_{lm}(0) = \begin{cases} 0 & (m > 0 \text{ and } l - m \text{ is odd}), \\ (-)^{(l-m)/2}\frac{(l+m-1)!!}{(l-M)!!} & (m > 0 \text{ and } l - m \text{ is even}). \end{cases} \tag{K.56}$$

K.2 Clebsch-Gordan coefficients

K.2.1 Definition

Let us consider a coupling of angular momenta. When the total angular momentum $\boldsymbol{j} = (j_x, j_y, j_z)$ is produced by the linear combination of the angular momenta $\boldsymbol{j}_1 = (j_{1x}, j_{1y}, j_{1z})$ and $\boldsymbol{j}_2 = (j_{2x}, j_{2y}, j_{2z})$, that is

$$\boldsymbol{j} = \boldsymbol{j}_1 + \boldsymbol{j}_2, \tag{K.57}$$

the eigenvalue j of $\boldsymbol{j}$ is in the range

$$|j_1 - j_2| \leq j \leq j_1 + j_2, \tag{K.58}$$

and its z-component m satisfies

$$m = m_1 + m_2, \tag{K.59}$$

where m_1 (m_2) is the eigenvalue of j_{1z} (j_{2z}). When the simultaneous eigenfunction of $\boldsymbol{j}_1$ and j_{1z} ($\boldsymbol{j}_2$ and j_{2z}) is expressed by $\psi_1(j_1 m_1)$ ($\psi_2(j_2 m_2)$) and they form the simultaneous eigenfunction $\psi(jm)$ of $\boldsymbol{j}$ and j_z, the probability amplitude $(j_1 m_1 j_2 m_2 | jm)$ is called the Clebsch-Gordan coefficient, that is

$$\psi(jm) = \sum_{m_1 m_2} (j_1 m_1 j_2 m_2 | jm)\, \psi_1(j_1 m_1) \psi_2(j_2 m_2). \tag{K.60}$$

K.2.2 Orthogonality

$$\sum_{m_1 m_2} (j_1 m_1 j_2 m_2 | jm) \left(j_1 m_1 j_2 m_2 | j' m'\right) = \delta_{jj'} \delta m m', \tag{K.61}$$

$$\sum_{j(m)} (j_1 m_1 j_2 m_2 | jm) \left(j_1 m_1' j_2 m_2' | jm\right) = \delta_{m_1 m_1'} \delta_{m_2 m_2'}. \tag{K.62}$$

From these orthogonalities, we obtain

$$\psi_1(j_1 m_1) \psi_2(j_2 m_2) = \sum_{j(m)} (j_1 m_1 j_2 m_2 | jm)\, \psi(jm). \tag{K.63}$$

K.2.3 Symmetric properties

$$\begin{aligned}
(j_1 m_1 j_2 m_2 | jm) &= (-)^{j_1 + j_2 - j} (j_2 m_2 j_1 m_1 | jm) \\
&= (-)^{j_1 + j_2 - j} (j_1, -m_1 j_2, -m_1 | j, -m) \\
&= (-)^{j_1 - m_1} \frac{\hat{j}}{\hat{j}_2} (j_1 m_1 j, -m | j_2, -m_2) \\
&= (-)^{j_2 - m_2} \frac{\hat{j}}{\hat{j}_1} (j, -m j_2 m_2 | j_1, -m_1)\,.
\end{aligned} \tag{K.64}$$

K.2.4 Special values

$$\sum_m (j_1 0 j m|j m) = \sum_m (j m j_1 0|j m) = \hat{j}^2 \delta_{j_1 0}. \tag{K.65}$$

$$(j_1 m_1 0 0|j m) = \delta_{j_1 j}\delta_{m_1 m}. \tag{K.66}$$

$$(j_1 m_1 j_2 m_2|0 0) = \delta_{j_1 j_2}\delta_{m_1 m_2}\frac{(-)^{j_1-m_1}}{\hat{j}_1}. \tag{K.67}$$

$$(j_1 0 j_2 0|j 0) = \begin{cases} (-)^{j+g}\hat{j}\frac{g!}{(g-j_1)!(g-j_2)!(g-j)!} \\ \times \left[\frac{(j_1+j_2-j)!(j_1+j-j_2)!(j_2+j-j_1)!}{(j_1+j_2+j+1)!}\right]^{1/2}, & (\text{if } j_1+j_2+j=2g), \\ 0, & (\text{if } j_1+j_2+j=2g+1), \end{cases} \tag{K.68}$$

where g is a positive integer.

K.2.5 Relation with 3-j symbol

$$\begin{pmatrix} j_1 & j_2 & j \\ m_1 & m_2 & m \end{pmatrix} = \frac{(-)^{j+m+2j_1}}{\hat{j}}\,(j_1, -m_1 j_2, -m_2|j m) \tag{K.69}$$

K.2.6 Explicit forms

$$\begin{aligned} &(j_1 m_1 j_2 m_2|j m) \\ &\quad = \delta_{m,m_1+m_2}\Delta(j_1 j_2 j) \\ &\quad \times [(j_1+m_1)!(j_1-m_1)!(j_2+m_2)!(j_2-m_2)!(j+m)!(j-m)!(2j+1)!]^{1/2} \\ &\quad \times \sum_z \frac{(-)^z}{z!(j_1+j_2-j-z)!(j_1-m_1-z)!(j_2-m_2-z)!(j-j_2+j_1+z)!(j-j_1-j_2+z)!}, \end{aligned} \tag{K.70}$$

$$\Delta(j_1 j_2 j) = \left[\frac{(j_! + j_2 - j)!(j_1 - j_2 + j)!(-j_1 + j_2 + j)}{(j_1+j_2+j+1)!}\right], \tag{K.71}$$

where the summation index z assumes integer values for which all the factorial arguments are non-negative.

$$\left(j_1 m_1 \frac{1}{2} m_2 | jm\right)$$

j \ m_2	$\frac{1}{2}$	$-\frac{1}{2}$
$j_1 + \frac{1}{2}$	$\sqrt{\frac{j_1+m+\frac{1}{2}}{2j_1+1}}$	$\sqrt{\frac{j_1-m+\frac{1}{2}}{2j_1+1}}$
$j_1 - \frac{1}{2}$	$-\sqrt{\frac{j_1-m+\frac{1}{2}}{2j_1+1}}$	$\sqrt{\frac{j_1+m+\frac{1}{2}}{2j_1+1}}$

$$(j_1 m_1 1 m_2 | jm)$$

j \ m_2	-1	0	1
$j_1 - 1$	$\sqrt{\frac{(j_1+m)(j_1+m+1)}{2j_1(2j_1+1)}}$	$-\sqrt{\frac{(j_1-m)(j_1+m)}{j_1(2j_1+1)}}$	$\sqrt{\frac{(j_1-m)(j_1-m+1)}{2j_1(2j_1+1)}}$
j_1	$\sqrt{\frac{(j_1-m)(j_1+m+1)}{2j_1(j_1+1)}}$	$\frac{m}{\sqrt{j_1(j_1+1)}}$	$-\sqrt{\frac{(j_1+m)(j_1-m+1)}{2j_1(j_1+1)}}$
$j_1 + 1$	$\sqrt{\frac{(j_1-m)(j_1-m+1)}{(2j_1+1)(2j_1+2)}}$	$\sqrt{\frac{(j_1-m+1)(j_1+m+1)}{(2j_1+1)(j_1+1)}}$	$\sqrt{\frac{(j_1+m)(j_1+m+1)}{(2j_1+1)(2j_1+2)}}$

K.2.7 Sums involving products of three Clebsch-Gordan coefficients

$$\sum_{\alpha\beta\delta} (a\alpha b\beta|c\gamma)\,(d\delta b\beta|e\varepsilon)\,(a\alpha f\varphi|d\delta) = p\hat{c}\hat{d}\,(c\gamma f\varphi|e\varepsilon) \begin{Bmatrix} a & b & c \\ e & f & d \end{Bmatrix}, \tag{K.72}$$

$$\sum_{\alpha\beta\delta} (b\beta c\gamma|a\alpha)\,(b\beta e\varepsilon|d\delta)\,(a\alpha f\varphi|d\delta) = p\frac{\hat{a}\hat{d}^2}{\hat{e}}\,(c\gamma f\varphi|e\varepsilon) \begin{Bmatrix} a & b & c \\ e & f & d \end{Bmatrix}, \tag{K.73}$$

$$\sum_{\alpha\beta\delta} (-)^{a-\alpha}\,(a\alpha b\beta|c\gamma)\,(d\delta b\beta|e\varepsilon)\,(d\delta a,-\alpha|f\varphi) = p\hat{c}\hat{f}\,(c\gamma f\varphi|e\varepsilon) \begin{Bmatrix} a & b & c \\ e & f & d \end{Bmatrix}, \tag{K.74}$$

$$\sum_{\alpha\beta\delta} (-)^{b-\beta}\,(a\alpha b\beta|c\gamma)\,(b,-\beta e\varepsilon|d\delta)\,(a\alpha f\varphi|d\delta) = p\frac{\hat{c}\hat{d}^2}{\hat{e}}\,(c\gamma f\varphi|e\varepsilon) \begin{Bmatrix} a & b & c \\ e & f & d \end{Bmatrix}, \tag{K.75}$$

$$\sum_{\alpha\beta\delta} (-)^{a-\alpha}\,(a\alpha c,-\gamma|b\beta)\,(d\delta b,-\beta|e\varepsilon)\,(a\alpha f\varphi|d\delta) = p\hat{b}\hat{d}\,(c\gamma f\varphi|e\varepsilon) \begin{Bmatrix} a & b & c \\ e & f & d \end{Bmatrix}, \tag{K.76}$$

where $p = (-)^{b+c+d+f}$, and the factor $\begin{Bmatrix} a & b & c \\ e & f & d \end{Bmatrix}$ is the Wigner 6-j symbol.

K.2.8 Sums involving products of four Clebsch-Gordan coefficients

$$\sum_{\beta\gamma\varepsilon\varphi} (b\beta c\gamma|a\alpha)\,(e\varepsilon f\varphi|d\delta)\,(e\varepsilon b\beta|g\eta)\,(f\varphi c\gamma|j\mu)$$

$$= (-)^{a-b+c+d+e-f}\hat{a}\hat{g}\sum_{s\sigma}\hat{s}^2\,(a\alpha s\sigma|j\mu)\,(g\eta s\sigma|d\delta)\begin{Bmatrix} b & c & a \\ j & s & f \end{Bmatrix}\begin{Bmatrix} b & e & g \\ d & s & f \end{Bmatrix}$$

$$= \hat{a}\hat{d}\hat{g}\hat{j}\sum_{k\kappa}(g\eta j\mu|k\kappa)\,(d\delta a\alpha|k\kappa)\begin{Bmatrix} c & b & a \\ f & e & d \\ j & g & k \end{Bmatrix}, \tag{K.77}$$

$$\sum_{\beta\gamma\varepsilon\varphi} (b\beta a\alpha|c\gamma)\,(f\varphi j\mu|c\gamma)\,(b\beta g\eta|e\varepsilon)\,(f\varphi d\delta|e\varepsilon)$$

$$= (-)^{a-b+f-j}\hat{c}^2\hat{e}^2\sum_{k\kappa}(g\eta j\mu|k\kappa)\,(d\delta a\alpha|k\kappa)\begin{Bmatrix} c & b & a \\ f & e & d \\ j & g & k \end{Bmatrix}, \tag{K.78}$$

$$\sum_{\beta\gamma\varepsilon\varphi} (a\alpha b\beta|c\gamma)\,(g\eta e\varepsilon|b\beta)\,(d\delta f\varphi|e\varepsilon)\,(j\mu c\gamma|f\varphi)$$

$$= (-)^{d+e-c-j}\hat{b}\hat{c}\hat{e}\hat{f}\sum_{k\kappa}(-)^{k-\kappa}\,(g\eta j\mu|k,-\kappa)\,(d\delta a\alpha|k\kappa)\begin{Bmatrix} c & b & a \\ f & e & d \\ j & g & k \end{Bmatrix}, \tag{K.79}$$

$$\sum_{\beta\gamma\varepsilon\varphi} (b\beta a,-\alpha|c\gamma)\,(e\varepsilon d,-\delta|f\varphi)\,(g\eta b,-\beta|e\varepsilon)\,(j\mu c,-\gamma|f\varphi)$$

$$= (-)^{b-c-g-\alpha-\eta}\hat{c}\hat{e}\hat{f}^2\sum_{k\kappa}(g\eta j,-\mu|k\kappa)\,(d\delta a\alpha|k\kappa)\begin{Bmatrix} c & b & a \\ f & e & d \\ j & g & k \end{Bmatrix}, \tag{K.80}$$

$$\sum_{\beta\gamma\varepsilon\varphi} (b\beta c,-\gamma|a\alpha)\,(e\varepsilon f\varphi|d\delta)\,(e,-\varepsilon g\eta|b\beta)\,(f\varphi j\mu|c\gamma)$$

$$= (-)^{b+f-g-\delta}\hat{a}\hat{b}\hat{c}\hat{d}\sum_{k\kappa}(g\eta j,-\mu|k\kappa)\,(d\delta a\alpha|k\kappa)\begin{Bmatrix} c & b & a \\ f & e & d \\ j & g & k \end{Bmatrix}, \tag{K.81}$$

$$\sum_{\beta\gamma\varepsilon\varphi} (b\beta c\gamma|a\alpha)\,(e\varepsilon f\varphi|d\delta)\,(e\varepsilon g\eta|b\beta)\,(f\varphi j\mu|c\gamma)$$

$$= \hat{b}\hat{c}\hat{d}\sum_{k\kappa}\hat{k}\,(g\eta j\mu|k\kappa)\,(d\delta k\kappa|a\alpha)\begin{Bmatrix} a & b & c \\ d & e & f \\ k & g & j \end{Bmatrix}, \tag{K.82}$$

$$\sum_{\beta\gamma\varepsilon\varphi} (b\beta c,-\gamma|a\alpha)\,(e\varepsilon f,-\varphi|d\delta)\,(g\eta b,-\beta|e\varepsilon)\,(j\mu f,-\varphi|c\gamma)$$

$$= (-)^{c+e-g+j+\alpha-\mu}\hat{a}\hat{d}\hat{e}\hat{c}\sum_{k\kappa}(g\eta j,-\mu|k\kappa)\,(d\delta a\alpha|k\kappa)\begin{Bmatrix} c & b & a \\ f & e & d \\ j & g & k \end{Bmatrix}, \tag{K.83}$$

$$\sum_{\beta\gamma\varepsilon\varphi} (b\beta c\gamma|a\alpha)\,(b\beta g\eta|e\varepsilon)\,(f\varphi d\delta|e\varepsilon)\,(f\varphi c\gamma|j\mu)$$

$$= (-)^{j-a+\delta-\eta}\hat{a}\hat{e}^2\hat{j}\sum_{k\kappa}(g\eta j,-\mu|k\kappa)\,(d\delta a,-\alpha|k\kappa)\begin{Bmatrix} c & b & a \\ f & e & d \\ j & g & k \end{Bmatrix}, \tag{K.84}$$

$$\sum_{\beta\gamma\varepsilon\varphi} (b\beta c\gamma|a\alpha)\,(g\eta e\varepsilon|b\beta)\,(f\varphi d\delta|e\varepsilon)\,(f\varphi c\gamma|j\mu)$$

$$= (-)^{j-a-g+\delta}\hat{a}\hat{b}\hat{e}\hat{j}\sum_{k\kappa}(g,-\eta j,-\mu|k\kappa)\,(d\delta a,-\alpha|k\kappa)\begin{Bmatrix} c & b & a \\ f & e & d \\ j & g & k \end{Bmatrix}, \tag{K.85}$$

$$\sum_{\beta\gamma\varepsilon\varphi} (-)^{c-\gamma+e-\varepsilon}\,(a\alpha b\beta|c\gamma)\,(d\delta f\varphi|e\varepsilon)\,(e\varepsilon b\beta|g\eta)\,(c\gamma f\varphi|j\mu)$$

$$= (-)^{a+d-\alpha-\delta}\hat{c}\hat{e}\hat{g}\hat{j}\sum_{k\kappa}(g\eta j,-\mu|k\kappa)\,(d\delta a,-\alpha|k\kappa)\begin{Bmatrix} c & b & a \\ f & e & d \\ j & g & k \end{Bmatrix}, \tag{K.86}$$

where the factor $\begin{Bmatrix} c & b & a \\ f & e & d \\ j & g & k \end{Bmatrix}$ is the Wigner 9-j symbol.

K.2.9 Sums involving products of the Clebsch-Gordan coefficients and one 6-j symbol

$$\sum_{e\varepsilon}(-)^{2e}\hat{c}\hat{d}\,(b\beta d\delta|e\varepsilon)\,(f\varphi c\gamma|e\varepsilon)\begin{Bmatrix} a & b & c \\ e & f & d \end{Bmatrix} = (a\alpha b\beta|c\gamma)\,(a\alpha f\varphi|d\delta)\,, \tag{K.87}$$

$$\sum_{f\varphi}(-)^{c+d+f}\hat{c}\hat{e}\,(e\varepsilon a\alpha|f\varphi)\,(d\delta c\gamma|f\varphi)\begin{Bmatrix} b & a & c \\ f & d & e \end{Bmatrix} = (a\alpha b\beta|c\gamma)\,(d\delta b\beta|e\varepsilon)\,, \tag{K.88}$$

$$\sum_{c\gamma}(-)^{2e-d+\alpha+\varphi}\hat{a}\hat{e}\,(f,-\varphi b\beta|c\gamma)\,(e\varepsilon a,-\alpha|c\gamma)\begin{Bmatrix} c & f & b \\ d & e & a \end{Bmatrix} = (b\beta d\delta|e\varepsilon)\,(f\varphi d\delta|a\alpha)\,, \tag{K.89}$$

$$\sum_{c\gamma}(-)^{c+d-\beta-\varphi}\hat{d}^2\,(a\alpha b\beta|c\gamma)\,(f,-\varphi e\varepsilon|c\gamma)\begin{Bmatrix} a & b & c \\ e & f & d \end{Bmatrix} = (a\alpha f\varphi|d\delta)\,(b,-\beta e\varepsilon|d\delta)\,, \tag{K.90}$$

$$\sum_{c\gamma}(-)^{2e}\hat{c}\hat{d}\,(a\alpha b\beta|c\gamma)\,(f\varphi c\gamma|e\varepsilon)\begin{Bmatrix} a & b & c \\ e & f & d \end{Bmatrix} = (b\beta d\delta|e\varepsilon)\,(a\alpha f\varphi|d\delta)\,, \tag{K.91}$$

$$\sum_{f\varphi}(-)^{2c}\hat{e}\hat{f}\,(b\beta d\delta|f\varphi)\,(a\alpha f\varphi|c\gamma)\begin{Bmatrix} a & b & e \\ d & c & f \end{Bmatrix} = (b\beta a\alpha|e\varepsilon)\,(d\delta e\varepsilon|c\gamma)\,. \tag{K.92}$$

K.2.10 Sums involving products of the Clebsch-Gordan coefficients and one 9-j symbol

$$\sum_{ak}\hat{a}\hat{d}\hat{g}\hat{j}\,(b\beta c\gamma|a\alpha)\,(g\eta j\mu|k\kappa)\,(d\delta a\alpha|k\kappa)\begin{Bmatrix}c & b & a\\ f & e & d\\ j & g & k\end{Bmatrix}$$
$$=(e\varepsilon f\varphi|d\delta)\,(e\varepsilon b\beta|g\eta)\,(f\varphi c\gamma|j\mu)\,, \tag{K.93}$$

$$\sum_{gj}\hat{a}\hat{d}\hat{g}\hat{j}\,(g\eta j\mu|k\kappa)\,(e\varepsilon b\beta|g\eta)\,(f\varphi c\gamma|j\mu)\begin{Bmatrix}c & b & a\\ f & e & d\\ j & g & k\end{Bmatrix}$$
$$=(d\delta a\alpha|k\kappa)\,(e\varepsilon f\varphi|d\delta)\,(b\beta c\gamma|a\alpha)\,, \tag{K.94}$$

$$\sum_{gj}(-)^{b+f-g-\delta}\hat{a}\hat{b}\hat{c}\hat{d}\,(b\beta c,-\gamma|a\alpha)\,(e\varepsilon f\varphi|d\delta)\,(d\delta a\alpha|k\kappa)\begin{Bmatrix}c & b & a\\ f & e & d\\ j & g & k\end{Bmatrix}$$
$$=(g\eta j,-\mu|k\kappa)\,(e,-\varepsilon g\eta|b\beta)\,(f\varphi j\mu|c\gamma)\,. \tag{K.95}$$

K.3 6-j symbols and the Racah coefficients

K.3.1 Definition

We consider the vector coupling of the three angular momenta, $\boldsymbol{j}_1$, $\boldsymbol{j}_2$, and $\boldsymbol{j}_3$, which reproduce the total angular momentum $\boldsymbol{j}$ and its projection m. The combination of the couplings for these vectors can be categorized as follows;

$$\text{(I)}\quad \boldsymbol{j}_1+\boldsymbol{j}_2=\boldsymbol{j}_{12},\quad \boldsymbol{j}_{12}+\boldsymbol{j}_3=\boldsymbol{j}, \tag{K.96}$$
$$\text{(II)}\quad \boldsymbol{j}_2+\boldsymbol{j}_3=\boldsymbol{j}_{23},\quad \boldsymbol{j}_1+\boldsymbol{j}_{23}=\boldsymbol{j}, \tag{K.97}$$
$$\text{(III)}\quad \boldsymbol{j}_1+\boldsymbol{j}_3=\boldsymbol{j}_{13},\quad \boldsymbol{j}_{13}+\boldsymbol{j}_2=\boldsymbol{j}. \tag{K.98}$$

For the scheme (I), the eigenstate of the operators $\boldsymbol{j}_1^2$, $\boldsymbol{j}_2^2$, $\boldsymbol{j}_3^2$, $\boldsymbol{j}_{12}^2$, $\boldsymbol{j}^2$, and $\boldsymbol{j}_z$ can be written as

$$\left|\left[[j_1\otimes j_2]_{j_{12}}\otimes j_3\right]_{jm}\right\rangle=\sum_{m_1m_2m_3}(j_1m_1j_2m_2|j_{12}m_{12})\,(j_{12}m_{12}j_3m_3|jm)$$
$$\times|j_1m_1\rangle\,|j_2m_2\rangle\,|j_3m_3\rangle\,, \tag{K.99}$$

where $|j_nm_n\rangle$ is the simultaneous eigenstate for the operators $\boldsymbol{j}_n^2$ and $\boldsymbol{j}_{nz}$. Similarly one can define the eigenstate for the schemes (II) and (III), respectively;

$$\left|\left[j_1\otimes[j_2\otimes j_3]_{j_{23}}\right]_{jm}\right\rangle=\sum_{m_1m_2m_3}(j_2m_2j_3m_3|j_{23}m_{23})\,(j_1m_1j_{23}m_{23}|jm)$$
$$\times|j_1m_1\rangle\,|j_2m_2\rangle\,|j_3m_3\rangle\,, \tag{K.100}$$

$$\left|\left[[j_1\otimes j_3]_{j_{13}}\otimes j_2\right]_{jm}\right\rangle=\sum_{m_1m_2m_3}(j_1m_1j_3m_3|j_{13}m_{13})\,(j_{13}m_{13}j_2m_2|jm)$$
$$\times|j_1m_1\rangle\,|j_2m_2\rangle\,|j_3m_3\rangle\,. \tag{K.101}$$

The Wigner 6-j symbols $\begin{Bmatrix} j_1 & j_2 & j_{12} \\ j_3 & j & j_{23} \end{Bmatrix}$ is the coefficient for the overlap of two eigenstates $\left| \left[[j_1 \otimes j_2]_{j_{12}} \otimes j_3 \right]_{jm} \right\rangle$ and $\left| \left[j_1 \otimes [j_2 \otimes j_3]_{j_{23}} \right]_{jm} \right\rangle$;

$$\begin{aligned} &\left\langle \left[[j_1 \otimes j_2]_{j_{12}} \otimes j_3 \right]_{jm} \middle| \left[j_1 \otimes [j_2 \otimes j_3]_{j_{23}} \right]_{j'm'} \right\rangle \\ &\quad = \delta_{jj'}\delta_{mm'}(-)^{j_1+j_2+j_3+j}\hat{j}_{12}\hat{j}_{23} \begin{Bmatrix} j_1 & j_2 & j_{12} \\ j_3 & j & j_{23} \end{Bmatrix}. \end{aligned} \tag{K.102}$$

One can also define the 6-j symbol from other overlaps as

$$\begin{aligned} &\left\langle \left[[j_1 \otimes j_2]_{j_{12}} \otimes j_3 \right]_{jm} \middle| \left[[j_1 \otimes j_3]_{j_{13}} \otimes j_2 \right]_{j'm'} \right\rangle \\ &\quad = \delta_{jj'}\delta_{mm'}(-)^{j_2+j_3+j_{12}+j_{13}}\hat{j}_{12}\hat{j}_{13} \begin{Bmatrix} j_2 & j_1 & j_{12} \\ j_3 & j & j_{13} \end{Bmatrix}, \end{aligned} \tag{K.103}$$

$$\begin{aligned} &\left\langle \left[j_1 \otimes [j_2 \otimes j_3]_{j_{23}} \right]_{jm} \middle| \left[[j_1 \otimes j_3]_{j_{13}} \otimes j_2 \right]_{j'm'} \right\rangle \\ &\quad = \delta_{jj'}\delta_{mm'}(-)^{j_1+j+j_{23}}\hat{j}_{13}\hat{j}_{23} \begin{Bmatrix} j_1 & j_3 & j_{13} \\ j_2 & j & j_{23} \end{Bmatrix}. \end{aligned} \tag{K.104}$$

The 6-j symbol can be written with the Clebsch-Gordan coefficients;

$$\begin{aligned} \sum_{m_1,m_2,m_3,m_{12},m_{23}} &(j_{12}m_{12}j_3m_3|jm)\,(j_1m_1j_2m_2|j_{12}m_{12}) \\ &\times \left(j_1m_1j_{23}m_{23}|j'm'\right)(j_2m_2j_3m_3|j_{23}m_{23}) \\ &= \delta_{jj'}\delta_{mm'}(-)^{j_1+j_2+j_3+j}\hat{j}_{12}\hat{j}_{23} \begin{Bmatrix} j_1 & j_2 & j_{12} \\ j_3 & j & j_{23} \end{Bmatrix}, \end{aligned} \tag{K.105}$$

where m and m' are fixed. In the 6-j symbol, the following triangular conditions are satisfied;

$$|j_1 - j_2| \le j_{12} \le j_1 + j_2, \tag{K.106}$$
$$|j_{12} - j_3| \le j \le j_{12} + j_3, \tag{K.107}$$
$$|j_2 - j_3| \le j_{23} \le j_2 + j_3, \tag{K.108}$$
$$|j_{23} - j_1| \le j \le j_{23} + j_1. \tag{K.109}$$

If, at least, one of these triangular conditions is not satisfied, the 6-j symbol vanishes.

K.3.2 Racah coefficient

The Racah coefficient $W(abed;cf)$ differs from the 6-j symbols only by a phase factor;

$$\begin{Bmatrix} a & b & c \\ d & e & f \end{Bmatrix} \equiv (-)^{a+b+d+e}W(abed;cf). \tag{K.110}$$

K.3.3 Orthonormality

$$\sum_{j_{12}} \hat{j}_{12}^2 \hat{j}_{23}^2 \begin{Bmatrix} j_1 & j_2 & j_{12} \\ j_3 & j & j_{23} \end{Bmatrix} \begin{Bmatrix} j_1 & j_2 & j_{12} \\ j_3 & j & j'_{23} \end{Bmatrix} = \delta_{j_{23} j'_{23}}, \tag{K.111}$$

$$\sum_{j_{23}} \hat{j}_{12}^2 \hat{j}_{23}^2 \begin{Bmatrix} j_1 & j_2 & j_{12} \\ j_3 & j & j_{23} \end{Bmatrix} \begin{Bmatrix} j_1 & j_2 & j'_{12} \\ j_3 & j & j_{23} \end{Bmatrix} = \delta_{j_{12} j'_{12}}. \tag{K.112}$$

K.3.4 Symmetric properties

1. **Classical symmetries**

$$\begin{aligned}
&\begin{Bmatrix} a & b & c \\ d & e & f \end{Bmatrix} = \begin{Bmatrix} a & c & b \\ d & f & e \end{Bmatrix} = \begin{Bmatrix} b & a & c \\ e & d & f \end{Bmatrix} \\
=&\begin{Bmatrix} b & c & a \\ e & f & d \end{Bmatrix} = \begin{Bmatrix} c & a & b \\ f & d & e \end{Bmatrix} = \begin{Bmatrix} c & b & a \\ f & e & d \end{Bmatrix} \\
=&\begin{Bmatrix} a & e & f \\ d & b & c \end{Bmatrix} = \begin{Bmatrix} a & f & e \\ d & c & b \end{Bmatrix} = \begin{Bmatrix} e & a & f \\ b & d & c \end{Bmatrix} \\
=&\begin{Bmatrix} e & f & a \\ b & c & d \end{Bmatrix} = \begin{Bmatrix} f & a & e \\ c & d & b \end{Bmatrix} = \begin{Bmatrix} f & e & a \\ c & b & d \end{Bmatrix} \\
=&\begin{Bmatrix} d & e & c \\ a & b & f \end{Bmatrix} = \begin{Bmatrix} d & c & e \\ a & f & b \end{Bmatrix} = \begin{Bmatrix} e & d & c \\ b & a & f \end{Bmatrix} \\
=&\begin{Bmatrix} e & c & d \\ b & f & a \end{Bmatrix} = \begin{Bmatrix} c & d & e \\ f & a & b \end{Bmatrix} = \begin{Bmatrix} c & e & d \\ f & b & a \end{Bmatrix} \\
=&\begin{Bmatrix} d & b & f \\ a & e & c \end{Bmatrix} = \begin{Bmatrix} d & f & b \\ a & c & e \end{Bmatrix} = \begin{Bmatrix} b & d & f \\ e & a & c \end{Bmatrix} \\
=&\begin{Bmatrix} b & f & d \\ e & c & a \end{Bmatrix} = \begin{Bmatrix} f & d & b \\ c & a & e \end{Bmatrix} = \begin{Bmatrix} f & b & d \\ c & e & a \end{Bmatrix}.
\end{aligned} \tag{K.113}$$

   These relations involve $3! \times 4 = 24$ different 6-j symbols.

2. **Regge symmetries**

$$\begin{aligned}
&\begin{Bmatrix} a & b & c \\ d & e & f \end{Bmatrix} = \begin{Bmatrix} a & s_1 - b & s_1 - c \\ d & s_1 - e & s_1 - f \end{Bmatrix} = \begin{Bmatrix} s_2 - a & b & s_2 - c \\ s_2 - d & e & s_2 - f \end{Bmatrix} \\
=&\begin{Bmatrix} s_3 - a & s_3 - b & c \\ s_3 - d & s_3 - e & f \end{Bmatrix} = \begin{Bmatrix} s_2 - d & s_3 - e & s_1 - f \\ s_2 - a & s_3 - b & s_1 - c \end{Bmatrix} \\
=&\begin{Bmatrix} s_3 - d & s_1 - e & s_2 - f \\ s_3 - a & s_1 - b & s_2 - c \end{Bmatrix},
\end{aligned} \tag{K.114}$$

   where

$$s_1 = \frac{b + c + e + f}{2}, \quad s_2 = \frac{a + c + d + f}{2}, \quad s_3 = \frac{a + b + d + e}{2}. \tag{K.115}$$

Combining the classical symmetries and the Regge symmetries, it reproduces totally 144 symmetry relations.

3. **"Mirror" symmetries**
The arguments of the 6-j symbols can be extended to negative integer or half-integer values. For

$$\bar{x} = -x - 1 \quad (x = a, b, c, d, e, \text{ or } f), \tag{K.116}$$

we have

$$\begin{aligned}
\begin{Bmatrix} a & b & c \\ d & e & f \end{Bmatrix} &= - \begin{Bmatrix} \bar{a} & \bar{b} & \bar{c} \\ \bar{d} & \bar{e} & \bar{f} \end{Bmatrix} \\
= (-)^{\varphi_1} \begin{Bmatrix} \bar{a} & b & c \\ d & e & f \end{Bmatrix} &= (-)^{\varphi_1+1} \begin{Bmatrix} a & \bar{b} & \bar{c} \\ \bar{d} & \bar{e} & \bar{f} \end{Bmatrix} \\
= (-)^{\varphi_2} \begin{Bmatrix} \bar{a} & b & c \\ \bar{d} & e & f \end{Bmatrix} &= (-)^{\varphi_2+1} \begin{Bmatrix} a & \bar{b} & \bar{c} \\ d & \bar{e} & \bar{f} \end{Bmatrix} \\
= i(-)^{\varphi_3} \begin{Bmatrix} \bar{a} & \bar{b} & c \\ d & e & f \end{Bmatrix} &= i(-)^{\varphi_3} \begin{Bmatrix} a & b & \bar{c} \\ \bar{d} & \bar{e} & \bar{f} \end{Bmatrix} \\
= i(-)^{\varphi_4} \begin{Bmatrix} \bar{a} & \bar{b} & \bar{c} \\ d & e & f \end{Bmatrix} &= i(-)^{\varphi_4} \begin{Bmatrix} a & b & c \\ \bar{d} & \bar{e} & \bar{f} \end{Bmatrix} \\
= (-)^{\varphi_5} \begin{Bmatrix} \bar{a} & \bar{b} & c \\ \bar{d} & e & f \end{Bmatrix} &= (-)^{\varphi_5+1} \begin{Bmatrix} a & b & \bar{c} \\ d & \bar{e} & \bar{f} \end{Bmatrix},
\end{aligned} \tag{K.117}$$

with

$$\begin{aligned}
&\varphi_1 = b - c - e + f, \quad \varphi_2 = 2(a + d), \\
&\varphi_3 = c + d + e + 2f, \quad \varphi_4 = a + b + c, \quad \varphi_5 = 2(c + f) + 1.
\end{aligned} \tag{K.118}$$

K.3.5 Special values

$$\begin{Bmatrix} 0 & b & c \\ d & e & f \end{Bmatrix} = \frac{(-)^{b+e+d}}{\hat{b}\hat{e}} \delta_{bc}\delta_{ef}, \tag{K.119}$$

$$\begin{Bmatrix} a & 0 & c \\ d & e & f \end{Bmatrix} = \frac{(-)^{a+d+e}}{\hat{a}\hat{d}} \delta_{ac}\delta_{df}, \tag{K.120}$$

$$\begin{Bmatrix} a & b & 0 \\ d & e & f \end{Bmatrix} = \frac{(-)^{a+e+f}}{\hat{a}\hat{d}} \delta_{ab}\delta_{de}, \tag{K.121}$$

$$\begin{Bmatrix} a & b & c \\ 0 & e & f \end{Bmatrix} = \frac{(-)^{a+d+e}}{\hat{b}\hat{c}} \delta_{bf}\delta_{ce}, \tag{K.122}$$

$$\begin{Bmatrix} a & b & c \\ d & 0 & f \end{Bmatrix} = \frac{(-)^{a+b+d}}{\hat{a}\hat{c}} \delta_{af}\delta_{cd}, \tag{K.123}$$

$$\begin{Bmatrix} a & b & c \\ d & e & 0 \end{Bmatrix} = \frac{(-)^{a+b+c}}{\hat{a}\hat{b}} \delta_{ae}\delta_{bd}. \tag{K.124}$$

K.3.6 Useful relations

$$\sum_X \hat{X}^2 \begin{Bmatrix} a & b & X \\ a & b & c \end{Bmatrix} = (-)^{2c}, \tag{K.125}$$

$$\sum_X (-)^{a+b+X} \hat{X}^2 \begin{Bmatrix} a & b & X \\ a & b & c \end{Bmatrix} = \hat{a}\hat{b}\delta_{c0}, \tag{K.126}$$

$$\sum_X (-)^{p+q+X} \hat{X}^2 \begin{Bmatrix} a & b & X \\ c & d & p \end{Bmatrix} \begin{Bmatrix} a & b & X \\ d & c & q \end{Bmatrix} = \begin{Bmatrix} a & c & q \\ b & d & p \end{Bmatrix}, \tag{K.127}$$

$$\sum_X (-)^{2X} \hat{X}^2 \begin{Bmatrix} a & b & X \\ c & d & p \end{Bmatrix} \begin{Bmatrix} c & d & X \\ e & f & q \end{Bmatrix} \begin{Bmatrix} e & f & X \\ a & b & r \end{Bmatrix} = \begin{Bmatrix} a & f & r \\ d & q & e \\ p & c & b \end{Bmatrix}, \tag{K.128}$$

$$\sum_X (-)^{R+X} \hat{X}^2 \begin{Bmatrix} a & b & X \\ c & d & p \end{Bmatrix} \begin{Bmatrix} c & d & X \\ e & f & q \end{Bmatrix} \begin{Bmatrix} e & f & X \\ a & b & r \end{Bmatrix} = \begin{Bmatrix} p & q & r \\ e & a & d \end{Bmatrix} \begin{Bmatrix} p & q & r \\ f & b & c \end{Bmatrix}, \tag{K.129}$$

where $R = a + b + c + d + e + f + p + q + r$.

K.4 9-j symbols

K.4.1 Definition

The Wigner 6-j symbol described above is the coefficient for which one transfers a coupling scheme of three angular momenta to another coupling scheme. The Wigner 9-j symbol is a same kind of it for not three but four angular momenta. The coupling schemes of four angular momenta $\boldsymbol{j}_1$, $\boldsymbol{j}_2$, $\boldsymbol{j}_3$, and $\boldsymbol{j}_4$ can be written down as

$$\text{(I)} \quad \boldsymbol{j}_1 + \boldsymbol{j}_2 = \boldsymbol{j}_{12}, \quad \boldsymbol{j}_3 + \boldsymbol{j}_4 = \boldsymbol{j}_{34}, \quad \boldsymbol{j}_{12} + \boldsymbol{j}_{34} = \boldsymbol{j}, \tag{K.130}$$

$$\text{(II)} \quad \boldsymbol{j}_1 + \boldsymbol{j}_3 = \boldsymbol{j}_{13}, \quad \boldsymbol{j}_2 + \boldsymbol{j}_4 = \boldsymbol{j}_{24}, \quad \boldsymbol{j}_{13} + \boldsymbol{j}_{24} = \boldsymbol{j}, \tag{K.131}$$

$$\text{(III)} \quad \boldsymbol{j}_1 + \boldsymbol{j}_4 = \boldsymbol{j}_{14}, \quad \boldsymbol{j}_2 + \boldsymbol{j}_3 = \boldsymbol{j}_{23}, \quad \boldsymbol{j}_{14} + \boldsymbol{j}_{23} = \boldsymbol{j}, \tag{K.132}$$

$$\text{(IV)} \quad \boldsymbol{j}_1 + \boldsymbol{j}_2 = \boldsymbol{j}_{12}, \quad \boldsymbol{j}_{12} + \boldsymbol{j}_3 = \boldsymbol{j}_{123}, \quad \boldsymbol{j}_{123} + \boldsymbol{j}_4 = \boldsymbol{j}, \tag{K.133}$$

where $\boldsymbol{j}$ is the total angular momentum. For the scheme (I), the eigenstate of the operators $\boldsymbol{j}_1^2$, $\boldsymbol{j}_2^2$, $\boldsymbol{j}_3^2$, $\boldsymbol{j}_4^2$, $\boldsymbol{j}_{12}^2$, $\boldsymbol{j}_{34}^2$, $\boldsymbol{j}^2$, and $\boldsymbol{j}_z$ can be written as

$$\begin{aligned} &\left| \left[[j_1 \otimes j_2]_{j_{12}} \otimes [j_3 \otimes j_4]_{j_{34}} \right]_{jm} \right\rangle \\ &\quad = \sum_{\substack{m_1 m_2 m_3 \\ m_4 m_{12} m_{34}}} (j_1 m_1 j_2 m_2 | j_{12} m_{12}) \, (j_3 m_3 j_4 m_4 | j_{34} m_{34}) \, (j_{12} m_{12} j_{34} m_{34} | jm) \\ &\quad \times |j_1 m_1\rangle \, |j_2 m_2\rangle \, |j_3 m_3\rangle \, |j_4 m_4\rangle \,, \end{aligned} \tag{K.134}$$

where $|j_n m_n\rangle$ is same as that in Eq. (K.99). Similarly, for the schemes (II), (III), and (IV), the eigenstates are respectively defined by

$$\begin{aligned}
&\left|\left[\left[j_1\otimes j_3\right]_{j_{13}}\otimes\left[j_2\otimes j_4\right]_{j_{24}}\right]_{jm}\right\rangle \\
&\quad=\sum_{\substack{m_1m_2m_3\\ m_4m_{12}m_{34}}}\left(j_1m_1j_3m_3|j_{13}m_{13}\right)\left(j_2m_2j_4m_4|j_{24}m_{24}\right)\left(j_{13}m_{13}j_{24}m_{24}|jm\right) \\
&\quad\times|j_1m_1\rangle\,|j_2m_2\rangle\,|j_3m_3\rangle\,|j_4m_4\rangle\,, \qquad \text{(K.135)}\\
&\left|\left[\left[j_1\otimes j_4\right]_{j_{14}}\otimes\left[j_2\otimes j_3\right]_{j_{23}}\right]_{jm}\right\rangle \\
&\quad=\sum_{\substack{m_1m_2m_3\\ m_4m_{14}m_{23}}}\left(j_1m_1j_4m_4|j_{14}m_{14}\right)\left(j_2m_2j_3m_3|j_{23}m_{23}\right)\left(j_{14}m_{14}j_{23}m_{23}|jm\right) \\
&\quad\times|j_1m_1\rangle\,|j_2m_2\rangle\,|j_3m_3\rangle\,|j_4m_4\rangle\,, \qquad \text{(K.136)}\\
&\left|\left[\left[\left[j_1\otimes j_2\right]_{j_{12}}\otimes j_3\right]_{j_{123}}\otimes j_4\right]_{jm}\right\rangle \\
&\quad=\sum_{\substack{m_1m_2m_3\\ m_4m_{12}m_{123}}}\left(j_1m_1j_2m_2|j_{12}m_{12}\right)\left(j_{12}m_{12}j_3m_3|j_{123}m_{123}\right)\left(j_{123}m_{123}j_4m_4|jm\right) \\
&\quad\times|j_1m_1\rangle\,|j_2m_2\rangle\,|j_3m_3\rangle\,|j_4m_4\rangle\,. \qquad \text{(K.137)}
\end{aligned}$$

The Wigner 9-j symbol or equivalently the Fano coefficient $\begin{Bmatrix} j_1 & j_2 & j_{12}\\ j_3 & j_4 & j_{34}\\ j_{13} & j_{24} & j\end{Bmatrix}$ is defined from the overlap of two eigenstates Eqs. (K.134) and (K.134);

$$\begin{aligned}
&\left\langle\left[\left[j_1\otimes j_2\right]_{j_{12}}\otimes\left[j_3\otimes j_4\right]_{j_{34}}\right]_{jm}\,\middle|\,\left[\left[j_1\otimes j_3\right]_{j_{13}}\otimes\left[j_2\otimes j_4\right]_{j_{24}}\right]_{j'm'}\right\rangle \\
&\qquad=\delta_{jj'}\delta_{mm'}\hat{j}_{12}\hat{j}_{13}\hat{j}_{24}\hat{j}_{34}\begin{Bmatrix} j_1 & j_2 & j_{12}\\ j_3 & j_4 & j_{34}\\ j_{13} & j_{24} & j\end{Bmatrix}. \qquad \text{(K.138)}
\end{aligned}$$

Using this definition one can obtain

$$\begin{aligned}
&\left\langle\left[\left[j_1\otimes j_2\right]_{j_{12}}\otimes\left[j_3\otimes j_4\right]_{j_{34}}\right]_{jm}\,\middle|\,\left[\left[j_1\otimes j_4\right]_{j_{14}}\otimes\left[j_2\otimes j_3\right]_{j_{23}}\right]_{j'm'}\right\rangle \\
&\qquad=\delta_{jj'}\delta_{mm'}(-)^{j_3+j_4-j_{34}}\hat{j}_{12}\hat{j}_{14}\hat{j}_{23}\hat{j}_{34}\begin{Bmatrix} j_1 & j_2 & j_{12}\\ j_4 & j_3 & j_{34}\\ j_{14} & j_{23} & j\end{Bmatrix}, \qquad \text{(K.139)}\\
&\left\langle\left[\left[j_1\otimes j_3\right]_{j_{13}}\otimes\left[j_2\otimes j_4\right]_{j_{24}}\right]_{jm}\,\middle|\,\left[\left[j_1\otimes j_4\right]_{j_{14}}\otimes\left[j_2\otimes j_3\right]_{j_{23}}\right]_{j'm'}\right\rangle \\
&\qquad=\delta_{jj'}\delta_{mm'}(-)^{j_3-j_4-j_{23}+j_{24}}\hat{j}_{13}\hat{j}_{14}\hat{j}_{24}\hat{j}_{23}\begin{Bmatrix} j_1 & j_3 & j_{13}\\ j_4 & j_2 & j_{24}\\ j_{14} & j_{23} & j\end{Bmatrix}. \qquad \text{(K.140)}
\end{aligned}$$

Note that the overlap with the coupling scheme Eq. (K.137) does not lead the 9-j symbol. It generate the product of two 6-j symbols.

From Eq. (K.138), we have

$$\begin{aligned}\sum_{m_i m_{ik}} &(j_1 m_1 j_2 m_2|j_{12} m_{12})\,(j_3 m_3 j_4 m_4|j_{34} m_{34})\,(j_{12} m_{12} j_{34} m_{34}|jm)\\ &\times (j_1 m_1 j_3 m_3|j_{13} m_{13})\,(j_2 m_2 j_4 m_4|j_{24} m_{24})\,\left(j_{13} m_{13} j_{24} m_{24}|j' m'\right)\\ &= \delta_{jj'}\delta_{mm'}\hat{j}_{12}\hat{j}_{13}\hat{j}_{24}\hat{j}_{34}\begin{Bmatrix} j_1 & j_2 & j_{12}\\ j_3 & j_4 & j_{34}\\ j_{13} & j_{24} & j\end{Bmatrix},\end{aligned} \tag{K.141}$$

where $m_i = m_1,\ m_2,\ m_3,$ and m_4 and $m_{ik} = m_{12},\ m_{13},\ m_{24},$ and m_{34}. The triangular conditions for the angular momenta in the Clebsch-Gordan coefficients in Eq. (K.141) must be satisfied for the finite value of the 9-j symbol.

K.4.2 Orthonormality

$$\sum_{gh}\hat{g}^2\hat{h}^2\begin{Bmatrix} a & b & c\\ d & e & f\\ g & h & j\end{Bmatrix}\begin{Bmatrix} a & b & c'\\ d & e & f'\\ g & h & j\end{Bmatrix} = \frac{\delta_{cc'}\delta_{ff'}}{\hat{c}^2\hat{f}^2}, \tag{K.142}$$

$$\sum_{cf}\hat{c}^2\hat{f}^2\begin{Bmatrix} a & b & c\\ d & e & f\\ g & h & j\end{Bmatrix}\begin{Bmatrix} a & b & c\\ d & e & f\\ g' & h' & j\end{Bmatrix} = \frac{\delta_{gg'}\delta_{hh'}}{\hat{g}^2\hat{h}^2}. \tag{K.143}$$

K.4.3 Symmetric properties

1. **Permutation symmetries**

(a) Column permutations

$$\begin{Bmatrix} j_{11} & j_{12} & j_{13}\\ j_{21} & j_{22} & j_{23}\\ j_{31} & j_{32} & j_{33}\end{Bmatrix} = \varepsilon\begin{Bmatrix} j_{1i} & j_{1k} & j_{1l}\\ j_{2i} & j_{2k} & j_{2l}\\ j_{3i} & j_{3k} & j_{3l}\end{Bmatrix}. \tag{K.144}$$

(b) Row permutations

$$\begin{Bmatrix} j_{11} & j_{12} & j_{13}\\ j_{21} & j_{22} & j_{23}\\ j_{31} & j_{32} & j_{33}\end{Bmatrix} = \varepsilon\begin{Bmatrix} j_{i1} & j_{i2} & j_{i3}\\ j_{k1} & j_{k2} & j_{k3}\\ j_{l1} & j_{l2} & j_{l3}\end{Bmatrix}. \tag{K.145}$$

(c) Transposition

$$\begin{Bmatrix} j_{11} & j_{12} & j_{13}\\ j_{21} & j_{22} & j_{23}\\ j_{31} & j_{32} & j_{33}\end{Bmatrix} = \begin{Bmatrix} j_{11} & j_{21} & j_{31}\\ j_{12} & j_{22} & j_{32}\\ j_{13} & j_{23} & j_{33}\end{Bmatrix}. \tag{K.146}$$

Here the phase factor ε is defined by

$$\varepsilon = \begin{cases} 1 & \text{for even permutations} \\ & \text{(cyclic permutations),} \\ (-)^R & \text{for odd permutations} \\ & \text{(non-cyclic permutations),} \end{cases} \tag{K.147}$$

$$R = \sum_{i,k=1}^{3} j_{ik}. \tag{K.148}$$

These symmetries generate different $3! \times 3! \times 2 = 72$ 9-j symbols. We list up some of them below when the even permutations are taken;

$$\begin{Bmatrix} j_{11} & j_{12} & j_{13} \\ j_{21} & j_{22} & j_{23} \\ j_{31} & j_{32} & j_{33} \end{Bmatrix} = \begin{Bmatrix} j_{21} & j_{31} & j_{11} \\ j_{22} & j_{32} & j_{12} \\ j_{23} & j_{33} & j_{13} \end{Bmatrix} = \begin{Bmatrix} j_{31} & j_{11} & j_{21} \\ j_{32} & j_{12} & j_{22} \\ j_{33} & j_{13} & j_{23} \end{Bmatrix}$$
$$= \begin{Bmatrix} j_{21} & j_{22} & j_{23} \\ j_{31} & j_{32} & j_{33} \\ j_{11} & j_{12} & j_{13} \end{Bmatrix} = \begin{Bmatrix} j_{31} & j_{32} & j_{33} \\ j_{11} & j_{12} & j_{13} \\ j_{21} & j_{22} & j_{23} \end{Bmatrix}. \tag{K.149}$$

2. **"Mirror" symmetries**
These symmetries correspond to them of the 6-j symbols. For

$$\bar{x} = -x - 1 \quad (x = a, b, c, d, e, f, g, h, \text{ or } j), \tag{K.150}$$

we obtain

$$
\begin{aligned}
&\begin{Bmatrix} a & b & c \\ d & e & f \\ g & h & j \end{Bmatrix} = \begin{Bmatrix} \bar{a} & \bar{b} & \bar{c} \\ \bar{d} & \bar{e} & \bar{f} \\ \bar{g} & \bar{h} & \bar{j} \end{Bmatrix} = \eta_1 \begin{Bmatrix} \bar{a} & b & c \\ d & e & f \\ g & h & j \end{Bmatrix} = \eta_1 \begin{Bmatrix} a & \bar{b} & \bar{c} \\ \bar{d} & \bar{e} & \bar{f} \\ \bar{g} & \bar{h} & \bar{j} \end{Bmatrix} \\
= \; & i\eta_2 \begin{Bmatrix} \bar{a} & \bar{b} & c \\ d & e & f \\ g & h & j \end{Bmatrix} = -i\eta_2 \begin{Bmatrix} a & b & \bar{c} \\ \bar{d} & \bar{e} & \bar{f} \\ \bar{g} & \bar{h} & \bar{j} \end{Bmatrix} = \eta_3 \begin{Bmatrix} \bar{a} & b & c \\ d & \bar{e} & f \\ g & h & j \end{Bmatrix} = \eta_3 \begin{Bmatrix} a & \bar{b} & \bar{c} \\ \bar{d} & e & \bar{f} \\ \bar{g} & \bar{h} & \bar{j} \end{Bmatrix} \\
= \; & i\eta_4 \begin{Bmatrix} \bar{a} & \bar{b} & \bar{c} \\ d & e & f \\ g & h & j \end{Bmatrix} = -i\eta_4 \begin{Bmatrix} a & b & c \\ \bar{d} & \bar{e} & \bar{f} \\ \bar{g} & \bar{h} & \bar{j} \end{Bmatrix} = \eta_5 \begin{Bmatrix} \bar{a} & \bar{b} & c \\ \bar{d} & e & f \\ g & h & j \end{Bmatrix} = \eta_5 \begin{Bmatrix} a & b & \bar{c} \\ d & \bar{e} & \bar{f} \\ \bar{g} & \bar{h} & \bar{j} \end{Bmatrix} \\
= \; & i\eta_6 \begin{Bmatrix} \bar{a} & \bar{b} & c \\ d & e & \bar{f} \\ g & h & j \end{Bmatrix} = -i\eta_6 \begin{Bmatrix} a & b & \bar{c} \\ \bar{d} & \bar{e} & f \\ \bar{g} & \bar{h} & \bar{j} \end{Bmatrix} = \eta_7 \begin{Bmatrix} \bar{a} & b & c \\ d & \bar{e} & f \\ g & h & \bar{j} \end{Bmatrix} = \eta_7 \begin{Bmatrix} a & \bar{b} & \bar{c} \\ \bar{d} & e & \bar{f} \\ \bar{g} & \bar{h} & j \end{Bmatrix} \\
= \; & \eta_5 \begin{Bmatrix} \bar{a} & \bar{b} & c \\ \bar{d} & \bar{e} & f \\ g & h & j \end{Bmatrix} = \eta_5 \begin{Bmatrix} a & b & \bar{c} \\ d & e & \bar{f} \\ \bar{g} & \bar{h} & \bar{j} \end{Bmatrix} = \eta_8 \begin{Bmatrix} \bar{a} & \bar{b} & \bar{c} \\ \bar{d} & e & f \\ g & h & j \end{Bmatrix} = \eta_8 \begin{Bmatrix} a & b & c \\ d & \bar{e} & \bar{f} \\ \bar{g} & \bar{h} & \bar{j} \end{Bmatrix} \\
= \; & -i\eta_6 \begin{Bmatrix} \bar{a} & \bar{b} & c \\ \bar{d} & e & \bar{f} \\ g & h & j \end{Bmatrix} = -i\eta_6 \begin{Bmatrix} a & b & \bar{c} \\ d & \bar{e} & f \\ \bar{g} & \bar{h} & \bar{j} \end{Bmatrix} = -\begin{Bmatrix} \bar{a} & \bar{b} & c \\ \bar{d} & e & f \\ g & h & \bar{j} \end{Bmatrix} = \begin{Bmatrix} a & b & \bar{c} \\ d & \bar{e} & \bar{f} \\ \bar{g} & \bar{h} & j \end{Bmatrix} \\
= \; & -\begin{Bmatrix} \bar{a} & \bar{b} & c \\ d & e & \bar{f} \\ g & h & \bar{j} \end{Bmatrix} = -\begin{Bmatrix} a & b & \bar{c} \\ \bar{d} & \bar{e} & f \\ \bar{g} & \bar{h} & j \end{Bmatrix}, \qquad \text{(K.151)}
\end{aligned}
$$

where

$$\eta_1 = (-)^{b-c-d+g}, \qquad \text{(K.152)}$$
$$\eta_2 = (-)^{c+d-e-g+h}, \qquad \text{(K.153)}$$
$$\eta_3 = (-)^{c+f-g-h}, \qquad \text{(K.154)}$$
$$\eta_4 = (-)^{R}, \qquad \text{(K.155)}$$
$$\eta_5 = (-)^{c-f-g+h+1}, \qquad \text{(K.156)}$$
$$\eta_6 = (-)^{g-h-j}, \qquad \text{(K.157)}$$
$$\eta_7 = (-)^{2(a+e+j)}, \qquad \text{(K.158)}$$
$$\eta_8 = (-)^{R-d+e-f+1}, \qquad \text{(K.159)}$$

where R is the summation over all components of each 9-j symbol. When we use

the z-components δ, ε, and φ of angular momenta $\boldsymbol{d}$, $\boldsymbol{e}$, and $\boldsymbol{f}$, respectively, we have

$$\begin{Bmatrix} d-\delta & e+\varepsilon & f+\varphi \\ d & e & f \\ g & h & j \end{Bmatrix} = i(-)^{g+\varepsilon-\varphi} \begin{Bmatrix} \bar{d}+\delta & e+\varepsilon & f+\varphi \\ \bar{d} & e & f \\ g & h & j \end{Bmatrix}, \tag{K.160}$$

$$\begin{Bmatrix} d+\delta & e-\varepsilon & f+\varphi \\ d & e & f \\ g & h & j \end{Bmatrix} = i(-)^{h+\varphi-\delta} \begin{Bmatrix} d+\delta & \bar{e}+\varepsilon & f+\varphi \\ d & \bar{e} & f \\ g & h & j \end{Bmatrix}, \tag{K.161}$$

$$\begin{Bmatrix} d+\delta & e+\varepsilon & f-\varphi \\ d & e & f \\ g & h & j \end{Bmatrix} = i(-)^{j+\delta-\varepsilon} \begin{Bmatrix} d+\delta & e+\varepsilon & \bar{f}+\varphi \\ d & e & \bar{f} \\ g & h & j \end{Bmatrix}, \tag{K.162}$$

$$\begin{Bmatrix} d-\delta & e-\varepsilon & f+\varphi \\ d & e & f \\ g & h & j \end{Bmatrix} = (-)^{h+\varphi-g+1} \begin{Bmatrix} \bar{d}+\delta & \bar{e}+\varepsilon & f+\varphi \\ \bar{d} & \bar{e} & f \\ g & h & j \end{Bmatrix}, \tag{K.163}$$

$$\begin{Bmatrix} d-\delta & e+\varepsilon & f-\varphi \\ d & e & f \\ g & h & j \end{Bmatrix} = (-)^{g+\varepsilon-j+1} \begin{Bmatrix} \bar{d}+\delta & e+\varepsilon & \bar{f}+\varphi \\ \bar{d} & e & \bar{f} \\ g & h & j \end{Bmatrix}, \tag{K.164}$$

$$\begin{Bmatrix} d+\delta & e-\varepsilon & f-\varphi \\ d & e & f \\ g & h & j \end{Bmatrix} = (-)^{j+\delta-h+1} \begin{Bmatrix} d+\delta & \bar{e}+\varepsilon & \bar{f}+\varphi \\ d & \bar{e} & \bar{f} \\ g & h & j \end{Bmatrix}, \tag{K.165}$$

$$\begin{Bmatrix} d-\delta & e-\varepsilon & f-\varphi \\ d & e & f \\ g & h & j \end{Bmatrix} = i(-)^{g+h+j+\delta+\varepsilon+\varphi+1} \begin{Bmatrix} \bar{d}+\delta & \bar{e}+\varepsilon & \bar{f}+\varphi \\ \bar{d} & \bar{e} & \bar{f} \\ g & h & j \end{Bmatrix}. \tag{K.166}$$

K.4.4 Special values

$$\begin{Bmatrix} a & b & c \\ a & b & c \\ g & h & j \end{Bmatrix} = 0 \quad \text{if } g+h+j = 2k+1, \tag{K.167}$$

$$\begin{Bmatrix} a & a & c \\ d & d & f \\ g & g & j \end{Bmatrix} = 0 \quad \text{if } c+f+j = 2k+1, \tag{K.168}$$

where k is positive integer.

$$\begin{Bmatrix} a & b & c \\ d & e & f \\ g & h & 0 \end{Bmatrix} = \delta_{cf}\delta_{gh}\frac{(-)^{b+c+d+g}}{\hat{c}\hat{g}} \begin{Bmatrix} a & b & c \\ e & d & g \end{Bmatrix}$$
$$= \delta_{cf}\delta_{gh}\frac{1}{\hat{c}\hat{g}}W(bcgd;ae), \tag{K.169}$$

$$\begin{Bmatrix} a & b & c \\ d & 0 & f \\ g & h & 0 \end{Bmatrix} = \delta_{df}\delta_{bh}\delta_{cf}\delta_{gh}\frac{(-)^{a-b-c}}{\hat{b}\hat{c}}, \tag{K.170}$$

$$\begin{Bmatrix} a & b & c \\ d & e & f \\ 0 & 0 & 0 \end{Bmatrix} = \delta_{ad}\delta_{be}\delta_{cf}\frac{1}{\hat{a}\hat{b}\hat{c}}, \tag{K.171}$$

$$\begin{Bmatrix} 0 & b & c \\ d & 0 & f \\ g & h & 0 \end{Bmatrix} = \delta_{bc}\delta_{bd}\delta_{bf}\delta_{bg}\delta_{bh}\frac{(-)^{2b}}{\hat{b}^2}. \tag{K.172}$$

K.4.5 Useful relations

$$\begin{Bmatrix} a & b & c \\ d & b & f \\ g & h & j \end{Bmatrix} = \frac{1}{\hat{c}\hat{f}\hat{g}\hat{h}\hat{j}^2}\sum_{\substack{\alpha\beta\gamma \\ \delta\varepsilon\varphi \\ \eta\mu\nu}} (a\alpha b\beta|c\gamma)\,(d\delta e\varepsilon|f\varphi)\,(c\varphi f\varphi|j\nu)$$
$$\times\,(a\alpha d\delta|g\eta)\,(b\beta e\varepsilon|h\mu)\,(g\eta h\mu|j\nu)$$
$$= \frac{(-)^{2(c+g)}}{\hat{a}^2\hat{e}^2\hat{j}^2}\sum_{\substack{\alpha\beta\gamma \\ \delta\varepsilon\varphi \\ \eta\mu\nu}} (c\gamma b\beta|a\alpha)\,(g\eta d\delta|a\alpha)\,(b\beta h\mu|e\varepsilon)$$
$$\times\,(d\delta f\varphi|e\varepsilon)\,(f\varphi c\varphi|j\nu)\,(h\mu g\eta|j\nu)\,, \tag{K.173}$$

$$\begin{Bmatrix} a & b & c \\ d & e & f \\ g & h & j \end{Bmatrix} = \sum_{j'}(-)^{2j'}\hat{j}'^2 \begin{Bmatrix} a & d & g \\ h & j & j' \end{Bmatrix} \begin{Bmatrix} b & e & h \\ c & j' & f \end{Bmatrix} \begin{Bmatrix} c & f & j \\ j' & a & b \end{Bmatrix}$$
$$= \sum_{j'}(-)^{2j'}\hat{j}'^2 \begin{Bmatrix} c & f & j \\ g & h & j' \end{Bmatrix} \begin{Bmatrix} a & d & g \\ f & j' & e \end{Bmatrix} \begin{Bmatrix} b & e & h \\ j' & c & a \end{Bmatrix}$$
$$= \sum_{j'}(-)^{2j'}\hat{j}'^2 \begin{Bmatrix} b & e & h \\ j & g & j' \end{Bmatrix} \begin{Bmatrix} c & f & j \\ e & j' & c \end{Bmatrix} \begin{Bmatrix} a & c & g \\ j' & b & c \end{Bmatrix}, \tag{K.174}$$

$$\sum_{cf}(-)^{d+e+f}(-)^{d+b+q}\hat{c}^2\hat{f}^2 \begin{Bmatrix} a & b & c \\ d & e & f \\ g & h & j \end{Bmatrix} \begin{Bmatrix} a & e & p \\ b & d & q \\ c & f & j \end{Bmatrix} = (-)^{b+d+h} \begin{Bmatrix} a & e & p \\ d & b & q \\ g & h & j \end{Bmatrix}, \tag{K.175}$$

$$(c\gamma f\varphi|j\nu)\begin{Bmatrix} a & b & c \\ d & e & f \\ g & h & j \end{Bmatrix} = \frac{1}{\hat{c}\hat{f}\hat{g}\hat{h}} \sum_{\substack{\alpha\beta\delta\varepsilon \\ \eta\mu\nu}} (a\alpha b\beta|c\gamma)\,(d\delta e\varepsilon|f\varphi) \times (a\alpha d\delta|g\eta)\,(b\beta e\varepsilon|h\mu)\,(g\eta h\mu|j\nu)\,, \tag{K.176}$$

$$\sum_j \hat{j}^2 \begin{Bmatrix} c & f & j \\ g & h & j' \end{Bmatrix} \begin{Bmatrix} a & b & c \\ d & e & f \\ g & h & j \end{Bmatrix} = (-)^{2j'} \begin{Bmatrix} a & d & g \\ f & j' & e \end{Bmatrix} \begin{Bmatrix} b & e & h \\ j' & c & a \end{Bmatrix}. \tag{K.177}$$

K.5 Wigner-Eckart theorem

K.5.1 Derivation

When we consider the eigenstate

$$|jm\rangle = \psi_{jm}(\xi), \tag{K.178}$$

of the square of the angular momentum $\boldsymbol{j}$ and its projection $\boldsymbol{j}_z$, the wave function ψ_{jm} can be regarded as an irreducible tensor operator which has the rank j, where $j(j+1)\hbar^2$ and $m\hbar$ are the eigenvalues of $\boldsymbol{j}^2$ and $\boldsymbol{j}_z$, respectively. The internal coordinate ξ involves coordinates both for real space and spin space. The matrix element $\langle j'm' \,|\, T_{\lambda\mu} \,|\, jm\rangle$ for an irreducible tensor operator $T_{\lambda\mu}$ with the rank λ is given by

$$\begin{aligned} &\langle j'm' \,|\, T_{\lambda\mu} \,|\, jm\rangle \\ &\quad = \int d\xi \psi^*_{j'm'}(\xi) T_{\lambda\mu}(\xi) \psi_{jm}(\xi) \\ &\quad = \int d\xi (-)^{j'-m'} \left[(-)^{j'+(-m')} \psi^*_{j',-(-m')}(\xi)\right] \sum_{JM} (\lambda\mu jm|JM)\,[T_\lambda \otimes \psi_j]_{JM} \\ &\quad = \int d\xi (-)^{j'-m'} \sum_{JJ'MM'} \left(j', -m'JM|J'M'\right) (\lambda\mu jm|JM)\left[\varphi_{j'} \otimes [T_\lambda \otimes \psi_j]_J\right]_{J'M'}, \end{aligned} \tag{K.179}$$

where the wave function $\varphi_{j'm'}$ is defend by

$$\varphi_{j'm'}(\xi) = (-)^{j'+m'} \psi^*_{j',-m'}(\xi). \tag{K.180}$$

From a symmetry of the integration, the spatial integration in Eq. (K.179) is non-zero only when $J' = M' = 0$. Thus the matrix element becomes

$$\begin{aligned} &\langle j'm' \,|\, T_{\lambda\mu} \,|\, jm\rangle \\ &\quad = \int d\xi (-)^{j'-m'} \sum_{JM} \left(j', -m'JM|00\right) (\lambda\mu jm|JM)\left[\varphi_{j'} \otimes [T_\lambda \otimes \psi_j]_J\right]_{00} \\ &\quad = (-)^{2j'} \left(\lambda\mu jm|j'm'\right) \int d\xi (-)^{j'-m'} \left[\varphi_{j'} \otimes [T_\lambda \otimes \psi_j]_{j'}\right]_{00}. \end{aligned} \tag{K.181}$$

Equation (K.181) can be written as

$$\begin{aligned}\left\langle j'm' \left| T_{\lambda\mu} \right| jm \right\rangle &= (-)^{j'-m'} \begin{pmatrix} j' & \lambda & j \\ -m' & \mu & m \end{pmatrix} \left\langle j' \left\| T_\lambda \right\| j \right\rangle, \\ &= \frac{1}{\hat{j}'} \left(jm\lambda\mu | j'm' \right) \left\langle j' \left\| T_\lambda \right\| j \right\rangle, \end{aligned} \tag{K.182}$$

$$\left\langle j' \left\| T_\lambda \right\| j \right\rangle = (-)^{j+j'-\lambda} \int d\xi (-)^{j'-m'} \left[\varphi_{j'} \otimes \left[T_\lambda \otimes \psi_j \right]_{j'} \right]_{00}. \tag{K.183}$$

Equation (K.182) is called the Wigner-Eckart theorem. The explicit form of the reduced matrix element $\langle j' \| T_\lambda \| j \rangle$ for the specific T_λ is shown in the next section. The Wigner-Eckart theorem means that the matrix element can be divided into two parts: The term $\left(jm\lambda\mu | j'm' \right) / \hat{j}'$ is a geometrical factor, which does not depend on a physical meanings of the operator T, while the reduced matrix element involves all of the physical contents of T.

K.5.2 Reduced matrix element

$$\left\langle j' \left\| 1 \right\| j \right\rangle = \hat{j} \delta_{jj'}, \tag{K.184}$$

$$\left\langle j' \left\| \boldsymbol{j} \right\| j \right\rangle = \sqrt{j(j+1)(2j+1)} \delta_{jj'}, \tag{K.185}$$

$$\left\langle Y_{l'} \left\| Y_\lambda \right\| Y_l \right\rangle = \frac{(-)^\lambda}{\sqrt{4\pi}} \hat{l}' \hat{\lambda} \left(l'0\lambda 0 | l0 \right), \tag{K.186}$$

$$\begin{aligned}\left\langle Y_{l'}(\hat{\boldsymbol{r}}) \left\| \nabla_{\boldsymbol{r}} \right\| Y_l(\hat{\boldsymbol{r}}) \right\rangle &= \hat{l} \left(l010 | l'0 \right) \\ &\times \left[\left(\frac{\partial}{\partial r} - \frac{l}{r} \right) \delta_{l',l+1} \left(\frac{\partial}{\partial r} + \frac{l+1}{r} \right) \delta_{l',l-1} \right], \end{aligned} \tag{K.187}$$

$$\left\langle \left[\eta_{1/2} \otimes Y_{l'} \right]_{j'} \left\| Y_\lambda \right\| \left[\eta_{1/2} \otimes Y_l \right]_j \right\rangle = \frac{(-)^{j+j'+1}}{2\sqrt{4\pi}} \hat{j}' \hat{\lambda} \left(j' \frac{1}{2} \lambda 0 | j \frac{1}{2} \right) \left[1 + (-)^{l+l'+\lambda} \right], \tag{K.188}$$

$$\left\langle j' \left\| \left[T_{\lambda_1} \otimes U_{\lambda_2} \right]_\lambda \right\| j \right\rangle = (-)^{j+j'+\lambda} \hat{\lambda} \sum_J \begin{Bmatrix} \lambda_1 & \lambda_2 & \lambda \\ j & j' & J \end{Bmatrix} \left\langle j' \left\| T_{\lambda_1} \right\| J \right\rangle \left\langle J \left\| U_{\lambda_2} \right\| j \right\rangle, \tag{K.189}$$

$$\left\langle j'_1 j'_2 j' \left\| \left[T_{\lambda_1} \otimes U_{\lambda_2} \right]_\lambda \right\| j_1 j_2 j \right\rangle = \hat{j} \hat{j}' \hat{\lambda} \begin{Bmatrix} j'_1 & j'_2 & j' \\ j_1 & j_2 & j \\ \lambda_1 & \lambda_2 & \lambda \end{Bmatrix} \left\langle j'_1 \left\| T_{\lambda_1} \right\| j_1 \right\rangle \left\langle j'_2 \left\| U_{\lambda_2} \right\| j_2 \right\rangle, \tag{K.190}$$

$$\begin{aligned}\left\langle j'_1 j'_2 j' \left\| \left(\boldsymbol{T}_{\lambda_1} \cdot \boldsymbol{U}_{\lambda_2} \right) \right\| j_1 j_2 j \right\rangle &= (-)^{\lambda_1} \hat{\lambda}_1 \left\langle j'_1 j'_2 j' \left\| \left[T_{\lambda_1} \otimes U_{\lambda_2} \right]_0 \right\| j_1 j_2 j \right\rangle \\ &= \delta_{jj'} \delta_{\lambda_1 \lambda_2} (-)^{j_1 + j'_2 + j} \hat{j} \begin{Bmatrix} j'_1 & j'_2 & j \\ j_2 & j_1 & \lambda_1 \end{Bmatrix} \\ &\times \left\langle j'_1 \left\| T_{\lambda_1} \right\| j_1 \right\rangle \left\langle j'_2 \left\| U_{\lambda_2} \right\| j_2 \right\rangle, \end{aligned} \tag{K.191}$$

where the eigenstate $|j_1 j_2 j\rangle$ is defined by $|j_1 j_2 j\rangle = \left| \left[\psi_{j_1} \otimes \psi_{j_2} \right]_j \right\rangle$.

Bibliography

[1] R. Serber, Phys. Rev. **72**, 1114 (1947). (Cited on page 1.)

[2] G. R. Satchler, *Direct Nuclear Reactions* (Oxford University Press, 1983). (Cited on pages 1, 32 and 104.)

[3] M. Kamimura *et al.*, Prog. Theor. Phys. Suppl. **89**, 1 (1986). (Cited on pages 2, 11, 80 and 111.)

[4] N. Matsuoka *et al.*, Nucl. Phys. **A455**, 413 (1986). (Cited on page 2.)

[5] N. Austern *et al.*, Phys. Rep. **154**, 125 (1987). (Cited on pages 2, 11, 80, 88 and 111.)

[6] M. Yahiro, K. Ogata, T. Matsumoto, and K. Minomo, Prog. Theor. Exp. Phys. **2012**, 01A206 (2012). (Cited on pages 2, 11, 70, 80 and 111.)

[7] N. Keeley, K. Kemper, and K. Rusek, Phys. Rev. C **88**, 017602 (2013). (Cited on pages 2, 3 and 4.)

[8] I. J. Thompson and F. M. Nunes, *Nuclear Reactions for Astrophysics* (Cambridge University Press, New York, 2009). (Cited on page 3.)

[9] M. Cubero *et al.*, Phys. Rev. Lett. **109**, 262701 (2012). (Cited on page 4.)

[10] N. Keeley *et al.*, Nucl. Phys. **A571**, 326 (1994). (Cited on page 4.)

[11] A. Sánchez-Benítez *et al.*, Nucl. Phys. **A803**, 30 (2008). (Cited on page 4.)

[12] G. Baur, C. Bertulani, and H. Rebel, Nucl. Phys. **A458**, 188 (1986). (Cited on pages 4 and 61.)

[13] K. Ogata, S. Hashimoto, Y. Iseri, M. Kamimura, and M. Yahiro, Phys. Rev. C **73**, 024605 (2006). (Cited on pages 4, 5 and 62.)

[14] K. Ogata, M. Yahiro, Y. Iseri, T. Matsumoto, and M. Kamimura, Phys. Rev. C **68**, 064609 (2003). (Cited on pages 5 and 62.)

[15] D. Baye, P. Capel, and G. Goldstein, Phys. Rev. Lett. **95**, 082502 (2005). (Cited on pages 5, 61, 62 and 63.)

[16] G. Goldstein, D. Baye, and P. Capel, Phys. Rev. C **73**, 024602 (2006). (Cited on pages 5, 61, 62, 63 and 69.)

[17] P. Capel, H. Esbensen, and F. Nunes, Phys. Rev. C **85**, 044604 (2012). (Cited on pages 6, 61, 65, 67, 68 and 72.)

[18] S. K. Penny and G. R. Satchler, Nucl. Phys. **53**, 145 (1964). (Cited on page 6.)

[19] P. J. Iano and N. Austern, Phys. Rev. **151**, 853 (1966). (Cited on page 6.)

[20] T. Tamura, Phys. Rev. **165**, 1123 (1968). (Cited on page 6.)

[21] R. Coker and T. Tamura, Phys. Rev. **182**, 1277 (1969). (Cited on page 6.)

[22] S. A. A. Zaidi, W. R. Coker, and D. G. Martin, Phys. Rev. C **2**, 1384 (1970). (Cited on page 6.)

[23] T. Tamura, D. R. Bes, R. A. Broglia, and S. Landowne, Phys. Rev. Lett. **25**, 1507 (1970). (Cited on page 6.)

[24] W. R. Coker, C. L. Hollas, P. J. Riley, and S. Sen, Phys. Rev. C **4**, 836 (1971). (Cited on page 6.)

[25] T. Udagawa, Nucl. Phys. **A164**, 484 (1971). (Cited on page 6.)

[26] T. Udagawa, T. Tamura, and T. Izumoto, Phys. Lett. **B35**, 129 (1971). (Cited on page 6.)

[27] D. Braunschweig, T. Tamura, and T. Udagawa, Phys. Lett. **B35**, 273 (1971). (Cited on page 6.)

[28] N. K. Glendenning and R. S. Mackintosh, Nucl. Phys. **A168**, 575 (1971). (Cited on page 6.)

[29] R. S. Mackintosh, Nucl. Phys. **A170**, 353 (1971). (Cited on page 6.)

[30] R. Broglia *et al.*, Phys. Lett. **B36**, 541 (1971). (Cited on page 6.)

[31] T. Tamura and T. Udagawa, Phys. Rev. C **5**, 1127 (1972). (Cited on page 6.)

[32] K. Yagi, K. Sato, Y. Aoki, T. Udagawa, and T. Tamura, Phys. Rev. Lett. **29**, 1334 (1972). (Cited on page 6.)

[33] P. K. Bindal and R. D. Koshel, Phys. Rev. C **6**, 2281 (1972). (Cited on page 6.)

[34] R. O. Nelson and N. R. Roberson, Phys. Rev. C **6**, 2153 (1972). (Cited on page 6.)

[35] G. Hoffmann, W. Coker, S. Zaidi, and D. E. Jr., Phys. Lett. **B41**, 47 (1972). (Cited on page 6.)

[36] D. K. Olsen, T. Udagawa, T. Tamura, and R. E. Brown, Phys. Rev. C **8**, 609 (1973). (Cited on page 6.)

[37] A. W. Obst and K. W. Kemper, Phys. Rev. C **8**, 1682 (1973). (Cited on page 6.)

[38] S. Landowne, R. Broglia, and R. Liotta, Phys. Lett. **B43**, 160 (1973). (Cited on page 6.)

[39] R. Nelson and N. Roberson, Phys. Lett. **B43**, 389 (1973). (Cited on page 6.)

[40] U. Scheib, A. Hofmann, G. Philipp, and F. Vogler, Nucl. Phys. **A203**, 177 (1973). (Cited on page 6.)

[41] R. Singh, N. D. Takacsy, S. Hayakawa, R. Hutson, and J. Kraushaar, Nucl. Phys. **A205**, 97 (1973). (Cited on page 6.)

[42] K. Yagi *et al.*, Phys. Lett. **B44**, 447 (1973). (Cited on page 6.)

[43] R. Ascuitto and N. Glendenning, Phys. Lett. **B45**, 85 (1973). (Cited on page 6.)

[44] W. Coker, J. Lin, J. Duggan, and P. Miller, Phys. Lett. **B45**, 321 (1973). (Cited on page 6.)

[45] F. Gareev, R. Jamalejev, H. Schulz, and J. Bang, Nucl. Phys. **A215**, 570 (1973). (Cited on page 6.)

[46] T. Udagawa, Phys. Rev. C **9**, 270 (1974). (Cited on page 6.)

[47] A. W. Obst and K. W. Kemper, Phys. Rev. C **9**, 1643 (1974). (Cited on page 6.)

[48] K. A. Erb *et al.*, Phys. Rev. Lett. **33**, 1102 (1974). (Cited on page 6.)

[49] W. R. Coker, T. Udagawa, and G. W. Hoffmann, Phys. Rev. C **10**, 1792 (1974). (Cited on page 6.)

[50] M. B. Lewis *et al.*, Phys. Rev. C **10**, 2441 (1974). (Cited on page 6.)

[51] O. Aspelund, D. Ingham, A. Djaloeis, H. Kelleter, and C. Mayer-Böricke, Phys. Lett. **B50**, 441 (1974). (Cited on page 6.)

[52] T. Tamura, K. Low, and T. Udagawa, Phys. Lett. **B51**, 116 (1974). (Cited on page 6.)

[53] T. Tamura, Phys. Rep. **14**, 59 (1974). (Cited on page 6.)

[54] P. Kunz and E. Rost, Phys. Lett. **B53**, 9 (1974). (Cited on page 6.)

[55] T. Udagawa and T. Tamura, Nucl. Phys. **A233**, 297 (1974). (Cited on page 6.)

[56] K. Yagi *et al.*, Phys. Rev. Lett. **34**, 96 (1975). (Cited on page 6.)

[57] D. K. Scott *et al.*, Phys. Rev. Lett. **34**, 895 (1975). (Cited on page 6.)

[58] D. K. Olsen, T. Udagawa, and R. E. Brown, Phys. Rev. C **11**, 1557 (1975). (Cited on page 6.)

[59] N. K. Glendenning, Rev. Mod. Phys. **47**, 659 (1975). (Cited on page 6.)

[60] W. S. Chien, C. H. King, J. A. Nolen, and M. A. M. Shahabuddin, Phys. Rev. C **12**, 332 (1975). (Cited on page 6.)

[61] T. Udagawa and T. Tamura, Phys. Lett. **B57**, 135 (1975). (Cited on page 6.)

[62] P. Nagel and R. D. Koshel, Phys. Rev. C **13**, 907 (1976). (Cited on page 6.)

[63] M. E. Cobern *et al.*, Phys. Rev. C **13**, 1200 (1976). (Cited on page 6.)

[64] L. Ray and W. R. Coker, Phys. Rev. C **13**, 1367 (1976). (Cited on page 6.)

[65] K. S. Low, T. Tamura, and T. Udagawa, Phys. Rev. C **13**, 2579 (1976). (Cited on page 6.)

[66] L. Ray, J. Lynch, and G. Westfall, Phys. Rev. C **13**, 2366 (1976). (Cited on page 6.)

[67] D. J. Pisano, Phys. Rev. C **14**, 468 (1976). (Cited on page 6.)

[68] D. J. Pisano and P. D. Parker, Phys. Rev. C **14**, 475 (1976). (Cited on page 6.)

[69] M. E. Cobern, D. J. Pisano, and P. D. Parker, Phys. Rev. C **14**, 491 (1976). (Cited on page 6.)

[70] R. N. Boyd *et al.*, Phys. Rev. C **14**, 946 (1976). (Cited on page 6.)

[71] D. Sinclair, B. T. Chait, S. Kahana, and B. S. Nilsson, Phys. Rev. C **14**, 1033 (1976). (Cited on page 6.)

[72] P. Nagel and R. D. Koshel, Phys. Rev. C **14**, 1667 (1976). (Cited on page 6.)

[73] M. C. Mermaz, J. C. Peng, N. Lisbona, and A. Greiner, Phys. Rev. C **15**, 307 (1977). (Cited on page 6.)

[74] B.-t. Kim, Phys. Rev. C **15**, 818 (1977). (Cited on page 6.)

[75] J. Källne and A. W. Obst, Phys. Rev. C **15**, 477 (1977). (Cited on page 6.)

[76] K. Yagi, Y. Aoki, M. Matoba, and M. Hyakutake, Phys. Rev. C **15**, 1178 (1977). (Cited on page 6.)

[77] J. C. Peng, M. C. Mermaz, A. Greiner, N. Lisbona, and K. S. Low, Phys. Rev. C **15**, 1331 (1977). (Cited on page 6.)

[78] S. Kubono *et al.*, Phys. Rev. Lett. **38**, 817 (1977). (Cited on page 6.)

[79] J. J. Kolata and M. Oothoudt, Phys. Rev. C **15**, 1947 (1977). (Cited on page 6.)

[80] M.-C. Lemaire and K. S. Low, Phys. Rev. C **16**, 183 (1977). (Cited on page 6.)

[81] D. L. Hanson *et al.*, Phys. Rev. C **16**, 902 (1977). (Cited on page 6.)

[82] K. Yagi *et al.*, Phys. Rev. Lett. **40**, 161 (1978). (Cited on page 6.)

[83] A. J. Baltz and S. Kahana, Phys. Rev. C **17**, 555 (1978). (Cited on page 6.)

[84] C. F. Maguire *et al.*, Phys. Rev. Lett. **40**, 358 (1978). (Cited on page 6.)

[85] H. T. Fortune, M. E. Cobern, and G. E. Moore, Phys. Rev. C **17**, 888 (1978). (Cited on page 6.)

[86] J. C. Peng, H. S. Song, F. C. Wang, and J. V. Maher, Phys. Rev. Lett. **41**, 225 (1978). (Cited on page 6.)

[87] S. Kubono, S. J. Tripp, D. Dehnhard, T. Udagawa, and T. Tamura, Phys. Rev. C **18**, 1929 (1978). (Cited on page 6.)

[88] J. C. Peng, B. T. Kim, M. C. Mermaz, A. Greiner, and N. Lisbona, Phys. Rev. C **18**, 2179 (1978). (Cited on page 6.)

[89] P. Nagel, Phys. Rev. C **18**, 2617 (1978). (Cited on page 6.)

[90] G. B. Sherwood *et al.*, Phys. Rev. C **18**, 2574 (1978). (Cited on page 6.)

[91] K. Yagi *et al.*, Phys. Rev. C **19**, 285 (1979). (Cited on page 6.)

[92] P. J. Ellis, M. Strayer, and M. F. Werby, Phys. Rev. C **19**, 536 (1979). (Cited on page 6.)

[93] M. Bernas *et al.*, Phys. Rev. C **19**, 2246 (1979). (Cited on page 6.)

[94] C. F. Maguire, Phys. Rev. C **20**, 1037 (1979). (Cited on page 6.)

[95] M. C. Mermaz *et al.*, Phys. Rev. C **20**, 2130 (1979). (Cited on page 6.)

[96] D. W. Miller, W. P. Jones, D. W. Devins, R. E. Marrs, and J. Kehayias, Phys. Rev. C **20**, 2008 (1979). (Cited on page 6.)

[97] P. D. Kunz, unpublished. (Cited on page 6.)

[98] T. Tamura and K. Low, Comput. Phys. Comm. **8**, 349 (1974). (Cited on page 6.)

[99] T. Udagawa and T. Tamura, unpublished. (Cited on page 6.)

[100] P. Nagel and R. D. Koshel, unpublished. (Cited on page 6.)

[101] K. Low, T. Tamura, and T. Udagawa, Phys. Lett. **B67**, 5 (1977). (Cited on pages 6 and 7.)

[102] P. D. Bond *et al.*, Phys. Rev. Lett. **36**, 300 (1976). (Cited on pages 6 and 7.)

[103] I. J. Thompson, Comput. Phys. Rep. **7**, 167 (1988). (Cited on page 7.)

[104] I. J. Thompson, Fresco: Coupled reaction channels calculations (2011), [http://www.fresco.org.uk/]. (Cited on page 7.)

[105] Y. Iseri and K. Ogata, private communication. (Cited on page 7.)

[106] T. Fukui, K. Ogata, and M. Yahiro, Prog. Theor. Phys. **125**, 1193 (2011). (Cited on pages 7, 8, 51, 56 and 107.)

[107] A. M. Moro, F. M. Nunes, and R. C. Johnson, Phys. Rev. C **80**, 064606 (2009). (Cited on page 8.)

[108] D. Beaumel *et al.*, Phys. Lett. **B514**, 226 (2001). (Cited on pages 9, 46, 56 and 57.)

[109] N. Austern, M. Yahiro, and M. Kawai, Phys. Rev. Lett. **63**, 2649 (1989). (Cited on pages 11, 39, 85 and 88.)

[110] M. C. Birse and E. F. Redish, Nuclear Physics A **406**, 149 (1983). (Cited on pages 11 and 87.)

[111] T. Matsumoto *et al.*, Phys. Rev. C **68**, 064607 (2003). (Cited on pages 16 and 47.)

[112] W. H. Press, B. P. Flannery, S. A. Teukolosky, and W. T. Vetterling, *NUMERICAL RECIPES in C* (Cambridge University Press, New York, 1988). (Cited on page 19.)

[113] K. Ogata, M. Yahiro, Y. Iseri, T. Matsumoto, and M. Kamimura, Phys. Rev. C **68**, 064609 (2003). (Cited on pages 22, 24, 27, 64, 70, 71 and 72.)

[114] K. Ogata, S. Hashimoto, Y. Iseri, M. Kamimura, and M. Yahiro, Phys. Rev. C **73**, 024605 (2006). (Cited on pages 22, 24, 27, 64, 70, 71 and 72.)

[115] A. M. Messiah, *Quantum mechanics I and II* (North-Holland, Amsterdam, 1962). (Cited on page 32.)

[116] N. F. Mott and H. J. W. Massey, *The theory of atomic collisions, 3rd ed.* (Clarendon Press, Oxford, 1965). (Cited on page 32.)

[117] N. Austern, M. Kawai, and M. Yahiro, Phys. Rev. C **53**, 314 (1996). (Cited on pages 39 and 88.)

[118] G. R. Satchler, Nucl. Phys. **55**, 1 (1964). (Cited on page 39.)

[119] M. Wiescher, J. Görres, S. Graff, L. Buchman, and F.-K. Thieleman, Astrophys. J. **343**, 352 (1989). (Cited on page 46.)

[120] L. Trache, F. Carstoiu, A. M. Mukhamedzhanov, and R. E. Tribble, Phys. Rev. C **66**, 035801 (2002). (Cited on pages 46 and 57.)

[121] T. Motobayashi, Nucl. Phys. **A718**, 101c (2003). (Cited on pages 46 and 57.)

[122] T. Ohmura, B. Imanishi, M. Ichimura, and M. Kawai, Prog. Theor. Phys. **43**, 347 (1970). (Cited on pages 47 and 137.)

[123] B. A. Watson, P. P. Singh, and R. E. Segel, Phys. Rev. **182**, 997 (1969). (Cited on pages 48 and 140.)

[124] N. K. Timofeyuk and R. C. Johnson, Phys. Rev. Lett. **110**, 112501 (2013). (Cited on pages 48 and 135.)

[125] N. K. Timofeyuk and R. C. Johnson, Phys. Rev. C **87**, 064610 (2013). (Cited on pages 48 and 135.)

[126] R. C. Johnson and N. K. Timofeyuk, Phys. Rev. C **89**, 024605 (2014). (Cited on pages 48 and 135.)

[127] G. Perey and B. Buck, Nucl. Phys. **32**, 353 (1962). (Cited on pages 48 and 140.)

[128] R. C. Johnson and P. J. R. Soper, Phys. Rev. C **1**, 976 (1970). (Cited on pages 50, 51 and 132.)

[129] J. P. Farrell Jr., C. M. Vincent, and N. Austern, Ann. of Phys. **96**, 333 (1973). (Cited on pages 50, 51 and 132.)

[130] N. Austern, C. Vincent, and J. P. Farrell Jr., Annals Phys. **114**, 93 (1978). (Cited on pages 50, 51 and 132.)

[131] H. Amakawa, S. Yamaji, A. Mori, and K. Yazaki, Phys. Lett. **B82**, 13 (1979). (Cited on pages 50, 51 and 132.)

[132] M. A. Nagarajan, I. J. Thompson, and R. C. Johnson, Nucl. Phys. **A385**, 525 (1982). (Cited on pages 50, 51 and 132.)

[133] Y. Sakuragi, M. Yahiro, and M. Kamimura, Prog. Theor. Phys. Supple. **89**, 136 (1986). (Cited on pages 52 and 75.)

[134] A. M. Mukhamedzhanov and N. K. Timofeyuk, Yad. Fiz. **51**, 679 (1990), [Sov. J. Nucl. Phys. **51**, 431 (1990)]. (Cited on page 56.)

[135] T. Fukui, K. Ogata, K. Minomo, and M. Yahiro, Phys. Rev. C **86**, 022801(R) (2012). (Cited on pages 56 and 57.)

[136] T. Fukui, K. Ogata, and M. Yahiro, Phys. Rev. C **91**, 014604 (2015). (Cited on page 56.)

[137] W. S. Pong and N. Austern, Ann. Phys. (N.Y.) **93**, 369 (1975). (Cited on page 57.)

[138] R. C. Johnson, N. Austern, and M. H. Lopes, Phys. Rev. C **26**, 348 (1982). (Cited on page 57.)

[139] R. Peterson, C. Fields, R. Raymond, J. Thieke, and J. Ullman, Nucl. Phys. **A408**, 221 (1983). (Cited on pages 58, 59, 108 and 109.)

[140] F. Becchetti and G. Greenlees, Phys. Rev. **182**, 1190 (1969). (Cited on pages 58 and 109.)

[141] R. J. Glauber, *High Energy Collision Theory, Lectures in Theoretical Physics* (Interscience, New York). (Cited on page 61.)

[142] C. A. Bertulani and P. Danielewicz, *Introduction to Nuclear Reactions* (Institute of Physics, Bristol, England, 2004). (Cited on pages 63, 67 and 68.)

[143] T. Fukui, K. Ogata, and P. Capel, Phys. Rev. C **90**, 034617 (2014). (Cited on page 65.)

[144] P. Capel, D. Baye, and V. S. Melezhik, Phys. Rev. C **68**, 014612 (2003). (Cited on page 66.)

[145] R. A. Broglia and A. Winther, *Heavy Ion Reactions, Lectures Notes, Vol. 1: Elastic and Inelastic Reactions* (Benjamin/Cummings, Reading, England, 1981). (Cited on pages 67 and 68.)

[146] C. A. Bertulani, C. M. Campbell, and T. Glasmacher, Comp. Phys. Comm. **152**, 317 (2003). (Cited on page 67.)

[147] K. Ogata and C. A. Bertulani, Prog. Theor. Phys. **121**, 1399 (2009). (Cited on page 70.)

[148] K. Ogata and C. A. Bertulani, Prog. Theor. Phys. **123**, 701 (2010). (Cited on page 70.)

[149] C. H. Dasso and A. Vitturi, Phys. Rev. C **79**, 064620 (2009). (Cited on page 70.)

[150] H. Horiuchi, K. Ikeda, and K. Katō, Prog. Theor. Phys. Suppl. **192**, 1 (2012). (Cited on page 73.)

[151] J. A. Wheeler, Phys. Rev. **52**, 1083 (1937). (Cited on page 74.)

[152] J. A. Wheeler, Phys. Rev. **52**, 1107 (1937). (Cited on page 74.)

[153] K. Wildermuth and T. Kanellopoulos, Nucl. Phys. **7**, 150 (1958). (Cited on page 74.)

[154] K. Wildermuth and T. Kanellopoulos, Nucl. Phys. **9**, 449 (1958/1959). (Cited on page 74.)

[155] K. Ikeda and R. Tamagaki, Prog. Theor. Phys. Suppl. **62**, 1 (1977). (Cited on page 74.)

[156] Y. Kanada-En'yo, T. Suhara, and Y. Taniguchi, Prog. Theor. Exp. Phys. **2014**, 073D02 (2014). (Cited on page 74.)

[157] A. B. Volkov, Nucl. Phys. **74**, 33 (1965). (Cited on page 75.)

[158] N. Anantaraman *et al.*, Nuclear Physics A **313**, 445 (1979). (Cited on pages 75, 77 and 79.)

[159] L. Chua, F. Becchetti, J. Jënecke, and F. Milder, Nucl. Phys. **A273**, 243 (1976). (Cited on page 75.)

[160] T. Tanabe *et al.*, Phys. Rev. C **24**, 2556 (1981). (Cited on pages 75, 77 and 79.)

[161] E. Newman, L. Becker, B. Preedom, and J. Hiebert, Nucl. Phys. **A100**, 225 (1967). (Cited on page 75.)

[162] F. Hinterberger, G. Mairle, U. Schmidt-Rohr, G. Wagner, and P. Turek, Nucl. Phys. **A111**, 265 (1968). (Cited on page 75.)

[163] F. Becchetti, J. Jënecke, and C. Thorn, Nucl. Phys. **A305**, 313 (1978). (Cited on pages 77 and 79.)

[164] L. D. Faddeev, ZhETF **39**, 1459 (1960), [Sov. Phys. JETP **12**, 1014 (1961).]. (Cited on pages 85 and 86.)

[165] L. D. Faddeev, *Mathematical Aspects of the Three-Body Probrem in the Quantum Scattering Theory* (Israel Program for Scientific Translation, Jerusalem, 1965). (Cited on pages 85 and 86.)

[166] T. Sawada and K. Thushima, Prog. Theor. Phys. **76**, 440 (1986). (Cited on page 88.)

[167] T. Sawada and K. Thushima, Prog. Theor. Phys. **79**, 1378 (1988). (Cited on page 88.)

[168] M. Yahiro, M. Nakano, Y. Iseri, and M. Kamimura, Prog. Theor. Phys. **67**, 1467 (1982). (Cited on page 88.)

[169] R. A. D. Piyadasa, M. Yahiro, M. Kamimura, and M. Kawai, Prog. Theor. Phys. **81**, 910 (1989). (Cited on page 88.)

[170] R. A. D. Piyadasa, M. Kawai, M. Kamimura, and M. Yahiro, Phys. Rev. C **60**, 044611 (1999). (Cited on page 88.)

[171] S. Okabe, *Ryhoshiron, Undo to hoho* (Kindai kagaku sha Co., Ltd., Tokyo, 1992). (Cited on pages 99 and 141.)

[172] F. D. Santos, Nucl. Phys. **A212**, 341 (1973). (Cited on pages 101, 104 and 113.)

[173] J. Poling, E. Norbeck, and R. Carlson, Phys. Rev. C **13**, 648 (1976). (Cited on page 107.)

[174] D. Drain, B. Chambon, J. L. Vidal, A. Dauchy, and H. Beaumevieille, Can. J. Phys. **53**, 882 (1975). (Cited on page 107.)

[175] E. Johnson *et al.*, Phys. Rev. Lett. **97**, 192701 (2006). (Cited on page 107.)

[176] C. Perey and F. Perey, Phys. Rev. **132**, 755 (1963). (Cited on page 109.)

[177] N. K. Timofeyuk and R. C. Johnson, Phys. Rev. C **59**, 1545 (1999). (Cited on pages 129 and 132.)

[178] Y. Yamaguchi, Phys. Rev. **95**, 1628 (1954). (Cited on page 136.)

[179] D. A. Varshalovich, A. N. Moskalev, and V. K. Khersonskii, *Quantum Theory of Angular Momentum* (World Scientific, 1988). (Cited on page 146.)